Norwegian University of Life Sciences
Faculty of Science and Technology

Philosophiae Doctor (PhD)
Thesis 2018:72

Geopolymer Concrete Incorporated with Microencapsulated Phase change materials for Energy Efficient Buildings

Geopolymer Betong med Mikrokapslede Faseendringsmaterialer for Energieffektive Bygninger

Vinh Duy Cao

Geopolymer Concrete Incorporated with Microencapsulated Phase change materials for Energy Efficient Buildings

Geopolymer Betong med Mikrokapslede Faseendringsmaterialer for Energieffektive Bygninger

Philosophiae Doctor (PhD) Thesis

Vinh Duy Cao

Norwegian University of Life Sciences
Faculty of Science and Technology

Ås 2018

Thesis number 2018:72
ISSN 1894-6402
ISBN 978-82-575-1540-9

Supervisors:

Dr. Carlos Salas-Bringas (main supervisor)
Associate Professor. Faculty of Science and Technology
Norwegian University of Life Sciences (NMBU)
P.O. Box 5003 REALTEK, N-1432, Ås, Norway

Dr. Anna-Lena Kjøniksen (co-supervisor)
Professor. Faculty of Engineering
Østfold University College (HIØF)
P.O.Box 700, 1757 NO-Halden, Norway

Evaluation Committee:

Dr. Juan Pedro Solano
Professor. Department of Thermal and Fluid Engineering
Technical University of Cartagena
30202 Cartagena, Murcia, Spain

Dr. Jessica Giro Paloma
Researcher. Department of Materials Science and Physical Chemistry
University of Barcelona
08028 Barcelona, Spain

Dr. Nils Bjugstad
Professor. Faculty of Science and Technology
Norwegian University of Life Sciences (NMBU)
P.O. Box 5003 REALTEK, N-1432, Ås, Norway

Preface

The doctoral thesis was submitted to the Faculty of Science and Technology at the Norwegian University of Life Sciences (NMBU, Ås, Norway). This PhD project is a part of *Microencapsulated phase change materials in concrete* project funded by Research Council of Norway (No. 238198). The thesis consists of seven scientific papers or manuscripts. The thesis includes the introduction to application of microencapsulated phase change materials in buildings, which summarizes and figure out the objectives of thesis, theoretical background, description of methodology, results-discussions and conclusions of the thesis. The work is supervised by Dr. Carlos Salas-Bringas and Prof. Anna-Lena Kjøniksen.

Acknowledgement

I would like to express my gratitude to my supervisor, Dr. Carlos Salas-Bringas, for his valuable guidance, supports and advices during my PhD. My expression of appreciation is to my supervisor, Prof. Anna-Lena Kjøniksen, for her enthusiastic and enduring guidance throughout this research and her constructive feedback on papers and thesis. Her encouraging nature, her outstanding knowledge and her dedication to research are great motivation to me. This thesis would not have been possible without their precious supports.

I would like to thank Prof. Juan F. Rodriguez, Dr. Manuel Carmona and Anna M. Szczotok at University of Castilla – La Mancha, Spain, for their microcapsules supply and for their valuable comments and discussion.

I am grateful to Prof. Lars Wadsö at Lund University, Sweden, Prof. Reidar Barfod Schüller at Norwegian University of Life Sciences and Prof. Marianne Hiorth at University of Oslo for carrying out some measurements in their lab.

I appreciate the assistance provided by Luca Valentini for his support at University of Padua, Italy to conduct X-ray micro-tomography measurements and his instructive comments.

I would like to thank colleagues at Engineering faculty, Østfold University College, especially Rino Nilsen, Trond Atle Drøbak and Reidar Nordby for their great supports with my experimental works.

I gratefully acknowledge funding from the Research Council of Norway.

Many thanks to my friends Anna, Shima, Susana, Tri, Loan for being such good friends, for sharing joys and knowledge.

I would like to thank all friends in Norway and in Vietnam for their priceless supports and the joyful time we had together since the first time I came to Norway. With your friendships, my PhD has been much more meaningful and the winters in Norway have safely passed without any depression.

The love and support of my parents, Cao Van Hien and Nguyen Thi Lien, my older brothers, Cao Duy Vu and Cao Duy Vuong, and my younger sister, Cao Nguyen Thao Linh, are the spring of motivation to me. Thank you for all your continuous encouragement and unconditional love.

At last but not least, a special thanks to my beloved wife, Nguyen Thi Ai Van, and my beautiful daughters, Cao Ha Ni and Cao Ha Mi, for their love, for their immeasurable support and for always being there to encourage me through the long process of completing this research.

Ås, August 2018

Vinh Duy Cao

Abstract

This study aims to develop new environmentally friendly construction materials with high energy storage capacity by using geopolymer concrete containing microencapsulated phase change materials (MPCM) to reduce energy consumption for buildings, which plays a key role to reduce global warming.

The rheological behavior of microcapsule suspensions revile the important role of non-encapsulated phase change materials on the physical properties and structure of microcapsules. This initial investigation provided valuable information for selecting the right kinds of microcapsules to integrate into concrete.

MPCM was integrated into Portland cement concrete (PCC) and geopolymer concrete (GPC), and a comparative analysis between PCC and GPC based on the thermal and mechanical properties was conducted.

The influence of the hygroscopic nature of polymer shell, core/shell ratio and size of the microcapsules on the microstructure, thermal properties and compressive strength of geopolymer concrete was investigated and discussed. The combination of a polymer shell containing polar functional groups and a small size of MPCM has a significant impact on the dispersion of MPCM in the GPC matrix and the porosity enhancement of GPC, which causes a reduction of both thermal conductivity and compressive strength. In addition, a high core/shell ratio contributes to an increase of the energy storage heat capacity during the phase change and a reduction of compressive strength when PCM changes from solid to liquid state. A better understanding of the effect of microcapsule properties on GPC is important to further investigations to maximize the thermal performance and minimize the mechanical strength reduction of GPC containing MPCM for building applications.

Thermal performance of GPC after incorporating MPCM was also investigated. Numerical modeling regarding the thermal performance of the materials was conducted and validated by experimental data. Systematic analysis of the effect of various climate conditions (outdoor temperature, maximum solar radiation) and MPCM-concrete design (wall thickness, MPCM concentration and core/shell ratio) on the energy efficiency of buildings using geopolymer concrete containing MPCM was examined.

The possibility of utilizing GPC containing MPCM at the environmental conditions of Oslo and Madrid during a one year period was numerically evaluated. It was found that the power

consumption for a heating/cooling system could be significantly reduced in both Oslo and Madrid after adding microcapsules into GPC walls. The wall orientations and the season have significant effect on energy efficiency of buildings, with the largest energy saving on the south and west facing walls and during summer.

Sammendrag

Formålet med dette studiet er å utvikle miljøvennlige konstruksjonsmaterialer med høy energilagringskapasitet ved å bruke geopolymerbetong som inneholder mikroinnkapslede faseovergangsmaterialer (MPCM) for å redusere bygningers energibehov og derved medvirke til redusert global oppvarming.

Reologiske målinger på suspensjoner av mikrokapslene viser at faseovergangsmaterialer som ikke er innkapslet har stor innvirkning på de fysiske egenskapene og strukturen til mikrokapslene. Resultatene fra dette innledende studiet resulterte i ny kunnskap som er essensiell for valg av riktig type mikrokapsler for bruk i betong.

MPCM ble blandet inn i Portland sement betong (PCC) og geopolymerbetong (GPC), og de termiske og mekaniske egenskapene til disse ble sammenlignet og analysert.

Påvirkningen av de hygroskopiske egenskapene til polymerskjellet, kjerne/skjell ratioer og størrelsen til mikrokapslene på mikrostrukturer, termiske egenskaper og trykkfasthet til geopolymerbetong ble undersøkt. Kombinasjonen av et polymerskjell som inneholder polare grupper og mikrokapsler med små størrelser har en signifikant innvirkning på dispersjonen av mikrokapsler i GPC-matrisen og på porøsitetsøkningen til GPC. Dette reduserer både den termiske konduktiviteten og slagstyrken til GPC. I tillegg vil en høy kjerne/skjell ratio øke energilagringskapasiteten under faseovergangen og redusere slagfastheten når faseovergangsmaterialet går fra fast til flytende form. En bedre forståelse av effekten av egenskapene til mikrokapslene er viktig for videre studier for å maksimere den termiske energisparingen og minimere styrkereduksjonen av betongen for videre bruk som bygningsmaterialer.

De termiske egenskapene til GPC med MPCM ble også undersøkt. Resultater av numerisk modellering av de termiske egenskapene til materialene ble validert ved sammenligning med eksperimentelle data. Effekten av forskjellige klimatiske forhold (utendørstemperatur, maksimal solstrålingsstyrke) og MPCM-betong design (veggtykkelse, MPCM-konsentrasjon og kjerne/skjell ratio) på energieffektiviteten til bygninger med geopolymerbetong med tilsatt MPCM ble systematisk studert og analysert.

Muligheten for å bruke GPC som inneholder MPCM under klimaforholdene i Oslo og Madrid under en ett års periode ble nummerisk modellert. Resultatene viste at energikonsumpsjonen for et varme/kjølesystem ble signifikant redusert i både Oslo og Madrid når MPCM ble tilsatt

til vegger av GPC. Veggenes retning har en stor innvirkning på energieffektiviteten. Mest energi ble spart på syd- og vestvegger under sommeren.

List of papers

Paper I: Vinh Duy Cao, Carlos Salas-Bringas, Reidar Barfod Schüller, Anna M. Szczotok, Marianne Hiorth, Manuel Carmona, Juan F. Rodriguez, Anna-Lena Kjøniksen. Rheological and thermal properties of suspensions of microcapsules containing phase change materials. *Colloid and Polymer Science* **2018**, 296, 981-988.

Paper II: Vinh Duy Cao, Carlos Salas-Bringas, Reidar Barfod Schüller, Anna M. Szczotok, Anna-Lena Kjøniksen. Time-dependent structural breakdown of microencapsulated phase change materials suspensions. *Journal of Dispersion Science and Technology* **2018**, in press.

Paper III: Vinh Duy Cao, Shima Pilehvar, Carlos Salas-Bringas, Anna M. Szczotok, Juan F. Rodriguez, Manuel Carmona, Nodar Al-Manasir, Anna-Lena Kjøniksen. Microcapsulated phase change materials for enhancing the thermal performance of Portland cement concrete and geopolymer concrete for passive building applications. *Energy Conversion and Management* **2017**, 133, 56–66.

Paper IV: Vinh Duy Cao, Shima Pilehvar, Carlos Salas-Bringas, Anna M. Szczotok, Nu Bich Duyen Do, Hoa Thanh Le, Manuel Carmona, Juan F. Rodriguez, Anna-Lena Kjøniksen. Influence of microcapsules size and shell polarity on the time-dependent viscosity of geopolymer paste. *Industrial& Engineering Chemistry Research* **2018**, 57, 9457-9464.

Paper V: Vinh Duy Cao, Shima Pilehvar, Carlos Salas-Bringas, Anna M. Szczotok, Luca Valentini, Manuel Carmona, Juan F. Rodriguez, Anna-Lena Kjøniksen. Influence of microcapsule size and shell polarity on thermal and mechanical properties of thermoregulating geopolymer concretes for passive building applications. *Energy Conversion and Management* **2018**, 164, 198-209.

Paper VI: Vinh Duy Cao, Shima Pilehvar, Carlos Salas-Bringas, Anna M. Szczotok, Tri Quang Bui, Manuel Carmona, Juan F. Rodriguez, Anna-Lena Kjøniksen. Thermal performance

and numerical simulation of geopolymer concrete containing different types of thermoregulating materials for passive building applications. *Energy and Buildings* **2018**, 173, 678-688.

Paper VII: Vinh Duy Cao, Shima Pilehvar, Carlos Salas-Bringas, Anna M. Szczotok, Tri Quang Bui, Manuel Carmona, Juan F. Rodriguez, Anna-Lena Kjøniksen. Thermal analysis of Geopolymer concrete containing microencapsulated phase change materials for passive building applications. Submitted to *Solar Energy* (Under review)

Table of Contents

Abbreviations and Symbols

Abbreviations

MPCM	Microcapsulated phase change materials
PCM	Phase change materials
GPC	Geopolymer concrete
GPP	Geopolymer paste
FA	Fly ash
GGBFS	Ground granulated blast furnace slag
PCC	Portland cement concrete
SEM	Scanning electron microscopy
XRF	X-ray Fluorescence
PMMA	Polymethyl methacrylate
PS-DVB	Polystyrene cross-linked with divinylbenzene
LDPE-EVA	Low density polyethylene copolymer with ethylvinylacetate
MF	Melamine-formaldehyde

Nomenclature

C_p	Specific heat capacity, J/kg °C
$Q_{convection}$	Convective heat transfer, W/m^2
Q_{rad}	Radiative heat transfer, W/m^2
T	Temperature, °C
t	Time, s
m	Mass, kg
P	Power consumption (Thermal load), kWh/m^2
Pr	Power reduction, %
h_i	Indoor heat transfer coefficient, W/m^2 °C
h_o	Outdoor heat transfer coefficient, W/m^2 °C
q_s"	Solar radiation, W/m^2
ΔH	Latent heat, J/g
K	The consistency index
n	Flow behaviour index
d	Thickness, m

A	Surface area, m^2
V	Volume, m^3

Subscripts

s	Saturated mass
d	Dry mass
b	Buoyant mass
solid	Solid state
liquid	Liquid state
init	Initial time of process
end	Final time of process
top	Top heat exchanger
bottom	Bottom heat exchanger
ave	Average
out	Outdoor environment
indoor	Indoor environment
max	Maximum temperature
min	Minimum temperature
sky	Average sky temperature
m	Melting

Greek symbols

η	Viscosity, Pa.s
$\dot{\gamma}$	Shear rate, 1/s
α	Thermal diffusivity, m^2/s
φ	Heat flux, W/m^2
λ	Thermal conductivity, W/m °C
ρ	Density, kg/m^3
σ	Stefan–Boltzmann constant, $W/m^2 \cdot K^4$
ε	Emissivity of the outdoor wall surface
α_s	Absorptivity of the outdoor wall surface

1. Introduction

Global warming is an important issue due to its significant and harmful influence on communities, health, and climate. The cause of global warming is increased amounts of greenhouse gases, especially carbon dioxide (CO_2) [1, 2]. The majority of CO_2 emissions are from the combustion of fossil fuels. The effort to slow the pace of global warming is closely related to the reduction of energy consumption. With approximately 40 % of the total global energy consumption contributed by buildings, reducing the energy consumption for buildings plays a key role to reduce global warming [3, 4].

Improved construction techniques and enhanced material technology can greatly reduce the energy consumption needed to keep a comfortable indoor temperature. Thermal energy storage systems, including sensible heat storage and latent heat storage materials, can be used to conserve and save energy [5-7]. Sensible heat storage materials store energy by raising the temperature of the storage materials such as concrete, rock, or steel. For latent heat storage materials, also known as phase change materials (PCM), the thermal energy is stored during the phase change of the materials (e.g. melting, evaporating, or crystallization) [8]. Unlike sensible heat storage, latent heat storage systems are capable of storing energy with higher storage density at an almost constant temperature, which is referred to as the phase transition temperature of the materials. This makes latent heat storage materials more attractive than sensible heat storage materials for improving thermal comfort and reducing the energy consumption for heating/cooling purposes.

The capability to store or release thermal energy from PCM strongly depends on the heat storage capacity, thermal conductivity, the melting temperature of the PCM, and the outdoor environment that it is exposed to [8, 9]. Building materials with a high volume and surface area exposed to the indoor environment are potential candidates for integration with PCM [10]. The incorporation of PCM into building materials can significantly improve the thermal energy storage capacity of building structures [8, 10-12]. Therefore, the development of building materials with a direct addition of PCM could reduce the energy consumption for heating/cooling systems. However, interaction with surrounding materials and low heat transfer coefficients limit the direct application of PCM [9, 13, 14]. In order to overcome these problems, microencapsulation may be utilized for incorporation of PCM into small polymeric capsules [15-18]. This provides not only an extremely high heat transfer area, but also prevents the leakage of PCM and interactions with the building structure. Microencapsulated phase

change materials (MPCM) are able to support PCM for utilization as thermal storage materials in building applications and energy storage systems [19-25]. Concrete-based materials with high thermal properties and high mechanical strength are potential candidates for MPCM integration [10]. Concrete materials provide the possibility to alter both thermal and mechanical properties of the MPCM-concrete. The integration of MPCM in concrete is therefore a good strategy of passive building technology to reduce the energy consumption.

MPCM can store and release large amounts of energy during the phase transition [16, 17]. This is a promising technology for improving the energy efficiency of buildings, with reduced power consumption for heating and cooling [10, 26-31]. Due to the low thermal conductivity of MPCM and an enhanced porosity, the thermal conductivity of concrete is decreased after addition of MPCM [10, 32]. This is advantageous for reducing the energy consumption. The decline in the compressive strength of concrete is the main drawback of MPCM addition [10, 26-28]. The destruction of microcapsules during the mixing process can contribute to the reduction of the compressive strength [26]. The soft nature of MPCM may weaken the concrete [10], and a complete cement hydration may be prevented due to the hygroscopic nature of microencapsulated phase change materials [28]. In addition, the enhancement of porosity after MPCM addition is probably an important factor for the strength reduction [10, 26, 29]. Although several explanations have been suggested, the exact mechanism causing the compressive strength reduction is still not clear. Furthermore, the effect of the properties of the microcapsules, such as the hygroscopic nature of the polymer shell, microcapsule size, and heat storage capacity on thermal and mechanical properties of concrete has not been explored. It is also important to evaluate the effect of PCM states (solid or liquid) on the compressive strength of concrete

Portland cement concrete is among the best known concrete-based materials for integration of MPCM [10, 26-31]. However, the main drawback of producing Portland cement is CO_2 emission, which contributes to about 5-8 % of the total CO_2 emissions, and is the third man-made CO_2 source after transport and energy generation [2]. Accordingly, it is advantageous to use green materials to partly replace Portland cement concrete. Geopolymers are synthesized by alkali activation of aluminosilicate materials in amorphous form (from industrial waste materials), providing environmentally friendly materials [33, 34]. It is interesting to replace Portland cement by geopolymer as the main binder for concrete, since this can significantly reduce the amount of CO_2 emission from the cement industry [35]. Although geopolymer

concrete containing microencapsulated phase change materials is very interesting, research regarding these materials is limited [10, 29].

Aim

The aim of this thesis is to develop a new environmental friendly geopolymer concrete containing microencapsulated phase change materials, which has high heat storage capacity and high thermal insulation properties while still keeping the mechanical properties at an acceptable level for passive building applications.

Main objectives

- Evaluating the effect of shear force and non-encapsulated phase change materials on microcapsule agglomeration (**Paper I and II).**
- Investigating the integration of microencapsulated phase change materials into concrete, comparing geopolymer concrete (GPC) and Portland cement concrete (PCC). (**Paper III**).
- Investigating the effect of microencapsulated phase change materials on the time dependent viscosity of geopolymer paste (**Paper IV**).
- Investigating the influence of the hygroscopic nature of the MPCM polymer shell, size and concentration on the thermal and mechanical properties of geopolymer concrete (**Paper IV and V**)
- Developing an accurate numerical method to predict the energy efficiency of buildings using concrete containing MPCM (**Paper VI**).
- Predicting the potential energy saving of buildings employing geopolymer concrete containing microencapsulated phase change materials at various European climate conditions (**Paper VII**).

2. Background

2.1. Microencapsulated phase change materials

2.1.1. Phase change materials

Phase Change Materials are capable of storing or releasing energy by changing phases [8, 9]. The mechanism of the thermal energy storage of PCM is simple (Figure 1). When the temperature rises above melting point, PCM will absorb energy and transfer from solid state to liquid state. When the temperature decreases below the melting point, the PCM will release the stored energy when it re-solidifies. Accordingly, PCM can provide a high energy storage capacity at an almost constant temperature (the phase change temperature point) [8, 9]. The high energy storage capacity of PCM can be applied in buildings to reduce the effect of external weather conditions on the indoor temperature fluctuations. This will enhance the energy efficiency and thermal comfort of buildings [10, 32]. The melting point depends on the chosen PCM. Accordingly, the desired interior temperature can be easily controlled by selecting a suitable PCM. The PCM can therefore be selected and applied to various climate conditions to maintain an interior temperature within the human comfort zone and thereby minimize the power consumption for the heating/cooling system.

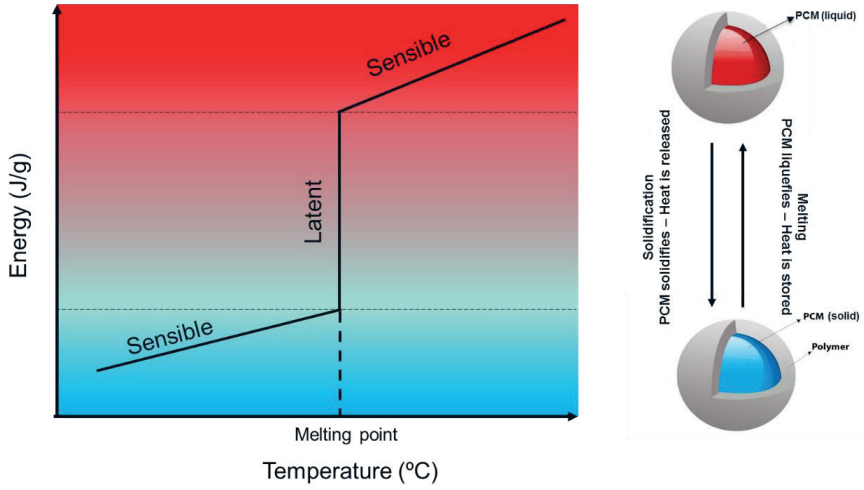

Figure 1. Schematic representation of phase change process

PCM can be classified into three categories: organic, inorganic, and eutectic materials. Inorganic PCM (salt hydrates and metallic materials) are the most common form of PCM, exhibiting attractive properties such as high latent heat, high thermal conductivity, non-

flammable, relatively low cost. However, the drawbacks of inorganic PCM are corrosiveness, instability, and a high tendency of super cooling [5-7]. Inorganic PCM tends to degrade after repeated cycles. Organic PCM includes paraffin and fatty acids [6, 7]. Organic PCM are chemically stable, safe and non-corrosive. They have a high latent heat per unit weight, and little super cooling. Moreover, they are compatible and suitable for integration into various building materials. These organic materials do have some undesirable properties such as a higher price than inorganic PCM, low thermal conductivity, and high changes in volume during phase change. In addition, they are flammable and they may generate harmful fumes on combustion.

Generally, the latent heat of paraffin are lower than that of inorganic materials, but they have a wider range of melting points and are more compatible with building materials. Paraffin PCM is therefore utilized in this thesis.

2.1.2. Microcapsules containing PCM

The incorporation of PCM into building materials can significantly improve the thermal energy storage capacity of building structures around the melting range of PCM [9, 11, 27]. Therefore, the development of smart building materials with the direct addition of PCM could reduce the energy consumption for heating/cooling systems. However, interactions with surrounding materials and low heat transfer coefficients limit the direct application of PCM. In order to overcome these problems, microencapsulation may be utilized for incorporation of PCM into small polymeric capsules [15-18]. This provides not only an extremely high heat transfer area, but also prevents the leakage of PCM and interactions with the building structure. Microencapsulated phase change materials (MPCM) are therefore able to support PCM for utilization as thermal storage materials in building applications and energy storage systems [13, 19, 26, 36-38]

The main component of microencapsulated phase change materials (Figure 2) is the phase change material core, which provides the high thermal energy storage of the microcapsules, while the polymer shell act as a protective barrier between PCM and the surrounding environment.

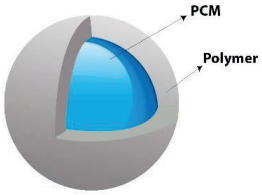

Figure 2. Schematic representation of microencapsulated phase change materials.

Microencapsulation is a process in which tiny particles or droplets are surrounded by a thin layer of encapsulating materials to give small capsules with many useful properties [8-19]. All three states of material (solids, liquids, and gases) can be microencapsulated. Since the PCM is within a solid polymer shell, the material can still be treated as a solid, even when the core is a liquid or gas. The encapsulated particles can be integrated into any matrix that is compatible with the encapsulating film. The shell materials provide a physical barrier between core and matrix. Organic or inorganic materials can be used for the shell material. However, polymers are commonly used. An important key for the shell material selection is the physical properties. The encapsulating material must be thick enough to avoid diffusion of the encapsulated material out through the shell. High resistance to mechanical and thermal stresses is an important requirement MPCM for building applications. It is important that the PCM exhibits good stability over numerous phase transition cycles. Accordingly, the PCM should be retained within an impermeable microcapsule for the whole product lifetime. Commonly used shell materials are: polystyrene, polymethylmethacrylate, Arabic gum, gelatin, amino plastics, gelatin-gum Arabic, urea formaldehyde resin, melamine formaldehyde resin, and gelatin formaldehyde resin [8-19].

2.2. Geopolymer concrete

Geopolymers are synthesized by alkali activation of materials rich in silica and alumina from industrial waste materials such as fly ash (FA), coal ash, rice-husk ash, red mud and ground granulated blast furnace slag (GGBFS) [33, 34, 39, 40]. The polymerization process involves a chemical reaction of aluminosilicate minerals under alkaline conditions that results in a three dimensional polymeric network. The polymerization process (Figure 3) includes: Stage I: Silicate and Alumina from the source materials react with hydroxide ions to form geopolymer

precursor ions/gel (monomers), which is known as aluminosilicate hydrate (A–S–H) gel, Stage II: polymerization of precursor ions (monomers) to form the 3-D geopolymer structure [41, 42].

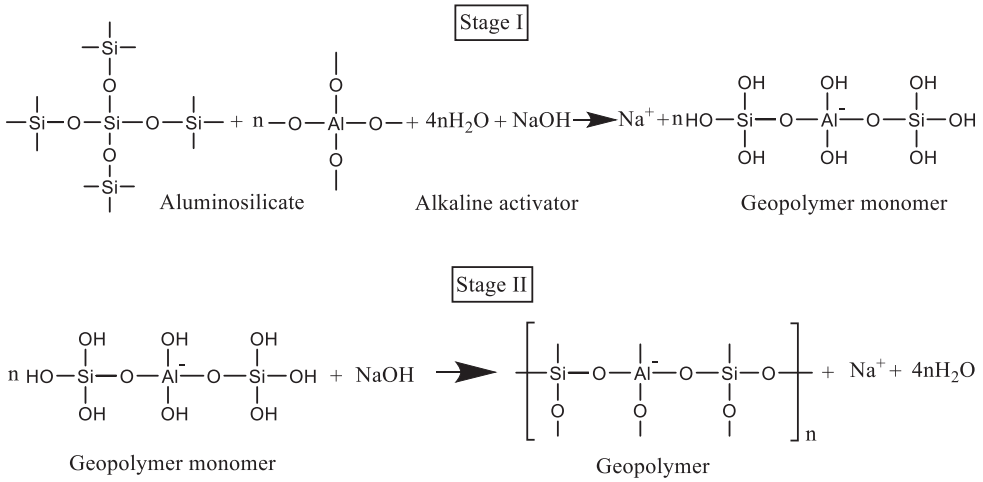

Figure 3. The geopolymer reaction mechanism between the sodium hydroxide activator and the Si-Al source materials **(Paper IV)**.

The structure and resulting properties of geopolymers are strongly depending on the alkaline activators and source materials that contain silica and alumina. The alumina and silicate from source materials are dissolved by alkaline solution to form the precursor/monomer (e.g. sodium aluminosilicate hydrate (N–A–S–H) gels). Furthermore, due to the existence of calcium oxide (CaO) in some source materials, calcium-silicate hydrates (C-S-H) gels and aluminium-modified calcium silicate hydrate (C–A–S–H) gels can be formed [43, 44]. These gels are responsible for the mechanical strength of geopolymers. Therefore, the structure and resulting properties of geopolymers can be varied by altering the silicate to alumina amorphous molar ratio, the amount of CaO in the source materials [45], and the kind and concentration of the alkali metal cation [46, 47]. Other important factors are geopolymerization temperature, water content, and the utilization of admixtures in the geopolymer synthesis process [48, 49].

The alumina-silicate source materials for geopolymers should contain a high amount of alumina (Al_2O_3) and silicate (SiO_2). Recently, fly ash (FA) based geopolymers have received special attention [43-50]. Fly ash is an industrial waste product from the coal combustion process, and contains high amounts of silica (SiO_2) and alumina (Al_2O_3). It is produced in huge amounts, and is extremely cheap [50]. It also has a favorable shape and size to with respect to improving the workability of geopolymers [50]. According to ASTM C618 [51], fly ash includes class C

FA and class F FA. The FA classification is based on the chemical composition. Class F fly ash contains high amounts of SiO_2, Al_2O_3, Fe_2O_3 (≥ 70%) and low amounts of CaO (< 10 wt.%) while class C FA has more than 50 wt.% of total SiO_2, Al_2O_3, Fe_2O_3 and more than 20 wt.% of CaO. Fly ash also contains low concentrations of other components such as magnesium, potassium, sodium, titanium, and sulfurat.

In comparison to class C fly ash, class F fly ash contains higher amounts of SiO_2, Al_2O_3 and Fe_2O_3 and lower content of CaO. The higher CaO fly ashes (Class C) generally have shorter setting time than low CaO fly ashes (class F). This causes difficulties in the fabrication process. A possible explanation is that the hydraulic reactivity of fly ash increases as the content of CaO increases [47]. On the other hand, a low amount of CaO in FA can reduce the hydrated products such as calcium silicate hydrate (C-S-H) [52, 53] and aluminium-modified calcium silicate hydrate (C–A–S–H), which decreases the compressive strength and the durability of GPC. In order to balance the advantage and disadvantage of CaO on the geopolymer properties, FA class F is mixed with substances which contain high amounts of CaO such as ground granulated blast furnace slag, silica fume, or natural pozzolan [47, 54-57]. Accordingly, the compressive strength and setting time of geopolymers can be controlled by adjusting the content of each component. The incorporation of ground granulated blast furnace slag (GGBFS) into FA geopolymers is a potential solution to obtain high mechanical properties [58-60]. GGBFS is an amorphous by-product of the steel industry with a high content of CaO, and renders the microstructure of geopolymers more compact and provides a reasonable setting time [58-60]. In some cases, it is necessary to add chemical admixtures to the geopolymer based FA+GGBFS recipe in order to increase the setting time [48, 49, 61].

The alkaline activator plays an important role in the geopolymerization process and final GPC properties due to its ability to dissolve the alumina-silicate from source materials to form the sodium aluminosilicate hydrate (N–A–S–H), aluminium-modified calcium silicate hydrate (C–A–S–H) the calcium silicate hydrate (C-S-H) [43, 44]. The common alkaline solutions for making geopolymer are sodium hydroxide (NaOH), potassium hydroxide (KOH), sodium silicate (Na_2SiO_3) and potassium silicate (K_2SiO_3) as individual components or a combination. An alkaline solution based on a combination of a sodium hydroxide solution (NaOH) and a sodium silicate solution (Na_2SiO_3) results in the best mechanical strength [44, 62]. It is possible that the sodium silicate addition can form more calcium silicate hydrate (C-S-H) in the final product, which can enhance the compressive strength [44, 62]. The ratio of sodium silicate to

sodium hydroxide is important since it has a significant effect on the workability and mechanical properties of GPC [46, 63].

In the current work, a mixture of GGBFS and class F fly ash was utilized as to improve the mechanical strength of geopolymer concrete, together with an alkaline activator based on a combination of sodium silicate and sodium hydroxide.

3. Materials

3.1. Microencapsulated phase change materials

Different kinds of microcapsules with variation of polymer shells, heat storage capacity and size distribution were utilized to explore their influence on the microstructure, thermal and mechanical properties of geopolymer concrete.

- LDPE-EVA/RT27 microcapsules consists of a paraffin Rubitherm®RT27 core coated with a hydrophobic LDPE-EVA (low density polyethylene copolymer with ethylvinylacetate) shell
- PS-DVB/RT27 microcapsules consists of a paraffin Rubitherm®RT27 core coated with a hydrophobic PS-DVB (polystyrene cross-linked with divinylbenzene) shell. These were made by a polymerization suspension process in our lab [64].
- Commercial Microtek MPCM24D (MF/PCM24) contains a paraffin core and a melamine-formaldehyde polymer shell (MF).
- Micronal DS-5038X (BASF, Germany) (PMMA/PCM26) is composed of a paraffin mixture core and a highly crosslinked polymethyl methacrylate (PMMA) shell.

The properties of the microcapsules are summarized in Table 1.

Table 1: The fundamental data of the microencapsulated phase change materials

MPCM name	Density (g/cm^3)	Melting point (ºC)	Latent heat (J/g)	Core/Shell ratio	Reference
LDPE-EVA/RT27	0.9	25.2	105	3:2	[65]
PS-DVB/RT27	0.9	24.9	100	11:9	[64]
PMMA/PCM26	0.9	24.7	110	7:3	[66]
MF/PCM24	0.9	21.9	154	9:1	[67]

3.2. Geopolymer concrete

Geopolymer concrete containing microencapsulated phase change materials (MPCM-GPC) was fabricated by mixing class F fly ash (FA), ground granulated blast furnace slag (GGBFS), sand, aggregates, retarder, an alkaline activator solution, and MPCM.

Sand (density of 2.7 g/cm^3) and aggregates (density of 2.6 g/cm^3) were supplied by Gunnar Holth and Skolt Pukkverk AS, Norway. In addition, the class F fly ash (density = 2.26±0.02 g/cm^3) and ground granulated blast furnace slag (GGBFS) (density = 2.85±0.02 g/cm^3) was purchased from Norcem, Germany and Cemex, Germany, respectively. The chemical composition of FA and GGBFS were obtained by X-ray Fluorescence (XRF) and is summarized in Table 2.

The alkaline activator solution was mixed at a ratio between sodium silicate solution (density = 1.93 g/cm^3, 35 wt.% solid) and 14M NaOH (560 g/L) solution of 1.5 [68]. Accordingly, $m_{Na2SiO3(aq)}$ = 120 g, and $m_{NaOH(aq)}$ = 80 g. In addition, fresh GPC possesses a poor workability due to the high viscosity of the alkaline solution and high geopolymerization reactivity. This results in a negative effect on the integration of MPCM into GPC [10, 29]. Therefore, a chemical admixture was utilized to improve the workability as well as the mixing ability of MPCM into GPC. A naphthalene based retarder, which has the density of 1.2 g/cm^3 and was purchased from FLUBE OS 39, Bozzetto Group, Italy, was selected due to its high effectiveness to fly ash class F [48, 49, 61], which was used in the current work.

Table 3 summarizes the composition of geopolymer concrete containing MPCM (MPCM-GPC). For the recipe, 1 L volume mix design was obtained [29, 68]. The sand was replaced by MPCM at the same volume percentage. The amounts of each component in weight were obtained by multiplying the volume of each component with the density.

In the first step, the homogenous binder was prepared by mixing fly ash, GGBFS and alkaline solution together for 1 minute. Afterward, the homogenous binder was mixed with the dried sand for 30 s using a drum mixer. Subsequently, the aggregates, retarder and extra water were consecutively added to the mixture and mixed for 2 minutes. In order to minimize the shearing effect of the mixing process, MPCM was only added into GPC during the final step and the final mixture was mixed for 2 more minutes. The whole mixing process was done at room temperature (20 ºC). PCM was incorporated into GPC at 0, 1.3, 2.6 and 5.2 wt.%. The concentration of MPCM was limited to 5.2 wt.% since higher concentrations of MPCM resulted

in too low workability of the geopolymer concrete. After mixing, MPCM-GPC was cast into molds at a size of 200 × 200 × 25 mm (for the thermal test) and 100 × 100 × 100 mm (for the compressive strength test). The samples were pre-cured at room temperature (20 ºC) for 24 hours. The samples were then demolded and kept in water at room temperature (20 ºC) for 28 days to reach a fully cured state. Before conducting the thermal test, the fully cured samples were dried in an oven at 40 °C until the sample weight remained unchanged.

In order to investigate the effect of MPCM on different types of concrete, Portland cement concrete was employed as a reference. Furthermore, the GPC without retarder (GPC-nonRetarder) was also tested. The recipe of PCC and GPC-nonRetarder can be found in **paper III**. It is important to note that the sand and aggregate used in **paper III** are different from the other papers due to a limitation from the supplier. Therefore, the comparison will be focused on the effect of MPCM on the changing rate (slope) of the properties rather than on the absolute values.

Table 2: Chemical composition of fly ash (FA) and ground granulated blast furnace slag (GGBFS) **(Paper V)**.

Chemical	Al_2O_3	SiO_2	CaO	Fe_2O_3	MgO	K_2O	TiO_2	Na_2O	P_2O_5	SO_3	SrO	CO_2
FA (wt.%)	23.15	50.83	6.87	6.82	1.70	2.14	1.01	1.29	1.14	1.24	0.19	3.07
GGBFS (wt.%)	10.30	34.51	42.84	0.60	7.41	0.52	0.66	0.40	0.02	1.95	0.05	0.30

Table 3: Composition of Geopolymer concretes **(Paper V, VI, VII)**

MPCM (wt.%)	Alkaline solution (g)	Water (g)	FA* (g)	GGBFS** (g)	Sand (g)	Aggregate (g)	Retarder (g)	MPCM (g)
0	200	50	300	200	871.2	851.7	5	0
1.3					784.1			30
2.6					696.9			63
5.2					522.7			117

3.3. Geopolymer paste for rheology

The viscosity of the pre-set geopolymer has a significant impact on fabricating process and properties of final product. In order to understand the effect of microcapsules on the geopolymer viscosity, the influence of the hygroscopic nature of the polymer shells, the size, and microcapsule concentration on the geopolymerization reaction and time dependent viscosity of the geopolymer paste was investigated.

Geopolymer paste containing microencapsulated phase change materials (MPCM-GPP) was fabricated by mixing fly ash (FA) (Norcem, Germany), ground granulated blast furnace slag (GGBFS) (Cemex, Germany), MPCM and an alkaline activator solution. The recipe of the GPP is shown in Table 4.

Table 4: Composition of Geopolymer paste (GPP) utilized in the rheology measurements **(Paper IV)**

Sample	MPCM (wt.%)	Alkaline solution (g)	Water (g)	FA (g)	GGBFS (g)	MPCM (g)
GPP0	0	220	55	300	200	0
GPP3	3					24
GPP6	6					50
GPP9	9					77
GPP12	12***					106

(***) MF/PCM24 was not utilized at concentration of 12 wt.% due to a too high viscosity.

For the rheological experiments, FA, GGBFS and MPCM were mixed together at room temperature (20 ºC) for 1 minute using a mixer (Electrolux EKM4300). The alkaline solution and water were added continuously into the mixed powder during 30 s, and the geopolymer paste was mixed for 3 more minutes. After mixing, the geopolymer paste was loaded into the rheometer measuring cell for testing.

4. Methodology

4.1. Size distribution

Low Angle Laser Light Scattering (LALLS) laser diffraction using a Malvern Mastersizer 2000 (Malvern Instruments Ltd., Malvern, UK) equipped with a Scirocco 2000 unit for analyzing dispersions of the particles in air was employed to determine the size distribution of MPCM.

4.2. SEM

The surface morphology and the micro structure of the microcapsules (powder form) were obtained by Scanning electron microscopy (SEM) (Quanta FEG-250, Spain). For MPCM-GPC samples, the fractured surfaces of samples containing 2.6 wt.% of MPCM were investigated using Zeiss EVO50 EP Scanning electron microscopy (Norway).

4.3. X-Ray tomography

The internal microstructure of GPC containing microcapsules was investigated using X-ray tomography. The X-ray micro-tomography cross-sectional slices of cylindrical samples were obtained using a Skyscan 1172 CT scanner (Bruker) with 80 kV incident radiation, 124 μA source current, 750 ms exposure time per frame and 0.3° rotation step. Tomographic reconstruction was performed using the Feldkamp algorithm [69] and the final pixel size was 6 μm. The samples were made in cylindrical form (1 cm diameter and 1 cm height) from completely cured GPC without MPCM and containing 2.6 wt.% of microcapsules (PS-DVB/RT27, PMMA/PCM26 and MF/PCM24).

4.4. Open porosity and density

The density of MPCM-concrete samples were determined using EN 12390-7[70]:

$$\rho = \frac{m_d}{V} \qquad \text{Eq. 1}$$

where ρ is the dry density of the MPCM-concrete, m_d is oven-dried weight and V is the volume of the sample.

The porosity test was done based on ASTM C1202-12 [71, 72]. The samples were oven-dried at 105 °C until a constant weight was achieved. It has previously been confirmed by thermogravimetric analysis (TGA) that the microcapsules are completely stable at temperatures lower than 150 °C [73]. The samples were cooled down to room temperature before recording the oven dried mass m_d. Afterwards, the samples were immersed in water at room temperature until the weight of the sample in water remains constant, and the buoyant mass of the saturated samples in water m_b were recorded. Finally, the saturated sample was moved out of water, the surplus water wiped from the surface, and the saturated sample in air m_s was recorded. The open porosity of MPCM-concrete samples can be calculated by:

$$Open\ Porosity\ (\%) = \frac{m_s - m_d}{m_s - m_b} \times 100 \qquad \text{Eq. 2}$$

4.5. Trapped water content

The ability of microcapsules to trap water was determined to compare the polarity of the microcapsules polymer shell. 5.0 ± 0.1 g of each type of microcapsules were immersed in 50 ml of alkaline solution at room temperature (20 ℃). After 24 hours, the dispersion of microcapsules in alkaline solution was placed into filter test tubes (0.45 μm filter membrane) and centrifuged at 4500 rpm for 5 min (Mega Star 1.6R) to separate the microcapsules from the alkaline solution. The remaining water trapped on the microcapsules were determined utilizing a moisture analyzer (MB 64M-VWR, Italy). The temperature for this test was set at 70 ℃. The final trapped water can be obtained after subtracting the water content of the initial microcapsules, which were also determined by the moisture analyzer.

4.6. Non-encapsulated PCM content

Microcapsules were weighed (0.5 g), and placed on an oil absorbing paper at room temperature. The paper was transferred to an oven at 40 °C for 10 min. The change of color and gloss of the paper were compared to indicate the presence of non-encapsulated paraffin. The amount of non-encapsulated paraffin was determined by weighting the absorbing paper before and after heating at 40 ℃ and summarized in Figure 4. Accordingly, LDPE-EVA/RT27 contains a high amount of non-encapsulated PCM (2.5±0.4 %) while there is no non-encapsulated PCM on PMMA/PCM26 and MF/PCM24 or very low amount on PS-DVB/RT27 (0.3±0.1 %).

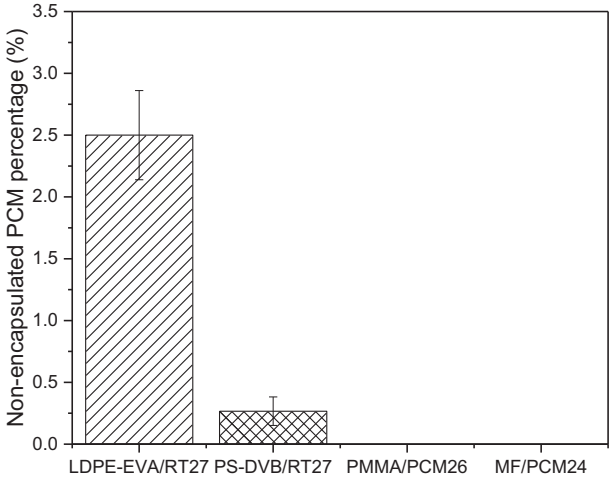

Figure 4. The non-encapsulated PCM percentage of different kinds of microcapsules. PMMA/PCM26 and MF/PCM24 contain no non-encapsulated PCM.

4.7. Rheology

4.7.1. MPCM suspensions

Suspensions of microencapsulated phase change materials were fabricated by dispensing different mass ratios of MPCM in glycerol at a room temperature. The mass concentration was varied from 0 to 30 wt.%.

Rheological measurements of MPCM suspensions were carried out using an Anton Paar MCR301 rheometer (Austria). The MPCM suspensions were tested using a CC27 bob/cop measuring system (cup diameter: 28.91 mm; bob diameter: 26.66 mm) mounted in a cylindrical Peltier for temperature control. A fresh sample was loaded into the measuring system. The sample was pre-sheared at shear rate of 50 s^{-1} for 5 min and rested for 5 min before any measurements were conducted. In order to investigate the reproducibility of the results, each measurement was repeated three times with fresh samples.

Flow curves were measured with a shear rate in the range of 10-500-10 s^{-1} at 10 °C, 20 °C (below the melting point of paraffin Rubitherm®RT27) and 40 °C, 50 °C (above the melting point of paraffin Rubitherm®RT27). The test was not performed at 30 °C to avoid the transition temperature of the melting process. The experimental data for the increasing shear rate curves were described by the Cross Model (Eq.3) and the power law model (Eq. 4) [74]. The hysteresis areas between the increasing and decreasing shear rate curves were obtained using OriginPro 2016 Sr2.

The Cross model is usually used to describe the viscosity over a wide range of shear rates. The Cross model describes the suspension as a Newtonian fluid at low shear rates, and as a power-law fluid at high shear rates:

$$\eta = \eta_\infty + (\eta_0 - \eta_\infty)\left(1 + \left(\frac{\dot{\gamma}}{\dot{\gamma}_0}\right)^2\right)^{\frac{n-1}{2}} \quad \text{Eq. 3}$$

where η_∞, η_0 and n are the viscosity at an infinite shear rate, the zero shear rate viscosity and the dimensionless flow behaviour index, respectively. $\dot{\gamma}$ and $\dot{\gamma}_0$ are the shear rate and the critical shear rate where the fluid transits from Newtonian to power law behavior, respectively. In order to avoid unreliable data due to over-parameterization of the fitting procedure, the number of fitting parameters was reduced by subtracting the temperature-dependent viscosity of glycerol from the measured viscosity values. The resulting reduced viscosity values were then fitted to Eq. 1, fixing η_∞ at zero. Although there are some deviation between the Cross model and the

experimental data at low shear rates, the model gives a reasonably good fit to the data below the phase transition temperature of the paraffin core (**Paper I**). Above the melting temperature of the paraffin core, the curves did not exhibit a Newtonian region in the considered shear rate range. Accordingly, at high temperatures Eq. 3 includes too many fitting parameters to achieve good fit of the data, and a simple power law behavior (Eq. 4) was therefore used instead:

$$\eta = K\dot{\gamma}^{n-1} \quad \text{Eq. 4}$$

where K is the consistency index.

Additionally, the MPCM suspensions were subjected to constant shear rates of 100, 300, 500 and 700 s^{-1} at 20 °C for a period of 30 min at different microcapsule concentrations in order to determine the influence of steady shear on the time-dependent structural breakdown of microencapsulated phase change materials (MPCM) (**Paper II**).

4.7.2. Geopolymer paste

Rheological measurements for geopolymer paste were carried out using an Anton Paar MCR302 rheometer (Austria). The MPCM-geopolymer paste were tested using a BMC-90 (building materials cell) measuring system (cup diameter: 74 mm; bob (stirrer ST59-2V-44.3/120) diameter: 59 mm) mounted in a cylindrical Peltier system for temperature control.

After mixing, geopolymer paste was loaded into the rheometer measuring cell for testing. The sample was left in the cell for 30 s before pre-shearing at 50 s^{-1} for 1 minute to ensure that the samples has the same shear history. After the pre-shear, the samples were left to equilibrate for 1 min to achieve a uniform state. The MPCM-geopolymer paste was sheared at a constant shear rate of 10 s^{-1} at 20 °C until the viscosity increases too much to continue the measurements.

In order to quantify the time-dependent changes of the viscosities of MPCM-geopolymer paste, a new empirical equation (Eq.5) was developed:

$$\eta(t) = (\eta_0 - 1) + a \cdot t + \exp\left[\left(\frac{t}{t_t}\right)^b\right] \quad \text{Eq. 5}$$

Where $\eta(t)$ and η_0 are the viscosity as function of time (t) and the initial viscosity of the MPCM-geopolymer paste, respectively. a, b, and t_t are the kinetic constants for the initial linear viscosity increase, the exponential growth kinetic constant and the transition time from linear increase to exponential growth, respectively.

4.8. Compressive strength

The effect of different kinds of microcapsules and their concentration on the compressive strength of geopolymer concrete were investigated. An Alpha 3-3000 system (Form+Test Seidner&Co.GmbH) was employed to determine the compressive strength of MPCM-GPC samples based on EN 12390-3. In addition, the measurement was conducted at different temperatures including 20 ºC (below the melting range) and 40 ºC (above the melting range) to examine effect of temperature on the compressive strength of MPCM-GPC samples. The cubes were left in the room for 3 h to remove free water before they were tested at 20 ºC. For the test at 40 °C, the temperature of the compressive strength machine was kept at 40 °C by thermal insulation combined with utilization of a temperature regulating incubator connected by an isolated tube. Before the compressive strength test, cubes were kept in a room temperature for 3 h to remove free water. Afterwards they were placed in a heating chamber at 40 °C for 12 h to obtain a uniform temperature through the whole samples, immediately afterward the cubes were tested. Three cubes were tested for each sample.

4.9. Guarded hot plate system

The guarded hot plates method, which is well suited for concrete samples, was utilized in order to characterize the thermal performance of the MPCM-concrete samples [13, 75]. This method allows recording of temperature variations and heat fluxes exchanged through the sample during the testing process. The guarded hot plates system is presented in Figure 5.

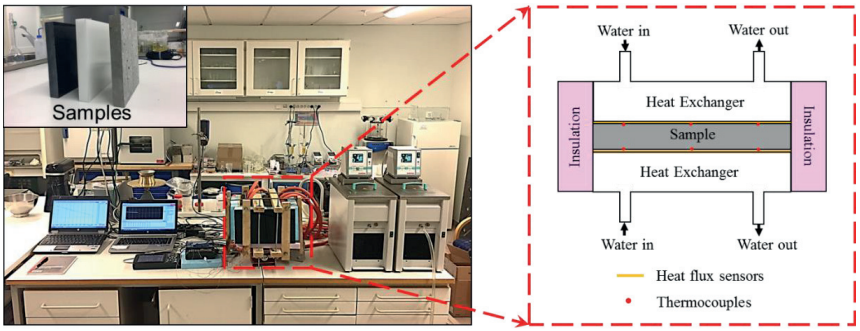

Figure 5. The guarded hot plates system and sketch of the cross-section of system.

The thermal system includes two aluminum plate heat exchangers connected to thermal regulated baths that define the thermal conditions. The MPCM-concrete sample was sandwiched between two aluminum plate heat exchangers. A 40 mm thick polyethylene

expanded foam (PEF) is used to form an insulated cover around the sample. This insulated cover will minimize the heat transfer from the lateral side face of the sample into the surrounding environment. Accordingly, the heat transfer through the MPCM-concrete sample can be calculated assuming one-dimensional thermal condition. Heat flux sensors (Captecv, France) and K-type thermocouples (TC Ltd., UK) were inserted on both sides of the sample to measure the temperature variations and heat fluxes through sample during testing processes. All sensors were connected to a multichannel multimeter (LR8410-20 Hioki, Japan) to record the data.

4.9.1. Thermal conductivity

The conductivity of the sample is defined according to the European standard EN-12667.
The thermal conductivity of the MPCM-concrete samples was determined at temperatures below and above melting range of MPCM (20-32 °C) [73]. They are denoted solid thermal conductivity (below the melting point) and liquid thermal conductivity (above the melting point). Both aluminum plate heat exchangers were first kept at a constant temperature T_{init} until the heat fluxes were constant (thermal steady-state condition). Then, a temperature variation was imposed on the top aluminum plate heat exchanger from T_{init} to T_{end} and kept at T_{end} while the other aluminum plate heat exchanger was kept at T_{init} until a thermal steady state was reached. After reaching a thermal steady state condition, the average temperature on the top (T_{top}) and bottom (T_{bottom}) faces of the block and the average heat fluxes (φ_{ave}) on both faces were recorded (Figure 6). The thermal conductivity (k) can be calculated by [10]:

$$k = \frac{\varphi d}{(T_{top} - T_{bottom})} \quad \text{Eq. 6}$$

where d is the thickness of the sample. In these experiments the dimension of the concrete samples is d=25±1 mm. For the solid thermal conductivity, T_{init} and T_{end} are set at 5 and 10 °C, respectively. While values of T_{init} and T_{end} of 45 and 50 °C are set to calculate the liquid thermal conductivity of the MPCM-concrete.

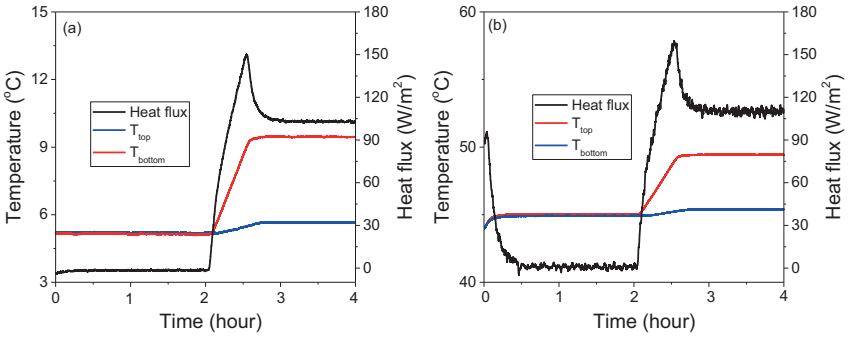

Figure 6. Heat flux and temperatures versus time for determination of (a) the solid thermal conductivity and (b) the liquid thermal conductivity of GPC-5.2-(MF/PCM24).

4.9.2. Specific heat capacity/latent heat

The latent heat and the specific heat capacity of the MPCM-concrete sample were measured by the same testing system as the thermal conductivity. The MPCM-concrete sample is initially isothermal at T_{init}. Afterwards, it was heated by raising the temperature of both aluminum plate heat exchangers from T_{init} to T_{end} by using thermostatic baths and at a heating rate of 10 °C/hour. In this experiment, T_{init} and T_{end} were set equal to 5 °C and 45 °C, respectively. The average heat fluxes (φ_{ave}) and temperature on both faces of MPCM-concrete sample (T_{top} and T_{bottom}) during the test is determined via heat flux sensors and thermocouples, respectively. The solid specific heat capacity, $C_{p\text{-}solid}$ (below melting range) and the liquid specific heat capacity, $C_{p\text{-}liquid}$ (above melting range) were estimated in the temperature range of 10-15 °C and 35-40 °C, respectively. Figure 7 shows the specific heat capacity of concrete containing MPCM samples as a function of temperature, determined by [10, 36]:

$$C_p(\mathrm{T}) = \frac{A\varphi(\mathrm{T})}{m\frac{dT}{dt}} \quad \text{Eq. 7}$$

The latent heat was calculated in the temperature range of 10-35 ºC by Eq.8 [36] using OriginPro 2016 Sr2.

$$\Delta H = \frac{A}{m}\left(\int_{T1}^{T2}\varphi(T)dT\right) - C_{p-ave}\cdot(T_2 - T_1) \quad \text{Eq. 8}$$

where $C_{p\text{-}ave}=(C_{p\text{-}solid} + C_{p\text{-}liquid})/2$ is the average specific heat capacity, ΔH is the latent heat. T_1=10 ºC and T_2=35 ºC. A=400 cm^2 is the area of the sample.

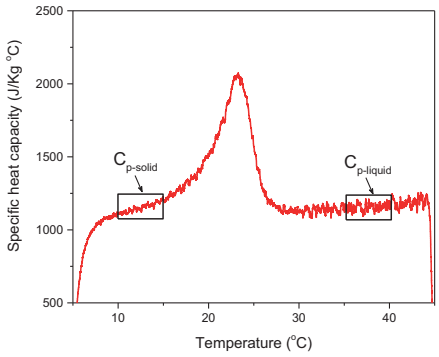

Figure 7. Specific heat capacity as function of temperature of GPC-5.2-(MF/PCM24).

Furthermore, a new equation was developed to represent the experimental data of the specific heat capacity function ($C_p(T)$). Most of the literature define $C_p(T)$ assuming that the melting peak is symmetric, utilizing the piecewise function of temperature [76, 77] or the Gauss function of temperature [78] for modelling purposes. However, this assumption is not in agreement with the experimental curve of $C_p(T)$ of concrete containing microcapsules, which presents an asymmetric shape of the melting peak [10, 13, 14, 36]. We have therefore utilized a new equation (Eq.9) based on the Pearson IV function to fit the specific heat capacity ($C_p(T)$) to the asymmetric shape:

$$Cp(T) = \begin{cases} Cp_o + h * \dfrac{{w_l}^{2m_l}}{\left({w_l}^2 + \left(2^{\frac{1}{m_l}} - 1\right) * (2T - 2T_m)^2\right)^{m_l}} & for\ T \le T_m \\ Cp_o + h * \dfrac{{w_r}^{2m_r}}{\left({w_r}^2 + \left(2^{\frac{1}{m_r}} - 1\right) * (2T - 2T_m)^2\right)^{m_r}} & for\ T > T_m \end{cases} \quad \text{Eq. 9}$$

h, T_m, w_l and w_r are the height of the melting peak, the melting peak temperature, the phase change temperature range on the left side and right side of the melting peak, respectively; m_l and m_r are shape parameters for the left and right side of the peak, respectively. The specific heat capacity of concrete is almost the same when the PCM is in solid and in liquid state (**Paper III, V and VI**). To simplify the fitting process, the same value of the specific heat capacity (Cp_o) is therefore used for both the solid and liquid state of PCM.

In addition, the thermal conductivity and specific heat capacity of a homogeneous reference sample (granite rock-Nero Assoluto, Zimbabwe) were determined by using the homemade hot plate system and a TPS2500 hotdisk system (Lund) to evaluate the accuracy of the homemade system compared to the commercial one. The test was performed at room temperature (≈ 20

°C) for the TPS2500 hotdisk system and a temperature range of 15-25 °C for the homemade system. The results are summarized in Table 5. The data shows a good agreement between the results measured by the homemade system and the TPS2500 with approximately 7 % and 10 % relative differences for the specific heat capacity and the thermal conductivity, respectively. In addition, the values are close to the litterature values of the specific heat capacity and thermal conductivity of granite rock (approximately 790 J/kg ºC and 2.68-3.07 W/m ºC [79]). Accordingly, the homemade sytem can be utilized to determine the thermal properties of building materials.

Table 5: Summarization of the specific heat capacity and thermal conductivity of granite rock determined by Homemade system and TPS2500 system **(Paper VI)**.

	Methods			Relative differences (%) $\frac{TPS2500-Homemade}{TPS2500} * 100\%$
	Homemade system	TPS2500	Liturature	
Specific heat capacity (J/Kg ºC)	704±9	755	790	6.7
Thermal conductivity	2.65±0.03	2.93	2.68-3.07	9.6

4.9.3. Thermal diffusivity

Because the thermal conductivity and heat storage capacity (specific heat capacity and latent heat) are inherent capacities of the materials, it is important to reveal their effect on the heat transfer process and on the energy consumption of the heating/cooling system to maintain a constant indoor temperature.

Thermal diffusivity is used to estimate the rate of heat transfer through a material. It also provides a relation between the thermal conductivity and heat storage capacity on the energy performance of building materials. The thermal diffusivity (α) is dependent on the thermal conductivity, the specific heat capacity and the density (ρ) [80]:

$$\alpha(T) = \frac{k_{ave}}{\rho C_p(T)} \quad \text{Eq. 10}$$

Where $k_{ave}=(k_{solid}+k_{liquid})/2$ is the average thermal conductivity. The average is used since there is little difference between the thermal conductivity of samples where is PCM in a solid or liquid state (**Paper III, V and VI**).

4.10. Numerical modelling

It is important to utilize a numerical model to estimate the thermal impact geopolymer concrete containing MPCM in building envelopes. Some numerical methods have been developed to simulate the effect of heat transfer during the solid–liquid phase change. These are the temperature transforming model, the heat source method, the enthalpy method and the heat capacity method [76, 77, 81-84]. One of the most commonly used numerical methods is the heat capacity method [76, 77, 84]. For this method, a good agreement between experimental data and the numerical methods are found. Nevertheless, this method defines the apparent specific heat capacity as a stepwise function of temperature, which exhibits a discontinuity of the specific heat capacity at the start and end of the melting point range, which can produce a mismatch between the model and realistic conditions. Furthermore, most of reports assume that the melting peak is symmetric to define $C_p(T)$ as the piecewise function of temperature [76, 77] or the Gauss function of temperature [78]. However, this assumption shows a mismatch with the experimental curve of $C_p(T)$ of concrete containing microcapsules, which exhibit an asymmetric shape of the melting peak [10, 13, 14, 36].

In the present study, a numerical model was developed to investigate the effect of MPCM addition on the thermal impact of MPCM concrete walls. For this purpose, a simplified and uninsulated concrete wall was utilized. The thermal performance including the indoor surface temperature of the concrete wall, and the power consumption and the power reduction for the heating and cooling system to maintain a constant indoor temperature were numerically calculated.

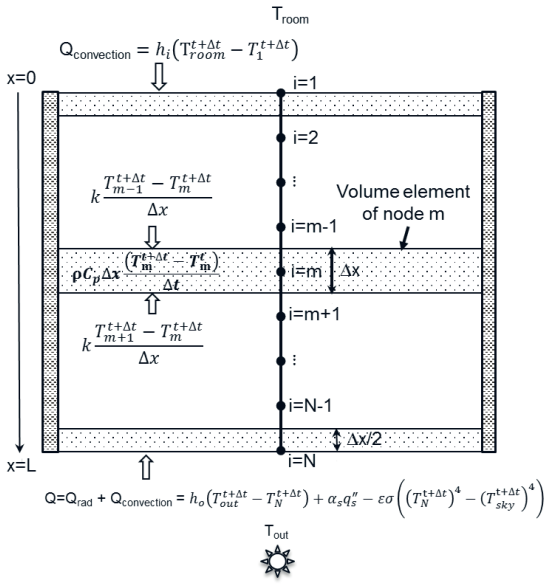

Figure 8. Schematic representation of the MPCM-concrete wall and implicit finite differences method using the energy balance approach with the boundary conditions. The energy balance states that heat transferred into the volume element from all of its surfaces is equal to the change in the energy content of the volume element during Δt [80] **(Paper VI)**.

The model used to investigate the thermal behavior of the concrete wall is shown in Figure 8 including some simplifying assumptions:

- The heat transfer through the wall is a one-dimensional condition.
- The GPC containing microcapsules is homogeneous and isotropic.
- There is no heat generation in the samples.
- The convection effect in the melted PCM and super-cooling effects are neglectable.
- The indoor and outdoor heat transfer coefficients are assumed to be constant and are obtained from the literature.
- The heat from people and devices are neglected.

The mathematical model for one-dimensional heat transfer through the wall is [76, 77, 80]:

$$k\frac{\partial^2 T}{\partial x^2} = \rho C_p(T)\frac{\partial T}{\partial t} \qquad \text{Eq. 11}$$

where k, ρ, x are the thermal conductivity, density, and thickness of the wall, respectively. $C_p(T)$ is the specific heat capacity as a function of the temperature of GPC containing microcapsules, which can be defined by Eq.9.

The implicit finite difference method using the energy balance approach is used to solve the mathematic model and is illustrated in Figure 8 [80]. According to the method, the concrete wall is firstly discretized into a number of nodes (N) with the Δx-distance between two adjacent nodes. Then, the volume elements over the nodes, where energy balance is applied, are formed to determine the temperatures at all nodes of the sample.

In order to solve Eq. 11, the convective heat transfer was imposed at the indoor wall surface while the combined convective and radiative heat transfer was imposed at the outdoor wall surface. The boundary conditions were shown in Eq. 12 and Eq. 13 as below:

- Interior node i=1 (x=0, boundary condition on indoor wall surface) [80]:

$$k\frac{\partial T}{\partial x}(x,t) + h_i\big(T(room,t) - \mathrm{T(x,t)}\big) = \rho C_p(T)\frac{\Delta x}{2}\frac{\partial T}{\partial t}(x,t) \quad \text{Eq. 12}$$

- Exterior node i=N (x=L, boundary condition on outdoor wall surface) [77, 78, 80, 85]:

$$k\frac{\partial T}{\partial x}(x,t) + h_o\big(T(out,t) - \mathrm{T(x,t)}\big) + \alpha_s q_s'' - \varepsilon\sigma\big((T_N^{\mathrm{t}})^4 - (T_{sky}^{\mathrm{t}})^4\big) = \rho C_p(T)\frac{\Delta x}{2}\frac{\partial T}{\partial t}(x,t) \quad \text{Eq. 13}$$

For the simulation, a time step Δt=60 s and a distance step Δx=0.005 m were selected for all cases in the current simulation. The initial temperature of the system was set to 23 ºC. h_i and h_o represent the indoor heat transfer coefficient and the outdoor heat transfer coefficient, respectively. The heat transfer coefficient depends on the surface orientation, the direction of the heat flow and the velocity of the heat flow [86]. To simplify the complex determination, the heat transfer coefficient values were selected from the literature. The indoor heat transfer coefficient h_i was set to 8 W/m^2 K while the outdoor heat transfer coefficient h_o was set to 20 W/m^2 K. These values are similar to the values recommended by ASHRAE [86], and has been utilized for similar calculations previously [77, 87, 88].

T_{out}, T_{sky} and T_N represent the outdoor temperature, the average sky temperature and the outdoor wall surface temperature (x=L), σ is the Stefan–Boltzmann constant, α_s and ε are the total absorptivity and emissivity of the outdoor wall surface, respectively [77, 89]. The total hemispherical solar absorptivity and surface emissivity of the outdoor wall surface were 0.65 and 0.87, respectively [89]. An average sky temperature $T_{sky} = (T_{out}-12)$ ºC was used [88, 90]

Finally, MATLAB (Mathworks Inc., Natick, MA, USA) was employed to solve Eq.11 to Eq.13 for all nodes. Relevant output data including the temperature across the thickness of the concrete samples, and the heat flux on the indoor surface (φ_{indoor}) were collected:

$$\varphi_{indoor}(\mathrm{t}) = h_i(T_{room}^t - T_1^t) \quad \text{Eq. 14}$$

Accordingly, the power required for a heating/cooling system to keep the indoor temperature stable was determined from Eq.15 while the power reduction Pr was calculated from Eq.16.

$$P = \frac{\int_0^{24h} |\varphi_{indoor}| dt}{3600 \cdot 10^3} \quad \text{Eq. 15}$$

Where φ_{indoor} is the heat flux on the indoor side of the sample.

The power reduction Pr is defined as:

$$Pr = \frac{P_{GPC} - P_{MPCM-GPC}}{P_{GPC}} \cdot 100\% \quad \text{Eq. 16}$$

Where P_{GPC} and $P_{MPCM\text{-}GPC}$ are the power consumption of the heating and cooling system working one day for geopolymer concrete without MPCM and with MPCM respectively.

- **MPCM concentration**

The MPCM concentration was varied to evaluate effect on the thermal performance of concrete. The simulation conditions were selected to reflect the real experimental conditions of MPCM-concrete. Accordingly, three MPCM concentrations of 0, 2.6 and 5.2 wt.% MPCM per solid of content concrete were selected. The concentration of MPCM was limited to 5.2 wt.% since higher concentrations of MPCM resulted in too low workability of the concrete.

- **Concrete thickness**

The thickness of the concrete wall affects the heat transfer process, and is therefore important for the thermal performance of buildings. The thickness of the concrete walls was varied from 5 to 20 cm to investigate the effect on the thermal performance.

- **Solar radiation**

The time dependent solar radiation heat flux q''_s which mimics maximum solar radiation conditions during summer time (July) of the city of Madrid, Spain [91] was utilized:

$$q_s'' = \begin{cases} 0 & for\ 21{:}00 \le t \le 5{:}00 \\ q''_{s,max} \sin\left(\frac{\pi}{57600} t - \frac{5\pi}{16}\right) & for\ 5{:}00 < t < 21{:}00 \end{cases} \quad \text{Eq. 17}$$

where $q''_{s,max}$ is the maximum daily solar radiation heat flux. In this article, the maximum daily solar radiation heat flux was varied from 0-1000 W/m^2 in steps of 250 W/m^2 to cover European

conditions during summer time. The maximum daily solar heat flux was assumed to occur at 13:00 [91].

- **Outdoor temperature**

To mimic outdoor conditions, the ambient outdoor temperature T_{out} was imposed as a sinusoidal function of time as:

$$T_{out}(t) = \frac{T_{max}+T_{min}}{2} + \frac{T_{max}-T_{min}}{2}\sin(\frac{\pi}{43200}t - \frac{2\pi}{3}) \quad \text{Eq. 18}$$

where T_{max} and T_{min} are the maximum and minimum outdoor temperatures during a day, respectively. The maximum outdoor temperature T_{max} were set at 14:00. The efficiency of MPCM addition on the thermal performance of concrete buildings is strongly dependent on the interplay between the phase change temperature and the outdoor temperature. Therefore, the outdoor temperature conditions were varied to evaluate the optimal temperature conditions for the MPCM utilized in this study. An outdoor temperature variation of $(T_{max}-T_{min})/2$ = 5, 7.5 and 10 ºC were utilized, and the average outdoor temperatures $(T_{max}+T_{min})/2$ was varied from 0 ºC to 40 ºC.

- **Evaluation of building envelopes using geopolymer concrete containing MPCM as single wall in European city conditions**

The possibility of utilizing the geopolymer concrete containing MPCM as the simple single wall for a single family home in Oslo climate zones and Madrid climate zone were evaluated. The outdoor temperature and solar radiation as function of time for a typical year in Oslo and Madrid used in Equation (13) were obtained from weather data (Climate Consultant software) [92]. The effect of wall orientation (South, East, North and West facing walls) and the season during a typical year on power consumption and power reduction were evaluated. GPC without MPCM and GPC containing 5.2 wt.% of PS-DVB/RT27 and MF/PCM24 were selected for the evaluation.

4.11. Experimental validation of numerical models

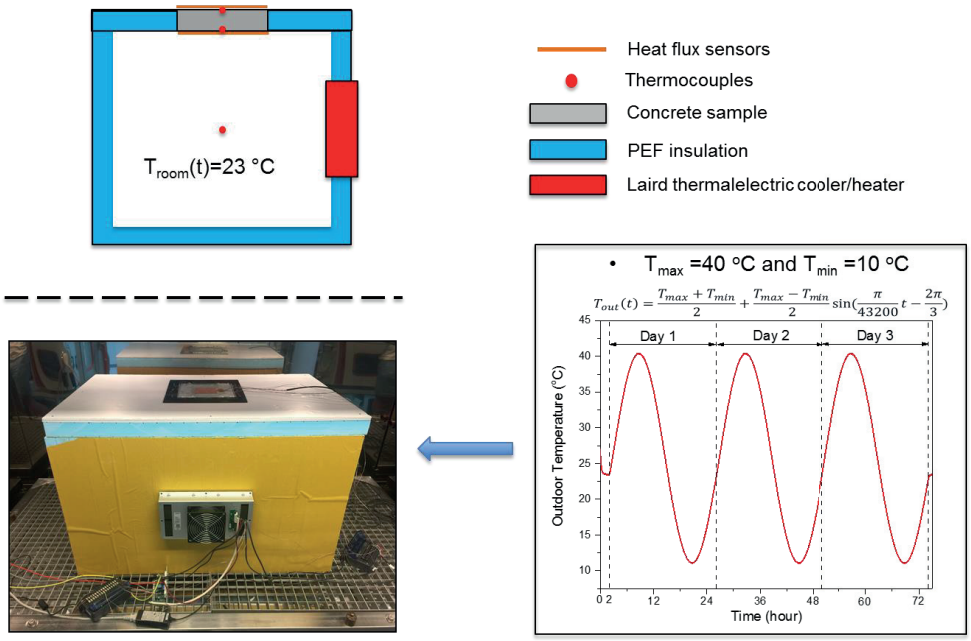

Figure 9. The thermal performance testing system with sketch of cross-section of the system and the simulated outdoor temperature profile **(Paper V)**.

Figure 9 shows the thermal testing system, which was utilized to investigate the thermal impact of geopolymer concrete containing microcapsules and to verify the numerical model. A small test box with inner dimensions of 60 × 80 × 60 cm was made of 5 cm panels of polyethylene expanded foam (PEF) (Figure 9) and was placed inside an environmental chamber to model outdoor temperature fluctuations. The concrete sample was placed in a rectangular opening (20 × 20 cm) in the middle of the top insulation panel.

For the test, the small test box was exposed to a daily sinusoidal temperature oscillation $T_{out}(t)$ (Eq.18) using an environmental chamber (VT³ 4250, Vötsch, Germany) while the temperature inside the test box (T_{room}) was kept constant at 23 °C by a temperature regulator (AA150-Laird Technologies). For verifying purpose, T_{max}=40 ºC and T_{min} =10 ºC were set as the maximum and minimum outdoor temperatures during one day, respectively. The maximum outdoor temperature T_{max} were set at 14:00. In order to simplify the thermal system, the effect of solar radiation is not considered. At the initial stage, both the indoor temperature (T_{room}) and outdoor temperature (T_{out}) were set at 23 ºC for 2 hours to reach a steady-state condition. Afterwards, the outdoor temperature cycles (Eq.18) were run continuously for 72 hours.

The thermocouples were installed at different depths of the concrete wall in steps of 2.5 cm to measure the temperature across the samples. The heat flux sensors were installed on both surfaces of the concrete sample to measure the heat fluxes on both surfaces of the sample. Thermocouples were also placed at different positions in both the test room and the environmental chamber to record the indoor temperature and the outdoor temperature. All data were recorded every 60 s using a multichannel multimeter (LR8410-20 Hioki, Japan).

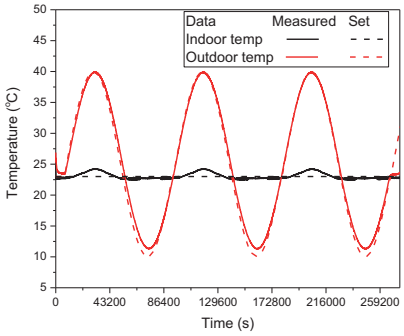

Figure 10. The setting temperature and measured temperature of the indoor and outdoor temperatures **(Paper VI)**.

The outdoor and indoor temperatures during the experiments were recorded and are shown in Figure 10. There is the slight mismatch between the setting temperature (Eq.18) and the mean collected temperature for both the outdoor and indoor temperature. This is more pronounced for the indoor temperature, which is probably due to the limits of the heating/cooling capacity of the temperature regulator. Therefore, the real experimental data collected using the calibrated thermal couples was utilized as input temperature data for the numerical calculation to improve the reality and accuracy of the method.

MPCM concentrations were selected at 0, 2.6 and 5.2 wt.% of the total solid of concrete to evaluate effect of MPCM concentration on the thermal performance of MPCM concrete while the thickness of 2.5, 5 and 7.5 cm were utilized for validation process. More information can be found in **Paper VI**.

Finally, some important parameters for numerical model were selected based on the experimental conditions. Both heat transfer coefficient h_i and h_o were considered to have the same value of 8 W/m^2 K for the horizontal wall to fit well to experimental conditions. This is similar to the recommended values of ASHRAE [86] and has been utilized for similar

calculations previously [77, 87, 88]. Furthermore, the effect of radiation was neglected giving $\alpha_s q_s'' - \varepsilon\sigma\left(\left(T_N^{t+\Delta t}\right)^4 - (T_{sky}^{t+\Delta t})^4\right) = 0$.

5. Results and Discussions

5.1. Rheological properties of MPCM suspensions

In **Paper I and II**, the rheological behavior of MPCM suspensions were investigated utilizing the LDPE-EVA/RT27 microcapsules. It was found that non-encapsulated phase change materials play an important role regarding the properties of the suspensions.

Figure 11 shows the influence of temperature and shear rate on the viscosity of 20 wt.% microcapsule suspensions (LDPE-EVA/RT27 in glycerol). The viscosity below the melting point of the paraffin core material (< 27 °C) exhibits a clear Newtonian region at low shear rates (10 – 100 s^{-1}) followed by a power law region at high shear rates. However, above the melting point of paraffin, the Newtonian region is not reached within the considered shear rate range, and only the power law region is observed. The non-encapsulated paraffin (insert in Figure 11) is probably causing this temperature dependent effect. Non-encapsulated paraffin can contribute to the agglomeration of the microcapsules. When the sample is heated, paraffin becomes softer, and the associative forces within the agglomerates are reduced. Accordingly, less force is needed to break the agglomerates apart (Figure 12). After the paraffin has melted, the agglomerates are easily disrupted and can be broken apart even at low shear rates, which is why no Newtonian plateau is observed at high temperatures.

In addition, the microencapsulated phase change materials (MPCM) suspensions were subjected to various constant shear force at 20 ºC for 30 min in order to investigate the effect of steady shear on the structural breakdown of MPCM (**Paper II).** The applied shear force has a significant impact on breaking down the agglomerated microcapsules to smaller sizes during the initial stage. However, at longer times, the agglomerates become smaller, and the shear forces do not have any significant effect on the overall size of the agglomerates (Figure 13). Furthermore, the breakdown of the agglomerated structures is most pronounced at high shear rates where the microcapsules are subjected to stronger disruptive forces while there is a stronger breakdown of the agglomerated structures when the concentration is raised. (Figure 5, **Paper II**).

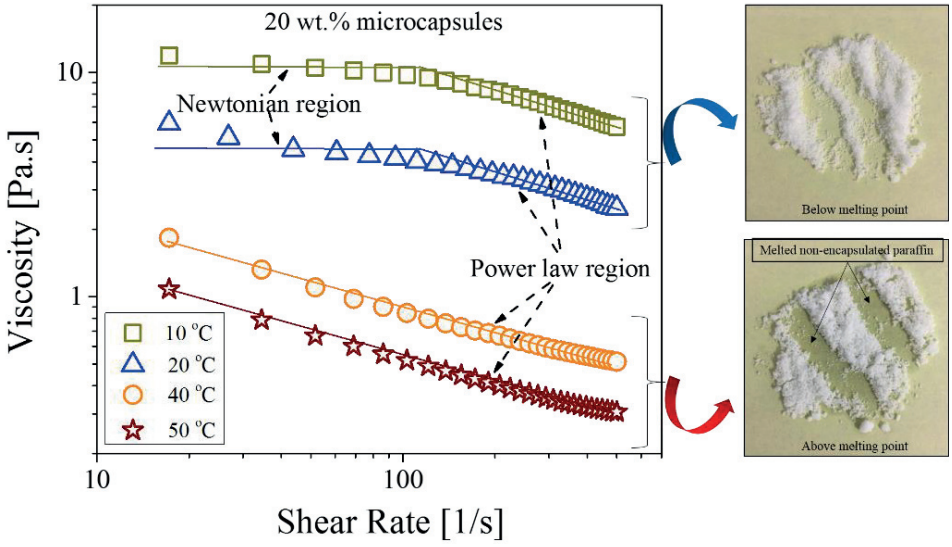

Figure 11. The effect of temperature and shear rate on the viscosity of 20 wt.% MPCM suspensions. The inserted images show an absorbing paper with microcapsules before heating to 40 °C and after heating to 40 °C for 10 min.

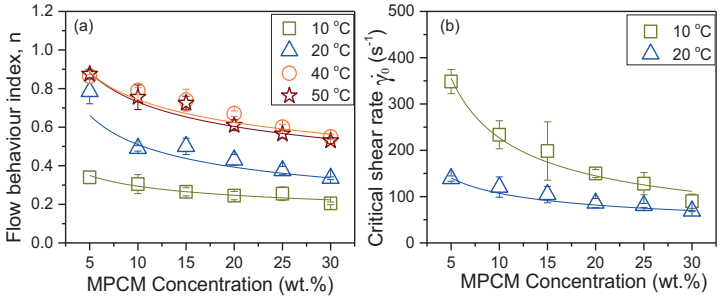

Figure 12. (a) The flow behavior index n and (b) the critical shear rate $\dot{\gamma}_o$ from power law and Cross models as a function of MPCM concentration and temperature **(Paper I)**.

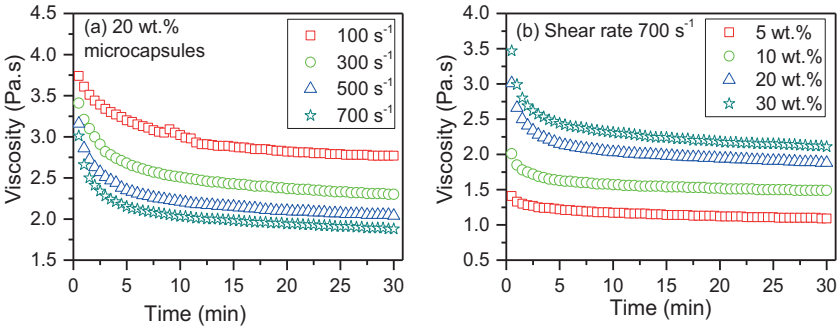

Figure 13. Viscosity at (a) different shear rates, MPCM concentration 20 wt.%, and (b) different concentration, shear rate 700 s^{-1} as a function of shearing time at 20 °C **(Paper II)**.

The results from **Paper I and II** demonstrate that LDPE-EVA/RT27 has a significant amount of non-encapsulated PCM, which cause agglomeration of the microcapsules. Free PCM can also interact with the cement matrix, especially at temperatures above the melting point of PCM. It is therefore important to avoid utilizing MPCM containing significant amounts of non-encapsulated PCM.

5.2. Comparison of Portland cement concrete and geopolymer concrete

The integration of microencapsulated phase change materials to geopolymer concrete (MPCM-GPC) is a promising method to produce not only high energy storage materials but also green building materials. It is interesting to compare Portland cement concrete (PCC) containing MPCM as reference materials for MPCM-GPC to evaluate the effect of MPCM on both types of concrete.

Figure 14a presents the average thermal conductivity of concrete containing LDPE-EVA/RT27. There is a clear reduction of the thermal conductivity when the concentration of microcapsules is increased. This can be explained by the lower thermal conductivity of the microcapsules compared to the sand it replaces. The thermal conductivity of paraffin Rubitherm®RT27 (0.2 W/m ºC [93]) and the LDPE-EVA shell (0.14-0.34 W/m ºC [93]) are approximately ten times lower than the average thermal conductivity of sand (1.80-2.50 W/m ºC) [10]. Additionally, the increased porosity (Figure 14b) and the poor interface between microcapsules and the concrete

matrix due to air gaps (Figure 19) will contribute to the decline in the thermal conductivity of MPCM-concrete.

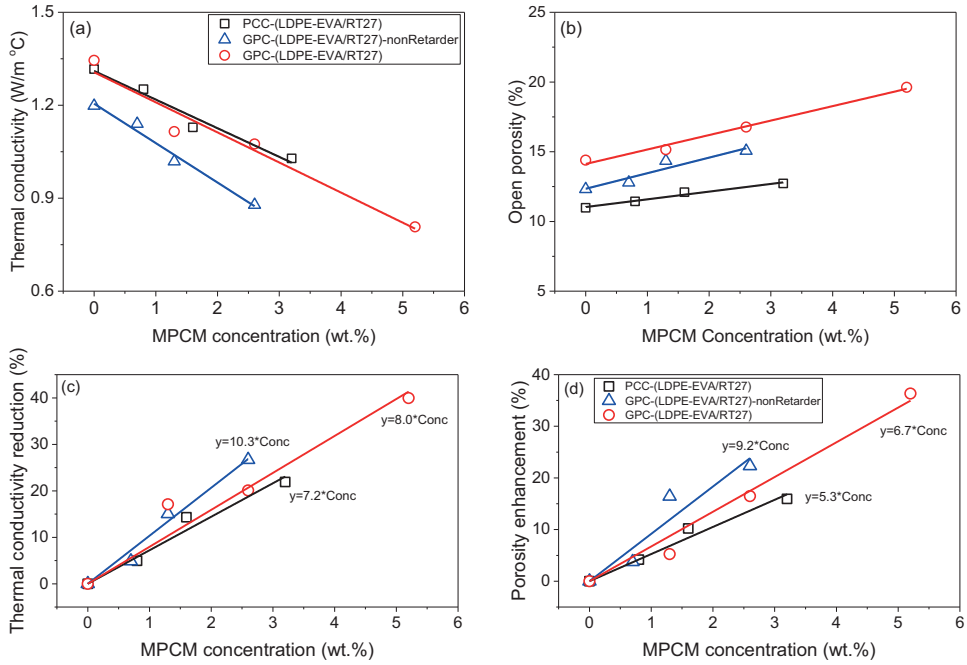

Figure 14. (a) The thermal conductivity, (b) the open porosity, (c) the thermal conductivity reduction and (d) the porosity enhancement of GPC and PCC as a function of MPCM concentration.

Comparing PCC and GPC, the reduction rate of thermal conductivity of PCC is slightly lower than for both types of GPC (Figure 14c). The slightly different MPCM concentration dependencies of GPC and PCC might be related to the corresponding change in porosity (Figure 14d). According to Figure 14d, the porosity enhancement of GPC increases at a higher rate than that of PCC when the concentration of MPCM is raised. The reason for this is unclear, as several effects may come into play. The effect of MPCM on the particle packing density might be different between GPC and PCC due to the different binders. The compatibility between the microcapsule shell and the binder is not necessarily the same for the two systems. It is also possible that the higher workability and shorter setting time of GPC compared to PCC could increase the probability of forming entrapped air voids during the mixing and pouring process. Interestingly, after MPCM addition, GPC with retarder has lower porosity increase rate than

without retarder. A possible explanation is that the better workability and longer setting times of geopolymer concrete after adding retarder increases the possibility to wet the surface of MPCM and remove the air.

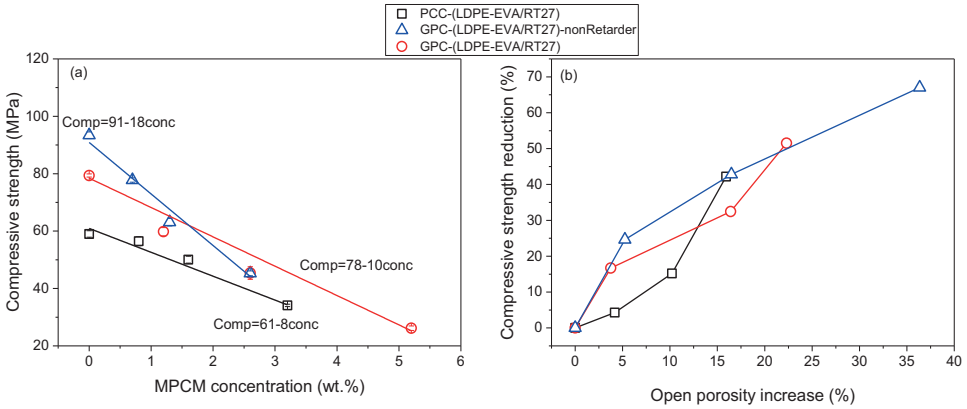

Figure 15. (a) Compressive strength of Portland cement concrete and geopolymer concrete containing MPCM and (b) their compressive strength reduction as function of open porosity increase.

The compressive strength (Figure 15a) shows that increasing the amount of MPCM reduces the compressive strength. This is probably because MPCM has a low mechanical strength and stiffness and can be easily broken under compressive force [26, 27, 93]. Furthermore, the higher porosity after adding MPCM can contribute to the reduction of the compressive strength. The compressive strength reduction rate of concrete containing microcapsules follows the order of PCC (8.3±0.7) <GPC with retarder (10.2±0.7) <GPC without retarder (18.0±1.5). This is consistent with the rate of the porosity enhancement (PCC<GPC with retarder<GPC without retarder). Specially, after adding the retarder, the compressive strength reduction rate of GPC decreases significantly from 18.0±1.5 (without retarder) to 10.2±0.7 (with retarder). Accordingly, more MPCM can be added to the sample with the retarder (2.6 wt.% without retarder can be raised to 5.2 wt.% with retarder). This will not just increase the heat storage capacity of GPC, but also results in compressive strengths that satisfy the demand for structural applications (EN 206-1, compressive strength class C20/25).

In order to examine the relationship between the compressive strength and the porosities, the compressive strength reduction is plotted as a function of the open porosity increase in Figure 15b. It is obvious that for all three samples the compressive strength is reduced when the

porosity becomes higher. The GPC with and without retarder mostly follow the same curve, confirming that the open porosity is the main influence on the changing the compressive strength (the one deviating point might be within the experimental errors of the open porosities). For PCC the open porosity increase has less effect on the compressive strength at low open porosities. However, for the last point the values are similar to that of GPC. The differences might be due to the lower absolute values of the PCC porosities (Figure 14b).

The investigation revealed that the microcapsules have significant effect on thermal and mechanical properties of concrete. Microcapsules were found to have a stronger effect on GPC than on PCC causing a higher thermal conductivity reduction rate and compressive strength reduction rate. In addition, the retarder plays an important role on reducing the negative effect of MPCM addition on the compressive strength of GPC, due to the better workability and longer setting time of GPC after adding retarder.

5.3. Effect of the properties of microcapsulated phase change materials on geopolymer concrete

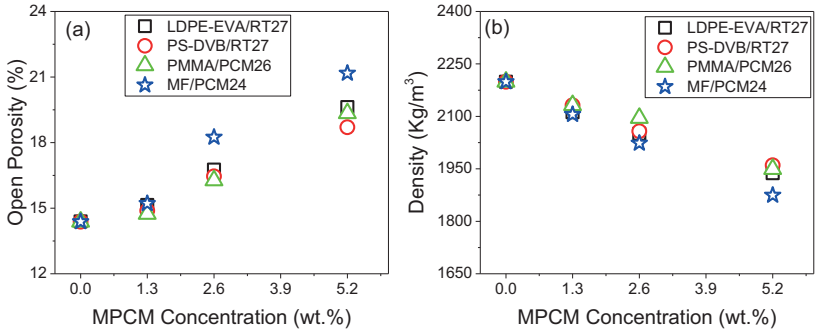

Figure 16. (a) Open porosity and (b) density of GPC containing different kinds of MPCM as a function of MPCM concentration.

The MPCM-GPC density and open porosity as a function of MPCM concentration are shown in Figure 16. The addition of microcapsules can affect the porosity of the geopolymer concrete in several ways. For the same volume, the total surface area of small particles is much higher than for larger particles. Accordingly, more binder paste adsorbs to the surface of small particles. This results in poorer workability, causing more voids between the particles (aggregates and microcapsules) and more trapped air. This is counteracted by the cavity filling effect [94-96]. The cavities between aggregates and sand can be filled up by small particles (≤

125 μm) [96] causing an increased packing density, thereby reducing the porosity of the concrete. The single microcapsules have a small size in the range of 1-100 μm (Figure 17). However, the effective size is larger due to agglomeration. The agglomerates of PS-DVB/RT27, PMMA/PCM26 and LDPE-EVA/RT27 are too large to fill in the cavities in the concrete structure [26, 97-99]. Only MF/PCM24 with a much smaller size distribution can fill up the cavities and thereby reduce the porosity. The properties of the polymer shell can also affect the porosity. As illustrated in Figure 18, PS-DVB/RT27 and LDPE-EVA/RT27 have little interaction with water. Accordingly, air gaps can be formed between the microcapsules and the geopolymer paste during the mixing process [10, 100, 101]. Although LDPE-EVA/RT27 contains some polar functional groups (ester groups), it is possible that the polarity of these functional groups on the copolymer LDPE-EVA shell are hindered or weakened by the long nonpolar hydrocarbon skeleton of LDPE. Furthermore, the non-encapsulated paraffin on the LDPE-EVA/RT27 surface can also contribute to non-polarity of these microcapsules. PMMA/PCM26 and MF/PCM24 have shells containing polar functional groups (Figure 18), providing better interaction with the aqueous alkaline environment. This results in better interface bonds between the microcapsules and the geopolymer paste, thereby reducing the air gaps between MPCM and geopolymer paste. The polar functional groups on the polymer shell also helps to disperse the microcapsules into the concrete matrix better than a hydrophobic shell. This is evident in the SEM images (Figure 19), which show obvious gaps between the concrete matrix and microcapsules (PS-DVB/RT27 and LDPE-EVA/RT27), while the polymers with polar functional groups exhibit almost no air gaps (PMMA/PCM26) or very small air gaps (MF/PCM24). However, the drawback of polar functional groups on the polymer shell is the poorer workability (Figure 23) since more water can be trapped on the surface of the particles (Figure 18). The porosity of the concrete will be governed by a combination of these effects.

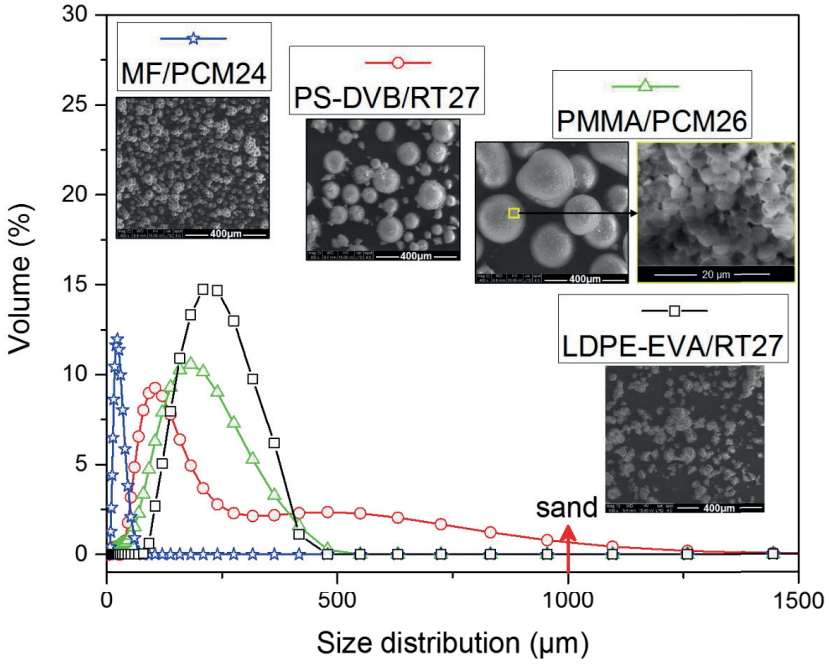

Figure 17. The size (diameter) distribution of the LDPE-EVA/RT27, PS-DVB/RT27, PMMA/PCM26, MF/PCM24 microcapsules (including aggregates) together with SEM images of the microcapsules.

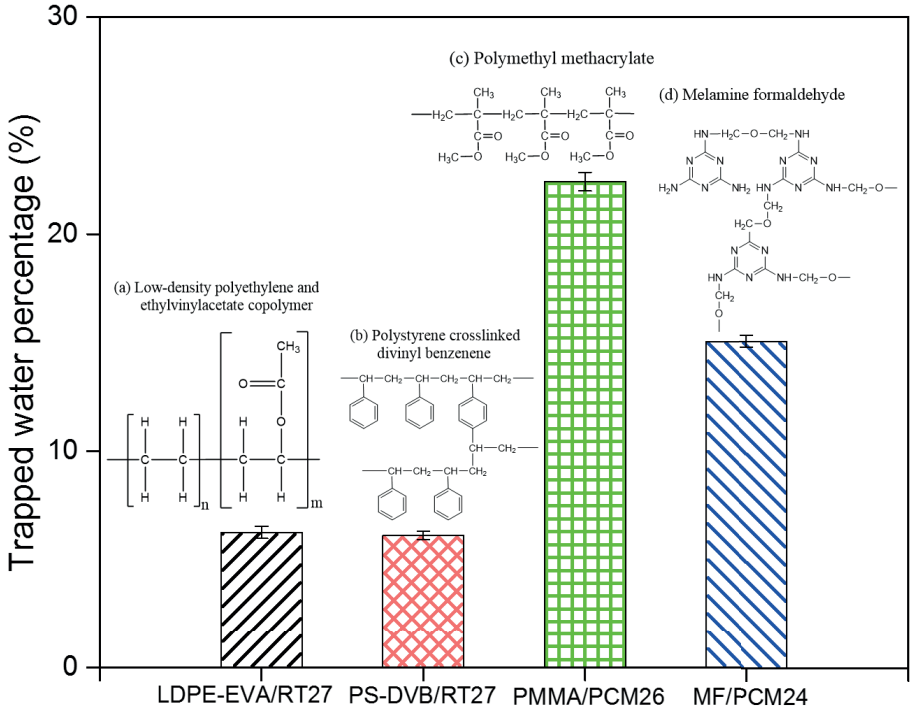

Figure 18. The effect of polymer shell structure on the trapped water of the microcapsules. The inserted images shows the chemical structure of (a) low density polyethylene and ethylvinylacetate copolymer (LDPE-EVA), (b) polystyrene crosslinked divinyl benzene (PS-DVB), (c) polymethyl methacrylate (PMMA) and (d) melamine formaldehyde (MF).

As can be seen from Figure 16a, the open porosity increases with microcapsule concentration. This can be explained by the smaller size of the microcapsule agglomerates compared to sand (Figure 17), causing a larger surface area that adsorbs more binder paste to the surface. The size of sand is approximately 4-5 times larger than for the PS-DVB/RT27, PMMA/PCM26 and LDPE-EVA/RT27 agglomerates and 30 times larger than MF/PCM24. When the concentration of MPCM is raised, the porosity of GPC with MF/PCM24 increases at a higher rate than PS-DVB/RT27, PMMA/PCM26 and LDPE-EVA/RT27. This is probably due to a combination of the small size and the polar functional groups on the microcapsule shell, which causes MF/PCM24 to adsorb more binder paste. This is in agreement with the X-ray micro-tomography data (Figure 20), which show that the amount of air bubbles present in GPC containing MF/PCM24 is higher than for the other samples.

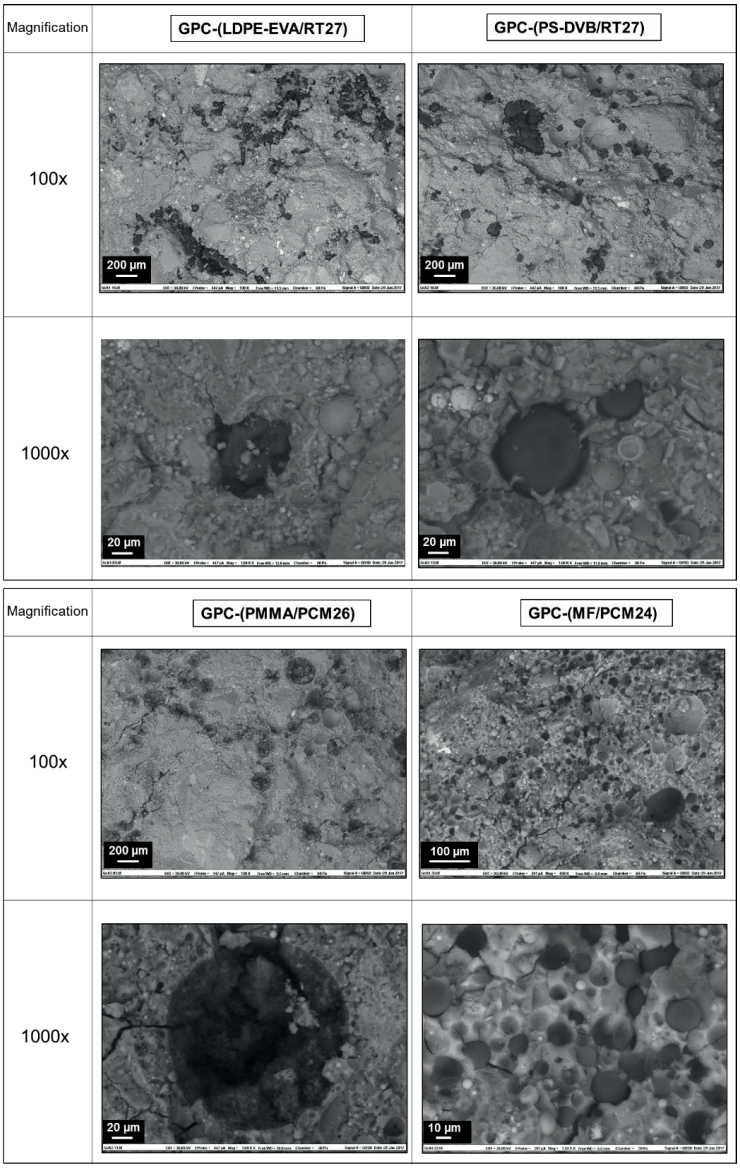

Figure 19. SEM images of GPC containing 2.6 wt.% of (a) LDPE-EVA/RT27, (b) PS-DVB/RT27, (c) PMMA/PCM26 and (d) MF/PCM24.

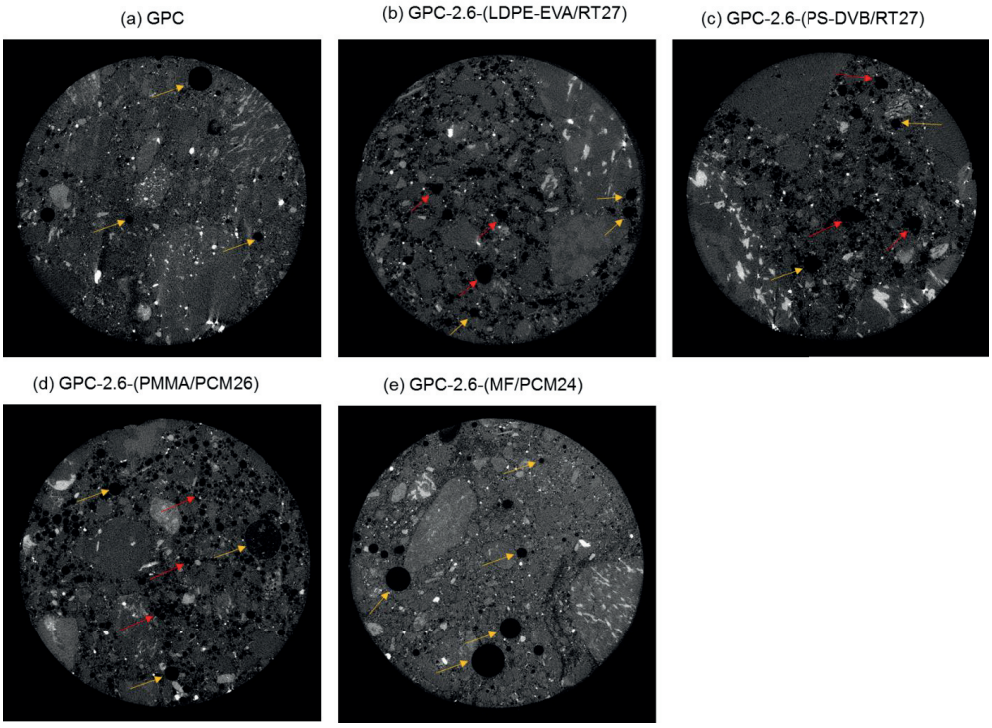

Figure 20. X-ray-tomography images of (a) GPC without MPCM, (b) GPC containing 2.6 wt.% PS-DVB/RT27, (c) GPC containing 2.6 wt.% PMMA/PCM26 and (d) GPC containing 2.6 wt.% MF/PCM24. The air bubbles and microcapsules are shown as dark colors due to low or no absorption of X-rays while bright colors represent sand and gravel, which can adsorb high amounts of X-rays. The yellow arrows point the air bubbles (spherical shape) and the red arrows indicate the microcapsules (irregular shape) [102]. The field of view is 1 cm.

The average thermal conductivity of GPC containing MPCM (MPCM-GPC) is summarized in Figure 21. There is a clear reduction of the thermal conductivity of MPCM-GPC when the amount of microcapsules is increased. It is believed that the lower thermal conductivity of the microcapsules compared to that of replaced sand, the enhancement of porosity (Figure 16a) and the poor interface between microcapsules and concrete matrix (Figure 19) are the main reasons for the decline in thermal conductivity. The reduction rates of the thermal conductivity of GPC after mixing with different kinds of microcapsules are slightly different, with reduction rates of 0.090±0.004, 0.095±0.012, 0.113±0.009 and 0.097±0.015 for GPC containing PS-DVB/RT27, PMMA/PCM26, MF/PCM24 and LDPE-EVA/RT27, respectively. Since air pores will reduce the thermal conductivity, the slightly different reduction rates are probably mostly due to the

change in porosity (Figure 16). Furthermore, the smaller size and better distribution of MF/PCM24 compared to PS-DVB/RT27, PMMA/PCM26 and LDPE-EVA/RT27 might contribute to this effect (Figure 19 and Figure 20). A better distribution of microcapsules in the concrete matrix can increase the MPCM thermal pathway through concrete matrix thereby facilitating lower thermal conductivity. The thermal conductivity of each microcapsule might also play a role, but unfortunately, the thermal conductivity of the considered microcapsules is unknown.

Figure 21b summarizes the latent heat of GPC as a function of microcapsule concentration within the temperature range of 10-35 ºC. The latent heat of concrete increases linearly when the microcapsule concentration is raised. MF/PCM24 increases fastest, with a slope of 0.93±0.03, while the lower slopes of PS-DVB/RT27 (0.70±0.02), PMMA/PCM26 (0.73±0.02) and LDPE-EVA/RT27 (0.69±0.03) are similar to each other. Several effects may cause γ to become lower than 1. A higher porosity of the concrete matrix might reduce the slope (Figure 9, **paper III**). However, this cannot explain the current results as MF/PCM24 exhibits the highest increase in open porosity (Figure 16) and the largest slope. A possible reason for this discrepancy is that the gaps between the particles and the GPC matrix play an important role. MF/PCM24 exhibits very little gaps between the microcapsules and the GPC matrix, which will improve the heat transfer to the particles and increase slope. In addition, MF/PCM24 is well dispersed as single, small microcapsules while PS-DVB/RT27, PMMA/PCM26 and LDPE-EVA/RT27 exist as agglomerates of approximately the same size as each other (Figure 19). Agglomerated structures can impede the heat transfer to the single microcapsules, thereby reducing slope.

The integration of microencapsulated phase change materials (MPCM) into geopolymer concrete (GPC) was found to improve the thermal energy storage capacity, reduce the thermal conductivity and decrease the density, resulting in an enhancement of the energy efficiency. MF/PCM24 with a polymer shell containing polar functional groups, the highest core/shell ratio (9:1) and the smallest size (10-100 μm) exhibited the largest increase of GPC porosity, lowest thermal conductivity, highest heat storage capacity, better interface bonds between microcapsules and the concrete matrix, and a more uniform dispersion in the concrete matrix compared to other microcapsules. Accordingly, MF/PCM24 exhibits the best thermal performance with the highest reduction of the energy consumption, both from experimental measurements (Figure 12, **paper V**) and from numerical calculations (**paper VI** and **paper VII**).

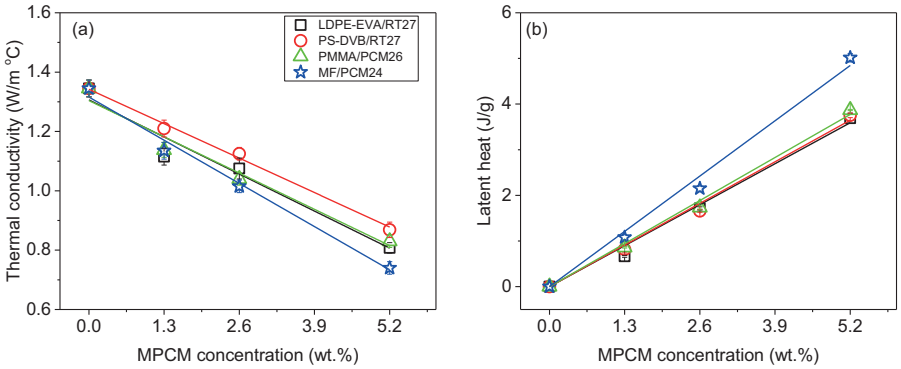

Figure 21. (a) Thermal conductivity and (b) latent heat of GPC containing different kinds of MPCM

Figure 22 presents the compressive strength of GPC containing microcapsules at 20 ºC (below the microcapsule melting point) and 40 ºC (above the microcapsule melting point) as a function of microcapsule concentration. The compressive strength of GPC declines significantly when the concentration of microcapsules increases for both states of PCM.

The compressive strength of GPC containing microcapsules follows the order of MF/PCM24<LDPE-EVA/RT27<PMMA/PCM26<PS-DVB/RT27. This trend is more obvious at high microcapsule concentrations (≥2.6 wt.%). The compressive strength of concrete will be lower when there are the more air voids (porosity) [10, 26], softer particles [102] and poorer dispersion of particles in the concrete matrix [103, 104]. Air gaps between microcapsules and concrete indicates poor interfacial bonds, which can result in a lower compressive strength [10, 26, 102]. Combination of these factors plays an important role regarding the effect of microcapsules on the compressive strength of geopolymer concrete. At high microcapsule concentrations, MF/PCM24 has a significantly lower compressive strength than the other samples even when the PCM is in a solid state. This might be due to the higher amounts of air bubbles in this sample and the higher core/shell ratio of MF/PCM24 that may result in softer particles. Although LDPE-EVA/RT27, PS-DVB/RT27 and PMMA/PCM26 have the similar porosity and size distribution in GPC, the lower compressive strength of GPC containing LDPE-EVA/RT27 compared to GPC containing PS-DVB/RT27 and PMMA/PCM26 can be explained by the poorer interface bonding (Figure 19) and the existence of non-encapsulated PCM in LDPE-EVA/RT27 agglomerate structure (Figure 4 and Figure 11).

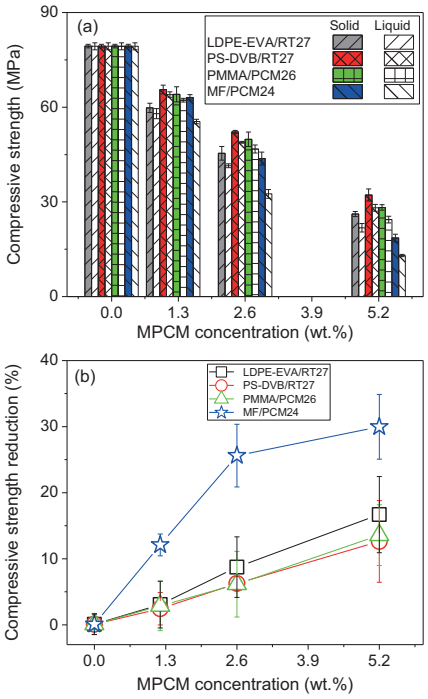

Figure 22. (a) The compressive strength of GPC containing microcapsules below (20 ºC) and above (40 ºC) the melting range of PCM and (b) the compressive strength reduction between the solid and liquid state of PCM.

Figure 22a shows that the compressive strength of GPC containing microcapsules with PCM in a solid state is higher than when PCM is in a liquid state. This might be due to an increase of the internal stress of the microcapsules at elevated temperatures (due to thermal expansion). It is also possible that the microcapsules become softer when they have a liquid core. Figure 22b shows the percentage reduction of the compressive strength of GPC containing microcapsules when PCM is changed from a solid to liquid state. The percentage reduction increases when the amount of microcapsules increases, confirming that the microcapsules are the cause of the decline in compressive strength. Furthermore, melting of the PCM affects the microcapsules as the orders of PS-DVB/RT27≈PMMA/PCM26<LDPE-EVA/RT27<MF/PCM24. This might be due to the higher paraffin core/polymer shell ratio of MF/PC24 compared to PS-DVB/RT27, PMMA/PCM26 and LDPE-EVA/RT27 (Table 1). In addition, the closer interface (lack of air gaps) between MF/PCM24 and concrete matrix facilitates better transfer of the compressive

force to the microcapsules, and makes the concrete more sensitive to a possible thermal expansion of the microcapsules. However, PMMA/PCM26 also has a good interface with the concrete matrix. PMMA/PCM26 exists as agglomerates, which can contain voids between the microcapsules. Accordingly, there will be less stress on the microcapsules during compression and when they expand. For LDPE-EVA/RT27, it is possible that non-encapsulated PCM will have a greater effect on the concrete structure when it is melted. MPCM agglomerates are probably held together by non-encapsulated PCM. When the PCM is melted the agglomerates are easily broken apart, which might weaken the concrete structure.

The compressive strength at 5.2 wt.% MPCM is 32 ± 2 MPa (solid state) and 28 ± 1 MPa (liquid sate) for PS-DVB/RT27, 26 ± 1 MPa (solid state) and 21 ± 1 MPa (liquid state) for LDPE-EVA/RT27 while the corresponding values for PMMA/PCM26 is 28 ± 1 MPa (solid state) and 24 ± 1 MPa (liquid state). Accordingly, the integration of PS-DVB/RT27 and PMMA/PCM26 into GPC at 5.2 wt.% satisfy the mechanical European regulation (EN 206-1, compressive strength class C20/25) for concrete for building construction, except for LDPE-EVA/RT27 at liquid state of PCM. Unfortunately, while 5.2 wt.% of MF/PCM24 shows the best thermal performance, its compressive strength is only 19 ± 1 MPa (solid state) and 13.0 ± 0.4 MPa (liquid state), which does not satisfy the European regulation for compressive strength. Therefore, further investigations to improve the mechanical strength to satisfy the mechanical regulation is needed in order to utilize MF/PCM24 as a thermoregulation component in geopolymer concrete for building applications.

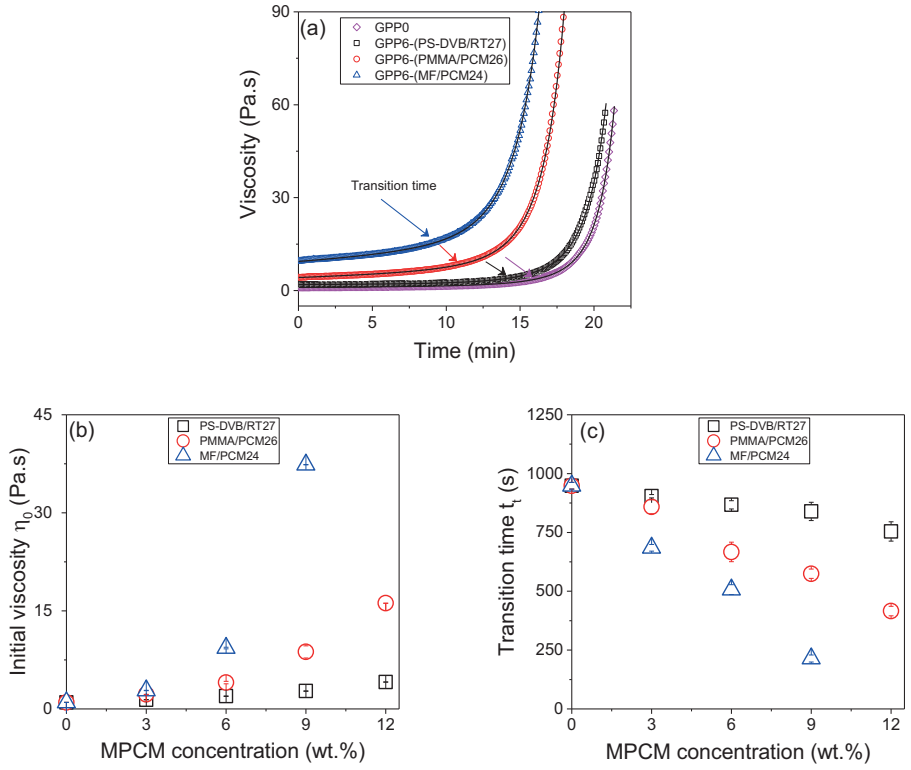

Figure 23. (a) The viscosity of geopolymer paste without MPCM and at 6 wt.% of MPCM as function of time at 20 ºC. Measured at a shear rate of 10 s^{-1}. The symbols are experimental values (every 5th point shown). The lines are fitted by to Eq.5. (b) Initial viscosity, η_0, (c) transition time t_t, of the geopolymer paste as a function of microcapsule concentration obtained by fitting by Eq.5. MF/PCM24 could not be measured at the highest concentration due to a too fast reaction rate.

In order to gain additional information regarding how the different microcapsules affect the properties of the pre-set geopolymer, rheological measurements were conducted on geopolymer paste. Figure 23a shows that the samples exhibit a slow increase in the viscosity at short times (stage 1 in Figure 3), followed by a much steeper raise at longer times (stage 2 in Figure 3). Figure 23b illustrates that an increase in the microcapsule concentration causes a higher initial viscosity (η_0). This is probably due to an increase of the total surface area of the particles in geopolymer paste after adding microcapsules, causing them to adsorb more water (Figure 18). In addition, as the concentration of microcapsules increases, the distance between the microcapsules becomes shorter causing an obstruction of the movement of fluid and thereby a

higher viscosity. The increase in the initial viscosity (η_0) as a function of MPCM concentration is fastest for MF/PCM24 and slowest for PS-DVB/RT 27. This probably reflects the polar/non-polar nature of the microcapsule shells (see **Paper IV** for details). The transition time (t_t) from stage 1 to stage 2 (Figure 23c) decreases when more MPCM is added to the samples, and the decline is most pronounced for MF/PCM24 and least evident for PS-DVB/RT27. This is contributed to a faster formation of the geopolymer precursor and monomer for MF/PCM24 due to the higher reduction of free water (see **Paper IV** for details).

5.4. Evaluation of building envelopes using geopolymer concrete containing MPCM as single wall in European city conditions (Oslo and Madrid).

A numerical model, which is based on the implicit finite differences method using an energy balance approach and the heat capacity method, was developed to determine the thermal impact of utilizing GPC containing MPCM in buildings (**paper VI**). The numerical model presented in this study was validated using the experimental results obtained by the system shown in Figure 9. Results from the numerical model were compared with the experimental measurements (Figure 24 and Figure 25). Although there is a small deviation between numerical data and experimental results, the numerical values obtained for GPC containing MPCM was in good agreement with the experimental data. This demonstrates that this numerical model can be used as a quantitative tool to predict the thermal impact of concrete containing microcapsules at different climate conditions and for varying building designs.

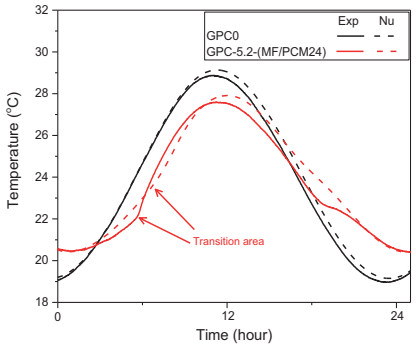

Figure 24: Comparison of numerical model with experimental measurements for the indoor surface temperature of GPC0 and GPC-5.2-(MF/PCM24). The wall thickness of all samples is 7.5 cm **(Paper VI)**.

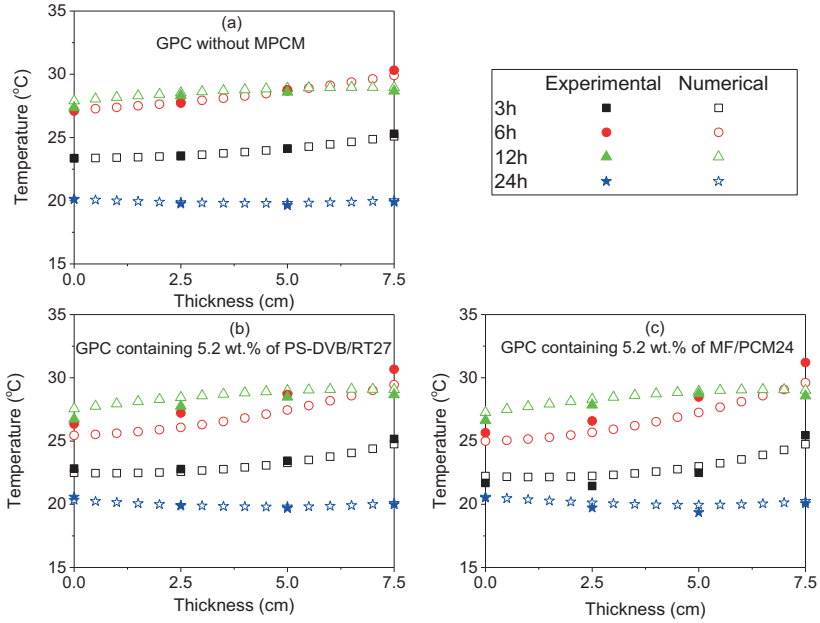

Figure 25: Comparison of numerical model with experimental measurements for temperature variations across the concrete thickness at different times for (a) GPC0, (b) GPC-5.2-(PS-DVB/RT27) and (c) GPC-5.2-(MF/PCM24). The thickness of all samples is 7.5 cm **(Paper VI)**.

In **paper VII,** the effect of various environmental conditions (e.g. solar radiation, outdoor temperature), and building design (e.g. wall thickness, MPCM concentration and MPCM types) on the thermal performance of buildings using MPCM-GPC walls was numerically investigated (Figure 26).

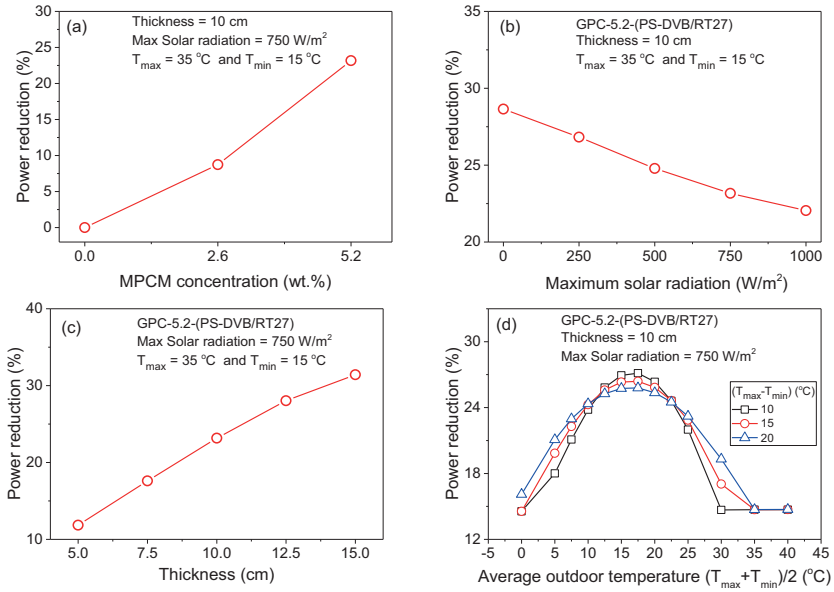

Figure 26. The effect of (a) MPCM concentration, (b) maximum solar radiation, (c) wall thickness and (d) average outdoor temperature and the outdoor temperature amplitude on power reduction. The data is GPC containing PS-DVB/RT27.

The simulations revealed that the power consumption could be significantly reduced by increasing the MPCM concentration. This is due to the higher heat storage capacity and lower thermal conductivity of MPCM-concrete when the amount of MPCM in GPC increases. As a result, the addition of 5.2 wt.% PS-DVB/RT27 can reduce the power consumption with approximately 25 % at the current numerical conditions (Figure 26a).

Increasing the maximum solar radiation leads to a higher power consumption to maintain an indoor temperature of 23 ºC (Figure 26b). The power reduction decreases from 29 to 22 % when the maximum solar radiation is raised from 0 to 1000 W/m^2. The heat transfer through the wall will increase with more solar radiation, while the MPCM can only absorb a certain amount of heat. During a hot summer, the capacity of the PCM will not be sufficient to compensate for the additional solar radiation.

By varying the thickness of the wall from 5 cm to 20 cm, the heat flux transfer to the indoor environment is decreased, resulting in a lower power consumption and higher power reduction for the heating and cooling system (Figure 26c). The decline in indoor surface heat flux is

caused by the rate of heat conduction through the sample, which is inversely proportional to the thickness of the sample.

The efficiency of utilizing a MPCM-GPC wall in a building is dependent on the outdoor temperature. The power consumption for both GPC0 and GPC containing 5.2 wt.% MPCM reaches a minimum power consumption when the average outdoor temperature is around 15-20 ºC, which is close to the desired indoor temperature (Figure 26d). At that outdoor temperature range (15-20 ºC), the power reduction with the addition of 5.2 wt.% PS-DVB/RT27 is about 25-27 %. However, too hot (40 ºC) or cold (0 ºC) outdoor temperature averages greatly reduce the efficiency of MPCM addition. At these conditions, the outdoor temperature fluctuations are mostly outside the melting range of the PCM, which greatly diminishes the effect of MPCM addition, reducing the efficiency of the MPCM. According to the simulated results, the power reduction of GPC containing 5.2 wt.% PS-DVB/RT27 can reach up to only 15 % in extreme hot or cold climate in comparison to GPC0. Although the effect of phase change is hindered in these conditions, the reduction of the thermal conductivity of concrete after adding MPCM provides a significant effect.

Based on this information, the numerical model was applied to the conditions of Oslo and Madrid in order to evaluate the potential of employing GPC-MPCM at different European conditions (**Paper VII**).

5.4.1. Effect of direction

Figure 27 shows the indoor surface heat flux as a function of time for a south-facing wall over one year at the conditions of Oslo and Madrid for GPC without MPCM and GPC containing 5.2 wt.% PS-DVB/RT27. The indoor surface heat flux throughout the year decreases after adding MPCM, leading to a reduction of the power consumption for the heating and cooling system to maintain the indoor temperature.

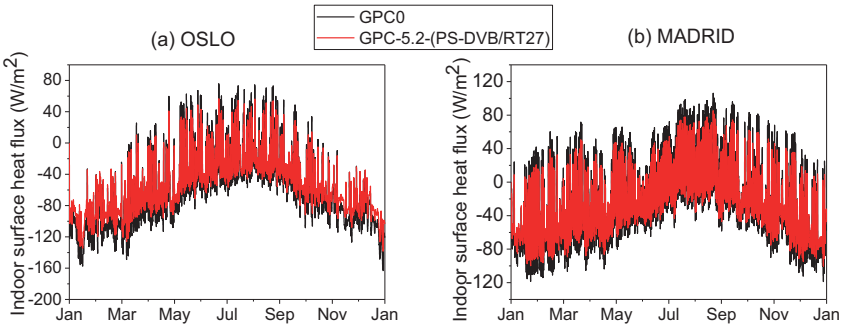

Figure 27. Indoor surface heat flux as a function of time for a south-facing wall over one year at the climate conditions of (a) Oslo and (b) Madrid for GPC without MPCM and GPC containing 5.2 wt.% PS-DVB/RT27 **(Paper VII)**.

The annual reduction of power consumption of concrete samples containing 5.2 wt.% MPCM compared to corresponding samples without MPCM (GPC0) facing different directions (south, east, north and west) at the conditions of Oslo and Madrid are presented in Figure 28. In both Oslo and Madrid, the power reduction for the south and west facing walls are higher than the east and north facing walls. The different solar radiation combined with the outdoor temperature (environmental temperature) contributes to these differences. In both cities, the solar radiation on the south and west walls are stronger than that for the walls facing east and north (Figure 30). The yearly outdoor temperature in Oslo and Madrid are lower than the maintained indoor temperature, except for some days in summer (Figure 29). The higher solar radiation on the south and west walls result in a higher energy absorption, and therefore less heat transfer from the indoor environment toward the outdoor environment. This shifts the indoor wall surface temperature on the south and west facing walls closer to the indoor temperature than the east and north facing walls (Figure 29). This is different from previous findings (Figure 26b) when the outdoor temperature was higher than the indoor temperature, where the solar radiation led to an increase of the heat transfer into the indoor environment.

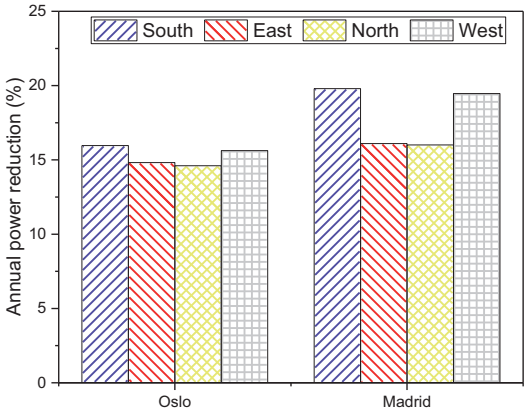

Figure 28. The annual power reduction for South, East, North and West facing walls in Oslo and Madrid using GPC-5.2-(PS-DVB/RT27) compared to GPC without MPCM.

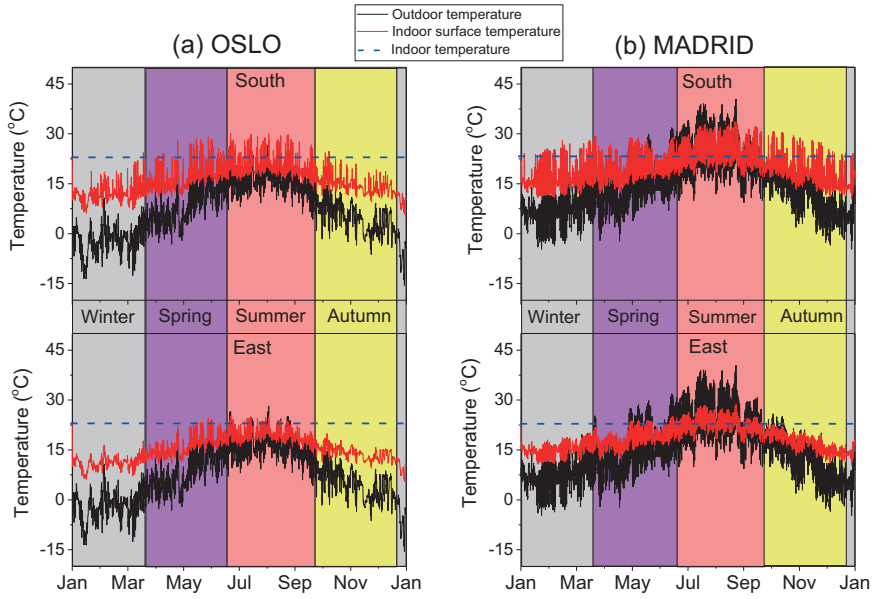

Figure 29. The outdoor temperature (obtained from weather data-Climate Consultant software [92]) and the effect of solar radiation on the indoor surface temperature of the south and east facing walls in (a) Oslo and (b) Madrid **(Paper VII)**.

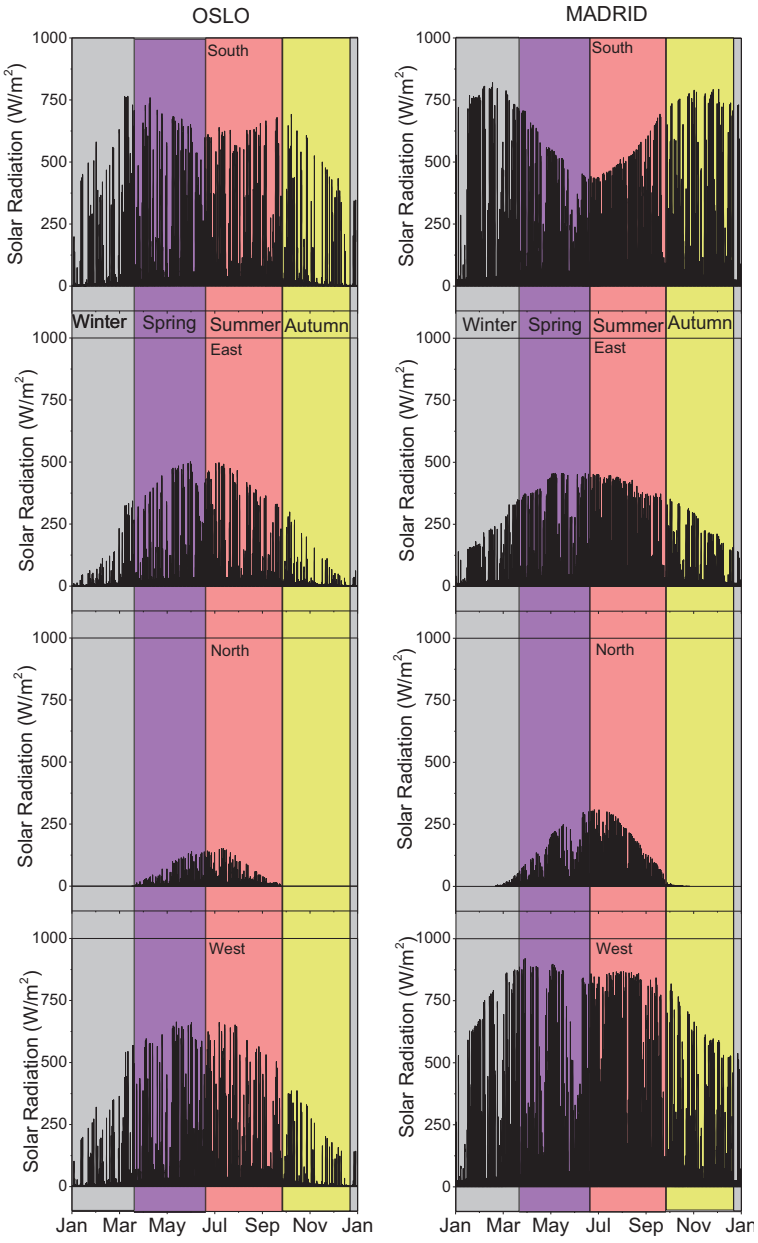

Figure 30. The solar radiation incident upon a south, east, north and west facing walls as functions of time Oslo and Madrid (obtained from weather data-Climate Consultant software [92]) **(Paper VII).**

5.4.2. Effect of season

Figure 31 shows the power consumption needed to maintain the indoor temperature at 23 ºC of a building utilizing GPC without MPCM and with 5.2 wt.% of MPCM (PS-DVB/RT27 and MF/PCM24); and the power reduction after adding 5.2 wt.% of MPCM at different seasons in Oslo an Madrid. The power consumption is lowest during the summer and highest during the winter in both cities and for all samples. Furthermore, the power reduction is highest for summer and lowest for winter. The average outdoor temperature in the summer months (15±2 ºC in Oslo and 22±2 ºC in Madrid) (Figure 29) is closest to the indoor temperature (23 ºC) and within the melting range of MPCM, which will improve the efficiency of utilizing the MPCM. The effect of the PCM latent heat during phase change is hindered during winter due to a too low average temperature. This is in good agreement with Figure 26d. In addition, the lower power consumption and higher power reduction of Madrid compared to Oslo demonstrates that MPCM has a higher impact on the conditions in Madrid than for Oslo. This can be explained by the higher average temperature of Madrid, which is also closer to the indoor temperature and the melting range of MPCM (Figure 29). Accordingly, by adding 5.2 wt.% of MPCM to GPC, a single family house in Madrid can reduce the power consumption with up to 24 % when utilizing PS-DVB/RT27 and 33 % for MF/PCM24 during summer and 16 % (PS-DVB/RT27) and 22 % (MF/PCM24) during winter (Figure 31). In the case of Oslo, the power reduction can reach to 18 % and 24 % during summer and 15 % and 20 % during winter after adding 5.2 wt.% of PS-DVB/RT27 and MF/PCM24, respectively. This demonstrates that MF/PCM24 has a greater thermal impact on GPC than PS-DVB/RT27. This is probably caused by the higher heat storage capacity of MF/PCM24 compared to PS-DVB/RT27, and the lower thermal conductivity of GPC containing MF/PCM24 (Figure 21).

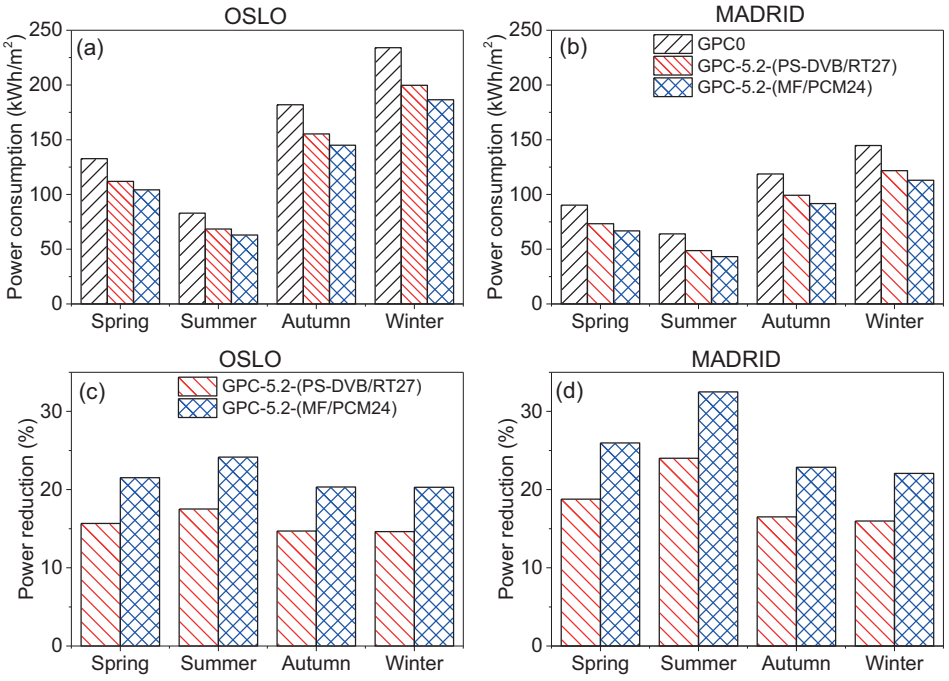

Figure 31. (a-b) The average power consumption (Eq.11) and (c-d) average power reduction (four wall orientations) of utilizing GPC-5.2-(PS-DVB/RT27) and GPC-5.2-(MF/PCM24) compared to GPC0 at different seasons during a year in Oslo and Madrid **(Paper VII)**.

6. Conclusions

This thesis has presented an investigation on the high thermal energy storage capacity of environmentally friendly geopolymer concrete containing microencapsulated phase change materials for building applications.

The rheological behavior of microcapsule suspensions in **Paper I and II** revile the important role of non-encapsulated phase change materials on the physical properties and structure of microcapsules. Free PCM can also interact with the cement matrix, especially when PCM is in liquid state. It is therefore important to select the microcapsules without the non-encapsulated PCM to integrate into concrete.

Materials with a high thermal energy storage capacity were fabricated by direct mixing of microencapsulated phase change materials (MPCM) to Portland cement concrete (PCC) and geopolymer concrete (GPC). The addition of MPCM strongly affects the thermal performance and compressive strength of PCC and GPC. Raising the amount of microcapsules was found to improve the thermal energy storage capacity, reduce the thermal conductivity and decrease the density, resulting in an enhancement of the energy efficiency. Unfortunately, the addition of microcapsules results in a significant loss of concrete compressive strength. The loss of compressive strength may be ascribed to low mechanical strength of the microcapsules combined with and an enhanced porosity.

The workability and types of microcapsules was found to have a significant impact on the concrete properties. GPC without retarder have a poorer workability and shorter setting time than PCC, causing a higher porosity, and a higher thermal conductivity reduction and higher compressive strength reduction of GPC compared to PCC. However, the addition of retarder to GPC caused a better workability and longer setting times (compared to GPC without retarder) leading to an increase in the amount of MPCM that was possible to add to the GPC and a smaller compressive strength reduction. Accordingly, the maximal amount of MPCM in GPC increased from 2.6 wt.% to 5.2 wt.%, while the slope of compressive strength reduction decreased from 18 to 10 after adding retarder.

The hygroscopic nature of polymer shell, core/shell ratio and the size of microcapsules play important roles on the concrete properties. It was found that, the microcapsules with polar functional groups on polymer shell and smaller size can adsorb more water resulting in a significant increase of the viscosity (**Paper IV**). The increase of viscosity of concrete after adding microcapsules caused a significant effect on the thermal performance as well as the mechanical strength of concrete. The results in **Paper III** and **V** prove the advantages in term of thermal performance of utilizing microcapsules with a polymer shell containing polar functional groups, a small size and a high core/shell ratio (MF/PCM24). The reduction of power consumption for stabilizing the indoor temperature at 23 ºC during one day for 5 cm thickness of GPC containing 5.2 wt.% of MF/PCM24 was highest at 25.9 ± 0.3 %. Unfortunately, due to the high amounts of air pockets and a high core/shell ratio, GPC containing 5.2 wt.% of MF/PCM24 had very low mechanical strength (19 ± 1 MPa in solid state and 13.0 ± 0.4 MPa in liquid state), which does not satisfy the European regulation for compressive strength (**Paper V**). Although the rest of the microcapsules had a lower thermal performance, their compressive strength at 5.2% MPCM satisfy the mechanical European regulation (EN 206-1, compressive strength class C20/25) for concrete for building construction.

The influence of PCM state on the thermal conductivity and compressive strength of GPC containing MPCM was examined. Although the thermal conductivity of GPC was independent on PCM state (**Paper III, V**), the compressive strength decreased when PCM changes from a solid to liquid state for all microcapsules (**Paper V**). The PCM state exhibited the largest impact on GPC containing MF/PCM24 and LDPE-EVA/RT27. It is believed that the lack of air gaps between MPCM and GPC combined with a high core/shell ratio (MF/PCM24) and the non-encapsulated PCM in MPCM structure (LDPE-EVA/RT27) contribute to this.

In **paper VI** and **VII** the energy saving aspect of buildings utilizing the GPC containing 5.2 wt.% at various environmental conditions were numerically evaluated. A numerical model was developed to determine the thermal impact of buildings utilizing GPC containing MPCM, and was successfully verified by experimental measurements (**paper VI**). In **paper VII**, the simulations reveal that increasing the MPCM concentration and the wall thickness significantly reduced the power consumption. Furthermore, the results illustrate the importance of utilizing a PCM with a melting temperature close to the average outdoor temperature and indoor temperature, so the effect of the high heat storage capacity during the phase change can be improved. Interestingly, the addition of MPCM reduced the power consumption even at conditions where the outdoor temperature is extremely warm or cold due to the increased porosity and the resulting lower thermal conductivities. Based on that information, a numerical model was applied for the conditions of Oslo and Madrid (**Paper VII).** The annual power reduction was dependent on the wall orientation. It was largest for the south- and west-facing walls in both Oslo and Madrid. The influence of MPCM addition on GPC was highest during summer and worst during winter, and the power reduction was highest during summer and lowest during winter. It is possible that the average outdoor temperature in the summer months (15±2 ºC in Oslo and 22±2 ºC in Madrid) is closest to the indoor temperature (23 ºC) and within the melting range of MPCM. The difference from the average outdoor temperature also contributed to the lower power consumption and higher power reduction of Madrid compared to Oslo.

7. Recommendations for future work

The current results show that the workability plays an important role on increasing amount of MPCM into geopolymer concrete as well as porosity enhancement. Those factors have a significant impact on improving thermal performance as well as reducing the mechanical properties of MPCM-GPC. It will be of significant interest to improve the GPC recipe to not

only increase the amount of MPCM but also control the porosity enhancement within an acceptable range. In this way, we can improve the thermal performance and minimize the compressive strength reduction to satisfy the demand of mechanical properties for structural applications.

Alternatively, improving microcapsules with higher thermal storage capacity and stronger polymer shell is a promising solution to achieve both good energy saving and high mechanical strength. The insertion of a suitable amount of nanomaterials to the microcapsule structure, especially the polymer shell [105-107], have showed promising potential in enhancing the mechanical stability of the microcapsules. An investigation of inserting nanomaterials to the microcapsules in order to enhance the thermal storage capacity and mechanical stability of the microcapsules should receive special attention.

A better understanding of the effect of microcapsule on the chemistry and the material structure of the geopolymer (e.g. the phases inside concrete structure, the reaction heat, etc) is important to further the understanding of mechanical and thermal properties of concrete. This can be achieved by utilizing advanced characterization methods (e.g. X-Ray diffraction (XRD), Calorimetry).

The durability of geopolymer concrete containing MPCM is another critical requirement. The durability tests including chemical attack, fire resistance, frost resistance, and weathering effects should be investigated in order to evaluate its potential for applications in buildings.

The heat transfer coefficient is strongly dependent on the indoor and outdoor environment conditions and building designs. This may contribute to the accuracy of numerical model. Therefore, it is necessary to employ the heat transfer coefficient as a function of various environmental conditions into the numerical model in order to improve the realisticity as well as the accuracy of model. Analytical approaches with correlations could be developed to estimate the heat transfer coefficient.

Evaluating the energy efficiency and developing the cost analysis method for buildings utilizing MPCM-GPC multi-walls will be very interesting topics.

8. Bibliography

[1] X.F. Zhang, S.Y. Zhang, Z.Y. Hu, G. Yu, C.H. Pei, R.N. Sa. Identification of connection units with high GHG emissions for low-carbon product structure design. J Cleaner Prod. 27 (2012) 118-25.
[2] E. Benhelal, G. Zahedi, E. Shamsaei, A. Bahadori. Global strategies and potentials to curb CO2 emissions in cement industry. J Cleaner Prod. 51 (2013) 142-61.
[3] E.P. EU Directive 2002/91/EC, Brussels, 2003.
[4] E.P. EU Directive 2010/31/UE, Strasburg, 2010.
[5] I. Dincer, M. A.Rosen. Thermal energy storage systems and applications. Second ed. A John Wiley and Sons, Ltd.2011.
[6] L.G. Socaciu. Thermal Energy Storage with Phase Change Material. Leonardo Electronic Journal of Practices and Technologies. (2012) 75-98.
[7] A.H. Abedin, M.A. Rosen. A Critical Review of Thermochemical Energy Storage Systems. The Open Renewable Energy Journal. 4 (2011) 42-6.
[8] M.F. Demirbas. Thermal Energy Storage and Phase Change Materials: An Overview. Energy Sources, Part B: Economics, Planning, and Policy. 1 (2006) 85-95.
[9] J.P.d. Cunha, P. Eames. Thermal energy storage for low and medium temperature applications using phase change materials – A review. Applied Energy. 177 (2016) 227-38.
[10] V.D. Cao, S. Pilehvar, C. Salas-Bringas, A.M. Szczotok, J.F. Rodriguez, M. Carmona, et al. Microencapsulated phase change materials for enhancing the thermal performance of Portland cement concrete and geopolymer concrete for passive building applications. Energy Convers Manage. 133 (2017) 56-66.
[11] A.d. Gracia, L.F. Cabeza. Phase change materials and thermal energy storage for buildings. ENERG BUILDINGS. 103 (2015) 414-9.
[12] A. Sharma, V.V. Tyagi, C.R. Chen, D. Buddhi. Review on thermal energy storage with phase change materials and applications. Renewable and Sustainable Energy Reviews. 13 (2009) 318-45.
[13] H. Cui, W. Liao, X. Mi, T.Y. Lo, D. Chen. Study on functional and mechanical properties of cement mortar withgraphite-modified microencapsulated phase-change materials. ENERG BUILDINGS. 105 (2015) 273-84.
[14] M. Lachheba, M. Karkri, S.B. Nasrallah. Development and thermal characterization of an innovativegypsum-based composite incorporating phase change material asbuilding energy storage system. ENERG BUILDINGS. 107 (2015) 93-102.
[15] P. Han, X. Qiu, L. Lu, L. Pan. Fabrication and characterization of a new enhanced hybrid shell microPCM for thermal energy storage. Energy Convers Manage. 126 (2016) 673-85.
[16] A.Jamekhorshid, S.M.Sadrameli, M.Farid. A review of microencapsulation methods of phase change materials (PCMs) as a thermal energy storage (TES) medium. Renewable and Sustainable Energy Reviews. 31 (2014) 531-42.
[17] V.V. Tyagi, S.C. Kaushik, S.K. Tyagi, T. Akiyama. Development of phase change materials based microencapsulated technology for buildings: A review. Renewable and Sustainable Energy Reviews. 15 (2011) 1373-91.
[18] Y. Zhu, S. Liang, H. Wang, K. Zhang, X. Jia, C. Tian, et al. Morphological control and thermal properties of nanoencapsulated n-octadecane phase change material with organosilica shell materials. Energy Convers Manage. 119 (2016) 151-62.
[19] A. Buscombe, M. Wu. A Review of PCM's Thermal Performance Within Lightweight Construction. International Journal of Engineering Practical Research (IJEPR). 2 (2013) 174-7.

[20] X. Wang, J. Niu, X.W. Yi Li, B. Chen, R. Zeng, Q. Song, et al. Flow and heat transfer behaviors of phase change material slurries in a horizontal circular tube. International Journal of Heat and Mass Transfer. 50 (2007) 2480-91.
[21] L. Chen, T. Wang, Y. Zhao, X.-R. Zhang. Characterization of thermal and hydrodynamic properties for microencapsulated phase change slurry (MPCS). Energy Convers Manage. 79 (2014) 317-33.
[22] G.H. Zhang, C.Y. Zhao. Thermal and rheological properties of microencapsulated phase change materials. Renewable Energy. 36 (2011) 2959-66.
[23] J.L. Alvarado, C. Marsh, C. Sohn, G. Phetteplace, T. Newell. Thermal performance of microencapsulated phase change material slurry in turbulent flow under constant heat flux. International Journal of Heat and Mass Transfer. 50 (2007) 1938-52.
[24] Y. Yamagishi, H. Takeuchi, A.T. Pyatenko, N. Kayukawa. Characteristics of Microencapsulated PCM Slurry as a Heat-Transfer Fluid. AIChE 45 (1999) 696-707.
[25] C. Pollerberg, C. Dotsch. Phase Changing Slurries in cooling and cold supply networks. 10th International Symposium on Disctrict Heating and Cooling, Hannover (Germany), 2006.
[26] A.G.E. M. Hunger, I. Mandilaras, H.J.H. Brouwers, M. Founti. The behavior of self-compacting concrete containing micro-encapsulated Phase Change Materials. Cem Concr Compos. 31 (2009) 731-43.
[27] J.L.M. María Fenollera, Itziar Goicoechea, Jaime Lorenzo and Miguel Ángel Álvarez. The Influence of Phase Change Materials on the Properties of Self-Compacting Concrete. Materials. 6 (2013) 3530-46.
[28] A. Eddhahak-Ouni, S. Drissi, J. Colin, J. Neji, S. Care. Experimental and multi-scale analysis of the thermal properties of Portland cement concretes embedded with microencapsulated Phase Change Materials (PCMs). Appl Therm Eng. 64 (2014) 32-9.
[29] S. Pilehvar, V.D. Cao, A.M. Szczotok, L. Valentini, D. Salvioni, M. Magistri, et al. Mechanical properties and microscale changes of geopolymer concrete and Portland cement concrete containing micro-encapsulated phase change materials. Cem Concr Res. 100 (2017).
[30] A.L. Pisello, A. D'Alessandro, C. Fabiani, A.P. Fiorelli, F. Ubertini, L. F.Cabeza, et al. Multifunctional Analysis of Innovative PCM-filled Concretes. Energy Procedia. 111 (2017) 81-90.
[31] Z. Wei, G. Falzone, B. Wang, A. Thiele, G. Puerta-Falla, L. Pilon, et al. The durability of cementitious composites containing microencapsulated phase change materials. Cem Concr Compos. 81 (2017) 66-76.
[32] V.D. Cao, S. Pilehvar, C. Salas-Bringas, A.M. Szczotok, L. Valentini, M. Carmona, et al. Influence of microcapsule size and shell polarity on thermal and mechanical properties of thermoregulating geopolymer concrete for passive building applications. Energy Convers Manage. 164 (2018) 198-209.
[33] P. Duxson, A. Fernandez-Jimenez, J.L. Provis, G.C. Lukey, A. Palomo, J.S.J.v. Deventer. Geopolymer technology: the current state of the art. J Mater Sci. 42 (2007) 2917-33.
[34] Z. Zuhua, Y. Xiao, Z. Huajun, C. Yue. Role of water in the synthesis of calcined kaolin-based geopolymer. Appl Clay Sci. 43 (2009) 218-23.
[35] L.K. Turner, F.G. Collins. Carbon dioxide equivalent (CO2-e) emissions: A comparison between geopolymer and OPC cement concrete. Construction and Building Materials. 43 (2013) 125-30.
[36] A. Joulin, L. Zalewski, S. Lassue, H. Naji. Experimental investigation of thermal characteristics of a mortar with or without a micro-encapsulated phase change material. Appl Therm Eng. 66 (2014) 171-80.
[37] R. Shadnia, L. Zhang, P. Li. Experimental study of geopolymer mortar with incorporated PCM. Constr Build Mater. 84 (2015) 95-102.

[38] A.M. Thiele, A. Jamet, G. Sant, L. Pilon. Annual energy analysis of concrete containing phase change materials for building envelopes. Energy Convers Manage. 103 (2015) 374-86.
[39] B. Nematollahi, R. Ranade, J. Sanjayan, S. Ramakrishnan. Thermal and mechanical properties of sustainable lightweight strain hardening geopolymer composites. Archives of Civil and Mechanical Engineering. 17 (2017) 55-64.
[40] B. Nematollahi, J. Sanjayan, F.U.A. Shaikh. Synthesis of heat and ambient cured one-part geopolymer mixes with different grades of sodium silicate. Ceramics International. 41 (2015) 5696-704.
[41] K.-t. Wang, Q. Tang, X.-m. Cui, Y. He, L.-p. Liu. Development of near-zero water consumption cement materials via the geopolymerization of tektites and its implication for lunar construction. Sci Rep. 6 (2016) 29659.
[42] A.M.M.A. Bakri, H. Kamarudin, M. Bnhussain, I.K. Nizar, W.I.W. Mastura. Mechanism and Chemical Reaction of Fly Ash Geopolymer Cement- A Review. JASR. 1 (2011) 247-53.
[43] G. Görhan, G. Kürklü. The influence of the NaOH solution on the properties of the fly ash-based geopolymer mortar cured at different temperatures. Composites Part B: Engineering. 58 (2014) 371-7.
[44] T. Phoo-ngernkham, A. Maegawa, N. Mishima, S. Hatanaka, P. Chindaprasirt. Effects of sodium hydroxide and sodium silicate solutions on compressive and shear bond strengths of FA–GBFS geopolymer. Construction and Building Materials. 91 (2015) 1-8.
[45] J. Temuujin, A.v. Riessen, R. Williams. Influence of calcium compounds on the mechanical properties of fly ash geopolymer pastes. Journal of Hazardous Materials. 167 (2009) 82-8.
[46] U. Rattanasak, P. Chindaprasirt. Influence of NaOH solution on the synthesis of fly ash geopolymer. Minerals Engineering. 22 (2009) 1073-8.
[47] P. Nath, P.K. Sarker. Effect of GGBFS on setting, workability and early strength properties of fly ash geopolymer concrete cured in ambient condition. Construction and Building Materials. 66 (2014) 163-71.
[48] B. Nematollahi, J. Sanjayan. Effect of different superplasticizers and activator combinations on workability and strength of fly ash based geopolymer. Materials and Design. 57 (2014) 667-72.
[49] J.G. Jang, N.K. Lee, H.K. Lee. Fresh and hardened properties of alkali-activated fly ash/slag pastes with superplasticizers. Constr Build Mater. 50 (2014) 169-76.
[50] N. Toniolo, A.R. Boccaccini. Fly ash-based geopolymers containing added silicate waste. A review. Ceramics International. 43 (2017) 14545-51.
[51] S.A. C618. Standard Specification for Coal Fly Ash and Raw or Calcined Natural Pozzolan for Use in Concrete.
[52] E.I. Diaz, E.N. Allouche, S. Eklund. Factors affecting the suitability of fly ash as source material for geopolymers. Fuel. 89 (2010) 992-6.
[53] C.K. Yip, G.C. Lukey, J.L. Provis, J.S.J. van Deventer. Effect of calcium silicate sources on geopolymerisation. Cement and Concrete Research. 38 (2008) 554-64.
[54] S. Kumar, R. Kumar, S.P. Mehrotra. Influence of granulated blast furnace slag on the reaction, structure and properties of fly ash based geopolymer. J Mater Sci. 45 (2010) 607-15.
[55] S. Thokchom, D. Dutta, S. Ghosh. Effect of incorporating silica fume in fly ash geopolymers. World Academy of Science, Engineering and Technology. 60 (2011) 243-7.
[56] A. Kusbiantoro, M.F. Nuruddin, N. Shafiq, S.A. Qazi. The effect of microwave incinerated rice husk ash on the compressive and bond strength of fly ash based geopolymer concrete. Construction and Building Materials. 36 (2012) 695-703.
[57] A.M. Rashad. A comprehensive overview about the influence of different admixtures and additives on the properties of alkali-activated fly ash. Materials & Design. 53 (2014) 1005-25.

[58] P.S. Deb, P. Nath, P.K. Sarker. The effects of ground granulated blast-furnace slag blending with fly ash and activator content on the workability and strength properties of geopolymer concrete cured at ambient temperature. Materials & Design. 62 (2014) 32-9.
[59] H. Xu, W. Gong, L. Syltebo, K. Izzo, W. Lutze, I.L. Pegg. Effect of blast furnace slag grades on fly ash based geopolymer waste forms. Fuel. 133 (2014) 332-40.
[60] A. Islam, U.J. Alengaram, M.Z. Jumaat, I.I. Bashar. The development of compressive strength of ground granulated blast furnace slag-palm oil fuel ash-fly ash based geopolymer mortar. Materials & Design. 56 (2014) 833-41.
[61] B. Nematollahi, J. Sanjayan. Efficacy of Available Superplasticizers on Geopolymers. Research Journal of Applied Sciences, Engineering and Technology. 7 (2014) 1278-82.
[62] M. Criado, A. Palomo, A. Fernández-Jiménez. Alkali activation of fly ashes. Part 1: Effect of curing conditions on the carbonation of the reaction products. Fuel. 84 (2005) 2048-54.
[63] A.A. Aliabdo, A.E.M. Abd Elmoaty, H.A. Salem. Effect of water addition, plasticizer and alkaline solution constitution on fly ash based geopolymer concrete performance. Construction and Building Materials. 121 (2016) 694-703.
[64] A.M. Szczotok, M. Carmona, A.-L. Kjøniksen, J.F. Rodriguez. Equilibrium adsorption of polyvinylpyrrolidone and its role on thermoregulating microcapsules synthesis process. Colloid Polym Sci. 40 (2017) 4061-71.
[65] A.M. Borreguero, J.L. Valverde, J.F. Rodríguez, A.H. Barber, J.J. Cubillo, M. Carmona. Synthesis and characterization of microcapsules containing Rubitherm®RT27 obtained by spray drying. Chemical Engineering Journal. 166 (2011) 384-90.
[66] http://www.micronal.de, datasheet of DS-5038X.
[67] http://www.microteklabs.com/data-sheets.html, Data sheet of MPCM24D.
[68] S. Pilehvar, V.D. Cao, A.M. Szczotok, M. Carmona, R. Pamies, A.-L. Kjøniksen. Mix design and mechanical properties of geopolymer concrete containing different types of micro-encapsulated phase change materials. Submitted for publication. (2017).
[69] L.A. Feldkamp, L.C. Davis, J.W. Kress. Practical cone-beam algorithm. J Opt Soc Am A. 1 (1984) 612-9.
[70] Standard BS EN 12390-7. Testing hardened concrete. Part 7: Density of hardened concrete, 2009.
[71] M.Y.J. Liu, U.J. Alengaram, M.Z. Jumaat, K.H. Mo. Evaluation of thermal conductivity, mechanical and transportproperties of lightweight aggregate foamed geopolymer concrete. ENERG BUILDINGS. 72 (2014) 238–45.
[72] M. Safiuddin, N. Hearn. Comparison of ASTM saturation techniques for measuring the permeable porosity of concrete. Cem Concr Res. 35 (2005) 1008-13.
[73] V.D. Cao, C. Salas-Bringas, R.B. Schüller, A.M. Szczotok, M. Hiorth, J.F. Rodriguez, et al. Rheological and thermal properties of suspensions of microcapsules containing phase change materials Colloid Polym Sci. 296 (2018) 981-8.
[74] C.W. Macosco. Rheology: Principles, Measurements, and Applications. Wiley–VCH, New York, 1994.
[75] P. Tittelein, S. Gibout, E. Franquet, K. Johannes, L. Zalewski, F. Kuznik, et al. Simulation of the thermal and energy behaviour of a composite material containing encapsulated-PCM: Influence of the thermodynamical modelling. Applied energy. 140 (2015) 269-74.
[76] P. Lamberg, R. Lehtiniemi, A.-M. Henell. Numerical and experimental investigation of melting and freezing processes in phase change material storage. International Journal of Thermal Sciences. 43 (2004) 277-87.
[77] A.M. Thiele, G. Sant, L. Pilon. Diurnal thermal analysis of microencapsulated PCM-concrete composite walls. Energy Convers Manage. 93 (2015) 215-27.
[78] B.M. Diaconu, M. Cruceru. Novel concept of composite phase change material wall system for year-round thermal energy savings. ENERG BUILDINGS. 42 (2010) 1759-72.

[79] E. Lev, I. Kutasov, A. Pilchin. Applied Geothermics. Springer-Verlag Berlin Heidelberg2014.
[80] Y.A. Cengel. Heat Transfer: A Practical Approach. 2nd ed. Mcgraw-Hill2002.
[81] S.N. AL-Saadi, Z.J. Zhai. Modeling phase change materials embedded in building enclosure: Areview. Renewable and Sustainable Energy Reviews. 21 (2013) 659-73.
[82] J. Darkwa, O. Su. Thermal simulation of composite high conductivity laminated microencapsulated phase change material (MEPCM) board. Applied Energy. 95 (2012) 246-52.
[83] B.L. Gowreesunker, S.A. Tassou, M. Kolokotroni. Improved simulation of phase change processes in applications where conduction is the dominant heat transfer mode. ENERG BUILDINGS. 47 (2012) 353-9.
[84] A.M. Borreguero, M.L. Sánchez, J.L. Valverde, M. Carmona, J.F. Rodríguez. Thermal testing and numerical simulation of gypsum wallboards incorporated with different PCMs content. Applied Energy. 88 (2011) 930-7.
[85] L.A. A. Pasupathy, R. Velraj, R.V. Seeniraj. Experimental investigation and numerical simulation analysis on the thermal performance of a building roof incorporating phase change material (PCM) for thermal management. Appl Therm Eng. 28 (2008) 556–65.
[86] ASHRAE. Handbook of Fundamentals. Atlanta: American Society of Heating, Refrigerating and Air-Conditioning Engineers. Inc.2013.
[87] E.M. Alawadhi. Thermal analysis of a building brick containing phase change material. Energy and Buildings. 40 (2008) 351-7.
[88] S.A. Al-Sanea. Thermal performance of building roof elements. Building and Environment. 37 (2002) 665-75.
[89] F. Kreith, R.M. Manglik, M.S. Bohn. Principles of Heat Transfer, SI Edition. Cengage Learning2012.
[90] H.P. Garg. Treatise on solar energy: Fundamentals of Solar Energy. Chichester: Wiley1982.
[91] A. Pérez-Burgos, J. Bilbao, A.d. Miguel, R. Román. Analysis of solar direct irradiance in spain. Energy Procedia. 57 (2014) 1070-6.
[92] U.E.D.T.G.C.C.h.w. energy-design-tools.aud.ucla.edu.
[93] A.M. Borreguero, I. Garrido, J.L. Valverdea, J.F. Rodríguez, M. Carmona. Development of smart gypsum composites by incorporatingthermoregulating microcapsules. ENERG BUILDINGS. 76 (2014) 631-9.
[94] U. Mucteba, Y. Kemalettin. Effect of mineral admixtures on properties of self-compacting concrete. Cem Concr Compos. 33 (2011) 771-6.
[95] I.M. Nikbin, M.H.A. Beygi, M.T. Kazemi, J. Vaseghi Amiri, S. Rabbanifar, E. Rahmani, et al. A comprehensive investigation into the effect of water to cement ratio and powder content on mechanical properties of self-compacting concrete. Constr Build Mater. 57 (2014) 69-80.
[96] D.J.S. Chad Norvell, Peter Dusicka. The Effect of Microencapsulated Phase-Change Material on the Compressive Strength of Structural Concrete. Journal of Green Building. 8 (2013) 116-24.
[97] P.K. Dehdezi, M.R. Hall, A.R. Dawson, S.P. Casey. Thermal, mechanical and microstructural analysis of concrete containing microencapsulated phase change materials. International Journal of Pavement Engineering. 14 (2012) 449-62.
[98] A.M. Borreguero, A. Serrano, I. Garrido, J.F. Rodríguez, M. Carmona. Polymeric-SiO2-PCMs for improving the thermal properties of gypsum applied in energy efficient buildings. Energy Convers Manage. 87 (2014) 138-44.
[99] H. Moosberg-Bustnes, B. Lagerblad, E. Forssberg. The function of fillers in concrete Materials and Structures. 37 (2004) 74-81.

[100] D. Fedroff, S. Ahmad, B. Savas. Mechanical properties of concrete with ground waste tire rubber. Transportation Research Board. 1532 (1996) 66-72.
[101] Z.K. Khatib, F.M. Bayomy. Rubberized Portland Cement Concrete. J Mater Civ Eng. 11 (1999) 206-13.
[102] S. Pilehvar, V.D. Cao, A.M. Szczotok, L. Valentini, D. Salvioni, M. Magistri, et al. Mechanical properties and microscale changes of geopolymer concrete and Portland cement concrete containing micro-encapsulated phase change materials. Cement and Concrete Research. 100 (2017) 341-9.
[103] F. Vahedi, H.R. Shahverdi, M.M. Shokrieh, M. Esmkhani. Effects of carbon nanotube content on the mechanical and electrical properties of epoxy-based composites. NEW CARBON MATERIALS. 29 (2014) 419-25.
[104] H. Elkady, M. I.Serag, M.S. Elfeky. Effect of Nano Silica De-agglomeration, and Methods of Adding Super-plasticizer on the Compressive Strength, and Workability of Nano Silica Concrete. Civil and Environmental Research. 3 (2013) 21-34.
[105] Y. Xuan, Y. Huang, Q. Li. Experimental investigation on thermal conductivity and specific heat capacity of magnetic microencapsulated phase change material suspension. Chemical Physics Letters. 479 (2009) 264-9.
[106] X. Jiang, R. Luo, F. Peng, Y. Fang, T. Akiyama, S. Wang. Synthesis, characterization and thermal properties of paraffin microcapsules modified with nano-Al2O3. Applied Energy. 137 (2015) 731-7.
[107] M. Li, M. Chen, Z. Wub. Enhancement in thermal property and mechanical property of phase change microcapsule with modified carbon nanotube. Applied Energy. 127 (2014) 166-71.

Errata list

Side	Line	Original text	Corrected text
XII(14)	17	Kg	kg
XII(14)	23	Power consumption	Power consumption (Thermal load)
XII(14)	25	Indoor heat coefficient	Indoor heat transfer coefficient
XII(14)	26	Outdoor heat coefficient	Outdoor heat transfer coefficient
XIII(14)	28	Stefan-Boltzmann constant	Stefan-Boltzmann constant, $W/m^2 \cdot K^4$
12(27)	18	…low angel…	…low angle…
24(39)	23	ASHAE	ASHRAE
28(43)	21	ASHEA	ASHRAE
45(60)	13	…by the system show in Figure…	…by the system shown in Figure
47(62)	1	…could be significant reduced…	…could be significantly reduced…
48(63)	13	…in compared to GPC0.	…in comparison to GPC0.

Publications

Paper I

Rheological and thermal properties of suspensions of microcapsules containing phase change materials.

Vinh Duy Cao, Carlos Salas-Bringas, Reidar Barfod Schüller, Anna M. Szczotok, Marianne Hiorth, Manuel Carmona, Juan F. Rodriguez, Anna-Lena Kjøniksen.

Colloid and Polymer Science **2018**, 296, 981-988.

Colloid and Polymer Science
https://doi.org/10.1007/s00396-018-4316-9

ORIGINAL CONTRIBUTION

Rheological and thermal properties of suspensions of microcapsules containing phase change materials

Vinh Duy Cao[1,2] · Carlos Salas-Bringas[2] · Reidar Barfod Schüller[3] · Anna M. Szczotok[1,4] · Marianne Hiorth[5] · Manuel Carmona[4] · Juan F. Rodriguez[4] · Anna-Lena Kjøniksen[1]

Received: 5 December 2017 / Revised: 13 March 2018 / Accepted: 16 March 2018

Abstract
The thermal and rheological properties of suspensions of microencapsulated phase change materials (MPCM) in glycerol were investigated. When the microcapsule concentration is raised, the heat storage capacity of the suspensions becomes higher and a slight decline in the thermal conductivity of the suspensions is observed. The temperature-dependent shear-thinning behaviour of the suspensions was found to be strongly affected by non-encapsulated phase change materials (PCM). Accordingly, the rheological properties of the MPCM suspensions could be described by the Cross model below the PCM melting point while a power law model best described the data above the PCM melting point. The MPCM suspensions are interesting for energy storage and heat transfer applications. However, the non-encapsulated PCM contributes to the agglomeration of the microcapsules, which can lead to higher pumping consumption and clogging of piping systems.

Keywords Microencapsulated phase change materials · Non-encapsulated phase change materials · Heat storage capacity · Thermal conductivity · Shear thinning behaviour · Time-dependent behaviour

Introduction

The increasing cost of energy for heating and cooling creates a demand for more energy efficient buildings. Thermal energy storage (TES) systems using phase change materials (PCM) can be used to conserve and save energy. PCM are efficient energy storing materials due to a high heat capacity and a high latent heat per unit volume makes [1–5]. The use of microencapsulated phase change materials (MPCM) is an efficient way to store thermal energy, and has mainly been used in energy storage systems and for heat transfer applications [6–12].

Microcapsules suspended in a fluid have a great potential for thermal energy storage and heat transfer fluid applications [7–12]. Such suspensions can solve the problem with low thermal conductivity of PCM, and improve the specific heat capacity of the fluid within the PCM melting temperature range [8–10]. The flow and heat transfer characteristics of the microcapsule suspensions, and the mechanical stability of microcapsules under high shear rates are important for the efficiency of the systems. The most utilized fluid for microcapsule suspensions is water [8–11]. Water has some obvious advantages, including high thermal conductivity and a large specific heat capacity. In addition, it is cheap and available. Previous studies on water-based microcapsule suspensions have mainly examined the effect of microcapsule concentration and temperature on the thermal performance and rheological properties of the suspensions. It has been shown that the thermal conductivity and the specific heat capacity decrease when the concentration is raised. The suspensions exhibit a Newtonian fluid behaviour at low concentrations and pseudoplastic behaviour at high concentrations, while the relative viscosity of the suspensions is temperature independent [9–12].

✉ Anna-Lena Kjøniksen
anna.l.kjoniksen@hiof.no

[1] Faculty of Engineering, Østfold University College, N-1757 Halden, Norway

[2] Department of Mathematical Sciences and Technology, Norwegian University of Life Sciences, N-1432 Ås, Norway

[3] Faculty of Chemistry, Biotechnology and Food Science, Norwegian University of Life Sciences, N-1432 Ås, Norway

[4] Department of Chemical Engineering, University of Castilla – La Mancha, 13004 Ciudad Real, Spain

[5] School of Pharmacy, University of Oslo, N-0316 Oslo, Norway

Published online: 04 April 2018

One of the main problems of water-based MPCM suspensions is the high rate of microcapsule floatation. To solve this problem, a small amount of surfactants or thickeners can be used for improving the stability of suspensions [9]. Another solution is to utilize a fluid with a higher viscosity, such as glycerol. Glycerol has higher viscosity than water, thereby providing more stable suspensions. Furthermore, glycerol has lower freezing point and higher boiling point than water [13]. Accordingly, glycerol with high thermal conductivity and large specific heat capacity is a very interesting alternative to water as a carrier fluid for microcapsule suspensions intended for applications as thermal energy storage and heat transfer media.

Another problem with MPCM suspension is the formation of agglomerates. Agglomeration is unwanted for applications as heat transfer fluids due to an increase in viscosity, which causes a higher power consumption for pumping. In addition, the agglomerates may lead to clogging of piping systems [14].

In this article, suspensions of microcapsules in glycerol were investigated. The microcapsules are composed of a shell of low-density polyethylene (LDPE) and ethylvinylacetate (EVA) copolymers, and a core of paraffin Rubitherm®RT27, abbreviated LDPE-EVA/RT27. The LDPE-EVA/RT27 is suitable for TES applications due to the high latent heat (100 J/g), a melting point around 27 °C and the lack of interactions with the surrounding environment [15]. The effects of the microcapsules on the thermal performance and the rheological properties were investigated.

Materials and methods

The microencapsulated phase change materials (MPCM) were made by a spray drying process [15]. The MPCM is composed of a paraffin Rubitherm®RT27 core coated with the LDPE-EVA (low-density polyethylene (LDPE) and ethylvinylacetate (EVA) copolymer) shell [15]. The surface morphology and the structure of the microcapsules were obtained by scanning electron microscopy (SEM) (FEI Quanta 200). The microcapsules size distribution was determined by laser light diffraction using a Malvern MasterSizer (Malvern Instruments Ltd., Malvern, Worcester, UK).

Suspensions of microencapsulated phase change materials were fabricated by dispensing different mass ratios of MPCM in glycerol at a room temperature. The mass concentration was varied from 0 to 30 wt.%.

Thermal properties of MPCM suspensions

A Mettler Toledo DSC822e fitted with a MultiSTAR HSS7 sensor, under an inert atmosphere at a heating rate of 5 °C/min and a Hot Disk Instrument TPS 2500S at a heating power of 20 mW were employed to determine the thermal properties of MPCM suspensions. The latent heat of MPCM suspensions were determined by DSC while The Hot Disk Instrument was utilized to evaluate the thermal conductivity and volumetric heat capacity of the MPCM suspensions at room temperature (≈ 20 °C). Finally, thermogravimetric analyses (TGA) (TA Instrument equipment model SDT Q600) was used to determine the thermal stability of MPCM.

Flow behaviour of MPCM suspensions

Rheological measurements were carried out using an Anton Paar MCR301 rheometer (Austria). The MPCM suspensions were tested using a CC27 bob/cop measuring system (cup diameter, 28.91 mm; bob diameter, 26.66 mm) mounted in a cylindrical Peltier for temperature control. A fresh sample was loaded into the measuring system. The sample was pre-sheared at shear rate of 50 s^{-1} for 5 min and rested for 5 min before any measurements were conducted. In order to investigate the reproducibility of the results, each measurement was repeated three times with fresh samples.

Flow curves were measured with a shear rate in the range of 10–500-10 s^{-1} at 10 °C, 20 °C (below the melting point of paraffin Rubitherm®RT27) and 40 °C, 50 °C (above the melting point of paraffin Rubitherm®RT27). The test was not performed at 30 °C to avoid the transition temperature of the melting process. The experimental data for the increasing shear rate curves were described by the Cross model (Eq.1) and the power law model (Eq. 2) [16]. The hysteresis areas between the increasing and decreasing shear rate curves were obtained using OriginPro 2016 Sr2.

The Cross model is usually used to describe the viscosity over a wide range of shear rates. The Cross model describes the suspension as a Newtonian fluid at low shear rates, and as a power law fluid at high shear rates:

$$\eta = \eta_\infty + (\eta_0 - \eta_\infty)\left(1 + \left(\frac{\dot{\gamma}}{\dot{\gamma}_0}\right)^2\right)^{\frac{n-1}{2}} \quad (1)$$

where η_∞, η_0, and n are the viscosity at an infinite shear rate, the zero shear rate viscosity and the dimensionless flow behaviour index, respectively. $\dot{\gamma}$ and $\dot{\gamma}_0$ are the shear rate and the critical shear rate where the fluid transits from Newtonian to power law behaviour, respectively. In order to avoid unreliable data due to over-parameterization of the fitting procedure, the number of fitting parameters was reduced by subtracting the temperature-dependent viscosity of glycerol from the measured viscosity values. The resulting reduced viscosity values were then fitted to Eq. 1, fixing η_∞ at zero. Although there are some deviation between the Cross model and the experimental data at low shear rates, the model gives a reasonably good fit to the data below the phase transition temperature of the paraffin core. Above the melting temperature of the paraffin core,

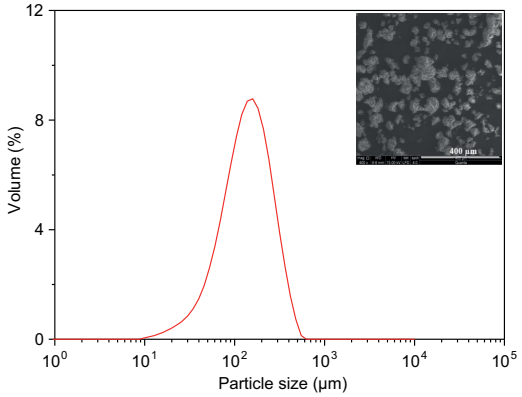

Fig. 1 The size (diameter) distribution and inserted SEM image of the microcapsules

the curves did not exhibit a Newtonian region in the considered shear rate range. Accordingly, at high temperatures Eq. 1 includes too many fitting parameters to achieve good fit of the data, and a simple power law behaviour (Eq. 2) was therefore used instead:

$$\eta = K\dot{\gamma}^{n-1} \tag{2}$$

where K is the consistency index.

Results and discussion

Size distribution

Before examining the rheological properties of the MPCM suspensions, it is important to know the size distribution of the microcapsules. Figure 1 illustrates that the particle size distribution (PSD) of the microcapsules are in the range of 10–550 μm with a median value of 170 μm (50% in the cumulative distribution). The inset plot in Fig. 1 shows a SEM image of the microcapsules, where the diameters of the single microcapsules is found to be about 3–10 μm. The much larger sizes observed in the particle size distribution indicates that the microcapsules form agglomerated structures.

Thermal properties

All MPCM samples exhibited two distinct DSC peaks (Fig. 2a). The main peak represents the melting range temperature of the paraffin Rubitherm®RT27 core. The minor peak (0–5 °C) to the left of the main peak corresponds to the melting of water, which is present in the supplied Rubitherm®RT27. As can be seen from Fig. 2b, the latent heat of the suspensions is directly proportional to the MPCM concentration, confirming that the main peak is due to the melting of the paraffin. Addition of 30 wt.% of MPCM gives a latent heat of approximately 27 J/g.

The thermal conductivity and the specific heat capacity of the MPCM suspensions were determined using the transient plane source method (TPS). The experimental error was estimated by comparing the experimental thermal conductivity and specific heat capacity with reference values of pure glycerol. Figure 3 shows that the experimental thermal conductivity and specific heat capacity of pure glycerol are 0.300 ± 0.004 W/(m·K) (reference value of 0.283 W/(m·K) [17]) and 2126 ± 103 J/(kg·K) (reference value of 2323 J/(kg·K) [17]), respectively. Accordingly, the experimental errors of the method are about 6% for the thermal conductivity and 9% for the specific heat capacity.

Figure 3 shows the effect of MPCM addition on the thermal conductivity and specific heat capacity of the MPCM suspensions. The addition of MPCM causes a reduction of the thermal conductivity of the microcapsule suspensions (Fig. 3a). This is due to the lower thermal conductivity of the microcapsules compared to glycerol. The thermal conductivity of the paraffin Rubitherm®RT27 and polymer LDPE-EVA shell are approximately 0.2 W/(m·K) and 0.13–0.34 W/(m·K) [15], respectively. The thermal conductivity of glycerol is approximately 0.283 W/(m·K) [17]. The specific heat capacity of the MPCM suspensions increases slightly when the

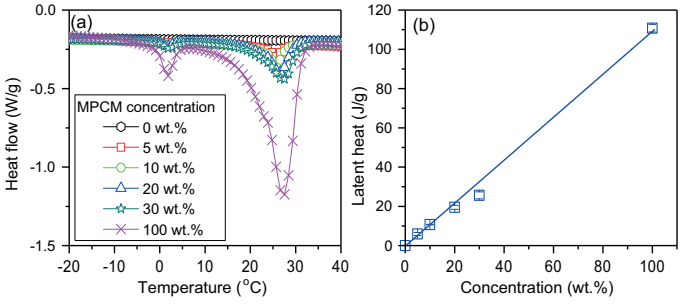

Fig. 2 **a** The specific heat capacity and **b** the latent heat of the MPCM suspensions at different concentrations of microcapsules

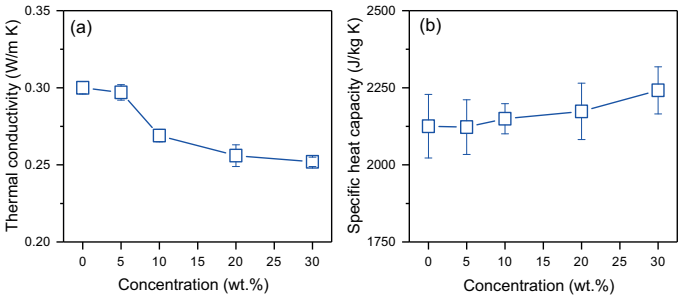

Fig. 3 **a** The thermal conductivity and **b** the specific heat capacity of MPCM suspensions

concentration of MPCM is raised (Fig. 3b). This is due to the higher specific heat capacity of microcapsules at 20 °C compared to that of glycerol [17, 18].

The thermogravimetric analysis of the microcapsules is shown in Fig. 4. There are two regions of weight loss in the thermal curve. The first region is between 150 and 250 °C, and is attributed to the evaporation of the paraffin Rubitherm®RT27. The second step is between 400 and 480 °C and is due to the degradation of the LDPE-EVA polymer shell [15, 19].

The thermal properties of the MPCM suspensions indicate that LDPE-EVA/RT27 is stable in the studied temperature range. Accordingly, the microcapsules are suited for integration into passive buildings, and the suspensions are interesting for heat transfer applications.

Flow behaviour

Figure 5 shows the influence of temperature and shear rate on the viscosity of 20 wt.% microcapsule suspensions. The viscosity below the melting point of the paraffin core material (< 27 °C) exhibits a clear Newtonian region at low shear rates (10–100 s^{-1}) followed by a power law region at high shear rates. However, above the melting point of paraffin, the Newtonian region is not reached within the considered shear rate range, and only the power law region is observed. Therefore, the flow curve of the MPCM suspensions was fitted to the Cross model (Eq. 1) below the melting point of paraffin, while the power law model (Eq. 2) was employed above the melting point.

Figure 6 shows the flow behaviour index (n) obtained by fitting the experimental data to the power law model (Eq. 2) (above the melting point) and the Cross model (Eq. 1) (below the melting point) as a function of concentration and temperature. High values of R^2 (0.98–1 for the Cross model and 0.99–1 for the power law model) reveals that both models are suitable for describing the flow behaviour of the MPCM suspensions in the considered temperature regions. The flow behaviour index n is less than one for all MPCM suspensions (0.21–0.88), illustrating that the samples exhibit strong and moderate shear-thinning behaviour. If the suspended microcapsules were present as single unagglomerated particles, a Newtonian behaviour without any shear-thinning effects would be expected. Accordingly, the shear-thinning behaviour suggests the presence of agglomerates that are broken down by the shear forces.

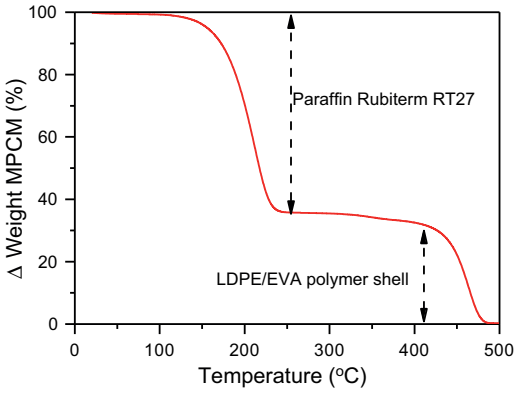

Fig. 4 Thermogravimetric curve of the microcapsules

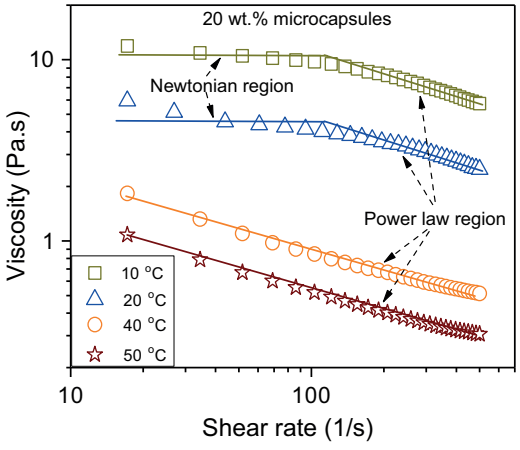

Fig. 5 The effect of temperature and shear rate on the viscosity of 20 wt.% MPCM suspensions

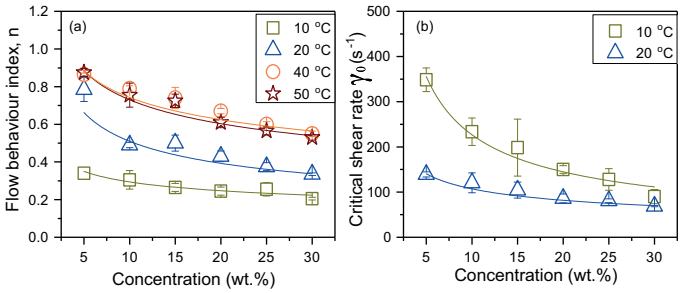

Fig. 6 **a** The flow behaviour index n and **b** the critical shear rate $\dot{\gamma}_0$ from power law and Cross models as a function of MPCM concentration and temperature

The flow behaviour index, n, decreases when the concentration is raised. This indicates a stronger shear thinning at higher concentrations, where there are more agglomerates that can be broken down by the shear forces. This is consistent with previous studies of other suspensions [20, 21]. As can be seen from Fig. 6a, the flow behaviour index, n, increases as the temperature is raised up to 40 °C, after which the temperature dependency is very small. Figure 6b shows the critical shear rate $\dot{\gamma}_0$ for the MPCM suspensions below the melting point of paraffin. The critical shear rate $\dot{\gamma}_0$ was found to decrease when the concentration of microcapsules was raised. This indicates that the agglomerates start to break down at lower shear rates when the concentration is increased. This suggests that the larger agglomerates present at high concentrations can be easier broken down compared to the smaller agglomerates at lower concentrations [22]. The critical shear rate $\dot{\gamma}_0$ decreases when the temperature is increased, and at high temperatures, the critical shear rate $\dot{\gamma}_0$ is below the considered shear rate range. Interestingly, both n and $\dot{\gamma}_0$ seem to be correlated with the melting point of paraffin. Until all paraffin has melted, n increases with temperature, while it is temperature independent when the sample is heated further. Below the melting point, $\dot{\gamma}_0$ becomes smaller with increasing temperature, while no Newtonian region is observed in the considered shear rate range above the melting point of paraffin. If all PCM were encapsulated in the microcapsules, we would not expect a distinct transition of the properties of the MPCM suspensions at the melting temperature of paraffin. Accordingly, non-encapsulated paraffin is probably causing this transition. Non-encapsulated paraffin can also contribute to the observed agglomeration of the microcapsules. When the sample is heated, paraffin becomes softer, and the associative forces within the agglomerates are reduced. This leads to higher values of n (reduced shear thinning), and shifts $\dot{\gamma}_0$ towards lower values (less force is needed to break the agglomerates apart). After the paraffin has melted, the agglomerates are easily disrupted and can be broken apart even at low shear rates, which is why no Newtonian plateau is observed at high temperatures.

Since the rheological data suggest the presence of non-encapsulated paraffin, an additional test was conducted to test this hypothesis. Microcapsules were weighed (0.5 g), and placed on an oil absorbing paper at room temperature. The paper was transferred to an oven at 40 °C for 10 min. Figure 7 shows the images of the absorbing paper with the microcapsules before and after the test. The change of colour and gloss of the paper indicates the presence of non-encapsulated paraffin. The amount of non-encapsulated paraffin was determined by weighting the absorbing paper before and after heating at 40 °C. According to this test, the MPCM contains approximately 2.5 wt.% non-encapsulated paraffin. Since the microcapsules utilized in this test were not subjected

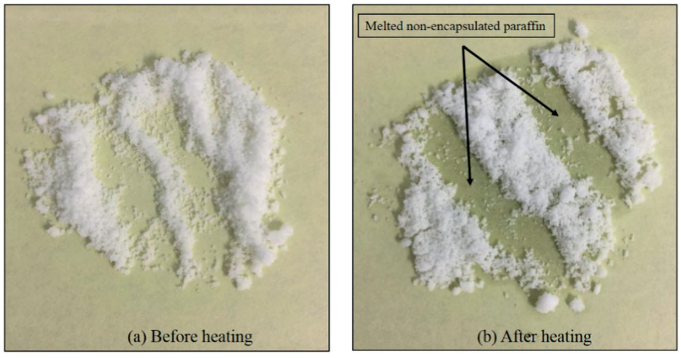

Fig. 7 Images of an absorbing paper with (**a**) microcapsules before heating to 40 °C and **b** after heating to 40 °C for 10 min

to disruptive forces, the non-encapsulated PCM is probably left from the synthesis process. The non-encapsulated paraffin will probably contribute to the observed agglomeration of the microcapsules. A disadvantage of free PCM is its tendency to clog distribution pipes for PCM heat transfer systems [23, 24].

The normalized viscosity at 500 s^{-1} of the MPCM suspensions is plotted in Fig. 8. The viscosity of all MPCM suspensions decreases as the temperature is raised. The reduction of the normalized viscosity at elevated temperatures occurs because the kinetic energy of the microcapsules increases, leading to breakage of the inter-microcapsule bonds. This observation is supported by Nguyen et al. [25] and Fei Duan [26] studying water-based nanofluids. Furthermore, when the sample is heated, the non-encapsulated paraffin becomes softer, and the associative forces within the agglomerates are reduced, leading to a decrease in the viscosity of the MPCM suspensions.

The flow curves of 20 wt.% of MPCM suspensions at different temperatures is shown in Fig. 9a. A hysteresis effect can be seen when the shear rate is increased and then decreased. When a sample is subjected to increasing shear rates followed by decreasing shear rates, the presence of a hysteresis area between the increasing curve and decreasing curve indicates that the flow of the sample is exhibiting a time-dependent behaviour [27]. The hysteresis effect suggests that the build-up of agglomerates when the shear rate is reduced is a slower process than the breakage of agglomerates at increasing shear rates. According to Roopa et al. [28] the loop area designates the energy required to break down the structure that is not recovered during the experimental period. The hysteresis area of the MPCM suspensions at different temperatures and concentrations are summarized in Fig. 9b.

Both the temperature and the concentration have a significant effect on the hysteresis loop area of the MPCM suspensions. The hysteresis area decreases as the temperature is increased from 10 to 50 °C at a constant concentration. The hysteresis area is much smaller at temperatures above the melting point of paraffin (40 and 50 °C) than for the lower temperatures. The hysteresis area of the MPCM suspensions are probably caused by the shear-induced break up of agglomerates, which need time to recover after being exposed to high shear forces [28]. Similar observations have been reported for hydrocolloid suspensions previously [29, 30]. Accordingly, the hysteresis effect is diminished when the non-encapsulated paraffin is melted, thereby reducing its effect on the agglomeration. The hysteresis area increases as the concentration is raised, which is probably due to the higher number of agglomerates in the sample.

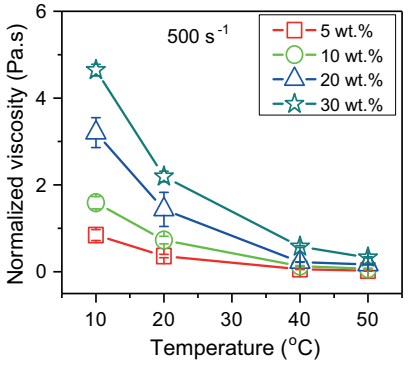

Fig. 8 Effect of temperature on the viscosity measured at a shear rate of 500 s^{-1}. Normalized by subtracting the viscosity of the solvent at the same temperatures

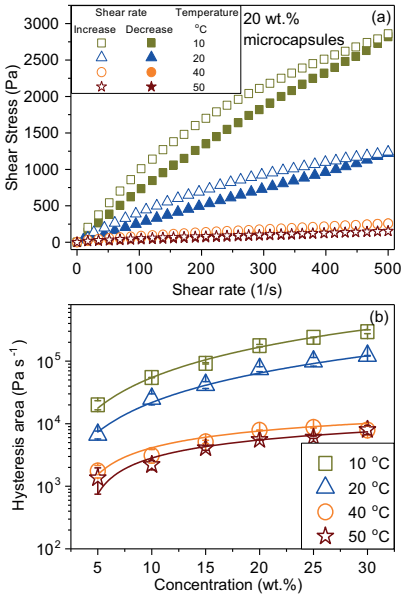

Fig. 9 **a** Flow curves of the MPCM suspensions measured with increasing and decreasing shear rates at different temperatures at a MPCM concentration of 20 wt.%. **b** The hysteresis area of the MPCM suspensions as function of concentration and temperature

Conclusions

The rheological and thermal properties of suspensions of microcapsules containing phase change materials (MPCM) were investigated. The small diameter of single microcapsules (3–10 μm), the high latent heat (100 J/g) and high thermal stability (> 140 °C) of microcapsules are satisfactory for utilization in thermal energy storage and heat transfer applications. The thermal conductivity of the MPCM suspensions decreased with increasing MPCM concentration below the PCM melting point, while the specific heat capacity of the MPCM suspensions increased with the MPCM concentration. The latent heat of the MPCM suspensions increased to approximately 27 J/g

by adding a 30 wt.% of MPCM, significantly improving the total heat storage capacity of the MPCM suspensions within the melting range of the phase change material (PCM).

Suspensions of microencapsulated phase change materials were found to exhibit shear-thinning behaviour. Interestingly, the rheological properties of the MPCM suspensions exhibited a transition around the melting temperature of the PCM. The presence of non-encapsulated PCM located outside the microcapsules was found to be the cause of this transition. The non-encapsulated PCM causes agglomeration of the microcapsules. Such structures will cause poor stability of MPCM suspensions and higher power consumption for pumping due to increased viscosity. When the PCM is melted, the binding force within the agglomerates becomes weaker. Accordingly, the hysteresis area of the flow curves decrease as the temperature is raised and it is significantly diminished above the PCM melting point. The Cross model was utilized to describe the rheological properties of the MPCM suspensions below the melting point of PCM, while a power law was used above the melting point due to the absence of a Newtonian region. The shear-thinning behaviour of the MPCM suspensions become stronger at higher MPCM concentrations and weaker at higher temperatures. The critical shear rate to break down the structure of the MPCM suspensions decreased when the temperature and concentration were increased.

Agglomerates may lead to clogging of piping systems. Improved microcapsules with reduced tendency for agglomerations and good mechanical properties would be interesting for further studies. In order to achieve such systems, it is important to avoid non-encapsulated PCM.

Acknowledgements We gratefully acknowledge funding from the Research Council of Norway, project number 238198. The authors gratefully acknowledge Prof. Lars Wadso, Bengt Nilsson and Stefan Backe at Lund University for their assistance with laboratory work.

Compliance with ethical standards

Conflict of interest The authors declare that they have no conflict of interest.

References

1. Demirbas MF (2006) Thermal energy storage and phase change materials: an overview. Energy Sources Part B Econ Plan Policy 1:85–95
2. Ad G, Cabeza LF (2015) Phase change materials and thermal energy storage for buildings. Energ Buildings 103:414–419
3. Sharma A, Tyagi VV, Chen CR, Buddhi D (2009) Review on thermal energy storage with phase change materials and applications. Renew Sust Energ Rev 13:318–345
4. Lachheba M, Karkri M, Nasrallah SB (2015) Development and thermal characterization of an innovative gypsum-based composite incorporating phase change material asbuilding energy storage system. Energ Buildings 107:93–102
5. Pomianowskia M, Heiselberg P, Zhang Y (2013) Review of thermal energy storage technologies based on PCM application in buildings. Energ Buildings 67:56–69
6. Buscombe A, Wu M (2013) A review of PCM's thermal performance within lightweight construction. Int J Eng Pract Res (IJEPR) 2:174–177
7. Wang X, Niu J, Yi Li XW, Chen B, Zeng R, Song Q, Zhang Y (2007) Flow and heat transfer behaviors of phase change material slurries in a horizontal circular tube. Int J Heat Mass Transf 50: 2480–2491
8. Chen L, Wang T, Zhao Y, Zhang X-R (2014) Characterization of thermal and hydrodynamic properties for microencapsulated phase change slurry (MPCS). Energy Convers Manag 79:317–333
9. Zhang GH, Zhao CY (2011) Thermal and rheological properties of microencapsulated phase change materials. Renew Energy 36: 2959–2966
10. Alvarado JL, Marsh C, Sohn C, Phetteplace G, Newell T (2007) Thermal performance of microencapsulated phase change material slurry in turbulent flow under constant heat flux. Int J Heat Mass Transf 50:1938–1952
11. Yamagishi Y, Takeuchi H, Pyatenko AT, Kayukawa N (1999) Characteristics of microencapsulated PCM slurry as a heat-transfer fluid. AIChE 45:696–707
12. Pollerberg C, Dotsch C (2006) Phase changing slurries in cooling and cold supply networks. In: 10th International Symposium on Disctrict Heating and Cooling, Hannover (Germany)
13. Melinder Å (2007) Thermophysical properties of aqueous solutions used as secondary working fluids. PhD Dissertation, Royal Institute of Technology
14. Dhiman N, Shah J, Agonafer D, Kannan N, Hoverson J, Kaler M (2013) Application of phase change material in sustainable cooling of data centers. In: ASME 2013 International Mechanical Engineering Congress and Exposition, San Diego, CA. American Society of Mechanical Engineers (ASME). https://doi.org/10.1115/IMECE2013-66515
15. Borreguero AM, Valverde JL, Rodríguez JF, Barber AH, Cubillo JJ, Carmona M (2011) Synthesis and characterization of microcapsules containing Rubitherm®RT27 obtained by spray drying. Chem Eng J 166:384–390
16. Macosco CW (1994) Rheology: principles, measurements, and applications. Wiley–VCH, New York
17. Green DW, Perry RH (1997) Perry's chemical engineers' handbook. Mc Graw Hill, Sydney, Australia
18. Cao VD, Pilehvar S, Salas-Bringas C, Szczotok AM, Rodriguez JF, Carmona M, Al-Manasir N, Kjøniksen A-L (2017) Microencapsulated phase change materials for enhancing the thermal performance of Portland cement concrete and geopolymer concrete for passive building applications. Energy Convers Manag 133: 56–66
19. Kayacan I, Dogan OM (2008) Pyrolysis of low and high density polyethylene. Part I: non-isothermal pyrolysis kinetics. Energy Sources 30:385–391
20. Cabaleiro D, Pastoriza-Gallego MJ, Gracia-Fernández C, Piñeiro MM, Lugo L (2013) Rheological and volumetric properties of TiO_2-ethylene glycol nanofluids. Nanoscale Res Lett 8:286–299
21. Behzadfar E, Abdolrasouli MH, Sharif F, Nazockdast H (2009) Effect of solid loading and aggregate size on the rheological behavior of pdms/calcium carbonate suspensions. Braz J Chem Eng 26: 713–721

22. Figoni PI, Shoemaker CF (1983) Characterization of time dependent flow properties of mayonnaise under steady shear. J Texture Stud 14:431–442
23. Eunsoo C, Cho Y, Lorsch HG (1994) Forced convection heat transfer with phase-change-material slurries: turbulent flow in a circular tube. Heat Mass Transf 37:207–215
24. Choi E, Cho YI, Lorsch HG (1991) Effects of emulsifier on particle size of a phase change material in a mixture with water. Int Commun Heat Mass Transf 18:759–766
25. Nguyen CT, Desgranges F, Roy G, Galanis N, Mare T, Boucher S, Mintsa HA (2007) Temperature and particle-size dependent viscosity data for water-based nanofluids—hysteresis phenomenon. Int J Heat Fluid Flow 28:1492–1506
26. Duan F (2012) Thermal property measurement of Al2O3-water nanofluids. In: Hashim DA (ed) Smart nanoparticles technology. InTech, China, pp 335–356
27. Tárrega A, Durán L, Costell E (2004) Flor behaviour of semi-solid dairy desserts. Effect of temperature. Int Dairy J 14:345–353
28. Roopa BS, Bhattacharya S (2009) Characterisation and modelling of time-independent and time-dependent flow behaviour of sodium alginate dispersions. Int J Food Sci Technol 44:2583–2589. https://doi.org/10.1111/j.1365-2621.2009.02088.x
29. Zhang LM, Kong T, Hui PS (2007) Semi-dilute solutions of hydroxypropyl guar gum: viscosity behaviour and thixotropic properties. J Sci Food Agric 87:684–688. https://doi.org/10.1002/jsfa.2769
30. Koocheki A, Razavi SMA (2009) Effect of concentration and temperature on flow properties of Alyssum homolocarpum seed gum solutions: assessment of time dependency and thixotropy. Food Biophys 4:353–364. https://doi.org/10.1007/s11483-009-9134-7

Paper II

Time-dependent structural breakdown of microencapsulated phase change materials suspensions.

Vinh Duy Cao, Carlos Salas-Bringas, Reidar Barfod Schüller, Anna M. Szczotok, Anna-Lena Kjøniksen.

Journal of Dispersion Science and Technology **2018**, in press.

Time-dependent structural breakdown of microencapsulated phase change materials suspensions

Vinh Duy Cao[1, 2], Carlos Salas-Bringas[2], Reidar Barfod Schüller[3], Anna M. Szczotok[1, 4] and Anna-Lena Kjøniksen[1*]

[1]Faculty of Engineering, Østfold University College, N-1757 Halden, Norway

[2]Department of Mathematical Sciences and Technology, Norwegian University of Life Sciences, N-1432 Ås, Norway

[3]Department of Chemistry, Biotechnology and Food Science, Norwegian University of Life Sciences, N-1432 Ås, Norway

[4]Department of Chemical Engineering, University of Castilla – La Mancha, 13004 Ciudad Real, Spain

[*]Corresponding author: anna.l.kjoniksen@hiof.no

Abstract

Microencapsulated phase change materials (MPCM) suspensions are multi-phase heat transfer fluids which exploit the latent heat of phase change materials. The effect of MPCM on the rheological properties of suspensions of microcapsules in glycerol were investigated to explore the suitability of the suspensions as a pumpable heat transfer fluid. Three different rheological models were utilized to characterize the time-dependent structural breakdown of the suspensions, and the second-order structural kinetic model was found to give a better fit to the experimental data than the Weltman and Figoni-Shoemaker models. The MPCM form agglomerates, which are disrupted by shear forces. The breakdown of the agglomerated structures was most pronounced at high shear rates where the microcapsules are subjected to stronger disruptive forces. More agglomerates are present at higher concentrations, which causes a stronger breakdown of the agglomerated structures when the concentration is raised.

The time-dependent structural breakdown of MPCM suspensions plays an important role for improving the efficiency of heat transfer liquids based on such materials.

Keywords: Microencapsulated phase change materials, Rheology, The second-order structural kinetic model, Time-dependent behaviour.

Introduction

Suspensions of microcapsules in heat transfer fluids have great potential for thermal energy storage and heat transfer fluid applications [1-6]. Microencapsulated phase change materials (MPCM) suspensions are multi-phase heat transfer fluids which exploit the latent heat of phase change materials. They are more efficient heat carriers than single-phase fluids. An increase in MPCM concentration improves the heat capacity and energy storage density during the phase change temperature range. Accordingly, reduced suspension flow rates can be utilized, leading to a lower pumping power consumption. However, this is counteracted by the MPCM induced viscosity increase of the suspensions, which raises the power consumption for pumping. It is therefore important to examine the rheological properties of the MPCM suspensions. Most studies of MPCM suspensions are only considering Newtonian liquids [2-5]. However, many such systems exhibit non-Newtonian and time-dependent behavior.

Water is the most utilized fluid for microcapsule suspensions due to its availability, cheap price, high thermal conductivity and large specific heat capacity [2-7]. The main problems of water based MPCM suspensions are the high floatation rate and the restricted usable temperature range. In addition, agglomeration of the microcapsules can cause problems such as increased viscosities. The agglomeration of the microcapsules can be reduced by utilizing a reasonable microcapsule concentration[8] and by using surfactants[3, 6]. Flotation can be adverted by using smaller microcapsules[8] and by balancing the density of the microcapsules and the carrier medium. In addition, a fluid with a higher viscosity, such as glycerol, can also reduce flotation. Glycerol exhibits a high thermal conductivity and large specific heat capacity,

and a lower freezing point and higher boiling point than water. This can extend the usable temperature range. However, the main drawback of utilizing glycerol as a carrier fluid is the higher viscosity, which increases the power consumption of the pumping process. It is therefore interesting to investigate the effect of MPCM on the rheological properties of glycerol suspensions.

In this study, the time-dependent structural breakdown of microcapsule suspensions in glycerol under the influence of a steady shear rate was investigated. The time-dependent behaviour of the MPCM suspensions were fitted to three different models in order to find which model is best suited to describe the experimental data (the Weltman model [9], the Figoni & Shoemaker model [10] and the second-order structural kinetic model [11, 12]). The investigation provide valuable rheological information which can be used to minimize the effect of MPCM on the viscosity increase of the suspensions. This can help enhancing the energy efficiency of this new type MPCM suspension.

Materials and methods

The microencapsulated phase change materials (MPCM) was made by a spray drying process [13]. The MPCM is composed of a paraffin Rubitherm®RT27 core coated with a LDPE-EVA (low density polyethylene (LDPE) and ethylvinylacetate (EVA) copolymer) shell [13]. The diameters of the single microcapsules are about 3-10 μm (SEM image-Figure 1a). However, the microcapsules are prone to agglomeration with an agglomerated particle size distribution (Malvern MasterSizer-UK) in the range of 10-550 μm with a median value of 170 μm (50% in the cumulative distribution) (Figure 1b).

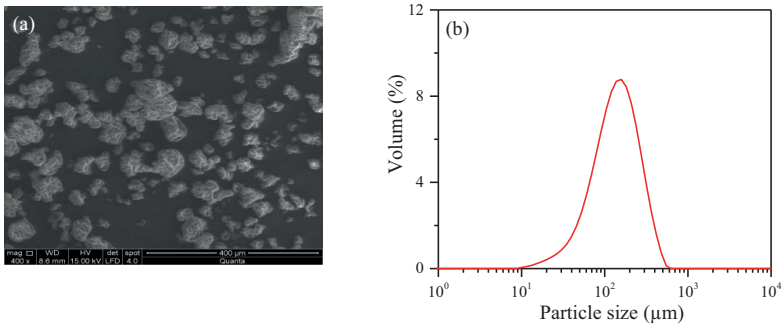

Figure 1. (a) SEM image and (b) size distribution of LDPE-EVA/RT27 microcapsules.

The LDPE-EVA/RT27 has a high latent heat of 110 J/g and a melting point of 27 °C. MPCM suspensions were fabricated by dispensing different mass ratios of MPCM in glycerol. The mass concentration was varied from 0 to 30 wt.%.

Thermal properties of MPCM suspensions

The latent heat of MPCM suspension was determined using a Mettler Toledo DSC822e fitted with a MultiSTAR HSS7 sensor, under an inert atmosphere. The heating rate for this process was set at 5 °C/min. The latent heat of the MPCM suspensions were determined over the range of -20 ℃ to 40 ℃.

Time-dependent structural breakdown of MPCM suspensions at constant shear

Time-dependent structural breakdown of MPCM suspension were carried out using an Anton Paar MCR301 rheometer (Austria). The MPCM suspensions were tested using a CC27 bob/cop measuring system (cup diameter: 28.91 mm; bob diameter: 26.66 mm) mounted in a cylindrical Peltier system for temperature control. A fresh sample was loaded into the measuring system, pre-sheared at shear rate of 50 s^{-1} for 5 min, and rested for 5 min before any measurements were conducted. A pre-test (data not shown) confirmed that a 5 min resting time was long enough to reach a steady state.

The time-dependent behaviour of the MPCM suspensions were investigated during a period of 30 min at 20 °C with a constant shear rate of 100, 300, 500 and 700 s^{-1}. In order to investigate

the reproducibility of the results, each measurement was repeated three times with fresh samples. Experimental data were fitted to three different models: the Weltman model, the Figoni-Shoemaker model and the second-order structural kinetic model.

The Weltman model (Eq. 1) is used to determine the logarithmic decrease of the shear stress with shearing time. The Weltman model includes two main parameters to estimate the time-dependent behaviour of suspensions. σ_0 represents the initial shear stress needed to start degrading the structure of the material. The quantity of structure degradation during shearing is estimated by the time coefficient of breakdown (B). This also indicates the reduced rate of shear stress from the initial value to the final equilibrium value [14].

$$\sigma(t) = \sigma_0 - B\ln(t) \quad (Eq.\,1)$$

The Figoni-Shoemaker model (Eq.2) describes the time-dependent behavior in a kinetic constant of breakdown of the internal structure of the MPCM suspensions. This model allows the quantification of the remaining structure and the structure breakdown by the parameters σ_e and $(\sigma_0 - \sigma_e)$, respectively.

$$\sigma_t = \sigma_e + (\sigma_0 - \sigma_e)\exp(-kt) \quad (Eq.\,2)$$

where k is the kinetic constant of structural breakdown.

Finally, the second-order structural kinetic model assumes that the change of structure is associated with breakdown of the internal fluid structure during the shearing process. The kinetics of the structured state to non-structured state process will define the structural breakdown rate during shearing process [12, 15].

$$\left(\frac{\eta - \eta_e}{\eta_0 - \eta_e}\right)^{1-m} = (m-1)k_s + 1 \quad (Eq.\,3)$$

where η_0 is the initial viscosity at $t = 0$ (structured state), η_e is the equilibrium viscosity as $t \to \infty$ (non-structured state), m is the order of the structure breakdown reaction, m=2 for second-order structural kinetic model [12].

The model selection for characterizing the time-dependent behaviour of the MPCM suspensions was evaluated using the determination coefficient R^2 and the normalized root mean squared error (NRMSE).

Results and Discussion

Figure 2 shows the DSC thermograms of the MPCM suspensions at different concentrations of MPCM. There are two distinct DSC peaks inFigure 3a: the main peak (10-40°C) which represents the melting range of the paraffin Rubitherm®RT27 core, and a minor peak (0-5 °C) which corresponds to the melting of water. Figure 2b illustrates the latent heat of the MPCM suspensions. As expected, the latent heat of the suspensions is directly proportional to the MPCM concentration. After adding 30 wt.% of MPCM, the latent heat is approximately 27 J/g.

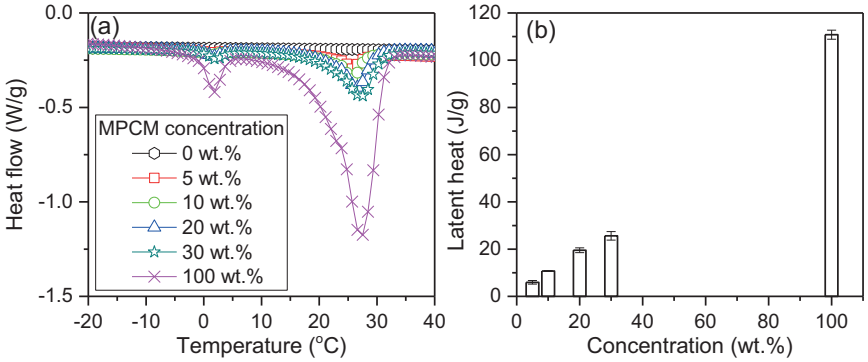

Figure 2. (a) The heat flow as function of temperature and (b) the latent heat of the MPCM suspensions at different concentrations of microcapsules.

The time-dependent behaviour of the MPCM suspensions were studied at constant shear rates of 100, 300, 500 and 700 s^{-1} at 20 °C for a period of 30 min at different microcapsule concentrations. The experimental data was fitted to three commonly used models (the second-order structural kinetic model, the Weltman model and the Figoni-Shoemaker model) to

investigate which of these models describes the time-dependent behaviour of the MPCM suspensions best.

Figure 3 illustrates that the experimental data fits reasonably well to the Weltman and Figoni-Shoemaker models, although there are some clear deviations at short times for some of the samples, especially for high concentrations and at high shear rates. As can be seen from Figure 4, the parameters σ_0 and B from the Weltman model exhibit higher values with increasing shear rates and concentrations. σ_0 is related to the shear stress at zero time, and becomes higher as the concentration is increased due to the higher viscosity of the samples, and will naturally increase at higher shear rates. When the microcapsule suspensions are subjected to a constant shear rate during the 30 min rheological experiment, the microcapsule agglomerates are gradually broken down by the shear forces. This structure break-down is quantified by the parameter B. As expected, more of the agglomerates are broken down when the samples are subjected to higher shear rates (higher values of B). In addition, B increases when the microcapsule concentration is raised. This is due to the enhanced tendency to form aggregates at higher concentrations, Accordingly, there are more agglomerates to break down, which causes higher values of B. Similar trends were also reported by Durairaj et al. [16].

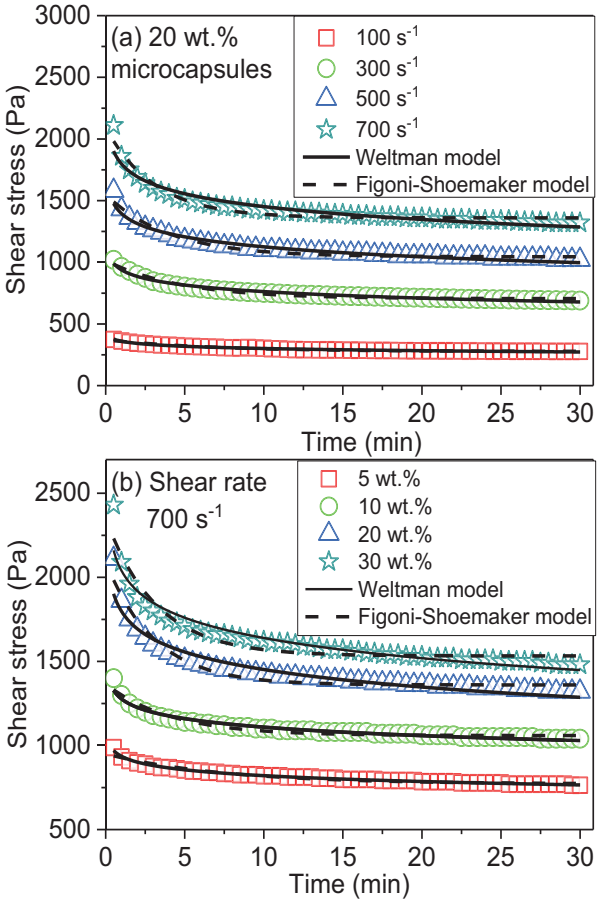

Figure 3. Shear stress at (a) different shear rates, MPCM concentration 20 wt.%, and (b) different concentrations, shear rate 700 s^{-1} as a function of shearing time at 20 °C. The points are experimental values. The solid and dashed lines show the fitted values according to the Weltman model (Eq.1) and the Figoni-Shoemaker model (Eq.2), respectively.

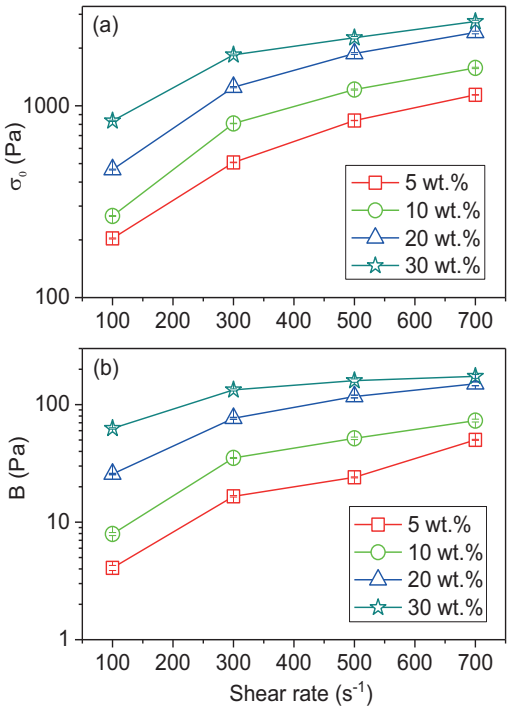

Figure 4. Rheological parameters of MPCM suspensions as a function of shear rates and concentration obtained by the Weltman model (Eq.1) at 20 °C, (a) σ_0 and (b) B.

Figure 5 shows the parameters from the fits to the Figoni-Shoemaker model, where all parameters increase when the shear rates and concentrations are raised. The initial shear stress (σ_0) (Figure 5a) have values close to that obtained from the Weltman model (Figure 4a). The equilibrium shear stress (σ_e) (Figure 5b) increases with concentration due to the viscosity increase caused by more microcapsules in the suspension. The quantity of structure breakdown ($\sigma_0 - \sigma_e$) (Figure 5c) becomes higher when the microcapsule concentration is raised, since there are more aggregates present that can be broken down by the shear stress. In addition, higher shear rates breaks down more of the aggregates. The kinetic constant of structural breakdown (k) illustrates how fast the stress of the MPCM suspensions reaches equilibrium under a constant shear. As can be seen from Figure 5d, the systems are approaching equilibrium

conditions faster at higher shear rates, where the agglomerates are broken down more quickly. This effect has also been reported previously for other systems [14]. It is interesting that an increasing concentration of the microcapsules also causes a faster approach to the equilibrium values. It is possible that the closer proximity of the agglomerates to each other speed up the process due to more frequent collisions between the agglomerated structures.

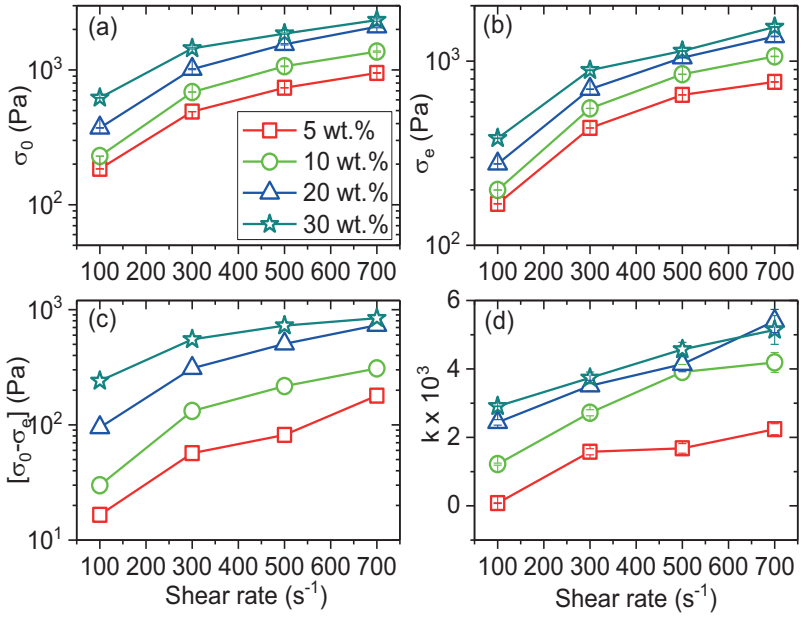

Figure 5. Rheological parameters of MPCM suspensions as a function of shear rates and concentration obtained by the Figoni-Shoemaker Model (Eq.2) at 20 °C, (a) σ_0, (b) σ_e, (c) [σ_0 – σ_e] and (d) k.

The rate constant (k_s), of the second-order structural kinetic model (Eq.3) probes the kinetics of the breakdown of structures in the liquid, while the ratio of initial to equilibrium viscosity (η_0/η_e) is related to the extent of structural decay due to the shear forces [12, 15, 17]. Figure 6 shows the fitted data curves of the MPCM suspensions using the second-order structural kinetic model. The model seems to fit well with the experimental data at all conditions. At a constant

shear rate, the viscosity decreases drastically with time in the first 5 min, before approaching a plateau region after approximately 15 min. This illustrates that the MPCM agglomerates are disrupted by the shear forces. Hammadi et al. [18] and Mallik et al. [19] observed similar trends for clays suspension and solder paste suspensions, respectively.

The viscosity decays more rapidly toward an equilibrium viscosity when the shear rates is raised (Figure 6a), illustrating that high shear rates accelerate the breakdown of the MPCM agglomerates. In addition, the rate constant (k_s) becomes higher with increasing shear rate and concentration (Figure 7c), revealing that the degradation rate of MPCM suspensions increases with increasing shear rates and concentrations. This is analogous to what was observed for he kinetic constant of structural breakdown (k) in the Figoni-Shoemaker model (Figure 5d).

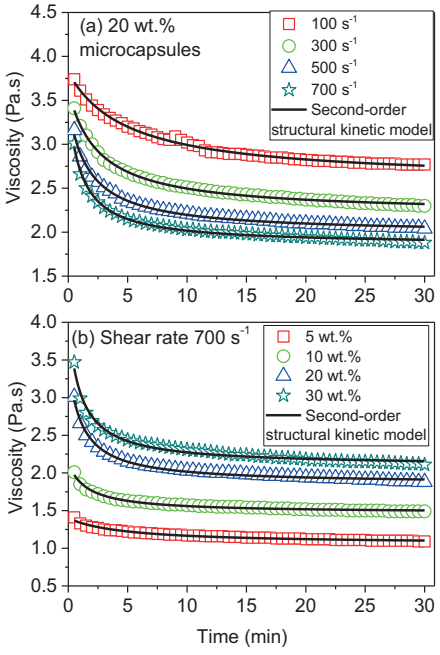

Figure 6. Viscosity at (a) different shear rates, MPCM concentration 20 wt.%, and (b) different concentration, shear rate 700 s^{-1} as a function of shearing time at 20 °C. The points are

experimental values. The solid lines show the fitted values according to the second-order structural kinetic model (Eq.3).

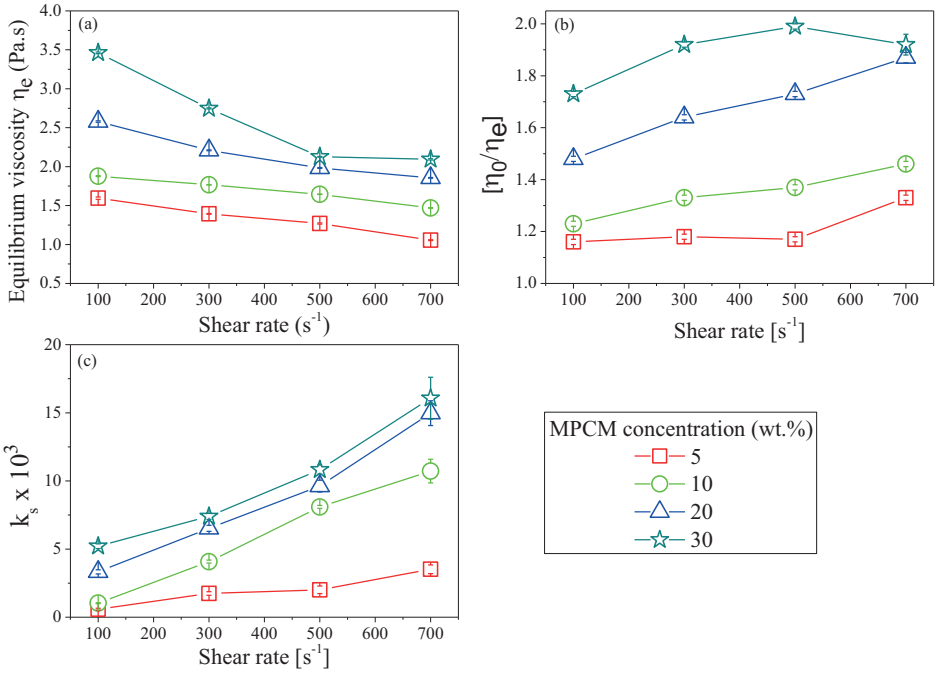

Figure 7. Rheological parameters of MPCM suspensions as the function of shear rates and concentration obtained by the Second-order structural kinetic model (Eq.3) at 20 °C, (a) Equilibrium viscosity η_e, (b) $[\eta_0/\eta_e]$ and (c) k_s.

The equilibrium viscosity (η_e) in Figure 7a illustrates the viscosity at long times where the agglomerates are broken down by the applied shear rate. As expected, the equilibrium viscosity becomes higher when the MPCM concentration increases due to the presence of more particles. When the shear rate is raised, η_e decreases since higher shear forces can break the agglomerates down to smaller structures. This illustrates the importance of avoiding large agglomerates for applications where a low viscosity fluid is preferred.

Figure 7b shows that the amount of structural breakdown (η_0/η_e) rises when the shear rate and the concentration are increased. Breakdown of flocculates/agglomerates and orientation or

deformation of suspended solid structures during the shearing process can cause a structural breakdown of suspensions [16, 20]. When shear forces are applied to the suspensions, the agglomerates can be broken apart by hydrodynamic shear stresses (deflocculating effect), and structures can be built up by the increased amount of collisions induced by the shear (flocculating effect) [21]. A balance of these two effects governs the breakdown process. At low shear rates, the forces are not large enough to break apart the agglomerated structures, and the flocculating effect dominates. At high shear rates the deflocculating effect is strong while the re-association rate is expected to be low, resulting in a significant viscosity decrease [19, 22]. As can be seen from Figure 3 and Figure 6, the agglomerated microcapsules breaks down to smaller sizes during the initial stage of applied shear forces. The deflocculating effect is dominant in this stage, resulting in a sharp decrease in the shear stress and the viscosity. At longer times, the agglomerates become smaller, and the shear forces do not have any significant effect on the overall size of the agglomerates.

The distance between the microcapsules becomes shorter at higher concentrations, leading to an increased interaction between the particles and the formation of larger agglomerates. When a shear force is applied, these large agglomerates are continuously sheared to smaller pieces. According to Figoni-Shoemaker [10], the extent of the attractive forces between agglomerates depend on the size of the agglomerates. They predicted that the breakdown rate of large agglomerates is higher than for the smaller ones.

If the deflocculation rate is higher than the flocculation rate, a decrease of the viscosity and shear stress occurs over time (the Weltman model). In addition, the Figoni-Shoemaker model and second-order structural kinetic model predicts that an equilibrium is reached after some time, where both of these effects are equal in magnitude. In order to examine which of the three models provide the best fit to the time-dependent rheological behaviour of the MPCM suspensions, the determination coefficient R^2 (Figure 8a) and normalized root mean squared

error (NRMSE) (Figure 8b) is compared for the three models. The coefficient of determination R^2 ($0 \leq R^2 \leq 1$) is an evaluation of how well the fitted curve represents the experimental data. $R^2 = 1$ would indicate that the fitted line fits the experimental data perfectly. As can be seen from Figure 8a, R^2 varies in the range of 0.92–1 for the Weltman model, 0.91-1 for the Figoni-Shoemaker model, and 0.99-1 for the second-order structural kinetic model. This indicates that the second-order structural kinetic models provided the best fit to the data. However, R^2 values may not always be a true indicator of how well the model fits the data, particularly when a large number of data points are analyzed [22]. The NRMSE values can therefore offer a better picture. NRMSE is frequently used to normalize the differences between fitted data and experimental data. It is employed to compare different models which do not utilize the same scales. A lower value of NRMSE indicates less residual variance and a model that fits the data better.

Figure 8b shows that the NRMSE values are 1.32-7.25 for the Weltman model, 1.39-9.84 for the Figoni-Shoemaker, and 0.95-3.2 for the second-order structural kinetic model. The much lower NRMSE values for the second-order structural kinetic model again illustrates that this model can be considered as the best model for characterizing these systems. This is also in agreement with a visual inspection of the fitted lines in Figure 3 and Figure 6, where the second-order structural kinetic model (Figure 6) follows the experimental data better than the Weltman and Figoni-Shoemaker models (Figure 3).

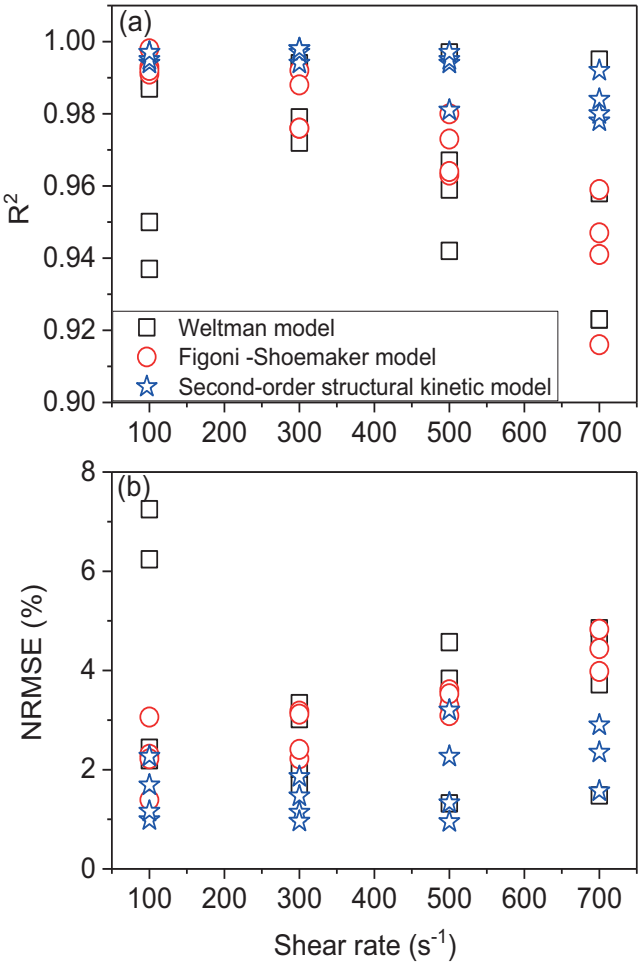

Figure 8. The comparison of (a) R^2 and (b) NRMSE for the Weltman model, the Figoni-Shoemaker model and the second-order structural kinetic model.

Conclusions

The influence of steady shear on the time-dependent structural breakdown of microencapsulated phase change materials (MPCM) suspensions were analysed by the Weltman model, the Figoni-Shoemaker model and the second-order structural kinetic model. The second-order structural kinetic model was found to exhibit the best correlation with the

experimental data. The MPCM form agglomerates, which are disrupted by shear forces. The breakdown of the agglomerated structures was most pronounced at high shear rates where the microcapsules are subjected to stronger disruptive forces. In addition, more and probably larger agglomerates are present at higher concentrations, which causes a stronger breakdown of the agglomerated structures when the concentration is raised.

References

[1] Chen, L.; Wang, T.; Zhao, Y.; Zhang, X.-R. Characterization of thermal and hydrodynamic properties for microencapsulated phase change slurry (MPCS). Energy Conversion and Management 2014, 79, 317-333.

[2] Delgado, M.; Lázaro, A.; Peñalosa, C.; Zalba, B. Experimental analysis of the influence of microcapsule mass fraction on the thermal and rheological behavior of a PCM slurry. Applied Thermal Engineering 2014, 63, 11-22.

[3] Zhang, G.H.; Zhao, C.Y. Thermal and rheological properties of microencapsulated phase change materials. Renewable Energy 2011, 36, 2959-2966.

[4] Wang, X.; Niu, J.; Yi Li, X.W.; Chen, B.; Zeng, R.; Song, Q.; Zhang, Y. Flow and heat transfer behaviors of phase change material slurries in a horizontal circular tube. International Journal of Heat and Mass Transfer 2007, 50, 2480-2491.

[5] Alvarado, J.L.; Marsh, C.; Sohn, C.; Phetteplace, G.; Newell, T. Thermal performance of microencapsulated phase change material slurry in turbulent flow under constant heat flux. International Journal of Heat and Mass Transfer 2007, 50, 1938-1952.

[6] Yamagishi, Y.; Takeuchi, H.; Pyatenko, A.T.; Kayukawa, N. Characteristics of Microencapsulated PCM Slurry as a Heat-Transfer Fluid. AIChE 1999, 45, 696-707.

[7] Dhiman, N.; Shah, J.; Agonafer, D.; Kannan, N.; Hoverson, J.; Kaler, M. Application of Phase Change Material in Sustainable Cooling of Data Centers. In ASME 2013 International

Mechanical Engineering Congress and Exposition; American Society of Mechanical Engineers (ASME): San Diego, CA, 2013.

[8] Zou, D.; Feng, Z.; Xiao, R.; Qin, K.; Zhang, J.; Song, W.; Tu, Q. Preparation and flow characteristic of a novel phase change fluid for latent heat transfer. Solar Energy Materials & Solar Cells 2010, 94, 2292-2297.

[9] Weltmann, R.N. Breakdown of Thixotropic Structure as Function of Time. Journal of Applied Physics 1943, 14, 343-350.

[10] Figoni, P.I.; Shoemaker, C.F. Characterization of time dependent flow properties of mayonnaise under steady shear. Journal of Texture Studies 1983, 14, 431-442.

[11] Nguyen, Q.D.; Jensen, C.T.B.; Kristensen, P.G. Experimental and modelling studies of the flow properties of maize and waxy maize starch pastes Chemical Engineering Journal 1998, 7, 165-171.

[12] Abu-Jdayil, B. Modelling the time-dependent rheological behavior of semisolid foodstuffs. Journal of Food Engineering 2003, 57, 97-102.

[13] Borreguero, A.M.; Valverde, J.L.; Rodríguez, J.F.; Barber, A.H.; Cubillo, J.J.; Carmona, M. Synthesis and characterization of microcapsules containing Rubitherm®RT27 obtained by spray drying. Chemical Engineering Journal 2011, 166, 384-390.

[14] Koocheki, A.; Razavi, S.M.A. Effect of Concentration and Temperature on Flow Properties of Alyssum homolocarpum Seed Gum Solutions: Assessment of Time Dependency and Thixotropy. Food Biophysics 2009, 4, 353-364.

[15] Tárrega, A.; Durán, L.; Costell, E. Flor behaviour of semi-solid dairy desserts. Effect of temperature. International Dairy Journal 2004, 14, 345–353.

[16] R.Durairaj; N.N.Ekere; B.Salam. Thixotropy flow behaviour of solder and conductive adhessive pastes. J Mater Sci: Mater Electron 2004, 15, 677-683.

[17] Abu-Jdayil, B. Flow properties of sweetened sesame paste (halawa tehineh). European Food Research & Technology 2004, 219, 265–272.

[18] Hammadi, L.; Boudjenane, N.; Houdjedje, R.; Reffis, R.; Belhadri, M. Modeling the Time-Dependent Rheological Behavior of Clays Used in Fabrication of Ceramic. International Journal of Mechanical, Aerospace, Industrial, Mechatronic and Manufacturing Engineering 2015, 9, 1377-1380.

[19] Mallik, S.; Ekere, N.N.; Marks, A.E.; Seman, A.; Durairaj, R. Modeling the Structural Breakdown of Solder Paste Using the Structural Kinetic Model. Journal of Materials Engineering and Performance 2009, 19, 40-45.

[20] Bhattacharya, S. Yield stress and time-dependent rheological properties of mango pulp. Journal of food science 1999, 64, 1029-1033.

[21] Barnes, H.A. Thixotropy a review. Journal of Non-Newtonian Fluid Mechanics 1997, 70, 1-33.

[22] Ravi, R.; Bhattacharya, S. The time-dependent rheological characteristics of a chickpea flour dispersion as a function of temperature and shear rate. International Journal of Food Science and Technology 2006, 41, 751-756.

Paper III

Microcapsulated phase change materials for enhancing the thermal performance of Portland cement concrete and geopolymer concrete for passive building applications.

Vinh Duy Cao, Shima Pilehvar, Carlos Salas-Bringas, Anna M. Szczotok, Juan F. Rodriguez, Manuel Carmona, Nodar Al-Manasir, Anna-Lena Kjøniksen.

Energy Conversion and Management **2017**, 133, 56–66.

Energy Conversion and Management 133 (2017) 56–66

Contents lists available at ScienceDirect

Energy Conversion and Management

journal homepage: www.elsevier.com/locate/enconman

Microencapsulated phase change materials for enhancing the thermal performance of Portland cement concrete and geopolymer concrete for passive building applications

Vinh Duy Cao [a,b], Shima Pilehvar [a,c], Carlos Salas-Bringas [b], Anna M. Szczotok [a,d], Juan F. Rodriguez [d], Manuel Carmona [d], Nodar Al-Manasir [e], Anna-Lena Kjøniksen [a,*]

[a] Faculty of Engineering, Østfold University College, N-1757 Halden, Norway
[b] Department of Mathematical Sciences and Technology, Norwegian University of Life Sciences, N-1432 Ås, Norway
[c] Department of Material Engineering and Manufacturing, Technical University of Cartagena, Cartagena, Murcia, Spain
[d] Department of Chemical Engineering, University of Castilla – La Mancha, 13004 Ciudad Real, Spain
[e] Mapei AS, Sagstua, Norway

ARTICLE INFO

Article history:
Received 5 October 2016
Received in revised form 23 November 2016
Accepted 28 November 2016

Keywords:
Microencapsulated phase change materials
Portland cement concrete
Geopolymer concrete
Specific heat capacity
Latent heat
Thermal conductivity

ABSTRACT

Concretes with a high thermal energy storage capacity were fabricated by mixing microencapsulated phase change materials (MPCM) into Portland cement concrete (PCC) and geopolymer concrete (GPC). The effect of MPCM on thermal performance and compressive strength of PCC and GPC were investigated. It was found that the replacement of sand by MPCM resulted in lower thermal conductivity and higher thermal energy storage, while the specific heat capacity of concrete remained practically stable when the phase change material (PCM) was in the liquid or solid phase. Furthermore, the thermal conductivity of GPC as function of MPCM concentration was reduced at a higher rate than that of PCC. The power consumption needed to stabilize a simulated indoor temperature of 23 °C was reduced after the addition of MPCM. GPC exhibited better energy saving properties than PCC at the same conditions.

A significant loss in compressive strength was observed due to the addition of MPCM to concrete. However, the compressive strength still satisfies the mechanical European regulation (EN 206-1, compressive strength class C20/25) for concrete applications. Finally, MPCM-concrete provided a good thermal stability after subjecting the samples to 100 thermal cycles at high heating/cooling rates.

1. Introduction

The total energy consumption is dramatically increasing all over the world. Much of the energy demand can be attributed to building energy consumption, and a significant proportion of this energy is for heating and cooling purposes [1]. Improved construction techniques and enhanced material technology can greatly reduce the energy consumption needed to keep a comfortable indoor temperature. Thermal energy storage systems, including sensible heat storage and latent heat storage materials, can be used to conserve and save energy [2–6]. Sensible heat storage materials store energy by raising the temperature of the storage materials such as concrete, rock, or steel. For latent heat storage materials, also known as phase change materials (PCM), the thermal energy is stored during the phase change of the materials (e.g. melting, evaporating, or crystallization). Unlike sensible heat storage, latent heat storage systems are capable of storing energy with higher storage density at an almost constant temperature, which is referred to as the phase transition temperature of the materials. This makes latent heat storage materials more attractive than sensible heat storage materials for improving thermal comfort and reducing the energy consumption for heating/cooling purposes.

The capability to store or release thermal energy from PCM strongly depends on the heat storage capacity, thermal conductivity, the melting temperature of the PCM, and the outdoor environment that it is exposed to. Building materials, especially concrete based materials, with a high volume and surface area exposed to the indoor environment, as well as a high mechanical strength are potential candidates for integration with PCM. Furthermore, concrete provide the possibility to alter both thermal and mechanical properties of the PCM-materials. The incorporation of PCM into concrete can significantly improve the thermal energy storage capacity of building structures around the melting range of PCM

* Corresponding author.
E-mail address: anna.l.kjoniksen@hiof.no (A.-L. Kjøniksen).

http://dx.doi.org/10.1016/j.enconman.2016.11.061
0196-8904/

Nomenclature

C_p	specific heat capacity, J/kg °C
Q	total energy consumption, kW h/m^2
T	temperature, °C
t	time, s
m	mass, kg
φ	heat flux, W/m^2
λ	thermal conductivity, W/m °C
ρ	density, kg/m^3
ε	concentration, wt.%
ΔH	latent heat, J/g

Subscripts/superscripts

s	saturated mass
d	dry mass
b	buoyant mass
S	solid state
L	liquid state
init	initial time of process
end	final time of process
top	top heat exchanger
bottom	bottom heat exchanger
ave	average
H	heating
C	cooling
MPCM	microencapsulated phase change materials

[7–9]. Therefore, the development of smart building materials with the direct addition of PCM could reduce the energy consumption for heating/cooling systems. However, interaction with surrounding materials and low heat transfer coefficients limit the direct application of PCM. In order to overcome these problems, microencapsulation may be utilized for incorporation of PCM into small polymeric capsules [10–13]. This provides not only an extremely high heat transfer area, but also prevents the leakage of PCM and interactions with the building structure. Microencapsulated phase change materials (MPCM) are therefore able to support PCM for utilization as thermal storage materials in building applications and energy storage systems [14–19]. Concrete-based materials with high thermal properties and high mechanical strength are potential candidates for MPCM integration. Concrete materials provide the possibility to alter both thermal and mechanical properties of the MPCM-concrete. The integration of MPCM in concrete is therefore a good strategy of passive building technology to reduce the energy consumption.

Portland cement concrete (PCC) is the most utilized concrete for applications utilizing microencapsulated phase change materials [15–17]. PCC has several advantageous properties, such as high thermal conductivity, high specific heat capacity, high density, and high mechanical strength. However, PCC exhibits a negative effect on the environment due to the emission of carbon dioxide (CO_2) during the production of cement [20]. In comparison to PCC, geopolymer concrete (GPC) not only exhibits corresponding advantageous properties as PCC, but also higher initial strength, small drying shrinkage, high fire resistance, superior acid resistance and shorter setting time [21]. The geopolymer binder is synthesized by alkali activation of aluminosilicate materials in amorphous form, which are produced from industrial waste materials. Geopolymer is therefore more environmentally friendly and cheaper than Portland cement [22,23]. The use of geopolymer concrete can significantly reduce the amount of CO_2 emission from the cement industry, the primary driver of global warming. Accordingly, geopolymer is a very interesting alternative to Portland cement as a binder for concrete. However, the thermal properties of geopolymer concrete containing MPCM have not been reported previously. Researchers utilizing MPCM have mostly utilized standard concrete recipes, which are more readily available for Portland cement. In addition, problems with short setting times of GPC [21,24], can be worsened when MPCM is added to the mixture. The comparison between Portland cement concrete and geopolymer concrete with the addition of MPCM is therefore very interesting.

While the integration of MPCM in concrete can improve the thermal energy storage capacity of the building structure, it also reduces the mechanical strength of concrete [9,15]. A good knowledge of the effect of microcapsules on the thermal and mechanical properties of concrete therefore plays an important role to optimize the efficiency of passive house construction.

In this article, the integration of MPCM into Portland and geopolymer concretes was investigated, respectively. The microcapsules have a shell of low density polyethylene (LDPE) and ethylvinylacetate (EVA) copolymer, and a core of paraffin Rubitherm®RT27, abbreviated LDPE-EVA/RT27. RT27 is selected as the PCM material due to the high latent heat (100 J/g), a melting point around 27 °C (which is suitable for achieving good temperature control in warm climates), and the lack of chemical interactions with the alkaline solution and the surrounding environment [25]. In addition, it will not corrode metal reinforcements within concrete structures. The effect of MPCM content on the thermal performance and mechanical properties (compressive strength) of PCC and GPC were investigated. MPCM were added by replacing the same volume percentage of sand, utilizing concentrations up to 3.2 and 2.7 wt.% for PCC and GPC, respectively. The comparative analysis between PCC and GPC was given special attention, since previous knowledge within this field is limited.

2. Experimental

2.1. Materials

The microencapsulated phase change materials (MPCM) were made by a spray drying process [25]. The MPCM are composed of a paraffin Rubitherm®RT27 core coated with the LDPE-EVA (low density polyethylene (LDPE) and ethylvinylacetate (EVA) copolymer) shell [25].

MPCM were integrated into two different types of concrete; Portland cement concrete (PCC) and geopolymer concrete (GPC) at various concentrations. Tables 1 and 2 present the composition of PCC and GPC mixtures. The MPCM replaced the same volume percentage of sand, and the MPCM concentration in total solid weight of concrete was calculated. PCC samples were fabricated with 0 wt.%, 0.8 wt.%, 1.6 wt.%, and 3.2 wt.% of incorporated MPCM (Table 1). For GPC (Table 2), the concentration of MPCM was 0 wt.%, 0.7 wt.%, 1.3 wt.%, and 2.7 wt.%. Higher amounts of MPCM resulted in too low workability of the concretes to produce usable samples. The dimensions of the samples were $20 \times 20 \times 2.53$ cm for the thermal test and $10 \times 10 \times 10$ cm for the compressive strength test. According to the mechanical regulations, the

Table 1
Composition of Portland cement concretes (PCCx[a]).

Sample	MPCM (wt.%)	Cement (g)	Water (g)	Admixture (g)	Sand (g)	Aggregate (g)	MPCM (g)
PCC0	0	434	192	5.6	1057	705	0
PCC0.8	0.8	434	192	5.6	1004.2	705	18
PCC1.6	1.6	434	192	5.6	951.3	705	36
PCC3.2	3.2	434	192	5.6	845.6	705	72

[a] x is the concentration (wt.%) of MPCM in the concrete.

Table 2
Composition of geopolymer concretes (GPCx[a]).

Sample	MPCM (wt.%)	Alkaline solution (g)	Water (g)	FA[b] (g)	GGBFS[c] (g)	Sand (g)	Aggregate (g)	MPCM (g)
GPC0	0	161.6	56.4	242.6	161.4	893.1	868.6	0
GPC0.7	0.7	161.6	56.4	242.6	161.4	848.6	868.6	15
GPC1.3	1.3	161.6	56.4	242.6	161.4	803.8	868.6	30
GPC2.7	2.7	161.6	56.4	242.6	161.4	714.5	868.6	60

[a] x is the concentration (wt.%) of MPCM in the concrete.
[b] FA: Flyash.
[c] GGBFS: Ground granulated blast-furnace slag.

MPCM-concrete samples were fully cured in water at room temperature for 28 days. For the thermal test, the fully cured samples were dried in an oven at 40 °C until the sample weight remained unchanged.

2.2. Scanning electron microscopy

The surface morphology and the structure of the microcapsules and MPCM-concrete were obtained by using scanning electron microscopy (SEM) (Quanta FEG-250 and Quanta FEI-200).

2.3. Size distribution of MPCM

The size distribution of MPCM were determined by Low Angel Laser Light Scattering (LALLS) laser diffraction using a Malvern Mastersizer 2000 (Malvern Instruments Ltd., Malvern, UK) equipped with a Scirocco 2000 unit for analyzing dispersions of the particles in air.

2.4. Density and porosity

The density of MPCM-concrete samples were determined using EN 12390-7 [26]:

$$\rho = \frac{m_d}{V} \quad (1)$$

where ρ is the dry density of the MPCM-concrete, m_d is oven-dried weight and V is the volume of the sample.

The porosity test was done based on ASTM C1202-12, which has been used by other researchers [27,28]. The samples were oven-dried at 105 °C until a constant weight was achieved. It was previously confirmed by thermogravimetric analysis (TGA) that the microcapsules were completely stable at temperatures lower than 150 °C [29]. The samples were cooled down to room temperature before recording the oven dried mass m_d. Afterwards, the samples were immersed in water at room temperature until the weight of sample in water remains constant, and the buoyant mass of the saturated samples in water m_b were recorded. Finally, the saturated sample was moved out of water, the surplus water wiped from the surface, and the saturated sample in air m_s was recorded. The open porosity of MPCM-concrete samples can be calculated by:

$$\textit{Open Porosity}\ (\%) = \frac{m_s - m_d}{m_s - m_b} \times 100 \quad (2)$$

2.5. Thermal properties

The guarded hot plates method, which is well suited for concrete samples, was utilized in order to characterize the thermal performance of the MPCM-concrete samples [16,30]. This method allows recording of temperature variations and heat fluxes exchanged through the sample during the testing process. The guarded hot plates system is presented in Fig. 1.

The thermal system includes two aluminum plate heat exchangers connected to thermal regulated baths that define the thermal conditions. The MPCM-concrete sample was sandwiched between two aluminum plate heat exchangers. A 40 mm thick polyethylene expanded foam (PEF) is used to form an insulated cover around the sample. This insulated cover will minimize the heat transfer from the lateral side face of the sample into the surrounding environment. Accordingly, the heat transfer through the MPCM-concrete sample can be calculated assuming one-dimensional thermal condition. Heat flux sensors (Captecv, France) and K-type thermocouples (TC Ltd., UK) were inserted on both sides of the sample to measure the temperature variations and heat fluxes through sample during testing processes. All sensors were connected to a multichannel multimeter (LR8410-20 Hioki, Japan) to record the data.

With the guarded hot plates system, the thermal properties of MPCM-concrete such as the thermal conductivity, its temperature in liquid and solid state for PCM, the specific heat capacity and the latent heat can be determined. Furthermore, it is possible to investigate the thermal performance of MPCM-concrete such as the thermal stability, and power consumption to stabilize the indoor temperature.

2.5.1. Thermal conductivity

The thermal conductivity of the MPCM-concrete samples was determined at temperatures below and above melting range of MPCM (20–32 °C) [29]. They are denoted solid thermal conductivity, λ_S (below melting point) and liquid thermal conductivity, λ_L (above melting point). Both aluminum plate heat exchangers were first kept at a constant temperature T_{init} until the heat fluxes were constant (thermal steady-state condition). Then, a temperature variation was imposed on the top aluminum plate heat exchanger from T_{init} to T_{end} and kept at T_{end} while the other aluminum plate heat exchanger was kept at T_{init} until a thermal steady state was reached. After reaching the thermal steady state condition, the average temperature on the top (T_{top}) and bottom (T_{bottom}) faces

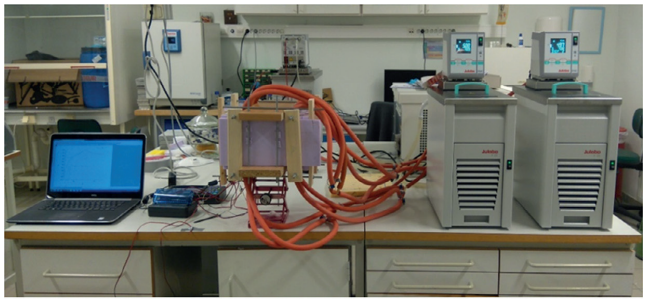

(a)

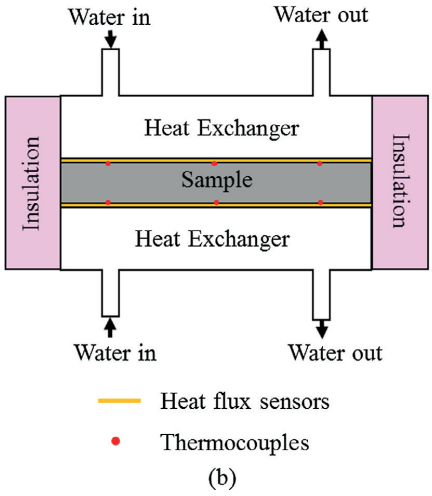

(b)

Fig. 1. (a) The guarded hot plates system and (b) sketch of the cross-section of system.

of the block and the average heat fluxes (φ_{ave}) on both faces were recorded for thermal conductivity (λ) calculation via the following relationship:

$$\lambda = \frac{\varphi_{ave} d}{A(T_{top} - T_{bottom})} \quad (3)$$

where A and d are the area and the thickness of the MPCM-concrete block, respectively. In these experiments the dimension of the concrete samples were A = 400 cm^2 and d = 2.53 ± 0.02 cm.

For solid thermal conductivity, T_{init} and T_{end} are set at 5 and 10 °C, respectively. While values of T_{init} and T_{end} of 45 and 50 °C are set to calculate the liquid thermal conductivity of MPCM-concrete.

2.5.2. Specific heat capacity/latent heat

The latent heat and the specific heat capacity (Eq. (4)) of the MPCMS-concrete sample were measured by the same testing system. The MPCM-concrete sample is initially isothermal at T_{init}. Afterwards, it was heated by raising the temperature of both aluminum plate heat exchangers from T_{init} to T_{end} by using oil thermostatic baths and at a heating rate of 10 °C/h. In this experiment, T_{init} and T_{end} were set equal to 5 °C and 45 °C, respectively. The average heat fluxes (φ_{ave}) and temperature on both faces of MPCM-concrete sample (T_{top} and T_{bottom}) during the test is determined via heat flux sensors and thermocouples, respectively. The solid specific heat capacity, $C_{p\text{-solid}}$ (below melting range) and the liquid specific heat capacity, $C_{p\text{-liquid}}$ (above melting range) were estimated in the temperature range of 10–15 °C and 35–40 °C, respectively.

$$C_p = \frac{A\varphi_{ave}}{m\frac{dT}{dt}} \quad (4)$$

where C_p is specific heat capacity, m is the mass of sample.

Paraffin Rubitherm®RT27 has a melting point of about 27 °C. However, since it is of an industrial standard, it is melting over a temperature range. Therefore, the latent heat was calculated over the range 10–35 °C to ensure that the whole melting temperature range is covered. A long as the whole melting point area of the paraffin is included in the temperature range the calculated latent heat is not affected by the utilized temperature range. OriginPro 9.0 R1 was employed to calculate the latent heat.

2.6. Energy saving aspect

The thermal system was employed to investigate the effect of MPCM on potential energy saving aspects. The appropriate temperature profiles were imposed on the two sides of the sample to simulate the indoor and outdoor temperature. First, both aluminum plate heat exchangers were set to 23 °C until reaching a thermal steady-state condition. Then, the temperature of the bot-

tom aluminum plate heat exchanger (the simulated outdoor temperature, $T_{outdoor}$) was varied in the sequence: 23–20–32–20 °C at a rate of 1 °C/h. The simulated indoor temperature (top aluminum plate heat exchanger, T_{indoor}) was set stable at 23 °C throughout the experiment. The temperature and heat fluxes on both surfaces of the sample were recorded to measure heat losses towards the simulated indoor environment during the testing process (Fig. 2). The total heat losses or the energy supplied for heating/cooling of the system to maintain the simulated indoor temperature at 23 °C can be calculated by:

$$Q = \frac{\int_{t_{ini}}^{t_{end}} |\varphi_{indoor}| dt}{3600 \cdot 10^3} \quad (5)$$

where φ_{indoor} is the heat flux on the simulated indoor side of the sample, t_{ini} and t_{end} are the initial time and end time of the thermal cycle.

2.7. Thermal stability

The MPCM-concrete samples were subjected to 100 identical thermal cycles to investigate their thermal stability. In order to accelerate the thermal cycling effect, each thermal cycle was set by linearly increasing the temperature from 20 °C to 32 °C for 30 min, followed by a linear decrease from 32 °C to 20 °C for the same period of time. Subsequently, the MPCM-concrete samples were subjected to the energy saving aspect process described above to investigate the thermal stability of samples. For this test, only the samples with the highest concentration of MPCM (PCC3.2 and GPC2.7) were tested.

2.8. Compressive strength test

The mechanical properties of the MPCM-concrete were analyzed by using an Alpha 3–3000 system (Form + Test Seidner&Co. GmbH) based on EN 12390-3. The measurement was conducted for samples without MPCM (PCC0 and GPC0) and samples at the highest amount of MPCM (PCC3.2 and GPC2.7) before and after subjecting the samples to 100 thermal cycles, in order to investigate the effect of MPCM and thermal stability on the mechanical compressive strength of MPCM-concrete.

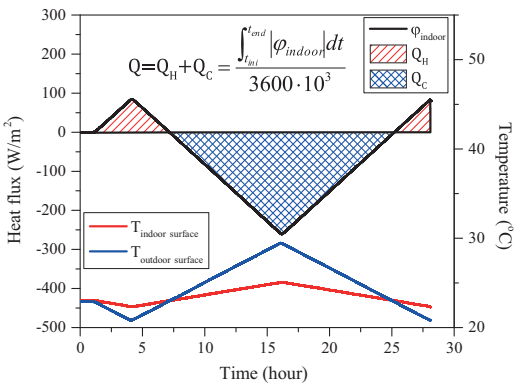

Fig. 2. Heat flux on the simulated indoor side (φ_{indoor}) and temperatures on the simulated indoor surface ($T_{indoor\ surface}$) and on the simulated outdoor surface ($T_{outdoor\ surface}$) of the sample versus time during a thermal cycle test. The total energy consumption for heating/cooling the system to maintain a stable simulated indoor temperature includes the energy used for heating (Q_H) when $T_{indoor\ surface} > T_{outdoor\ surface}$; and the energy used for cooling (Q_C) when $T_{indoor\ surface} < T_{outdoor\ surface}$.

3. Results and discussion

3.1. Size distribution

Fig. 3a shows a SEM image of the microcapsules. The diameters of the single microcapsules are in the range of 3–10 μm. However, it is clear that the microcapsules have a strong tendency to form agglomerated structures. This observation is in good agreement with the size distribution of the microcapsules (Fig. 3b). The volume average size distribution shows that the microcapsules have a diameter in the range between 10 and 1000 μm. The median value of the microcapsules diameter at 60% in the cumulative distribution (D_{60}) is 240 μm. The agglomerated microcapsule size is smaller than the size of sand (D_{60} = 1000 μm). The difference between the size distribution of agglomerated microcapsules and sand may alter the physical properties of the concrete samples.

3.2. MPCM-concrete density and porosity

SEM images (Fig. 4) present the microstructure of PCC0, PCC3.2, GPC0 and GPC2.7. For both types of concrete, the SEM images show no clear difference between the concrete matrix before and after addition of MPCM. This suggests that MPCM with components of low chemical reactivity (LDPE-EVA shell and paraffin core) does not have an obvious reaction with the concrete binder (cement hydration and geopolymerization process) at the current conditions. In addition, Fig. 4b and d illustrates that there are noticeable gaps between MPCM and both types of concrete matrix. These can cause a higher porosity in MPCM-concrete, which may influence the thermal properties and mechanical strength of MPCM-concrete.

Fig. 5 shows the MPCM-concrete density and open porosity. MPCM has the same effect on density and open porosity of both type of concrete. When the concentration of MPCM is raised, the density of MPCM-concrete decreases and the open porosity increases. This is consistent with previous studies of other MPCM-concretes [9,15]. The density decrease at higher concentrations can be explained by the replacement of sand by MPCM, which has a lower density. In addition, the increase of the porosity of the samples will also cause a density decrease.

The higher porosity of MPCM-concrete when the concentration of microcapsules is raised indicates that the addition of microcapsules plays an important role on the porosity of concrete. Three effects may affect the porosity of concrete when MPCM is included. The small size (3–10 μm) of single microcapsules can fill the cavity between aggregates, leading to improved particle packing density and decrease the porosity (first effect) [31–33]. On the other hand, the hydrophobic nature of LDPE-EVA/RT27 may cause an opposite effect. When microcapsules are added to concrete, they have a tendency to repel water, and air may adhere to the microcapsule leading to a higher porosity in concrete mixtures (second effect) [34,35]. The third possible effect is due to the smaller size of the microcapsule agglomerates compared to sand particles (Fig. 3). The surface area of microcapsules is much higher than that of sand for a unit replacement volume, resulting in an increase of the binder paste and water demand to cover the entire surface of the particles. Because the water content was kept constant for all samples in this study, more voids between particles (aggregates and microcapsules) might be formed [31]. This results in higher porosity of the concrete. A balance of these three effects governs the porosity of the concrete. Norvell et al. [33] demonstrated that the addition of BASF Mironal® microcapsules with an average diameter of 5 μm to cement mortal increased the packing density, resulting in the reduction of the porosity. However, he also revealed that the filling effect was significantly reduced for particle sizes larger than

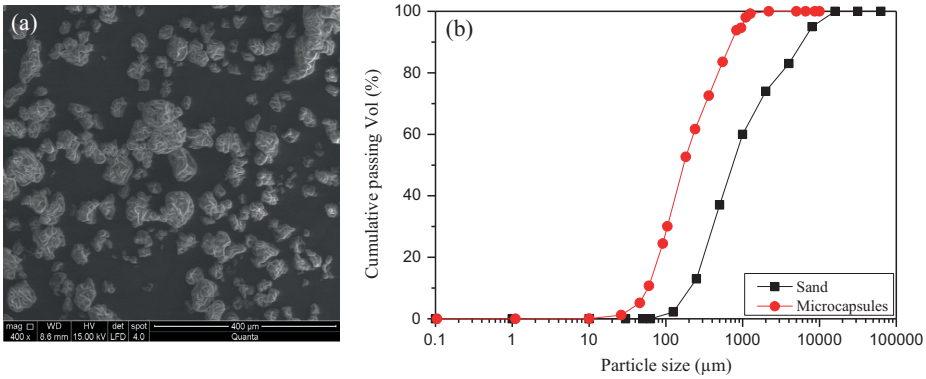

Fig. 3. (a) SEM image of the LDPE-EVA/RT27 microcapsules and (b) the size (diameter) distribution of the LDPE-EVA/RT27 microcapsules and sand.

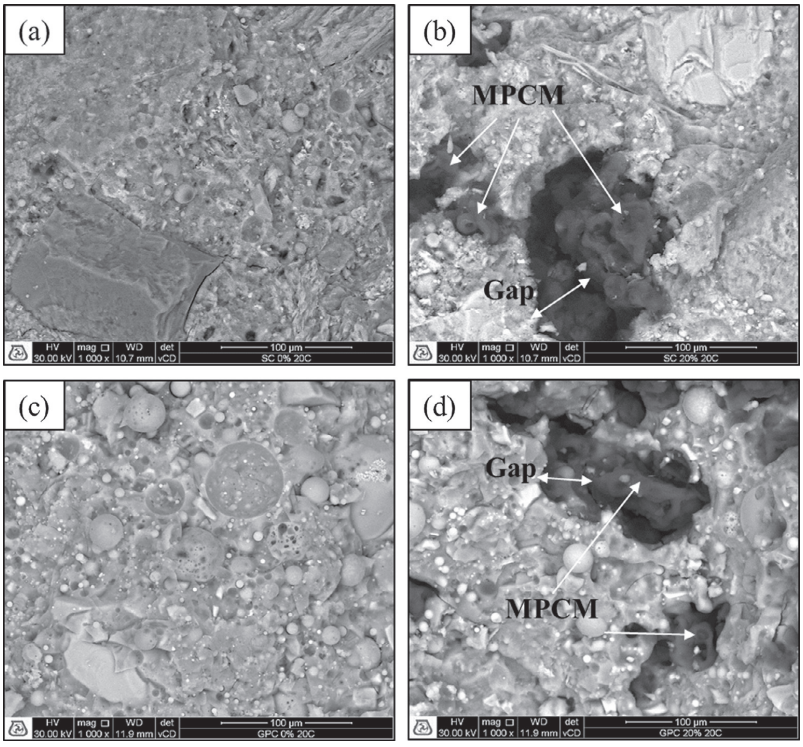

Fig. 4. SEM images of (a) PCC without MPCM (PCC0), (b) PCC containing 3.2 wt.% MPCM (PCC3.2), (c) GPC without MPCM (GPC0) and (d) GPC containing 2.7 wt.% MPCM (GPC2.7).

125 μm. This is in good agreement with Moosberg-Bustnes et al. [36] who studied the effect of average quartz size on the compressive strength of concrete. According to SEM images and MPCM size distribution (Fig. 3), MPCM has a tendency to form agglomerated structures with larger sizes (D_{60} = 240 μm). The agglomeration of the microcapsules is due to non-encapsulated PCM outside the microcapsules [29]. The large size of the agglomerates reduces the ability of the MPCM to fill up cavities and increase the tendency to entrap air on their surface and in their structure. Consequently, the second and third effects are probably the dominant effects, resulting in an increase of the porosity of the concrete. The result of these effects is the obvious gap between concrete matrix and microcapsules in the SEM images (Fig. 4). Similar observations were also found previously [15,37,38].

According to Fig. 5, PCC has higher density and lower porosity than GPC for all samples. Furthermore, the porosity of GPC increases at a higher rate than that of PCC when raising the concentration of MPCM. As can be seen from Fig. 5b, the porosity

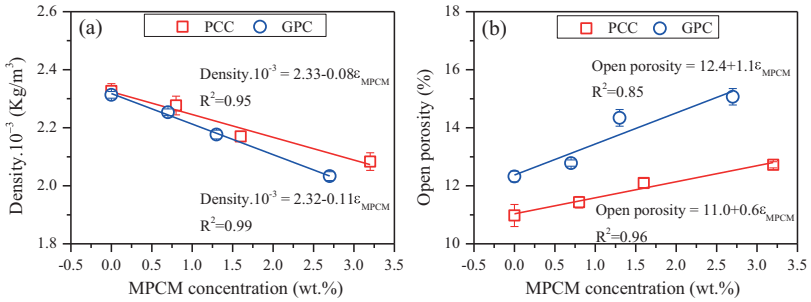

Fig. 5. (a) Density and (b) open porosity of GPC and PCC as a function of MPCM concentration (ε_{MPCM}).

increases with concentration at a rate of 1.1 for GPC and 0.6 for PCC. The reason for this is unclear, as several effects may come into play. The effect of MPCM on the particle packing density might be different between GPC and PCC due to the different binders. The compatibility between the microcapsule shell and the binder is not necessarily the same for the two systems. In addition, GPC has a much lower workability and shorter setting time than PCC. The lower workability of GPC could increase the probability of forming entrapped air voids during the mixing and pouring process.

3.3. Thermal properties

The thermal conductivity of MPCM-concrete is an important parameter for thermal energy storage applications. The heat fluxes and the measured temperatures on both sides of the MPCM-concrete when the paraffin Rubitherm®RT27 is in solid and in liquid state are shown in Fig. 6. The value of the temperature difference and the average value of the heat fluxes during a steady state were used to determine the apparent thermal conductivity of the MPCM-concrete via Eq. (3). The apparent thermal conductivity of MPCM-concrete in liquid and solid PCM state is summarized in Fig. 7.

According to Fig. 7, the thermal conductivity of MPCM-concrete decreases with the concentration of microcapsules. The addition of MPCM causes the reduction of thermal conductivity of the concrete due to the lower thermal conductivity of the microcapsules compared to that of replaced sand and also the porosity increase. The thermal conductivity of the paraffin Rubitherm®RT27 and polymer LDPE/EVA shell are approximately 0.2 W/m °C and 0.13–0.34 W/m °C [39], respectively, while the average thermal conductivity of

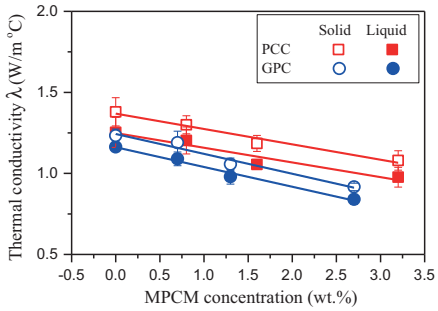

Fig. 7. The solid thermal conductivity and the liquid thermal conductivity of GPC and PCC as a function of MPCM concentration.

sand is in the range of 1.80–2.50 W/m °C depending on the degree of water saturation (information provided by the supplier). Moreover, for a constant MPCM concentration, the thermal conductivity of concrete in solid PCM state is higher than that in the liquid PCM state. This is because the thermal conductivity of PCM in a solid state is higher than that in a liquid state [16,40]. This observation is supported by Cui et al. [16] studying the effect of microcapsules on thermal properties of cement mortal.

Comparing PCC and GPC, the thermal conductivity of PCC is higher than for GPC. The reduction rates of thermal conductivity of GPC and PCC are similar for the liquid and solid states of PCM. They are 0.12 for GPC and 0.09 for PCC. The slightly different MPCM concentration dependencies of GPC and PCC might be related to

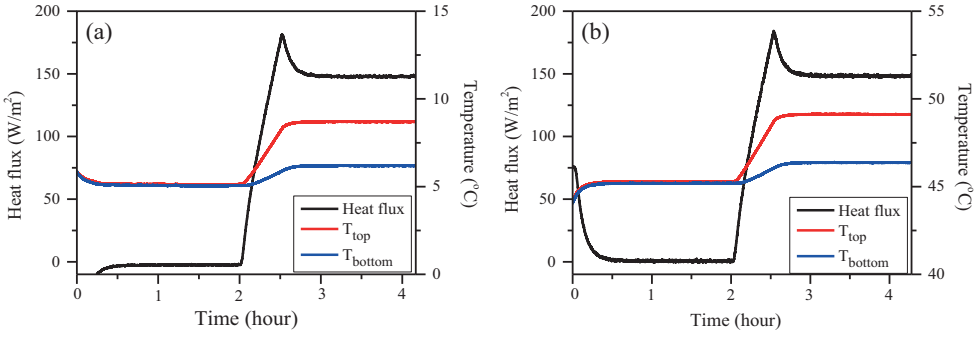

Fig. 6. Heat flux and temperatures versus time during (a) the solid thermal conductivity and (b) the liquid thermal conductivity test of PCC0.

the corresponding change in porosity (Fig. 5b), as air pockets will decrease the thermal conductivity.

The specific heat capacity of the PCC samples in the region 5–45 °C is shown in Fig. 8. In order to determine the specific heat capacity of samples containing PCM in solid and liquid state, the average value of specific heat capacity from 10 to 15 °C (below the melting range of PCM) and from 35 to 40 °C (above melting range of PCM) were employed. The specific heat capacity in both states is summarized in Fig. 9a.

The results show that the specific heat capacity of MPCM-concrete is nearly the same when the PCM is in solid or liquid state, although the specific heat capacity of microcapsules (determined by differential scanning calorimetry) is higher in solid state ($C_{p\text{-solid}}$ = 3050 J/kg °C) than in liquid state ($C_{p\text{-liquid}}$ = 2740 J/kg °C). This is possibly due to low microcapsule concentrations, which are too small to significantly affect the values of the specific heat capacity of the concrete samples. This observation is in good agreement with Joulin et al. [17]. Interestingly, the specific heat capacity is not changed when the concentration of MPCM is increased from 0 to 3.2 and 2.7 wt.% for PCC and GPC, respectively. This observation is different from Joulin et al. [17], who found that the specific heat capacity of MPCM-mortar increased with microcapsule concentration due to the higher specific heat capacity of microcapsule compared to mortar. The smaller microcapsule concentrations applied compared to that of Jourlin's (14 wt.%) is probably reason for this difference. The low concentrations of microcapsules utilized in the current study may be too small to significantly increase the specific heat capacity of the concrete.

The latent heat of the samples was determined within the temperature range of 10–35 °C and is presented in Fig. 9b. The latent heat exhibits a linear increase with respect to the microcapsule concentration. However, the latent heat of PCC increases at slightly higher rate than that of GPC (0.72 for PCC and 0.60 for GPC), as can be seen in Fig. 9b. This can be attributed to the different porosity of GPC and PCC.

3.4. Energy saving aspect

In order to investigate the influence of microcapsules on reducing energy consumption for heating and cooling systems, the indoor and outdoor temperatures were simulated utilizing the thermal analysis system. The samples were subjected to a simulated outdoor thermal cycle where the temperature was changed from 23–20–32–20 °C at a rate of 1 °C/h. The total duration of this heating-cooling cycle was 27 h. The simulated indoor temperature was set at 23 °C throughout the experiment.

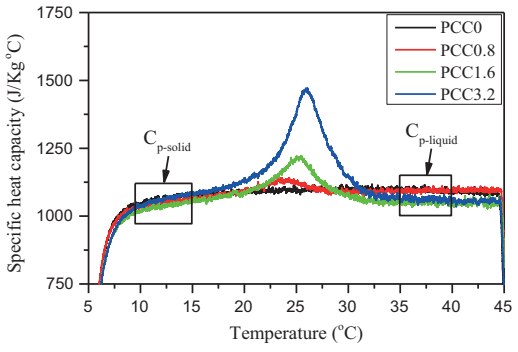

Fig. 8. The specific heat capacity of PCC at different concentrations of MPCM.

The total heat losses towards the indoor environment can be calculated by integration of the heat flux on the simulated indoor side of the sample (Fig. 10). This calculated energy corresponds to the energy consumed by the heating/cooling system to stabilize the simulated indoor temperature at 23 °C. According to Fig. 10a, the heat flux as function of time is a straight line without any obvious transition point from MPCM addition. This deviates from previous studies [15,16,38] where a transition point was found around the melting point of paraffin. When the paraffin is completely melted, the effect of the latent heat process ends, causing a steeper increase of the indoor surface temperature and the indoor heat flux. This should cause a transition point on the heat flux curve [16]. The lower microcapsule concentrations (3.2 wt.% for PCC and 2.7 wt.% for GPC) applied here compared to that of Borreguero (10–15 wt.%) [38] or Cui (5–20 wt.%) [16] is probably reason for this difference. This observation is in good agreement with Hunger et al. [15] who reported that there was no clear transition point until adding 5 wt.% of MPCM to concrete. The calculated energy consumption using Eq. (5) for a thermal cycle is shown in Fig. 10b.

According to Fig. 10, the addition of MPCM significantly improves the thermal performance of concrete in terms of saving energy. There is no significant difference in energy consumption between PCC and GPC in the absence of MPCM. However, the energy consumption decreases from 2.82 ± 0.10 kW h/m^2 (without MPCM) to 2.51 ± 0.03 kW h/m^2 (3.2 wt.% MPCM) for PCC and from 2.74 ± 0.13 kW h/m^2 (without MPCM) to 2.32 ± 0.03 kW h/m^2 (2.7 wt.% MPCM) for GPC after adding microcapsules. Accordingly, energy consumption for heating and cooling to maintain the indoor temperature can be reduced up to 11% for PCC (3.2 wt.% MPCM) and 15% for GPC (2.7 wt.% MPCM), compared to the samples without MPCM. The results reveal that in addition to the energy storage capacity of MPCM, the increase of thermal insulation (thermal conductivity reduction) plays an important role in the energy saving mechanism at the studied conditions. The improved properties of GPC containing MPCM compared to PCC is probably due to the formation of a structure with more insulating pores when MPCM is added to GPC.

Comparing the open porosity (Fig. 5b) with the thermal conductivity (Fig. 7), the latent heat (Fig. 9b), and the power consumption (Fig. 10b), it is evident that the enhanced porosity plays a vital role for the thermal properties of these samples. Addition of MPCM causes a higher porosity increase for GPC than for to PCC. The air pores provides an enhanced thermal insulation effect. Accordingly, GPC experience a stronger decrease in thermal conductivity, a lower increase in latent heat, and a higher energy saving efficiency. Adding MPCM to GPC causes a higher energy saving efficiency than for PCC (Fig. 10b) even though the latent heat increases more for PCC (Fig. 9b). It is therefore clear that for reducing the power consumption of these samples, the thermal insulation effect of the air voids is more important than the increased latent heat from the MPCM.

3.5. Thermal stability

The heat fluxes on the indoor side of MPCM-concrete before and after subjecting the samples to 100 thermal cycles are shown in Fig. 11. The results show that there is no detectable change in the energy consumption after subjecting the samples to 100 thermal cycles. Accordingly, MPCM-concrete possesses a good thermal stability over 100 accelerated melting/solidification cycles.

3.6. Compressive strength

Results of the compressive strength measurement are presented in Fig. 12. The results show that increasing the amount of MPCM causes significantly lower compressive strengths. This is

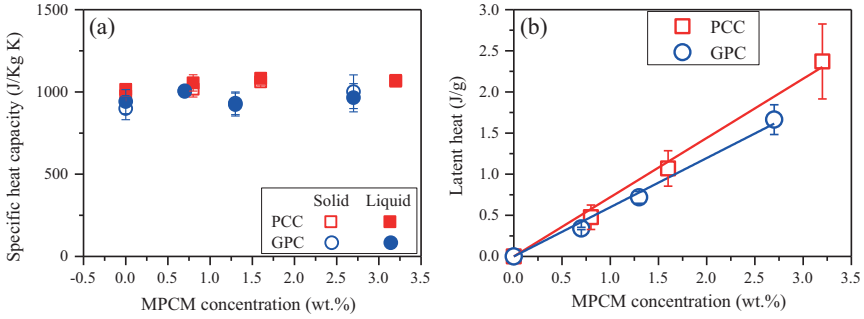

Fig. 9. (a) The specific heat capacity of GPC and PCC at solid and liquid state of PCM and (b) the latent heat of PCC and GPC at different concentrations of MPCM.

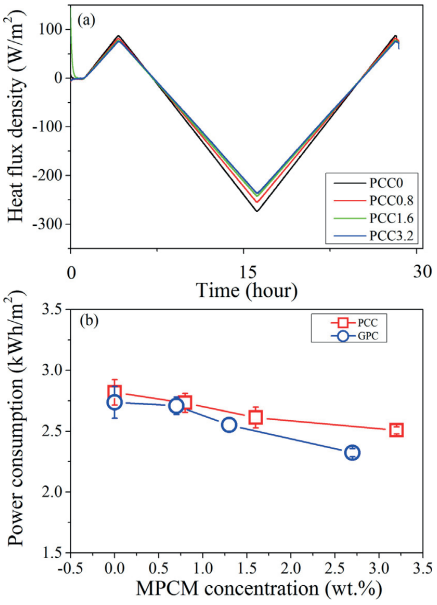

Fig. 10. (a) Heat flux density on the simulated indoor side of PCC at different MPCM concentrations and (b) the energy consumption needed for heating/cooling the system to maintain a simulated indoor temperature of 23 °C for PCC and GPC.

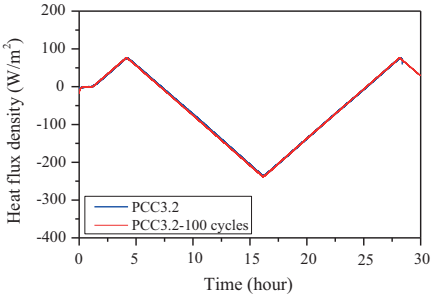

Fig. 11. Heat flux density on the indoor side of PCC containing 3.2 wt.% of MPCM before and after exposing the samples to 100 thermal cycles.

probably because MPCM is a material with low mechanical strength and stiffness and can be easily broken under compressive force [9,15,39]. Furthermore, the higher porosity after adding MPCM can contribute to the reduction the compressive strength of MPCM-concrete. In addition, the compressive strength of PCC and GPC decreases by 42% and 51% after adding 3.2 wt.% of MPCM to PCC and 2.7 wt.% of MPCM to GPC, respectively. This indicates that the compressive strength of GPC decreases at higher rate than that of PCC, although a smaller amount of MPCM is added to GPC than PCC. This might be caused by the higher porosity increase of the GPC samples.

Additionally, the gaps between concrete matrix and microcapsules (Fig. 4) reveal a poor interface between microcapsules and the concrete matrix. This leads to an increase of the thermal contact resistance and weakens the mechanical strength of concrete. In order to solve this negative effect, Zhang et al. [41] modified the surface of the microcapsules to improve the compatibility between the microcapsules and mortal matrix, thus improving the compressive strength of the MPCM-mortar. Future work could focus on improving microcapsules with low tendency of agglomeration, high compatibility to the concrete matrix and strong mechanical properties.

It is also important to point out that although the loss of compressive strength of concrete is significant after adding microcapsules, the compressive strength of GPC2.7 (45.3 ± 0.8 MPa) and PCC3.2 (34.1 ± 0.4 MPa) confirms to the mechanical European regulation (EN 206-1, compressive strength class C20/25) for concrete for building construction. An optimal system should contain as many microcapsules as possible (to improve the thermal

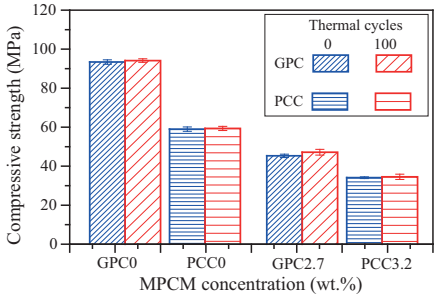

Fig. 12. The compressive strength of concrete including PCC without MPCM (PCC0), PCC containing 3.2 wt.% MPCM (PCC3.2), GPC without MPCM (GPC0) and GPC containing 2.7 wt.% MPCM (GPC2.7) before and after subjecting the samples to 100 accelerated thermal cycles.

performance), while still satisfying the European regulation for compressive strength. Unfortunately, further increasing the MPCM concentrations causes a too low workability of the concretes to produce usable samples.

Fig. 12 also shows that the compressive strength of MPCM-concrete is the same (within the experimental errors) before and after exposing the samples to 100 thermal cycles. This illustrates that the MPCM-concrete can experience temperature changes around the melting point of paraffin many times without changing the properties. A higher number of thermal cycles will be tested in the future to obtain more information about thermal cycling resistance of MPCM-concrete.

4. Conclusion

Materials with high thermal energy storage capacity were fabricated by direct mixing of microencapsulated phase change materials (MPCM) to Portland cement concrete (PCC) and geopolymer concrete (GPC). The addition of MPCM strongly affects the thermal performance and compressive strength of PCC and GPC. Raising the amount of microcapsules reduces the thermal conductivity and increases the latent heat of concrete. Interestingly, the replacement of sand by microcapsules did not change the specific heat capacity of concrete. Furthermore, the addition of microcapsules caused an increase of the porosity of the concrete. Microcapsules were found to have a stronger effect on GPC than on PCC, causing a higher porosity increase of GPC compared to PCC (slopes of 1.1 for GPC and 0.6 for PCC). The enhanced porosity is probably the reason for the higher thermal conductivity reduction rate of GPC (0.12) compared to PCC (0.09).

The increase in latent heat and the decrease in thermal conductivity could significantly improve the thermal performance of concrete building materials in terms of saving energy. The power consumption for stabilizing the indoor temperature at 23 °C may save up to 11% (PCC) and 15% (GPC) after adding 3.2 wt.% MPCM to PCC and 2.7 wt.% MPCM to GPC. This indicates that the thermal insulation effect play an important role on the energy saving in building applications.

Unfortunately, the addition of microcapsules resulted in a significant loss of concrete compressive strength. After adding 3.2 wt.% of microcapsules, the compressive strength of PCC decreased around 42%. For GPC, the reduction of compressive strength is higher than that of PCC. It is approximately 51% after integrating 2.7 wt.% of microcapsules. The loss of compressive strength may be ascribed to low mechanical strength of microcapsules and the enhanced porosity. Although the loss of compressive strength is significant, the compressive strength of MPCM-concrete satisfies the demand of mechanical properties for structural applications. It is therefore, possible to increase the amount of microcapsules to improve the thermal performance and still satisfy the demand of mechanical properties for structural applications. In addition, the agglomeration of microcapsules may reduce the ability of the microcapsules to fill in cavities in the concrete matrix, leading to higher porosity of the concrete. Improved microcapsules with reduced tendency for agglomerations and good mechanical properties would be interesting for further studies.

Acknowledgement

We gratefully acknowledge funding from the Research Council of Norway, project number 238198. The authors gratefully acknowledge Rino Nilsen, Trond Atle Drøbak at Østfold University College and Van Thi Ai Nguyen for their assistance with laboratory work.

References

[1] Allcott H, Greenstone M. Is there an energy efficiency gap? J Econ Perspect 2012;26:3–28.
[2] Khan Z, Khan Z, Ghafoor A. A review of performance enhancement of PCM based latent heat storage system within the context of materials, thermal stability and compatibility. Energy Convers Manage 2016;115.
[3] Khan Z, Khan Z, Tabeshf K. Parametric investigations to enhance thermal performance of paraffin through a novel geometrical configuration of shell and tube latent thermal storage system. Energy Convers Manage 2016;127:355–65.
[4] Dincer I, Rosen MA. Thermal energy storage systems and applications. 2nd ed. A John Wiley and Sons Ltd; 2011.
[5] Urschitz G, Walter H, Brier J. Experimental investigation on bimetallic tube compositions for the use in latent heat thermal energy storage units. Energy Convers Manage 2016;125:368–78.
[6] Abedin AH, Rosen MA. A critical review of thermochemical energy storage systems. Open Renew Energy J 2011;4:42–6.
[7] de Gracia A, Cabeza LF. Phase change materials and thermal energy storage for buildings. Energy Build 2015;103:414–9.
[8] da Cunha JP, Eames P. Thermal energy storage for low and medium temperature applications using phase change materials – a review. Appl Energy 2016;177:227–38.
[9] Fenollera María, Míguez José Luis, Goicoechea Itziar, Lorenzo Jaime, Ángel Álvarez Miguel. The influence of phase change materials on the properties of self-compacting concrete. Materials 2013;6:3530–46.
[10] Han P, Qiu X, Lu L, Pan L. Fabrication and characterization of a new enhanced hybrid shell microPCM for thermal energy storage. Energy Convers Manage 2016;126:673–85.
[11] Jamekhorshid A, Sadrameli SM, Farid M. A review of microencapsulation methods of phase change materials (PCMs) as a thermal energy storage (TES) medium. Renew Sustain Energy Rev 2014;31:531–42.
[12] Tyagi VV, Kaushik SC, Tyagi SK, Akiyama T. Development of phase change materials based microencapsulated technology for buildings: a review. Renew Sustain Energy Rev 2011;15:1373–91.
[13] Zhu Y, Liang S, Wang H, Zhang K, Jia X, Tian C, et al. Morphological control and thermal properties of nanoencapsulated n-octadecane phase change material with organosilica shell materials. Energy Convers Manage 2016;119:151–62.
[14] Buscombe A, Wu M. A review of PCM's thermal performance within lightweight construction. Int J Eng Pract Res (IJEPR) 2013;2:174–7.
[15] Hunger M, Entrop AG, Mandilaras I, Brouwers HJH, Founti M. The behavior of self-compacting concrete containing micro-encapsulated phase change materials. Cement Concrete Compos 2009;31:731–43.
[16] Cui H, Liao W, Mi X, Lo TY, Chen D. Study on functional and mechanical properties of cement mortar with graphite-modified microencapsulated phase-change materials. Energy Build 2015;105:273–84.
[17] Joulin A, Zalewski L, Lassue S, Naji H. Experimental investigation of thermal characteristics of a mortar with or without a micro-encapsulated phase change material. Appl Therm Eng 2014;66:171–80.
[18] Shadnia R, Zhang L, Li P. Experimental study of geopolymer mortar with incorporated PCM. Constr Build Mater 2015;84:95–102.
[19] Thiele AM, Jamet A, Sant G, Pilon L. Annual energy analysis of concrete containing phase change materials for building envelopes. Energy Convers Manage 2015;103:374–86.
[20] Benhelal E, Zahedi G, Shamsaei E, Bahadori A. Global strategies and potentials to curb CO_2 emissions in cement industry. J Clean Prod 2013;51:142–61.
[21] Rajini B, Rao AVN. Mechanical properties of geopolymer concrete with fly ash and GGBC as source materials. Int J Innov Res Sci Eng Technol 2014;3:15944–53.
[22] Duxson P, Fernandez-Jimenez A, Provis JL, Lukey GC, Palomo A, van Deventer JSJ. Geopolymer technology: the current state of the art. J Mater Sci 2007;42:2917–33.
[23] Zuhua Z, Xiao Y, Huajun Z, Yue C. Role of water in the synthesis of calcined kaolin-based geopolymer. Appl Clay Sci 2009;43:218–23.
[24] Neupane K. Investigation on modulus of elasticity of powder-activated geopolymer concrete. Int J Struct Eng 2016;7:262–78.
[25] Borreguero AM, Valverde JL, Rodríguez JF, Barber AH, Cubillo JJ, Carmona M. Synthesis and characterization of microcapsules containing Rubitherm® RT27 obtained by spray drying. Chem Eng J 2011;166:384–90.
[26] Standard BS EN 12390-7. Testing hardened concrete. Part 7: Density of hardened concrete; 2009.
[27] Liu MYJ, Alengaram UJ, Jumaat MZ, Mo KH. Evaluation of thermal conductivity, mechanical and transportproperties of lightweight aggregate foamed geopolymer concrete. Energy Build 2014;72:238–45.
[28] Safiuddin M, Hearn N. Comparison of ASTM saturation techniques for measuring the permeable porosity of concrete. Cem Concr Res 2005;35:1008–13.
[29] Cao VD, Salas-Bringas C, Schüller RB, Szczotok AM, Hiorth M, Rodriguez JF, et al. Rheological properties and thermal performance of suspensions of microcapsules containing phase change materials Submitted for publication; 2016.
[30] Tittelein P, Gibout S, Franquet E, Johannes K, Zalewski L, Kuznik F, et al. Simulation of the thermal and energy behaviour of a composite material containing encapsulated-PCM: influence of the thermodynamical modelling. Appl Energy 2015;140:269–74.

[31] Mucteba U, Kemalettin Y. Effect of mineral admixtures on properties of self-compacting concrete. Cement Concr Compos 2011;33:771–6.
[32] Nikbin IM, Beygi MHA, Kazemi MT, Vaseghi Amiri J, Rabbanifar S, Rahmani E, et al. A comprehensive investigation into the effect of water to cement ratio and powder content on mechanical properties of self-compacting concrete. Constr Build Mater 2014;57:69–80.
[33] Norvell C, Sailor DJ, Dusicka P. The effect of microencapsulated phase-change material on the compressive strength of structural concrete. J Green Build 2013;8:116–24.
[34] Fedroff D, Ahmad S, Savas B. Mechanical properties of concrete with ground waste tire rubber. Transport Res Board 1996;1532:66–72.
[35] Khatib ZK, Bayomy FM. Rubberized Portland cement concrete. J Mater Civil Eng 1999;11:206–13.
[36] Moosberg-Bustnes H, Lagerblad B, Forssberg E. The function of fillers in concrete. Mater Struct 2004;37:74–81.
[37] Dehdezi Pejman Keikhaei, Hall Matthew R, Dawson Andrew R, Casey Sean P. Thermal, mechanical and microstructural analysis of concrete containing microencapsulated phase change materials. Int J Pavement Eng 2012:449–62.
[38] Borreguero AM, Serrano A, Garrido I, Rodríguez JF, Carmona M. Polymeric-SiO_2-PCMs for improving the thermal properties of gypsum applied in energy efficient buildings. Energy Convers Manage 2014;87:138–44.
[39] Borreguero AM, Garrido I, Valverdea JL, Rodríguez JF, Carmona M. Development of smart gypsum composites by incorporating thermoregulating microcapsules. Energy Build 2014;76:631–9.
[40] Ukrainczyk N, Kurajica S, Šipušić J. Thermophysical comparison of five commercial paraffin waxes as latent heat storage materials. Chem Biochem Eng Quart 2010;24:129–37.
[41] Zhang J, Yan H, Chen SL, Wang XM, Gu ZD. The preparation and properties of the low melting point microencapsulated paraffin insulation mortar. Appl Mech Mater 2011;71–78:4835–8.

Paper IV

Influence of microcapsules size and shell polarity on the time-dependent viscosity of geopolymer paste.

Vinh Duy Cao, Shima Pilehvar, Carlos Salas-Bringas, Anna M. Szczotok, Nu Bich Duyen Do, Hoa Thanh Le, Manuel Carmona, Juan F. Rodriguez, Anna-Lena Kjøniksen.

Industrial& Engineering Chemistry Research **2018**, 57, 9457-9464.

I&EC research
Industrial & Engineering Chemistry Research

Article

Cite This: *Ind. Eng. Chem. Res.* 2018, 57, 9457−9464

pubs.acs.org/IECR

Influence of Microcapsule Size and Shell Polarity on the Time-Dependent Viscosity of Geopolymer Paste

Vinh Duy Cao,[†,‡] Shima Pilehvar,[†,§] Carlos Salas-Bringas,[‡] Anna M. Szczotok,[†,∥] Nu Bich Duyen Do,[⊥] Hoa Thanh Le,[¶] Manuel Carmona,[∥] Juan F. Rodriguez,[∥] and Anna-Lena Kjøniksen*[,†]

[†]Faculty of Engineering, Østfold University College, N-1757 Halden, Norway

[‡]Faculty of Science and Technology, Norwegian University of Life Sciences, N-1432 Ås, Norway

[§]Department of Material Engineering and Manufacturing, Technical University of Cartagena, 30202 Cartagena, Murcia, Spain

[∥]Department of Chemical Engineering, University of Castilla − La Mancha, 13004 Ciudad Real, Spain

[⊥]Faculty of Technology, Natural Sciences and Maritime Sciences, University College of Southeast Norway, N-3184 Borre, Norway

[¶]Department of Micro and Nanotechnology, DTU Nanotech, Technical University of Denmark, 2800 Kongens Lyngby, Denmark

Supporting Information

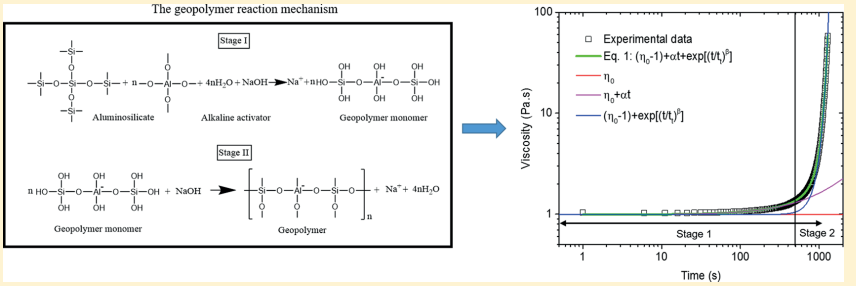

ABSTRACT: The effects of microencapsulated phase-change materials (MPCM) on the rheological properties of a geopolymer paste (GPP) were investigated. In order to quantify the time-dependent viscosity increase of the geopolymer paste containing MPCM (GPP-MPCM), a new rheological model was successfully developed. Three different MPCMs were compared in order to examine the effect of the hygroscopic nature of the microcapsule shells and the size distribution of the microcapsules. In addition, the effect of microcapsule concentration was investigated. It was found that microcapsules with polar functional groups on the shells affect the viscosity and the geopolymerization reaction of the geopolymer paste much more than microcapsules with hydrophobic shells. In addition, aggregated microcapsules influence the viscosities less than unaggregated microcapsules.

1. INTRODUCTION

Portland cement is one of the most important components in building materials because of its important role in producing high-performance concrete. However, producing this cement emits a huge amount of CO_2 into the environment.[1,2] This contributes to around 5−8% of the total worldwide CO_2 emission into the atmosphere.[1,3] Geopolymers synthesized by alkali activation of aluminosilicate in amorphous form (from industrial waste materials) have recently received considerable attention as an environmentally friendly material to partly replace Portland cement.[4,5] By replacing Portland cement with a geopolymer, CO_2 emission from the cement industry can be significantly reduced.

Approximately 40% of the total global energy consumption is from buildings; therefore, the reduction of energy consumption by buildings is important for the environment.[6,7] Phase-change materials (PCM), with the capability of storing and releasing high amounts of energy around the phase-change temperature, have been integrated into building materials to enhance the thermal performances of buildings. However, the practical applications are limited because of reactions with surrounding materials, which cause reductions of the mechanical strength of the building materials and deteriorate the thermal properties of PCM.[8,9] In order to avoid these adverse interactions, the PCM can be incorporated into protective microcapsules. Microencapsulated phase-change materials (MPCM) have therefore been utilized for integration into building materials to improve the heat-storage capacity and thermal insulation.[9−13] This is a promising solution to

Received: May 4, 2018
Revised: June 25, 2018
Accepted: June 26, 2018
Published: June 26, 2018

DOI: 10.1021/acs.iecr.8b01961
Ind. Eng. Chem. Res. 2018, 57, 9457−9464

Table 1. Composition of the Geopolymer Pastes (GPPs) Utilized in the Rheology Measurements

sample	MPCM (wt %)	alkaline solution (g)	water (g)	FA (g)	GGBFS (g)	MPCM (g)
GPP0	0	220	55	300	200	0
GPP3	3	220	55	300	200	24
GPP6	6	220	55	300	200	50
GPP9	9	220	55	300	200	77
GPP12	12[a]	220	55	300	200	106

[a]MF/PCM24 was not utilized at 12 wt % because its viscosity was too high.

enhance the energy efficiency of buildings. It is, however, important to ensure that the microcapsules do not break during the mixing process,[14] as this will adversely affect the thermal properties[15] and is expected to influence the rheological behavior.[16] The integration of MPCM into geopolymer materials has been investigated in recent years, showing promising results for reducing the energy consumption of buildings.[11−13] For incorporation into geopolymers, the MPCM should be able to withstand the highly alkaline environment of the geopolymer mixture. Previous investigations have mainly focused on the thermal and mechanical properties as well as the energy efficiency of these materials. However, studies on the effects of microencapsulated phase-change materials on the rheological properties and geopolymerization reaction of geopolymer pastes are scarce, even though the rheological behavior is important for the geopolymer properties. Previous studies revealed a correlation between rheology and the geopolymerization reaction of a geopolymer paste, where an increase in viscosity as a function of time corresponded to each geopolymerization stage.[17] Therefore, it is possible that the influence of microcapsules on the geopolymerization reaction can be investigated through their effect on the time-dependent viscosity.

In this article, a geopolymer paste is employed for the integration of microencapsulated phase-change materials. Special attention is focused on the influence of the hygroscopic nature of the polymer shells, the size distribution, and the microcapsule concentration on the geopolymerization reaction and time-dependent viscosity of the geopolymer paste. In order to quantify the time-dependent changes of the viscosities of the MPCM−geopolymer paste and the geopolymerization reaction, a new empirical equation that provides a good representation of the experimental data has been proposed. In addition, the microstructure of the geopolymer paste (GPP) containing the microcapsules was determined by SEM to evaluate whether the microcapsules can withstand the mixing process.

2. EXPERIMENTAL SECTION

2.1. Materials. A geopolymer paste containing microencapsulated phase-change materials (MPCM−GPP) was fabricated by mixing fly ash (FA, Norcem), ground granulated blast-furnace slag (GGBFS, Cemex), MPCM, and an alkaline activator solution that was a mixture of 120 g of a sodium silicate solution (35 wt % solids) and 80 g of a 14 M NaOH solution. The recipe of the GPP is shown in Table 1. The MPCM concentration, which was calculated as the weight percentage of the total geopolymer paste, was varied from 0 to 12 wt % in steps of 3 wt %. However, MF/PCM24 was not utilized at a concentration of 12 wt % because it had too high a viscosity for measurements.

Three different kinds of microcapsules were utilized. PS-DVB/*RT*27 is composed of a paraffin Rubitherm RT27 core coated with a shell of polystyrene cross-linked with divinylbenzene (PS-DVB).[18] Micronal DS-5038X (Microtek, USA) is composed of a paraffin-mixture core and a highly cross-linked poly(methyl methacrylate) (PMMA) shell.[19] Microtek MPCM24D (Microtek) is composed of a paraffin-mixture core and a melamine-formaldehyde polymer shell (MF).[20] Table 2 summarizes the properties of the three MPCMs.

Table 2. Fundamental Data of the Microencapsulated Phase-Change Materials

MPCM name	functional groups on the shell	melting point[a] (°C)	latent heat[a] (J/g)
PS-DVB/*RT*27	phenyl (nonpolar)	24.9	100
PMMA/PCM26	ester (polar)	24.7	110
MF/PCM24	amine (polar)	21.9	154

[a]The melting points and latent heats were determined by differential-scanning calorimetry (see the Supporting Information for details).

2.2. Rheology. Rheological measurements were carried out using an Anton Paar MCR302 rheometer. The MPCM−geopolymer pastes were tested using a building-materials-cell (BMC-90) measuring system (cup diameter: 74 mm; bob diameter: 59 mm, stirrer ST59-2 V-44.3/120) mounted in a cylindrical Peltier system for temperature control.

The MPCM can be broken during the concrete-mixing process, leading to leaching of PCM.[14] The nonencapsulated PCM can have a significant effect on the geopolymer properties. Nonencapsulated PCM can contribute to agglomeration of the microcapsules, leading to a decrease of the mechanical properties, reduced thermal performance of the concrete,[9,11] and an increase of the viscosity of the mixture.[16] Although the PCM (paraffin) in the current study is inert to the concrete environment (an alkaline solution),[9] it might retard the geopolymerization reaction by coating the binder particles (FA/GGBFS).[21] It is therefore important to prevent rupture of the MPCM, to avoid interference of nonencapsulated PCM in the rheological properties of the geopolymer.

In order to avoid MPCM damage, FA, GGBFS, and MPCM were gently mixed together at room temperature (20 ± 1 °C) for 1 min using a mixer (Electrolux EKM4300). The alkaline solution and water were added continuously into the mixed powder for 30 s, and the geopolymer paste was mixed for 3 more minutes. After mixing, the geopolymer paste was loaded into the rheometer measuring cell. The sample was left in the cell for 30 s before being presheared at 50 s^{-1} for 1 min to ensure that the samples had the same shear histories. After the preshear, the samples were left to equilibrate for 1 min to achieve a uniform state. The MPCM−geopolymer paste was

DOI: 10.1021/acs.iecr.8b01961
Ind. Eng. Chem. Res. 2018, 57, 9457−9464

sheared at a constant shear rate of 10 s^{-1} until the viscosity increased too much to continue the measurements. The testing temperature was set at 20 °C, which is close to room temperature and below the melting point of the phase-change materials, to minimize the possibility of rupturing the microcapsules during the rheology test.

In order to quantify the time-dependent changes of the viscosities, a new empirical equation (eq 1) was developed:

$$\eta(t) = (\eta_0 - 1) + \alpha t + \exp\left[\left(\frac{t}{t_t}\right)^{\beta}\right] \quad (1)$$

where $\eta(t)$ and η_0 are the viscosity as a function of time (t) and the initial viscosity of the MPCM−geopolymer paste, respectively. α, β, and t_t are the kinetic constants for the initial linear viscosity increase, the exponential-growth kinetic constant, and the transition time from linear increase to exponential growth, respectively.

2.3. Geopolymer-Paste Temperature during Geopolymerization. After being mixed, the geopolymer paste without MPCM and with 6 wt % MPCM were casted into a mold (50 × 50 × 50 mm) that was made of 20 mm thick wood with an open top surface. The temperature change of the geopolymer paste during the geopolymerization process was recorded using thermocouple type T (Omega) via a multichannel multimeter (LR8410-20, Hioki). The thermocouple was inserted into the center of the geopolymer-paste sample after casting. The data was recorded every 0.5 s for a period of 5 h. The test was conducted at room temperature (20 ± 1 °C). The temperature of the geopolymer paste during the mixing period was not recorded. The temperature increment due to the exothermic geopolymerization reaction during the mixing process was determined as the difference between the room temperature (20 ± 1 °C) and the geopolymer-paste temperature after the mixing process.

2.4. Size Distribution of MPCM. Low-angle laser-light-scattering (LALLS) laser diffraction using a Malvern Mastersizer 2000 (Malvern Instruments Ltd.) equipped with a Scirocco 2000 unit for analyzing dispersions of the particles in air was employed to determine the size distribution of the MPCMs.

2.5. Trapped-Water Test. The dispersion of microcapsules (5.0 ± 0.1 g) and alkaline solution (50 mL) was fabricated at room temperature (20 ± 1 °C) to compare the polarity of the polymer shell with the ability of the microcapsules to trap water. After immersing the MPCM in an alkaline solution for 24 h, MPCM was separated from the alkaline solution by centrifugation (Mega Star 1.6R) of the suspension in filter test tubes (0.45 μm filter membrane) at 4500 rpm for 5 min. Afterward, the remaining trapped water on the MPCM was determined by a moisture analyzer (MB 64M-VWR) at 70 °C to gently remove the adsorbed water without damaging the MPCM or degrading the PCM core.

2.6. Scanning Electron Microscopy. The microstructure and the surface morphology of the microcapsules in powder form was examined by scanning electron microscopy (SEM, Quanta FEG-250).

In order to determine the effect of the mixing process and the shear induced during the rheology measurements on the structure of the microcapsules, the microstructure of GPP containing 6 wt % microcapsules was investigated by SEM (Zeiss Supra 40 VP) at an accelerating voltage of 15 kV. Backscattered-electrons (BSE) mode was utilized to obtain good contrast between the microcapsules and the geopolymer matrix. For this test, the GPP containing 6 wt % microcapsules was collected after the rheology test of the sample.

3. RESULTS AND DISCUSSION

The size distribution and SEM images of the three types of microcapsules are shown in Figure 1. The SEM images show

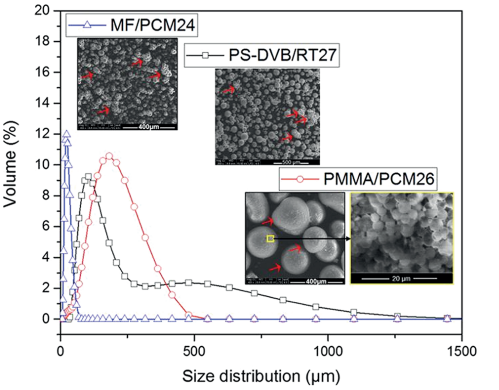

Figure 1. Size (diameter) distribution of the PS-DVB/*RT*27, PMMA/PCM26, and MF/PCM24 microcapsules (including aggregates) together with SEM images of the microcapsules. The red arrows show the microcapsule aggregates.

that PS-DVB/*RT*27, PMMA/PCM26, and MF/PCM24 exhibit spherical shapes with a strong tendency to form agglomerated structures (red arrows), especially PMMA/PCM26. The diameters of the single microcapsules, which were determined by SEM (Supporting Information), are in the ranges of 10−100, 1−3, and 10−30 μm for PS-DVB/*RT*27, PMMA/PCM26, and MF/PCM24, respectively. However, the mean agglomerated-microcapsule diameters determined by a Mastersizer are 130 μm for PS-DVB/*RT*27, 155 μm for PMMA/PCM26, and 21 μm for MF/PCM24. The differences in the size distributions of the three kinds of microcapsules may have an important impact on the rheological properties and geopolymerization properties of the geopolymer paste.

After immersing the MPCM in an alkaline solution (corresponding to the alkaline solution used in the geopolymer) for 24 h, the microcapsules remained stable, with a spherical shape and the same size as before (single microcapsules), (see Supporting Information Figure S3). This demonstrates that the microcapsules can withstand the alkaline solution of the geopolymer paste. This is in good agreement with previous findings.[9] The trapped water in the microcapsule structure is presented in Figure 2. Under alkaline conditions, the amount of trapped water is lowest for PS-DVB/*RT*27 and highest for PMMA/PCM26. Both the differences in the chemical structure of the polymer shells (Figure 2) and the size of the MPCM (Figure 1) can contribute to this. A higher amount of water is expected to be adsorbed on polymer shells containing polar functional groups compared with nonpolar shells. Accordingly, the nonpolar phenyl groups of PS-DVB are expected to adsorb less water than the polar groups of PMMA (ester groups) and MF (amine groups), which is in agreement with Figure 2. In addition, small particles have a larger surface

DOI: 10.1021/acs.iecr.8b01961
Ind. Eng. Chem. Res. 2018, 57, 9457−9464

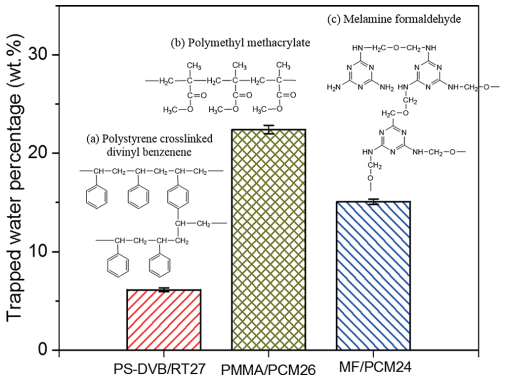

Figure 2. Effect of polymer-shell structure on the trapped water of the microcapsules. The inserted images show the chemical structures of (a) polystyrene cross-linked divinyl benzene (PS-DVB), (b) poly(methyl methacrylate) (PMMA), and (c) melamine formaldehyde (MF).

area per unit volume and can therefore adsorb more water on the surfaces of the particles. The smaller size of a single PMMA/PCM26 microcapsule (1−3 μm) compared with a single MF/PCM24 microcapsule (10−30 μm) can explain why PMMA/PCM26 exhibits the highest amount of trapped water. The different polarities of PMMA and MF might also play a role,[22] but unfortunately, the exact differences in polarities are unknown. To determine the exact polarity of each kind of microcapsule would be interesting for further studies.

The temperature of the geopolymer paste after the mixing process was recorded for a period of 5 h (Figure 3). The

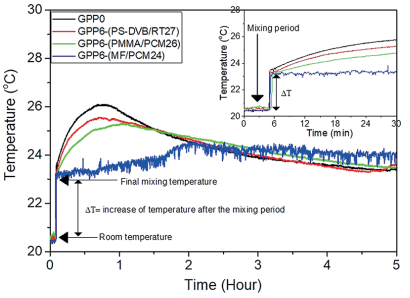

Figure 3. Temperature of geopolymer paste containing 6 wt % microcapsules during the first 5 h after mixing. The inserted graph shows a magnification of the first 30 min. The temperature of the geopolymer paste was not recorded during the mixing process.

temperature of the geopolymer paste increased from room temperature (20 ± 1 °C before mixing) to approximately 23 °C after the mixing process. The temperature increase during the mixing process is due to the exothermic geopolymerization process.[23] The temperature of the geopolymer paste continued to increase after the mixing stage. For geopolymer paste without MPCM, a peak was reached at approximately 26 °C. This is in good agreement with Suwan et al., who studied the internal heat liberation of geopolymers at ambient curing conditions.[23] As can be seen from Figure 3, the peak temperature decreased after the addition of microcapsules. The microcapsules can absorb a high amount of heat during the phase change, which can reduce the temperature increase of the GPP.[14] The lowest peak temperature (about 24 °C) and longest time to reach the peak (2 h) was observed for GPP containing MF/PCM24, which has the highest latent heat (Table 2). In addition, MF/PCM24 has the lowest melting temperature (21.9 °C), which is closest to the temperature of the geopolymer paste. However, the latent heat of the microcapsules is not the only mechanism that might cause the reduced temperature of the geopolymer paste. It is also possible that the addition of microcapsules might interfere with the geopolymerization reaction, thereby reducing the heat release and peak temperature of the geopolymer paste. Further studies are needed to explore this possibility in more detail.

SEM images of MPCM−GPP with 6 wt % microcapsules are shown in Figure 4. Most of the single microcapsules were

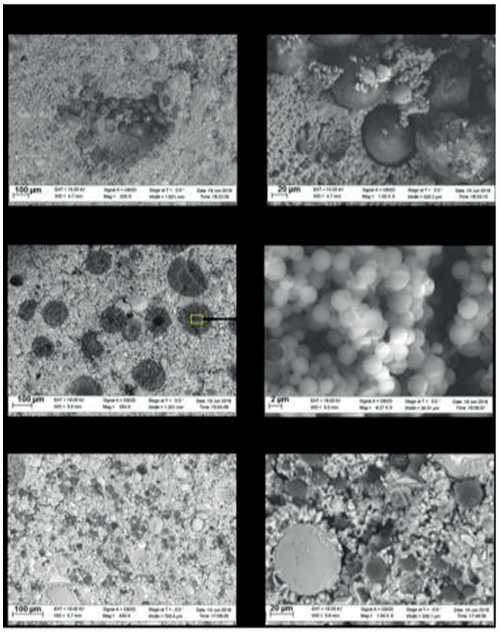

Figure 4. SEM images of geopolymer paste containing 6 wt % microcapsules: (a) GPP6−(PS-DVB/*RT*27), (b) GPP6−(PMMA/PCM26), and (c) GPP6−(MF/PCM24).

observed to be stable after the mixing process. There is no evidence of any cracks in the microcapsules, and no leached PCM is observed on the structures of the microcapsules. This demonstrates that the microcapsules can withstand the current mixing process, even though the exothermic-reaction heat of the geopolymerization process will cause the PCM to be in a liquid state during the mixing process. This is in good agreement with previous studies, where the MPCM remained stable after concrete-, mortar-, and cement-paste mixing.[24−27] However, this observation is different from that of Hunger et al.,[14] who reported that microcapsules were damaged after the concrete-mixing process. This was explained by the intensive

DOI: 10.1021/acs.iecr.8b01961
Ind. Eng. Chem. Res. 2018, 57, 9457−9464

mixing of a horizontal concrete mixer, which can produce a high shear stress on the microcapsules. The absence of sand and gravel combined with a relatively gentle mixing force in the current study probably contributes to the prevention of microcapsule rupture during the mixing process. In addition, the mechanical strength of the utilized microcapsules contributes to their ability to withstand the mixing process.

Rheology of MPCM−Geopolymer Paste. The geopolymer binder is an inorganic material based on the polymerization of aluminosilicate materials and a concentrated alkaline solution (Figure 5). The polymerization process

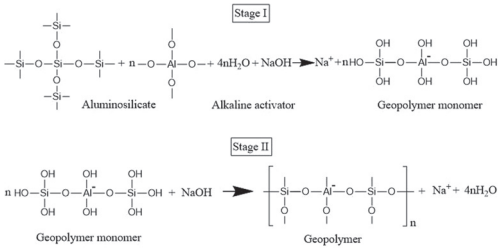

Figure 5. Geopolymer-reaction mechanism between the sodium hydroxide activator and the Si−Al source materials.

includes two stages. In Stage I, Si and Al atoms from the source material react with hydroxide ions to form geopolymer precursor ions (monomers). In Stage II, the precursor ions (monomers) polymerize to form the 3-D geopolymer structure.[28,29]

Figure 6a illustrates how the viscosity changes during the different stages of the geopolymerization procedure. After the initial 7 min mixing procedure (see the Experimental Section for details), the viscosity measurements were started. Each stage of the polymerization process (Figure 5) can be correlated to the time-dependent viscosity of the geopolymer paste. Accordingly, the viscosity of the geopolymer paste as function of time includes two main regions:

Stage I: The viscosity increases linearly with time as a result of the formation of the higher-molecular-weight precursor or monomer.

Stage II: The polymerization process that forms 3-D geopolymer structures dominates the viscosity profile, causing an exponential growth of the viscosity. This is consistent with previous findings.[17]

By utilizing eq 1, it is possible to quantify these two stages, and evaluate the effect of microcapsules on the polymerization process of a geopolymer paste. The experimental data of the viscosity versus time of the geopolymer paste after adding 0 and 6 wt % microcapsules (PS-DVB/*RT*27, PMMA/PCM26, and MF/PCM24) at a shear rate of 10 s^{-1} is shown in Figure 6b together with lines fitted by eq 1.

The various parts of the fitting function are illustrated in Figure 7a. The figure is plotted on a log−log scale to better show the effects at short times and low viscosities. The initial viscosity (η_0) shows where the viscosity starts at the beginning of the measurements. The η_0 obtained from the fitting procedure corresponds well with the initial values of the viscosities measured at short times. During Stage I, the viscosity increases linearly ($\eta = \eta_0 + \alpha t$). When Stage II of the geopolymerization reaction starts to dominate, an exponential increase is observed. Because the exponential equation starts at 1 when t approaches 0, −1 is introduced in the fitting function to obtain the correct value of η_0 from the fitting procedure. A stretched exponential is used, where the exponent, β, indicates how fast the viscosity is increasing. A higher β value indicates a steeper increase of the viscosity.

The new model (eq 1) was found to fit well with the experimental data, as illustrated by the high values of R^2 (0.99−1) and the fitted lines that follow the experimental data very well both in linear and logarithmic plots (Figures 6 and 7). In order to further examine how well the equation describes the experimental data, residual plots are shown in Figure 7b. The residuals are mostly nonsystematic, illustrating that the equation provides a good fit of the data. The large values and small peaks in the residuals at long times are due to the transition between Stage I and Stage II combined with the higher viscosity values at long times.

Figure 8 shows the parameters from the fits by eq 1. The concentration and the type of microcapsule have a significant effect on the polymerization reaction of the geopolymer paste. The fitted parameters show that an increase in the microcapsule concentration causes a higher initial viscosity (η_0, Figure 8a). This is probably due to the increase of the total surface area of the particles in the geopolymer paste after

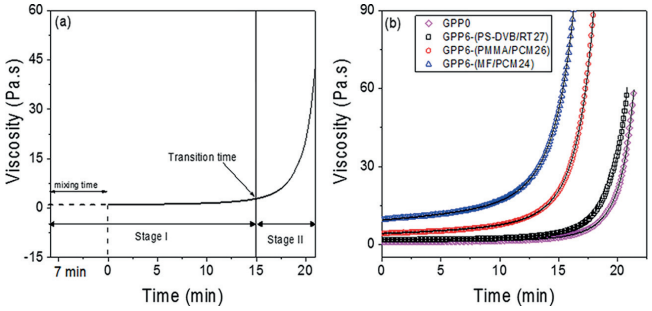

Figure 6. (a) Illustration of the stages of the formation of the geopolymer paste related to the viscosity as function of time. (b) Viscosity of the geopolymer paste without MPCM and with 6 wt % MPCM as functions of time at 20 °C and measured at a shear rate of 10 s^{-1}. The symbols are experimental values (every fifth point is shown). The lines are fitted by eq 1.

DOI: 10.1021/acs.iecr.8b01961
Ind. Eng. Chem. Res. 2018, 57, 9457−9464

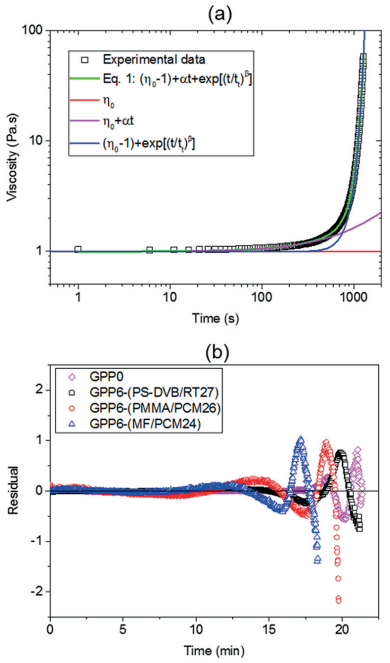

Figure 7. (a) Viscosity of the geopolymer paste without MPCM as a function of time at 20 °C. The symbols are experimental values (every fifth point is shown). The lines illustrate how the various parts of eq 1 model the different stages of the experimental data. (b) Residuals between experimental and fitted data as a function of time for the viscosity of the geopolymer paste without MPCM and with 6 wt % MPCM.

microcapsules are added.[11] Water can be adsorbed onto the surfaces of the microcapsules. A higher surface area can therefore reduce the free water in the sample, thereby increasing the viscosity. In addition, as the concentration of microcapsules increases, the distance between the microcapsules becomes shorter, causing an obstruction of the movement of the fluid around them, which results in higher viscosity.[11,30] The increase in the initial viscosity (η_0) as a function of MPCM concentration is fastest for MF/PCM24 and slowest for PS-DVB/*RT*27. This might reflect the polar and nonpolar natures of the microcapsule shells. The hydrophobic PS-DVB/*RT*27 adsorbs much less water on the surface than MF/PCM24 and PMMA/PCM26 (Figure 2) and therefore affects the initial viscosity (η_0) to a smaller degree (Figure 8a). The initial viscosity (η_0) increases faster when the concentration is raised for MF/PCM24 than for PMMA/PCM26. However, according to Figure 2, PMMA/PCM26 adsorbs more water than MF/PCM24. The different testing conditions can contribute to this discrepancy. For the trapped-water test, the long immersion time (24 h) and the low viscosity of the alkaline solution allows the solution to easily penetrate deeply inside the structure of the PMMA/PCM26 agglomerates. Accordingly, all the single PMMA/PCM26 microcapsules can be covered by the alkaline solution, thereby causing more water to be adsorbed by PMMA/PCM26 compared with by MF/PCM24. However, for the rheology test, the higher viscosities of the geopolymer paste and the shorter contact times might prevent water from penetrating into the PMMA/PCM26 agglomerates. This can cause a lower effective water adsorption, because only the outer parts of the agglomerates adsorb water.

The precursor kinetic constant, α, which indicates how fast the viscosity increases during the first stage, rises as the microcapsule concentration becomes higher (Figure 8c). This indicates that the reaction forming the geopolymer precursor and monomer is faster. When the microcapsule concentrations are raised, α increases much faster for the MPCMs with polar

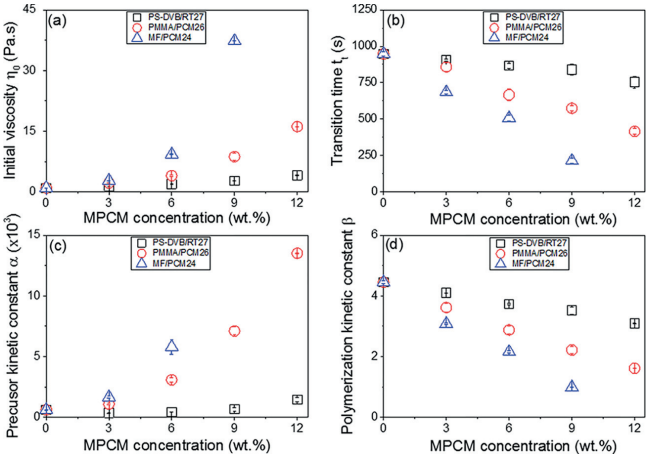

Figure 8. Rheological parameters of the geopolymer paste as functions of microcapsule concentration obtained by fitting eq 1. (a) Initial viscosity, η_0; (b) transition time, t_t; (c) precursor kinetic constant, α; and (d) polymerization kinetic constant, β. MF/PCM24 could not be measured at the highest concentration because the reaction rate was too fast.

DOI: 10.1021/acs.iecr.8b01961
Ind. Eng. Chem. Res. 2018, 57, 9457−9464

groups on the polymer shells (MF/PCM24 and PMMA/PCM26) than for PS-DVB/*RT*27, which has a nonpolar shell. As for η_0, α increases faster for MF/PCM24 than for PMMA/PCM26. This suggests that the faster reaction rates forming the geopolymer precursor and monomer are due to the reduction of free water in the sample when water is adsorbed onto the microcapsule surfaces. Less free water might increase the concentration of the Si−Al source material (Figure 5) in the liquid phase, thereby speeding up the reaction rate. It should be noted that the precursor kinetic constant, α, of the geopolymer paste containing 9 wt % MF/PCM24 gave a slightly negative value after fitting to eq 1. This is unrealistic because the viscosity increases with time (Figure 9). It is

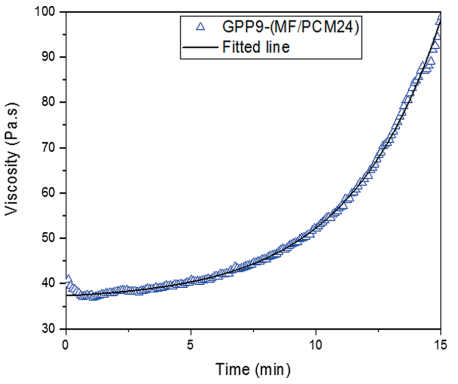

Figure 9. Viscosity of the geopolymer paste containing 9 wt % MF/PCM24 as a function of time at 20 °C. The symbols are experimental values (every fifth point is shown). The line shows the fitted values according to eq 1 with the precursor kinetic constant, α, fixed equal to 0.

possible that at this high concentration of MF/PCM24 (9 wt %), the formation of the precursor during Stage I occurs very fast (i.e., it mostly finishes during the 7 min mixing process, Figure 6a). Accordingly, the measured viscosity only represents Stage II of the geopolymerization reaction. Working from this assumption, the precursor kinetic constant, α, of the geopolymer paste containing 9 wt % MF/PCM24 was set to 0 during the fitting procedure. As can be seen from Figure 9, this assumption seems reasonable because the fitted line is in good agreement with the experimental data, with a high value of R^2 (0.99).

The transition time (t_t) from Stage I to Stage II indicates where the viscosity curve goes from the initial moderate increase to a much steeper curve (Figure 6a). As can be seen from Figure 8b, t_t decreases when more MPCM is added to the samples, and the decline is most pronounced for MF/PCM24 and least evident for PS-DVB/*RT*27. This is in agreement with the faster formation of the geopolymer precursor and monomer for MF/PCM24. Interestingly, the polymerization kinetic constant, β, decreases at higher concentrations of microcapsules, illustrating that at Stage II, the geopolymerization reaction is slowed down by the addition of MPCM. As for the other parameters, the concentration dependence is strongest for MF/PCM24 and weakest for PS-DVB/*RT*27. The slower reaction rates are probably caused by the higher viscosities of the systems, which slow down the transportation of monomers to build up the 3-D structure.

4. CONCLUSION

A new rheological model was successfully developed to investigate the effect of microcapsules on the time-dependent viscosity of a geopolymer paste, obtaining good correlation with the geopolymerization reaction.

The important role of the hygroscopic nature, the sizes and concentrations of microcapsules on the time-dependent viscosity and geopolymerization-reaction rate were investigated. It was found that a higher microcapsule concentration caused an increase of initial viscosity, η_0; faster reaction rates for the formation of the geopolymer precursor and monomer; and a shorter transition time, t_t, to the change from the first stage (the formation of the precursor and monomer) to the second stage (geopolymer formation). Interestingly, at higher concentrations of microcapsules, the polymerization kinetic constant, β, decreased. This demonstrates that the geopolymerization reaction during the second stage is slowed down by the addition of MPCM, probably as a result of the higher viscosities. Overall, MF/PCM24, which has a polymer shell containing polar functional groups and the smallest size distribution (mean size of 21 μm), was found to have the strongest impact on the time-dependent viscosity and geopolymerization-reaction rate of the geopolymer paste when the concentration of MPCM was raised, whereas the weakest dependency was found for PS-DVB/*RT*27, which has a hydrophobic polymer shell. This effect is probably due to the higher amount of water adsorbed onto the microcapsules with more polar functional groups. The PMMA/PCM26 microcapsules affected the viscosities less than the MF/PCM24 microcapsules, although both of these microcapsules had shells with polar groups. The reason for this is probably the agglomerated nature of PMMA/PCM26, which provides a smaller effective surface area on which the water can adsorb.

The developed model can be used as a quantitative tool to design the mixing recipe and mixing process of a geopolymer paste containing MPCM. Further work will focus on the effects of microencapsulated phase-change materials on the rheology and geopolymerization reactions of geopolymer mortar and geopolymer concrete for buildings applications.

■ ASSOCIATED CONTENT

Supporting Information

The Supporting Information is available free of charge on the ACS Publications website at DOI: 10.1021/acs.iecr.8b01961.

Microstructures and sizes of single microcapsules, additional DSC thermograms of different types of microcapsules for determining microcapsule melting points and latent heats, and additional optical-microscope images of microcapsules before and after immersion in alkaline activator solution for 24 h (PDF)

■ AUTHOR INFORMATION

Corresponding Author

*E-mail: anna.l.kjoniksen@hiof.no.

ORCID

Vinh Duy Cao: 0000-0001-5387-3874

Manuel Carmona: 0000-0002-1464-5067

DOI: 10.1021/acs.iecr.8b01961
Ind. Eng. Chem. Res. 2018, 57, 9457−9464

Anna-Lena Kjøniksen: 0000-0003-4864-4043

Notes

The authors declare no competing financial interest.

■ ACKNOWLEDGMENTS

We gratefully acknowledge funding from the Research Council of Norway, project number 238198. The authors gratefully acknowledge Rino Nilsen and Trond Atle Drøbak at Østfold University College for their assistance with laboratory work.

■ REFERENCES

(1) Benhelal, E.; Zahedi, G.; Shamsaei, E.; Bahadori, A. Global strategies and potentials to curb CO2 emissions in cement industry. *J. Cleaner Prod.* **2013**, *51*, 142−161.

(2) Chen, C.; Habert, G.; Bouzidi, Y.; Jullien, A. Environmental impact of cement production: detail of the different processes and cement plant variability evaluation. *J. Cleaner Prod.* **2010**, *18*, 478−485.

(3) Chen, C.; Habert, G.; Bouzidi, Y.; Jullien, A. Environmental impact of cement production: detail of the different processes and cement plant variability evaluation. *J. Cleaner Prod.* **2010**, *18*, 478−485.

(4) Duxson, P.; Fernandez-Jimenez, A.; Provis, J. L.; Lukey, G. C.; Palomo, A.; van Deventer, J. S. J. Geopolymer technology: the current state of the art. *J. Mater. Sci.* **2007**, *42*, 2917−2933.

(5) Zuhua, Z.; Xiao, Y.; Huajun, Z.; Yue, C. Role of water in the synthesis of calcined kaolin-based geopolymer. *Appl. Clay Sci.* **2009**, *43*, 218−223.

(6) *Directive 2002/91/EC of the European Parliament and of the Council of 16 December 2002 on the energy performance of buildings*; European Union: Brussels, 2002.

(7) *Directive 2010/31/EU of the European Parliament and of the Council of 19 May 2010 on the energy performance of buildings*; European Union: Brussels, 2010.

(8) Hunger, M.; Entrop, A. G.; Mandilaras, I.; Brouwers, H. J. H.; Founti, M. The behavior of self-compacting concrete containing micro-encapsulated Phase Change Materials. *Cem. Concr. Compos.* **2009**, *31*, 731−743.

(9) Wei, Z.; Falzone, G.; Wang, B.; Thiele, A.; Puerta-Falla, G.; Pilon, L.; Neithalath, N.; Sant, G. The durability of cementitious composites containing microencapsulated phase change materials. *Cem. Concr. Compos.* **2017**, *81*, 66−76.

(10) Eddhahak-Ouni, A.; Drissi, S.; Colin, J.; Neji, J.; Care, S. Experimental and multi-scale analysis of the thermal properties of Portland cement concretes embedded with microencapsulated Phase Change Materials (PCMs). *Appl. Therm. Eng.* **2014**, *64* (1−2), 32−39.

(11) Cao, V. D.; Pilehvar, S.; Salas-Bringas, C.; Szczotok, A. M.; Rodriguez, J. F.; Carmona, M.; Al-Manasir, N.; Kjøniksen, A.-L. Microencapsulated phase change materials for enhancing the thermal performance of Portland cement concrete and geopolymer concrete for passive building applications. *Energy Convers. Manage.* **2017**, *133*, 56−66.

(12) Pilehvar, S.; Cao, V. D.; Szczotok, A. M.; Valentini, L.; Salvioni, D.; Magistri, M.; Pamies, R.; Kjøniksen, A.-L. Mechanical properties and microscale changes of geopolymer concrete and Portland cement concrete containing micro-encapsulated phase change materials. *Cem. Concr. Res.* **2017**, *100*, 341−349.

(13) Shadnia, R.; Zhang, L.; Li, P. Experimental study of geopolymer mortar with incorporated PCM. *Construction and Building Materials* **2015**, *84*, 95−102.

(14) Hunger, M.; Entrop, A. G.; Mandilaras, I.; Brouwers, H. J. H.; Founti, M. The behavior of self-compacting concrete containing micro-encapsulated Phase Change Materials. *Cem. Concr. Compos.* **2009**, *31*, 731−743.

(15) Drissi, S.; Eddhahak, A.; Caré, S.; Neji, J. Thermal analysis by DSC of Phase Change Materials, study of the damage effect. *Journal of Building Engineering* **2015**, *1*, 13−19.

(16) Cao, V. D.; Salas-Bringas, C.; Schüller, R. B.; Szczotok, A. M.; Hiorth, M.; Rodriguez, J. F.; Carmona, M.; Kjøniksen, A.-L. Rheological and thermal properties of suspensions of microcapsules containing phase change materials. *Colloid Polym. Sci.* **2018**, *296*, 981−988.

(17) Vickers, L.; Rickard, W. D. A.; van Riessen, A. *Fire-Resistant Geopolymers: Role of Fibres and Fillers to Enhance Thermal Properties*; SpringerBriefs in Materials Series; Springer: Singapore, 2015.

(18) Szczotok, A. M.; Carmona, M.; Kjøniksen, A.-L.; Rodriguez, J. F. Equilibrium adsorption of polyvinylpyrrolidone and its role on thermoregulating microcapsules synthesis process. *Colloid Polym. Sci.* **2017**, *295*, 783−792.

(19) *Micronal DS 5038 X*; Datasheet; Microtek Laboratories: Dayton, OH, 2017.

(20) *MPCM 24D*; Datasheet MPDS3300-0026; Microtek Laboratories: Dayton, OH, 2017.

(21) Sakulich, A. R.; Bentz, D. P. Increasing the Service Life of Bridge Decks by Incorporating Phase-Change Materials to Reduce Freeze-Thaw Cycles. *J. Mater. Civ. Eng.* **2012**, *24*, 1034−1042.

(22) Ito, S.; Hashimoto, M.; Wadgaonkar, B.; Svizero, N.; Carvalho, R. M.; Yiu, C.; Rueggeberg, F. A.; Foulger, S.; Saito, T.; Nishitani, Y.; Yoshiyama, M.; Tay, F. R.; Pashley, D. H. Effects of resin hydrophilicity on water sorption and changes in modulus of elasticity. *Biomaterials* **2005**, *26*, 6449−6459.

(23) Suwan, T.; Fan, M.; Braimah, N. Internal heat liberation and strength development of self-cured geopolymers in ambient curing conditions. *Construction and Building Materials* **2016**, *114*, 297−306.

(24) Lucas, S. S.; Senff, L.; Ferreira, V. M.; Barroso de Aguiar, L.; Labrincha, J. A. Fresh State Characterization of Lime Mortars with PCM Additions. *Appl. Rheol.* **2010**, *20* (6), 63162.

(25) Norvell, C.; Sailor, D. J.; Dusicka, P. The Effect of Microencapsulated Phase-Change Material on the Compressive Strength of Structural Concrete. *J. Green Building* **2013**, *8*, 116−124.

(26) Beyhan, B.; Cellat, K.; Konuklu, Y.; Gungor, C.; Karahan, O.; Dundar, C.; Paksoy, H. Robust microencapsulated phase change materials in concrete mixes for sustainable buildings. *Int. J. Energy Res.* **2017**, *41*, 113−126.

(27) Cao, V. D.; Pilehvar, S.; Salas-Bringas, C.; Szczotok, A. M.; Valentini, L.; Carmona, M.; Rodriguez, J. F.; Kjøniksen, A.-L. Influence of microcapsule size and shell polarity on thermal and mechanical properties of thermoregulating geopolymer concrete for passive building applications. *Energy Convers. Manage.* **2018**, *164*, 198−209.

(28) Wang, K.-T.; Tang, Q.; Cui, X.-M.; He, Y.; Liu, L.-P. Development of near-zero water consumption cement materials via the geopolymerization of tektites and its implication for lunar construction. *Sci. Rep.* **2016**, *6*, 29659.

(29) Mustafa Al Bakri, A. M.; Kamarudin, H.; Bnhussain, M.; Khairul Nizar, I.; Mastura, W. I. W. Mechanism and Chemical Reaction of Fly Ash Geopolymer Cement − A Review. *J. Asian Sci. Res.* **2011**, *1*, 247−253.

(30) Kanellopoulos, A.; Giannaros, P.; Al-Tabbaa, A. The effect of varying volume fraction of microcapsules on fresh, mechanical and self-healing properties of mortars. *Construction and Building Materials* **2016**, *122*, 577−593.

DOI: 10.1021/acs.iecr.8b01961
Ind. Eng. Chem. Res. 2018, 57, 9457−9464

Paper V

Influence of microcapsule size and shell polarity on thermal and mechanical properties of thermoregulating geopolymer concretes for passive building applications.

Vinh Duy Cao, Shima Pilehvar, Carlos Salas-Bringas, Anna M. Szczotok, Luca Valentini, Manuel Carmona, Juan F. Rodriguez, Anna-Lena Kjøniksen.

Energy Conversion and Management **2018**, 164, 198-209.

Energy Conversion and Management 164 (2018) 198–209

Contents lists available at ScienceDirect

Energy Conversion and Management

journal homepage: www.elsevier.com/locate/enconman

Influence of microcapsule size and shell polarity on thermal and mechanical properties of thermoregulating geopolymer concrete for passive building applications

Vinh Duy Cao[a,b], Shima Pilehvar[a,c], Carlos Salas-Bringas[b], Anna M. Szczotok[a,d], Luca Valentini[e], Manuel Carmona[d], Juan F. Rodriguez[d], Anna-Lena Kjøniksen[a,*]

[a] Faculty of Engineering, Østfold University College, N-1757 Halden, Norway
[b] Faculty of Science and Technology, Norwegian University of Life Sciences, N-1432 Ås, Norway
[c] Department of Material Engineering and Manufacturing, Technical University of Cartagena, Cartagena, Murcia, Spain
[d] Department of Chemical Engineering, University of Castilla – La Mancha, 13004 Ciudad Real, Spain
[e] Department of Geosciences, University of Padua, 35131 Padua, Italy

ARTICLE INFO

Keywords:
Microencapsulated phase change materials
Geopolymer concrete
Thermal diffusivity
Energy efficiency
Thermal conductivity

ABSTRACT

Microencapsulated phase change materials (MPCM) were added to geopolymer concrete (GPC) for utilization as a thermal energy storage concrete for passive building applications. Three different MPCM were compared to examine the influence of the hygroscopic nature of the MPCM shell, the PCM core/polymer shell ratio, and the MPCM size on the microstructure, thermal properties and compressive strength of GPC. The combination of a hygroscopic nature of the polymer shell, a high core/shell ratio, and a small MPCM size were found to improve the interface bonds between microcapsules and the GPC matrix, increase the energy storage capacity of GPC, and results in a good dispersion of MPCM in the GPC matrix. After adding 5.2 wt% MPCM to GPC, the power consumption for stabilizing the indoor temperature at 23 °C may be reduced by up to 18.5 ± 0.3% for GPC containing PS-DVB/RT27 (paraffin Rubitherm®RT27 core and a shell of polystyrene cross-linked with divinylbenzene), 20.1 ± 0.7% for GPC containing PMMA/PCM26 (paraffin mixture core with a crosslinked polymethyl methacrylate shell) and 25.9 ± 0.3% for GPC containing MF/PCM24 (paraffin mixture core with a melamine–formaldehyde polymer shell). Adding MPCM to GPC induces a higher amount of air pockets, which weaken the compressive strength. Unfortunately, the same parameters that are advantageous for reducing the energy consumption also results in a greater decline of the compressive strength. The compressive strength is further reduced when the microcapsule core is in its liquid state. However, the compressive strength still satisfies the mechanical European regulation (EN 206-1, compressive strength class C20/25) for concrete applications, except for GPC containing 5.2 wt% of MF/PCM24.

1. Introduction

With approximately 40% of the total global energy consumption contributed by buildings, reducing the energy consumption for buildings plays a key role for reducing global warming [1,2]. In order to reduce the huge energy consumption of buildings, improved construction techniques and advanced material technology are required. Concrete-based materials are among the most used materials for building applications. With their high mechanical strength and the possibility of changing the properties by varying the concrete recipe, concrete can work not only as a structural material but also as a functional material for thermal energy storage. The energy storage capacity of concrete can be enhanced by integrating microencapsulated phase change materials (MPCM). MPCM can store and release large amounts of energy during the phase transition. This is a promising technology for improving the energy efficiency of buildings, with reduced power consumption for heating and cooling [3–9]. Due to the low thermal conductivity of MPCM and an enhanced porosity, the thermal conductivity of concrete is decreased after addition of MPCM [5]. The decline in the compressive strength of concrete is the main drawback of MPCM addition [3–6]. The destruction of microcapsules during the mixing process might be the reason for the reduction of the compressive strength [3]. The soft nature of MPCM may weaken the concrete [5], and a complete cement hydration may be prevented due to the hygroscopic nature of the

* Corresponding author.
E-mail address: anna.l.kjoniksen@hiof.no (A.-L. Kjøniksen).

https://doi.org/10.1016/j.enconman.2018.02.076
Received 7 December 2017; Received in revised form 1 February 2018; Accepted 22 February 2018

MPCM [6]. In addition, the higher porosity after MPCM addition is probably contributing to the reduced strength [3,5,7].

Most studies of including MPCM in concrete structures are based on Portland cement concrete [3–9]. However, the high amount of CO_2 emission from production of Portland cement is a drawback of utilizing this type of concrete [10]. It is therefore a great advantage to replace Portland cement concrete by more environmentally friendly construction materials such as geopolymer concrete. Geopolymer is synthesized by alkali activation of materials rich in silica and alumina (from industrial waste materials such as fly ash (FA), coal ash, rice-husk ash, red mud and ground granulated blast furnace slag (GGBFS)) [11–14]. Using geopolymer as an alternative binder for concrete can greatly reduce the CO_2 emission from the cement industry. A few studies have examined integration of MPCM to geopolymer concrete [5,7], with promising results for improving the energy efficiency of buildings. It was found that the higher porosity after adding microcapsules contributes to the improvement of the thermal properties and the reduction of the compressive strength of geopolymer concrete. However, the effect of the MPCM properties (hygroscopic nature of the polymer shell, size of the microcapsules, storage heat capacity) on the thermal and mechanical properties of geopolymer concrete was not investigated in previous studies. In addition, it is important to evaluate the effect of the PCM state (solid or liquid) on the compressive strength of concrete.

In the current study, geopolymer concrete is employed as the concrete-based material for integration of microencapsulated phase change materials. Three kinds of microcapsules with variation of polymer shells, heat storage capacity and size were utilized to explore the influence on the microstructure, thermal, and mechanical properties of geopolymer concrete. The effects of the hygroscopic nature of MPCM and different PCM states were given special attention, as previous knowledge within this field is very limited. The effect of MPCM on the energy efficiency of buildings was estimated by determining the power consumption and power reduction of a heating and cooling system.

2. Experimental

2.1. Materials

Three different kinds of microcapsules were utilized. PS-DVB/RT27 was produced by a suspension polymerization process [15]. The MPCM are composed of a paraffin Rubitherm®RT27 core coated with a PS-DVB (polystyrene cross-linked with divinylbenzene) shell. PMMA/PCM26 (Micronal DS-5038X, BASF, Germany) has a core which is a paraffin mixture and highly crosslinked polymethyl methacrylate (PMMA) shell, with a core/shell ratio of 7:3 [16]. MF/PCM24 (Microtek MPCM24D) has a paraffin mixture core and melamine-formaldehyde polymer shell (MF). The ratio between the paraffin core and polymer shell is 9:1 [17]. Table 1 summarizes the characteristics of the three MPCMs.

Geopolymer concrete containing microencapsulated phase change materials (MPCM-GPC) was fabricated by mixing class F fly ash (FA) (Norcem, Germany) (density = 2.26 ± 0.02 g/cm^3), ground granulated blast furnace slag (GGBFS) (Cemex, Germany) (density = 2.85 ± 0.02 g/cm^3), sand (Gunnar Holth and Skolt Pukkverk AS, Norway) (density of 2.7 g/cm^3), aggregates with an average size of approximately 10 mm (Gunnar Holth and Skolt Pukkverk AS, Norway) (density of 2.6 g/cm^3), retarder (FLUBE OS 39, Bozzetto Group, Italy) (density of 1.2 g/cm^3), an alkaline activator solution, and MPCM. The sand and aggregates were dried before use. The chemical composition of FA and GGBFS were obtained by X-ray Fluorescence (XRF) and is summarized in Table 2. Based on a previous study [19], the alkaline activator solution was mixed at a ratio of 1.5 of a sodium silicate solution (density = 1.93 g/cm^3, 35 wt% solid) and 14 M NaOH (560 g/L). Accordingly, $m_{Na2SiO3(aq)}$ = 120 g, and $m_{NaOH(aq)}$ = 80 g. Fresh GPC possesses a poor workability due to the high geopolymerization reaction rate, which has a negative effect on the integration of MPCM into GPC [5,7]. Therefore, a chemical admixture was utilized to improve the workability of the concrete and to facilitate a better distribution of MPCM in the GPC matrix. A naphthalene based retarder was selected due to its high effectiveness with geopolymer concrete containing fly ash class F [20–22].

Table 3 summarizes the composition of geopolymer concrete containing MPCM (MPCM-GPC). For the recipe, a 1 L mix design was obtained from previous studies [7,19]. To keep a constant volume, the sand was replaced by MPCM at the same volume percentage (see supporting document [18] for details). However, the MPCM content is calculated as a wt.% of the total concrete sample, for a clearer comparison of the energy reduction. The mixture was prepared by weighting the components. In order to minimize the effect of shear during the mixing process, MPCM was mixed into GPC during the final step. For more information about the mixing process and recipe, see Pilehvar et al. [7,19].

PCM was incorporated into GPC at 0, 1.3, 2.6 and 5.2 wt%. The concentration of MPCM was limited to 5.2 wt% since higher concentrations of MPCM resulted in too low workability of the geopolymer concrete. After mixing, MPCM-GPC were cast into molds at a size of 200 × 200 × 25 mm (for the thermal test) and 100 × 100 × 100 mm (for the compressive strength test). The samples were pre-cured at room temperature (20 °C) for 24 h. The samples were then demolded and kept in water at room temperature (20 °C) for 28 days to reach a fully cured state. Before conducting the thermal test, the fully cured samples were dried in an oven at 40 °C until the sample weight remained unchanged.

Table 1
The fundamental data of the microencapsulated phase change materials.

MPCM name	Density (g/cm^3)	Melting point* (°C)	Latent heat* (J/g)	Core/shell ratio	Refs.
PS-DVB/RT27	0.9	24.9	100	11:9	[15]
PMMA/PCM26	0.9	24.7	110	7:3	[16]
MF/PCM24	0.9	21.9	154	9:1	[17]

* The melting point and latent heat were determined by differential scanning calorimetry (DSC) (see Supporting document [18] for details).

2.2. Scanning electron microscopy

The surface morphology and the micro structure of the microcapsules (powder form) were obtained by Scanning electron microscopy (SEM) (Quanta FEG-250, Spain). For MPCM-GPC, the fractured surfaces of samples containing 2.6 wt% of MPCM were investigated using a Zeiss EVO50 EP Scanning electron microscope (Norway).

2.3. X-ray micro-tomography

The internal microstructure of GPC containing microcapsules were investigated using X-ray tomography. The X-ray micro-tomography cross-sectional slices of cylindrical samples were obtained using a Skyscan 1172 CT scanner (Bruker) with 80 kV incident radiation, 124 μA source current, 750 ms exposure time per frame and 0.3° rotation step. Tomographic reconstruction was performed using the Feldkamp algorithm [23] and the final pixel size was 6 μm. The samples were made in cylindrical form (1 cm diameter and 1 cm height) from completely curing GPC without MPCM and containing 2.6 wt% of microcapsules (PS-DVB/RT27, PMMA/PCM26 and MF/PCM24).

2.4. Size distribution of MPCM

Low Angel Laser Light Scattering (LALLS) laser diffraction using a Malvern Mastersizer 2000 (Malvern Instruments Ltd., Malvern, UK) equipped with a Scirocco 2000 unit for analyzing dispersions of the particles in air was employed to determine the size distribution of MPCM.

Table 2
Chemical composition of fly ash (FA) and ground granulated blast furnace slag (GGBFS).

Chemical	Al_2O_3	SiO_2	CaO	Fe_2O_3	MgO	K_2O	TiO_2	Na_2O	P_2O_5	SO_3	SrO	CO_2
FA (wt.%)	23.15	50.83	6.87	6.82	1.70	2.14	1.01	1.29	1.14	1.24	0.19	3.07
GGBFS (wt.%)	10.30	34.51	42.84	0.60	7.41	0.52	0.66	0.40	0.02	1.95	0.05	0.30

Table 3
Composition of geopolymer concretes.

MPCM (wt.%)	Alkaline solution (g)	Water (g)	FA* (g)	GGBFS** (g)	Sand (g)	Aggregate (g)	Retarder (g)	MPCM (g)
0	200	50	300	200	871.2	851.7	5	0
1.3	200	50	300	200	784.1	851.7	5	30
2.6	200	50	300	200	696.9	851.7	5	63
5.2	200	50	300	200	522.7	851.7	5	117

* FA: Flyash.
** GGBFS: Ground granulated blast-furnace slag.

2.5. Density and porosity

The density and open porosity of concrete samples were respectively determined by EN 12390-7 (Eq. (1)) [24] and ASTM C1202-12 (Eq. (2)) [25,26].

$$\rho = \frac{m_d}{V} \tag{1}$$

$$Open\ Porosity(\%) = \frac{m_s - m_d}{m_s - m_b} \times 100 \tag{2}$$

where ρ is the dry density of the sample, V is the volume of the sample, and m_d, m_b and m_s are oven-dried weight, the buoyant mass of the saturated sample in water and the mass of the saturated sample in air, respectively.

2.6. Trapped water content

The ability of microcapsules to trap water was determined to compare the polarity of the microcapsules polymer shell. 5.0 ± 0.1 g of each type of microcapsules were immersed in 50 ml of alkaline solution at room temperature (20 °C). After 24 h, the dispersion of microcapsules in alkaline solution was placed into filter test tubes (0.45 μm filter membrane) and centrifuged at 4500 rpm for 5 min (Mega Star 1.6R) to separate the microcapsules from the alkaline solution. The remaining water trapped on the microcapsules were determined utilizing a moisture analyzer (MB 64M-VWR, Italy). The temperature for this test was set at 70 °C. The final trapped water can be obtained after subtracting the water content of the initial microcapsules, which were also determined by the moisture analyzer.

2.7. Thermal properties

The thermal properties of concrete containing MPCM such as the thermal conductivity, the specific heat capacity and the latent heat was determined by the guarded hot plates method [5,27,28]. The sample was sandwiched between two aluminum plate heat exchangers which were connected to thermal regulated baths that define the thermal conditions. In order to minimize the heat transfer from the lateral side face of the samples into the external ambient conditions, a 40 mm thick polyethylene expanded foam (PEF) is used to cover the sample. Accordingly, the heat transfer through the sample can be calculated assuming one-dimensional thermal condition. The temperature variations and heat fluxes through sample during testing were recorded by heat flux sensors (Captecv, France) and T-type thermocouples (OMEGA, US) via a multichannel multimeter (LR8410-20 Hioki, Japan).

2.7.1. Thermal conductivity

The conductivity of the sample is defined according to the European standard EN-12667.

In order to determine the thermal conductivity of concrete containing MPCM, the temperature on the top and bottom aluminum plate heat exchanger were set at $T_{Al\text{-}top}$ and $T_{Al\text{-}bot}$ until a thermal steady state was reached. For solid thermal conductivity determination, $T_{Al\text{-}top}$ and $T_{Al\text{-}bot}$ are set at 5 and 10 °C while 45 and 50 °C are utilized to calculate the liquid thermal conductivity of MPCM-concrete.

The thermal conductivity of the sample in liquid state and solid state of PCM was determined by [5]:

$$k = \frac{\varphi d}{(T_{top} - T_{bottom})} \tag{3}$$

where d is the thickness of the sample. In these experiments the dimension of the concrete samples is d = 25 ± 1 mm. T_{top} and T_{bottom} are the temperature on the top face and bottom face of concrete sample while φ is the average heat fluxes on both faces of concrete sample.

2.7.2. Specific heat capacity/latent heat

In order to determine the specific heat capacity and the latent heat of the concrete containing MPCM, the temperature of both aluminum plate heat exchangers was raised from 5 °C to 45 °C. For this test, the heating rate was set at 10 °C/hour. The heat flux sensors and thermocouples were used to record the heat fluxes (φ) and temperature on both faces of the sample during the test. The specific heat capacity of concrete containing MPCM samples as a function of temperature can be determined by [5,29]:

$$C_p(\mathrm{T}) = \frac{A\varphi(\mathrm{T})}{m\frac{dT}{dt}} \tag{4}$$

Accordingly, the solid specific heat capacity, $C_{p\text{-}solid}$ (below the melting range of PCM) and the liquid specific heat capacity, $C_{p\text{-}liquid}$ (above the melting range of PCM) were estimated as the average value of $C_p(T)$ in the temperature range of 10–15 °C and 35–40 °C, respectively.

The latent heat was calculated in the temperature range of 10–35 °C by Eq. (5) [29] using OriginPro 2016 Sr2.

$$\Delta H = \frac{A}{m}\left(\int_{T1}^{T2} \varphi(T)dT\right) - C_{p-ave}\cdot(T_2 - T_1) \tag{5}$$

where $C_{p\text{-}ave} = (C_{p\text{-}solid} + C_{p\text{-}liquid})/2$ is the average specific heat capacity, ΔH is the latent heat. T_1 = 10 °C and T_2 = 35 °C. A = 400 cm^2 is the area of the sample.

2.7.3. Thermal diffusivity

Because the thermal conductivity and heat storage capacity (specific

heat capacity and latent heat) are inherent capacities of the materials, it is important to reveal their effect on the heat transfer process and on the energy consumption of the heating/cooling system to maintain a constant indoor temperature.

Thermal diffusivity is used to estimate the rate of heat transfer through a material. It also provides a relation between the thermal conductivity and heat storage capacity on the energy performance of building materials. The thermal diffusivity (α) is dependent on the thermal conductivity, the specific heat capacity and the density (ρ) [30]:

$$\alpha(T) = \frac{k_{ave}}{\rho C_p(T)} \tag{6}$$

where $k_{ave} = (k_{solid} + k_{liquid})/2$ is the average thermal conductivity. The average is used since there is little difference between the thermal conductivity of samples where is PCM in a solid or liquid state (see Section 3.3)

2.8. Energy saving aspect

To investigate the effect of microcapsules on the thermal performance (energy saving aspect) of geopolymer concrete, a thermal system was set up as illustrated in Fig. 1.

A small test room was made from a 50 mm of polyethylene expanded foam (PEF) panels for thermal insulation and has inner dimensions of 600 × 800 × 600 mm (Fig. 1). The concrete sample (200 × 200 × 50 mm) was inserted in a rectangular hole of 200 × 200 mm located in the middle of the top insulation panel of the box. The test room was placed inside an environmental chamber to mimic the outdoor environmental temperature variations. The simulated indoor temperature (T_{room}) was set at 23 °C throughout the experiment using a Laird temperature regulator (AA150-Laird Technologies). To mimic outdoor conditions, the outdoor temperature T_{out} was imposed as a sinusoidal function of time using an environmental chamber (VT^3 4250, Vötsch, Germany):

$$T_{out}(t) = \frac{T_{max} + T_{min}}{2} + \frac{T_{max} - T_{min}}{2}\sin\left(\frac{\pi}{43200}t - \frac{2\pi}{3}\right) \tag{7}$$

where T_{max} = 40 °C and T_{min} = 10 °C are the maximum and minimum outdoor temperatures during a day, respectively. The maximum outdoor temperature T_{max} were set at 14:00.

During the initial stage, both indoor temperature and outdoor temperature were set at 23 °C for 2 h to reach a steady-state condition. After that, the outdoor temperature cycles (Eq. (7)) were applied and run for 72 h to determine the thermal performance of the concrete samples and the repeatability of the measurements.

The temperature and heat fluxes on both surfaces of the sample were recorded by using thermocouples and heat flux sensors to measure heat losses towards the simulated indoor environment during the testing process.

It is assumed that there is no heat transfer through the insulation panels of the box. Accordingly, the total energy supplied to the heating/cooling system to maintain the simulated indoor temperature at 23 °C within one day can be calculated as the sum of the heating power consumption (the indoor surface temperature < T_{room}) and the cooling power consumption (the indoor surface temperature > T_{room}):

$$P = \frac{\int_{t_{ini}}^{t_{end}} |\varphi_{indoor}| dt}{3600 \cdot 10^3} \tag{8}$$

where φ_{indoor} is the heat flux on the simulated indoor side of the sample, t_{ini} and t_{end} are the initial time and end time of the thermal cycle.

The power reduction Pr was defined as:

$$Pr = \frac{P_{GPC} - P_{MPCM-GPC}}{P_{GPC}} \cdot 100\% \tag{9}$$

where P_{GPC} and $P_{MPCM\text{-}GPC}$ are the power consumption of the heating and cooling system working within one day for geopolymer concrete without MPCM and with MPCM, respectively.

2.9. Compressive strength test

The effect of different kinds of microcapsules and their concentration on the compressive strength of geopolymer concrete were investigated. An Alpha 3-3000 system (Form + Test Seidner&Co.GmbH) was employed to determine the compressive strength of MPCM-GPC

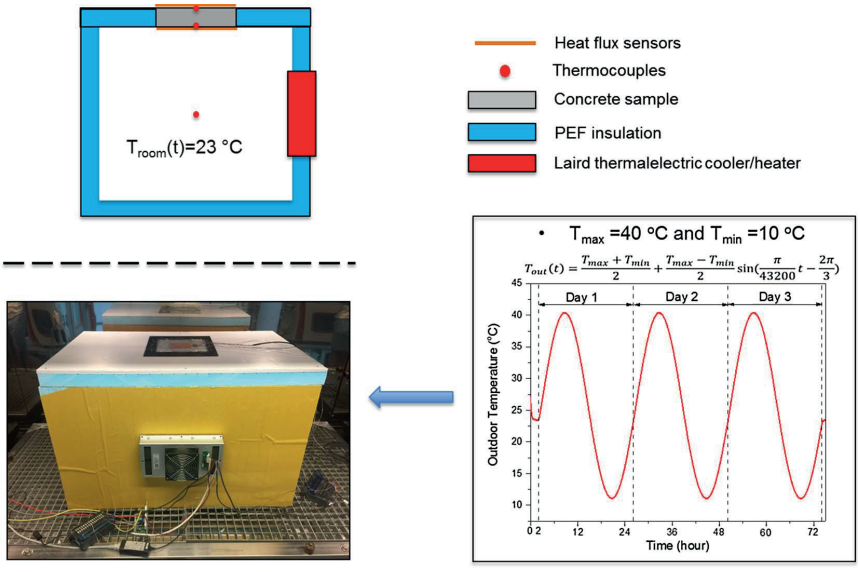

Fig. 1. The thermal performance testing system with sketch of cross-section of the system and the simulated outdoor temperature profile.

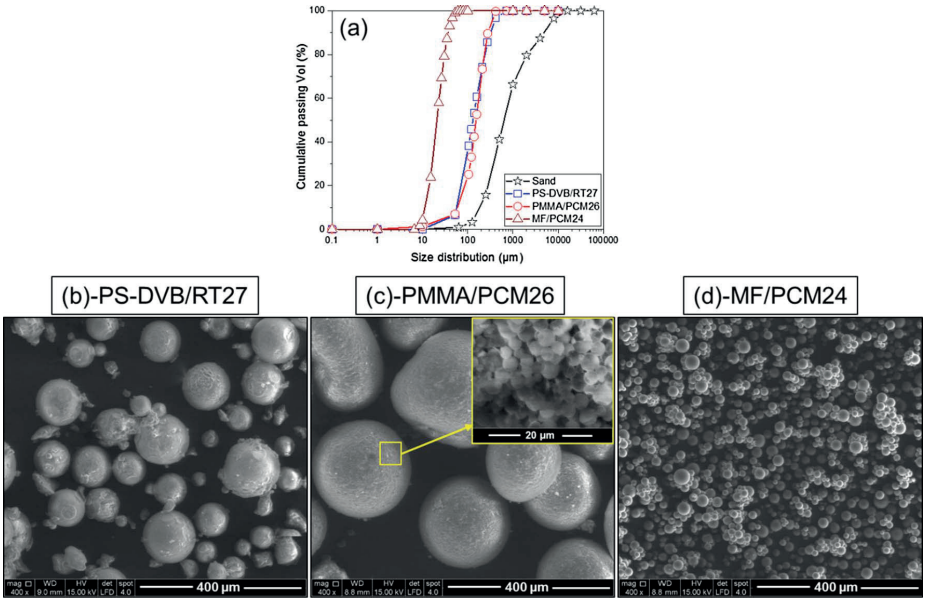

Fig. 2. (a) The size (diameter) distribution of the PS-DVB/RT27, PMMA/PCM26, MF/PCM24 microcapsules and sand, and SEM images of (b) PS-DVB/RT27, (c) PMMA/PCM26 and (d) MF/PCM24. The insert plot (c) shows the single PMMA/PCM26 microcapsules.

samples based on EN 12390-3. In addition, the measurement was conducted at different temperatures including 20 °C (below the melting range) and 40 °C (above the melting range) to examine effect of temperature on the compressive strength of MPCM-GPC samples. The cubes were left in the room for 3 h to remove free water before they were tested at 20 °C. For the test at 40 °C, the temperature of the compressive strength machine was kept at 40 °C by thermal insulation combined with utilization of a temperature regulating incubator connected by an isolated tube. Before the compressive strength test, cubes were kept in room temperature (20 °C) for 3 h to remove free water, followed by storage in a heating chamber at 40 °C for 12 h to obtain a uniform temperature through the whole samples, immediately afterward the cubes were tested. Three cubes were tested for each sample.

3. Results and discussion

Fig. 2 shows size distribution of the microcapsules and the sand, and SEM images of the microcapsules. As is evident from the SEM images, the microcapsules exhibit a spherical shape. They have a diameter in the range of 10–100 μm for PS-DVB/RT27; 1–3 μm for PMMA/PCM26 and 10–30 μm for MF/PCM24. However, all of them have a strong tendency to form agglomerated structures, especially PMMA/PCM26 (Fig. 2c). The size distribution of the agglomerated microcapsules is shown in Fig. 2a. The agglomerated microcapsules have a diameter in the range between 10 and 1000 μm for PS-DVB/RT27, 0.1–800 μm for PMMA/PCM26 and 0.1–100 μm for MF/PCM24. The mean agglomerated microcapsules diameter at 50% in the cumulative distribution (D_{50}) is 130 μm for PS-DVB/RT27, 155 μm for PMMA/PCM26 and 21 μm for MF/PCM24, which is smaller than the size of sand (D_{50} = 640 μm). This difference may have an important impact on the physical properties of the concrete samples.

Fig. 3 presents the trapped water of the microcapsules after immersion for 24 h in an alkaline solution (corresponding to the alkaline solution used in the geopolymer). PS-DVB/RT27 traps less water than PMMA/PCM26 and MF/PCM24. This is reasonable considering the difference in the chemical structures of the polymer shells of the

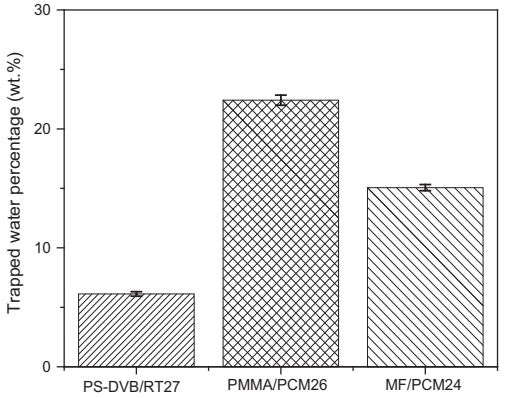

Fig. 3. The trapped water of microcapsules after immersion in an alkaline solution at room temperature (20 °C) for 24 h.

microcapsules. As can be seen from Fig. 4, PS-DVB contains non-polar functional groups (phenyl functional groups) while the functional groups PMMA (ester functional groups) and MF (amine functional groups) are more polar. The existence of polar functional groups renders the polymer shell more compatible with water, causing a higher amount of water to adsorb on the microcapsules.

Fig. 3 also illustrates that PMMA/PCM26 traps more water than MF/PCM24. Accordingly, at alkaline conditions PMMA/PCM26 and MF/PCM24 can trap approximately 22.4 ± 0.4 and 15.1 ± 0.3% of water, respectively. Both the difference in the functional groups (Fig. 4) and the size of the microcapsules (Fig. 2) can contribute to this difference. Although PMMA/PCM26 exists as agglomerated structures with a larger size than MF/PCM24, the single PMMA/PCM26 size (1–3 μm) is approximately 10 times smaller than MF/PCM24 (Fig. 2). After immersing in an alkaline solution for 24 h, the solution can

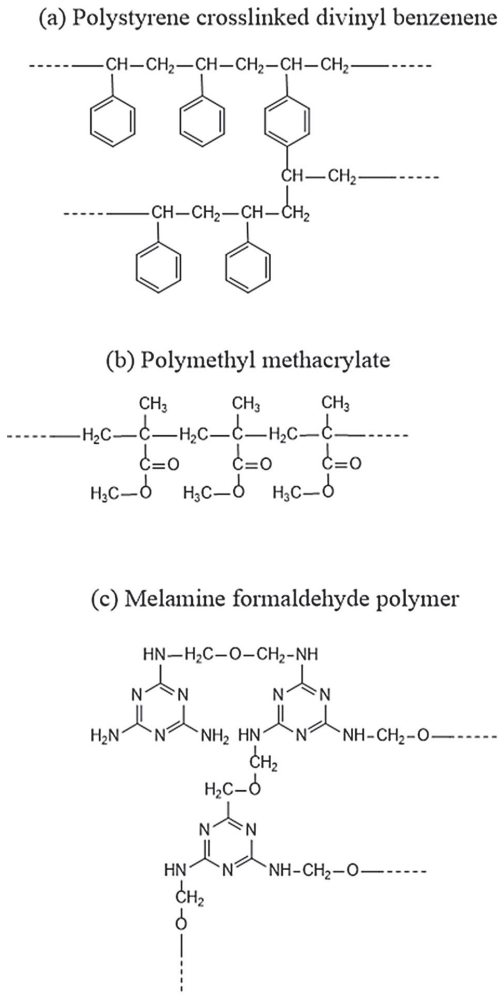

Fig. 4. The chemical structure of (a) polystyrene crosslinked divinyl benzene (PS-DVB) (b) polymethyl methacrylate (PMMA) and (c) Melamine formaldehyde polymer (MF).

penetrate deeply inside the structure of the PMMA/PCM26 aggregates to cover all the single microcapsules, thereby causing PMMA/PCM26 to adsorb more water.

3.1. MPCM-GPC density and porosity

The MPCM-GPC density and open porosity as a function of MPCM concentration are shown in Fig. 5. The addition of microcapsules can affect the porosity of the geopolymer concrete in several ways. For the same volume, the total surface area of small particles is much higher than for larger particles. Accordingly, more binder paste adsorbs to the surface of small particles. This can cause more voids between the particles (aggregates and microcapsules) [5]. This is counteracted by the cavity filling effect [31–33]. The cavity between aggregates and sand can be filled up by small particles ($\leq$125 μm) [33] causing an increase of the packing density, thereby reducing the porosity of the concrete. The single microcapsules have a small size in the range of 1–100 μm (Fig. 2). However, the effective size is larger due to agglomeration. The agglomerates of PS-DVB/RT27 and PMMA/PCM26 are too large to fill in the cavities in the concrete structure (Fig. 2a) [3,34–36]. Only MF/PCM24 with a much smaller size distribution (Fig. 2a) can fill up the cavities to reduce the porosity. In addition, the properties of the polymer shell can affect the porosity. As illustrated in Fig. 3, the hydrophobic PS-DVB/RT27 has little interaction with water. Accordingly, air gaps can be formed between the microcapsules and the geopolymer paste during the mixing process [5,37,38]. PMMA/PCM26 and MF/PCM24 have shells containing polar functional groups (Fig. 4), providing better interaction with the aqueous alkaline environment (Fig. 3). This results in better interface bonds between the microcapsules and the geopolymer paste, thereby reducing the air gaps between MPCM and geopolymer paste. The more polar functional groups on the polymer shell also helps to disperse the microcapsules into the concrete matrix better than a hydrophobic shell. This is evident in the SEM images (Fig. 6) which show obvious gaps between the concrete matrix and PS-DVB/RT27, while the polymers with polar functional groups exhibit almost no air gaps (PMMA/PCM26) or very small air gaps (MF/PCM24). The porosity of the concrete will be governed by a combination of these effects.

As can be seen from Fig. 5a, the open porosity increases with microcapsule concentration. This can be explained by the smaller size of the microcapsule agglomerates compared to sand (Fig. 2a), causing a larger surface area that adsorbs more binder paste to the surface. The D_{50} size of sand is approximately 4–5 times larger than the PS-DVB/RT27 and PMMA/PCM26 agglomerates and 30 times larger than MF/PCM24. When the concentration of MPCM is raised, the porosity of GPC with MF/PCM24 increases at a higher rate than PS-DVB/RT27 and PMMA/PCM26. This is probably due to the combination of the small size and the polar functional groups on the microcapsule shell, which causes MF/PCM24 to adsorb more binder paste. However, this is not consistent with the trapped water content (Fig. 3) where PMMA/PCM26 is shown to trap more water than MF/PCM24. This discrepancy might be due the high viscosity and short setting time of the geopolymer mixture, preventing the water to penetrate deeply into the PMMA/PCM26 agglomerates before the geopolymer sets. Accordingly, only the outer surface of the PMMA/PCM26 agglomerates are covered, reducing the amount of binder adsorption onto PMMA/PCM26. When more geopolymer paste is adsorbed onto the microcapsules, the viscosity increases and the probability of forming entrapped air voids during the mixing and pouring process is raised [5,7]. This is in agreement with the X-ray micro-tomography data (Fig. 7), which will be discussed in more details below.

The density of MPCM-GPC decreases when the MPCM concentration increases (Fig. 5b). This is due to the lower density of the microcapsules compared to the sand it replaces combined with the increase of the porosity. Similar observations have also been found previously [9,15].

3.2. Microstructure of MPCM-GPC

Fig. 6 shows the SEM images of geopolymer concrete with 2.6 wt% microcapsules. As is evident from Fig. 6b, the original PMMA/PCM26 agglomerates (Fig. 2b) are broken into smaller entities after mixing, resulting in a better dispersion of the single microcapsules. This indicates that the physical bonds holding the PMMA/PCM26 agglomerates together are relatively weak. It can be seen that PMMA/PCM26 and MF/PCM24 are well dispersed in the geopolymer concrete while the more hydrophobic PS-DVB/RT27 is not dispersed properly, as is evident from the presence of large irregular agglomerates. In addition, the SEM images reveal that the single microcapsules remain stable with a spherical shape in the concrete matrix. This demonstrates that the microcapsules can withstand the current mixing process of the concrete.

Fig. 7 presents X-ray micro-tomography cross-sectional slices obtained from GPC without MPCM and GPC containing 2.6 wt% of MPCM. In the X-ray micro-tomography images, the air bubbles and microcapsules are shown as dark colors due to low or no absorption of X-rays

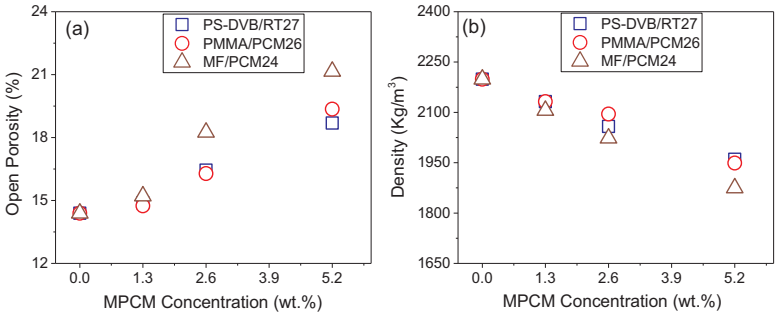

Fig. 5. Open porosity (a) and density (b) and of GPC at different MPCM concentrations.

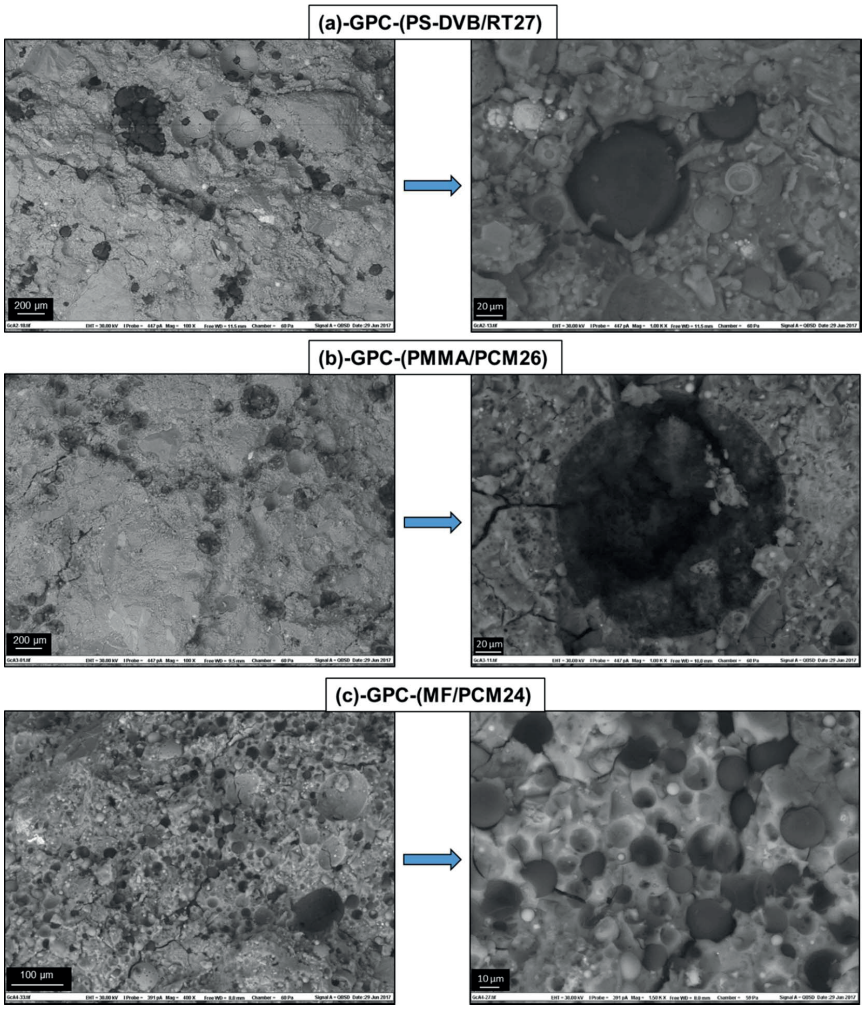

Fig. 6. SEM images of GPC containing 2.6 wt% of (a) PS-DVB/RT27, (b) PMMA/PCM26 and (c) MF/PCM24.

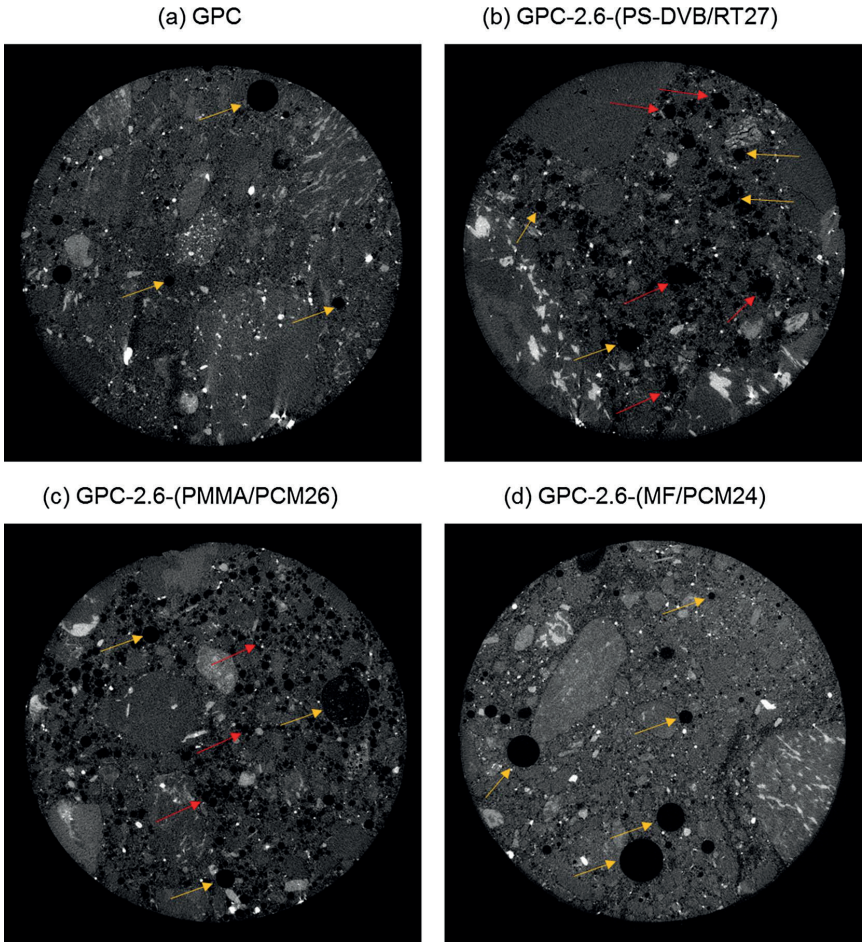

Fig. 7. X-ray-tomography images of (a) GPC without MPCM, (b) GPC containing 2.6 wt% PS-DVB/RT27, (c) GPC containing 2.6 wt% PMMA/PCM26 and (d) GPC containing 2.6 wt% MF/PCM24. The yellow arrows point the air bubbles and the red arrows indicate the microcapsules. The field of view is 1 cm. (For interpretation of the references to colour in this figure legend, the reader is referred to the web version of this article.)

while bright colors represent sand and gravel, which can adsorb high amounts of X-rays. The purpose of using X-ray micro-tomography is to investigate the internal microstructure of the concrete samples, and to evaluate how the microcapsules and the air bubbles are dispersed in the concrete matrix. This can provide important information for thermal and mechanical properties of concrete. It is difficult to discriminate between air bubbles and microcapsules based on grey scale values, due to the low level of X-ray attenuation of the organic materials constituting the MPCM [7]. However, air bubbles have tendency to be approximately spherical due to interfacial tension effects, while MPCM might exist as agglomerates with a more irregular shape [7]. For GPC containing PMMA/PCM26, it is difficult to distinguish air bubbles and MPCM based on the shape because the PMMA/PCM26 has a spherical aggregate structure (SEM, Fig. 6b). This is confirmed by Fig. 7c, where both MPCM and air bubbles appears in a spherical shape. However, some air bubbles can be distinguished (the yellow arrows) since the sizes are much larger than size distribution of PMMA/PCM26. For GPC containing MF/PCM24 (Fig. 7d), a high amount of spherical air bubbles can be observed (the yellow arrows) while the agglomerated microcapsules MF/PCM24 cannot be detected. The agglomerated microcapsules MF/PCM24 have a size of 21 μm (Fig. 2) which are too small to be easily visible in the X-ray tomography images. This illustrates that the MF/PCM24 microcapsules are well dispersed in GPC with no large agglomerates formed during the mixing process.

GPC containing the hydrophobic PS-DVB/RT27 microcapsules is different from GPC containing microcapsules with a polymer shell containing polar functional groups (PMMA/PCM26 and MF/PCM24). For PS-DVB/RT27, there is a clear difference between the spherical air bubbles and the irregular MPCM agglomerates (the yellow arrows and red arrows show air bubbles and MPCM, respectively). The presence of large agglomerates illustrates that PS-DVB/RT27 is not dispersed properly in the concrete matrix. A visual inspection of Fig. 7 show that the amount of air bubbles presented in GPC containing MF/PCM24 is higher than for the other samples. This is in agreement with the higher porosity of this sample (Fig. 5a).

3.3. Thermal properties of MPCM-GPC

The thermal conductivity of GPC containing MPCM (MPCM-GPC) at different temperatures (comparing the solid state and liquid states of

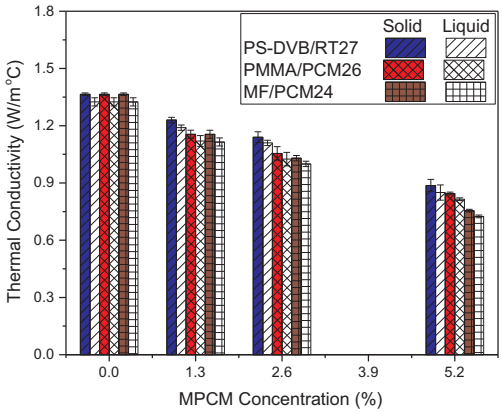

Fig. 8. Thermal conductivity of GPC containing microcapsules at the solid and liquid state of PCM as a function of microcapsule concentration.

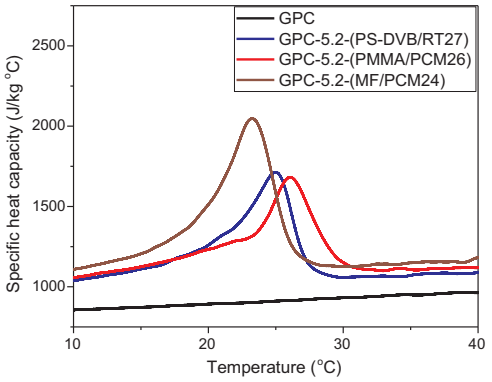

Fig. 9. The specific heat capacity as a function of temperature for GPC at 0 wt% and 5.2 wt% MPCM.

PCM) is summarized in Fig. 8. There is a clear reduction of the thermal conductivity of MPCM-GPC when the amount of microcapsules is increased. It is believed that the lower thermal conductivity of the microcapsules compared to that of replaced sand [5], the enhancement of porosity (Fig. 5a) and the poor interface between microcapsules and concrete matrix (Fig. 6) are the main reasons for the decline in thermal conductivity. The thermal conductivity of MPCM-GPC at low temperatures (5–10 °C) where PCM is in a solid state is slightly lower than at high temperatures (45–50 °C) where PCM is in a liquid state. The higher thermal conductivity of the solid PCM compared to the liquid PCM is a possible explanation [27,39]. However, since the difference between the thermal conductivity of MPCM-GPC for the solid PCM and liquid PCM is small, the average thermal conductivity will be used to calculate the thermal diffusivity of MPCM-GPC.

The reduction rates of thermal conductivity of GPC after mixing with different kinds of microcapsules are not significantly influenced by whether PCM is in a liquid or solid state. However, there is a slight difference between the different kinds of microcapsules, with reduction rates of 0.090, 0.096, 0.110 for GPC containing PS-DVB/RT27, PMMA/PCM26, MF/PCM24 respectively. Since air pores will reduce the thermal conductivity, the slightly different reduction rates are probably mostly due to the change in porosity (Fig. 5a). Furthermore, the smaller size and better distribution of MF/PCM24 compared to PS-DVB/RT27 and PMMA/PCM26 might contribute to this effect. A better distribution of microcapsules in the concrete matrix can increase the MPCM thermal pathway through concrete matrix thereby facilitating lower thermal conductivity. The thermal conductivity of each microcapsule might also play a role, but unfortunately, the thermal conductivity of the considered microcapsules is unknown.

Fig. 9 shows the specific heat capacity of GPC containing PS-DVB/RT27, PMMA/PCM26 and MF/PCM24 at a microcapsule concentration of 5.2 wt%. The specific heat capacity in the temperature range of 10–15 °C (below the melting range of PCM) and 35–40 °C (above melting range of PCM) were determined and is summarized in Fig. 10a.

As shown in Fig. 10a, for both liquid and solid PCMs the specific heat capacity of GPC increases slightly when the concentration of microcapsules is raised. This might be due to a lower specific heat capacity of geopolymer concrete compared to the microcapsules. In addition, there is almost no difference between the specific heat capacity of GPC containing microcapsules in the solid and liquid state of PCM (Fig. 10a). This observation is in good agreement with previous findings [5,29].

Fig. 10b summarizes the latent heat of GPC as a function of microcapsule concentration within the temperature range of 10–35 °C. The latent heat of concrete increases linearly when the microcapsule concentration is raised. MF/PCM24 increases fastest, with a slope (γ) of 0.93, while the lower slopes of PS-DVB/RT27 (γ = 0.70) and PMMA/PCM26 (γ = 0.73) are similar to each other. Several effects may cause γ to become lower than 1. A higher porosity of the concrete matrix might reduce γ [5]. However, this cannot explain the current results as MF/PCM24 exhibits the highest increase in open porosity (Fig. 5) and the largest γ. A possible reason for this discrepancy is that the gaps between the particles and the GPC matrix play an important role. MF/PCM24 exhibits very little gaps between the microcapsules and the GPC matrix, which will improve the heat transfer to the particles and increase γ. In addition, MF/PCM24 is well dispersed as single, small microcapsules while PS-DVB/RT27 and PMMA/PCM26 exist as agglomerates of approximately the same size as each other (Fig. 6). Agglomerated structures can impede the heat transfer to the single microcapsules, thereby reducing γ.

3.4. Thermal diffusivity

The calculated thermal diffusivity of GPC containing microcapsules (MPCM-GPC) are shown in Fig. 11. According to Fig. 11a, the thermal diffusivity of MPCM-GPC decreases with the concentration of microcapsules over the whole temperature range. Comparing the different microcapsules (Fig. 11b), the thermal diffusivity of GPC containing MF/PCM24 is lowest while GPC containing PMMA/PCM26 is slightly lower than that of PS-DVB/RT27. This is especially evident for the temperatures outside the melting range of the microcapsules. The lower thermal diffusivity of MF/PCM24 is probably related to the higher amount of air bubbles in this sample (the air will act as a thermal insulator), and the higher apparent heat capacity. The thermal diffusivity provides important information regarding the transient thermal conduction process through a wall. Materials with smaller thermal diffusivity can reduce the heat transfers through the wall, resulting a smaller effect of the outdoor environment on the indoor environment and cause a reduction in heating/cooling energy consumption to maintain the indoor temperature at the desired level. The results indicate that GPC containing MF/PCM24 can have better effect on reducing the heating/cooling energy consumption than PS-DVB/RT27 and PMMA/PCM26.

3.5. Energy saving

Fig. 12 presents the simulated indoor surface temperature, and the inner wall heat flux as a function of time and the total consumed power for heating and cooling of GPC containing 0 wt% and 5.2 wt% microcapsules.

The addition of microcapsules causes a higher heat storage capacity

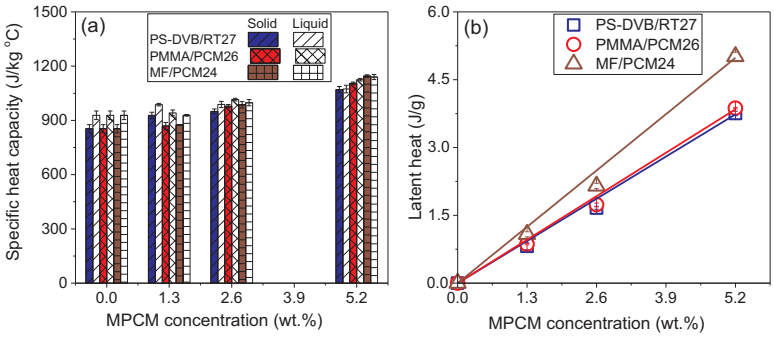

Fig. 10. (a) The specific heat capacity (b) the latent heat of GPC as a function of concentration of MPCM.

and lower thermal conductivity of the GPC samples, leading to a lower thermal diffusivity (Fig. 11). Accordingly, the heat transfers through the wall can be reduced, resulting in a smaller effect of the outdoor environment on the indoor temperature, and thereby causing a reduction in the energy consumption need to maintain the indoor temperature at 23 °C.

The effect of the PCM latent heat on the heat transfer process can be seen clearly as a slight transition point around the melting point of PCM for both the indoor surface temperature and the inner wall heat flux (Fig. 12a, b). This is especially evident for MF/PCM24. Similar observations were also found previously [3,27,35]. After adding 5.2 wt% of microcapsules to GPC, the variation of indoor surface temperature of the GPC is lower and closer to the human comfort zone than for pure GPC (0 wt%) (Fig. 12a). The microcapsules induce a lower heat transfer (heat flux) to the indoor side of the concrete wall (Fig. 12b). Accordingly, a lower power consumption is needed to maintain the indoor environment at the desired temperature (Fig. 12c). When utilizing 5.2 wt% of microcapsules, the total energy consumption for to maintain an indoor temperature of 23 °C is reduced by up to 18.5 ± 0.3% for PS-DVB/RT27, 20.1 ± 0.7% for PMMA/PCM26 and 25.9 ± 0.3% for MF/PCM24 (Fig. 12d). The higher energy saving potential of MF/PCM24 compared to PS-DVB/RT27 and PMMA/PCM26 can be explained by the formation of a structure with more insulating pores (higher porosity content) and the higher heat storage capacity of MF/PCM24. This is in agreement with the thermal diffusivity of GPC containing MPCM (Fig. 11).

3.6. Compressive strength

Fig. 13 presents the compressive strength of GPC containing microcapsules at 20 °C (below the microcapsule melting point) and 40 °C (above the microcapsule melting point) as a function of microcapsule concentration. The compressive strength of GPC declines significantly when the concentration of microcapsules increases for both states of PCM, in agreement with previous findings [3,5].

The compressive strength of GPC containing microcapsules follows the order of MF/PCM24 < PMMA/PCM26 < PS-DVB/RT27. This trend is more obvious at high microcapsule concentrations (≥ 2.6 wt%). The compressive strength of concrete will be lower when there are the more air voids (porosity) [3,5], softer particles [7] and poorer dispersion of particles in the concrete matrix [40,41]. Air gaps between microcapsules and concrete indicates poor interfacial bonds, which can result in a lower compressive strength [3,5,7]. Combination of these factors plays an important role regarding the effect of microcapsules on the compressive strength of geopolymer concrete. At high microcapsule concentrations, MF/PCM24 has a significantly lower compressive strength than the other samples even when the PCM is in a solid state. This might be due to the higher amounts of air bubbles in this sample and the higher core/shell ratio of MF/PCM24 which may result in softer particles.

Fig. 13a shows that the compressive strength of GPC containing microcapsules with PCM in a solid state is higher than when PCM is in a liquid state. This might be due to an increase of the internal stress of the microcapsules at elevated temperatures (due to thermal expansion). It is also possible that the microcapsules become softer when they have a liquid core. Fig. 13b shows the percentage reduction of the compressive strength of GPC containing microcapsules when PCM is changed from a solid to liquid state. The percentage reduction increases when the amount of microcapsules increases, confirming that the microcapsules are the cause of the decline in compressive strength. Furthermore,

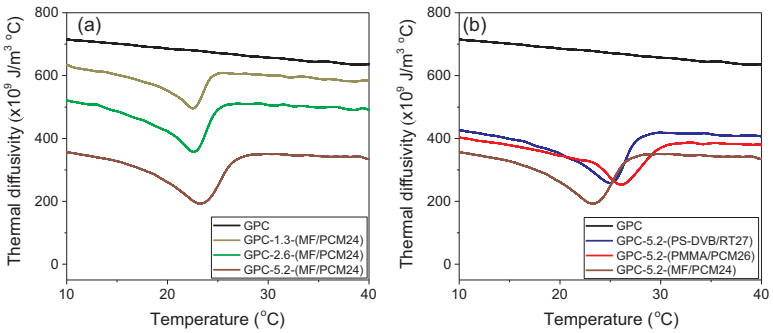

Fig. 11. Thermal diffusivity of (a) GPC containing different concentrations of MF/PCMPC24 and (b) GPC containing 5.2 wt% of PS-DVB/RT27, PMMA/PCM26 and MF/PCM24 as a function of temperature.

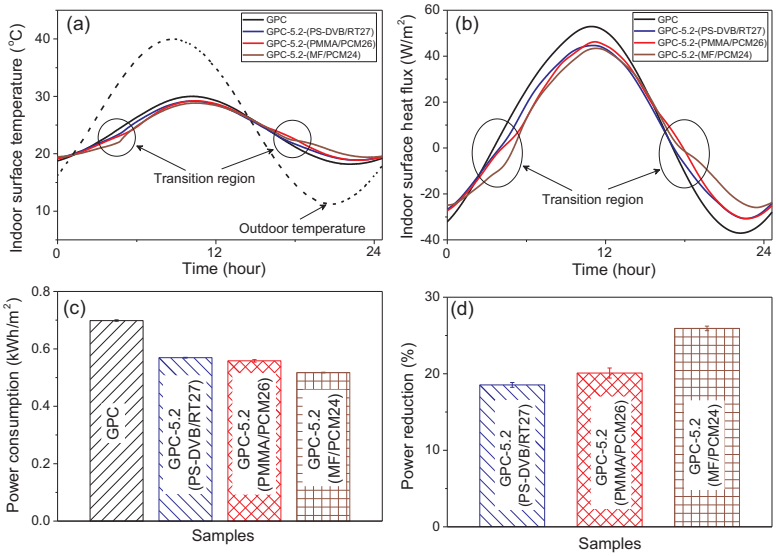

Fig. 12. (a) The simulated indoor surface temperature; (b) the simulated indoor surface heat flux through a 50 mm thick geopolymer concrete wall containing MPCM after exposing it to a sinusoidal outdoor temperature fluctuation (Eq. (8)); (c) the simulated power consumption for heating and cooling the system to maintain an indoor temperature of 23 °C and (d) the power reduction (%) after adding 5.2 wt% of MPCM compared to a corresponding sample without MPCM.

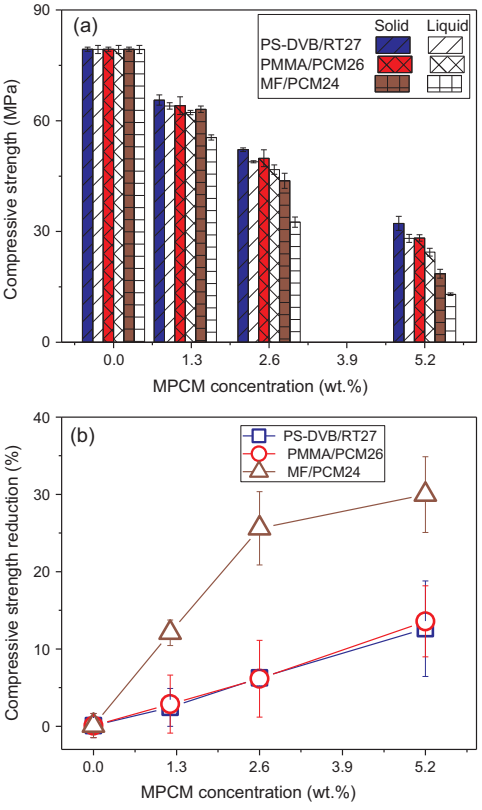

Fig. 13. (a) The compressive strength of GPC containing microcapsules below (20 °C) and above (40 °C) the melting range of PCM and (b) the compressive strength reduction between the solid and liquid state of PCM.

melting of the PCM core affects the MF/PCM24 much more than for PS-DVB/RT27 and PMMA/PCM26. This might be due to the higher paraffin core/polymer shell ratio of MF/PCM24 compared to PS-DVB/RT27 and PMMA/PCM26 (Table 1). In addition, the closer interface (lack of air gaps) between MF/PCM24 and concrete matrix facilitates better transfer of the compressive force to the microcapsules, and makes the concrete more sensitive to a possible thermal expansion of the microcapsules. However, PMMA/PCM26 also has a good interface with the concrete matrix. PMMA/PCM26 exists as agglomerates, which can contain voids between the microcapsules. Accordingly, there will be less stress on the microcapsules during compression and when they expand.

The compressive strength at 5.2% MPCM is 32 ± 2 MPa (solid state) and 28 ± 1 MPa (liquid sate) for PS-DVB/RT27 while for PMMA/PCM26 it is 28 ± 1 MPa (solid state) and 24 ± 1 MPa (liquid state). Accordingly, the integration of PS-DVB/RT27 and PMMA/PCM26 into GPC at 5.2 wt% satisfy the mechanical European regulation (EN 206-1, compressive strength class C20/25) for concrete for building construction. Unfortunately, while 5.2% of MF/PCM24 shows the best thermal performance, its compressive strength is only 19 ± 1 MPa (solid state) and 13.0 ± 0.4 MPa (liquid state), which does not satisfy the European regulation for compressive strength. Therefore, further investigations to improve the mechanical strength to satisfy the mechanical regulation is needed in order to utilize MF/PCM24 as a thermoregulation component in geopolymer concrete for building applications.

4. Conclusion

The integration of microencapsulated phase change materials (MPCM) into geopolymer concrete (GPC) was found to improve the thermal energy storage capacity, reduce the thermal conductivity and decrease the density, resulting in an enhancement of the energy efficiency. MF/PCM24 with a polymer shell containing polar functional groups, the highest core/shell ratio (9:1) and the smallest size (10–100 μm) exhibited the largest increase of GPC porosity, better interface bonds between microcapsules and the concrete matrix, and a more uniform dispersion in the concrete matrix compared to PS-DVB/RT27 and PMMA/PCM26. The reduction of power consumption for

stabilizing the indoor temperature at 23 °C was also highest for MF/PCM24 at 25.9 ± 0.3% utilizing 5.2 wt% microcapsules, while the corresponding values was 18.5 ± 0.3% for PS-DVB/RT27, and 20.1 ± 0.7% for PMMA/PCM26.

The main drawback of MPCM addition is the significant reduction of compressive strength, which is also more pronounced for MF/PCM24 due to the larger amount of air pockets and a higher core/shell ratio than PS-DVB/RT27 and PMMA/PCM26.

The compressive strength of GPC containing MPCM decreases when PCM changes from a solid to liquid state. The reduction is most pronounced for MF/PCM24, probably due to the lack of air gaps between MPCM and the GPC combined with a higher core/shell ratio.

The addition of PS-DVB/RT27 and PMMA/PCM26 to GPC was found to satisfy the demand of mechanical properties for structural applications. MF/PCM24 was found to be the best choice for saving energy, but unfortunately the mechanical strength is too low. This challenge needs to be overcome in order to facilitate utilization in building materials.

Acknowledgement

We gratefully acknowledge funding from the Research Council of Norway, project number 238198. The authors gratefully acknowledge Rino Nilsen, Trond Atle Drøbak at Østfold University College and Van Thi Ai Nguyen for their assistance with laboratory work.

References

[1] E.P. EU Directive 2002/91/EC. Brussels; 2003.
[2] E.P. EU Directive 2010/31/UE. Strasburg; 2010.
[3] Hunger AGEM, Mandilaras I, Brouwers HJH, Founti M. The behavior of self-compacting concrete containing micro-encapsulated Phase Change Materials. Cem Concr Compos 2009;31:731–43.
[4] María Fenollera JLM, Goicoechea Itziar, Lorenzo Jaime, Álvarez Miguel Ángel. The influence of phase change materials on the properties of self-compacting concrete. Materials 2013;6:3530–46.
[5] Cao VD, Pilehvar S, Salas-Bringas C, Szczotok AM, Rodriguez JF, Carmona M, et al. Microencapsulated phase change materials for enhancing the thermal performance of Portland cement concrete and geopolymer concrete for passive building applications. Energy Convers Manage 2017;133:56–66.
[6] Eddhahak-Ouni A, Drissi S, Colin J, Neji J, Care S. Experimental and multi-scale analysis of the thermal properties of Portland cement concretes embedded with microencapsulated Phase Change Materials (PCMs). Appl Therm Eng 2014;64:32–9.
[7] Pilehvar S, Cao VD, Szczotok AM, Valentini L, Salvioni D, Magistri M, et al. Mechanical properties and microscale changes of geopolymer concrete and Portland cement concrete containing micro-encapsulated phase change materials. Cem Concr Res 2017;100:341–9.
[8] Pisello AL, D'Alessandro A, Fabiani C, Fiorelli AP, Ubertini F, Cabeza LF, et al. Multifunctional analysis of innovative PCM-filled concretes. Energy Procedia 2017;111:81–90.
[9] Wei Z, Falzone G, Wang B, Thiele A, Puerta-Falla G, Pilon L, et al. The durability of cementitious composites containing microencapsulated phase change materials. Cem Concr Compos 2017;81:66–76.
[10] Benhelal E, Zahedi G, Shamsaei E, Bahadori A. Global strategies and potentials to curb CO_2 emissions in cement industry. J Cleaner Prod 2013;51:142–61.
[11] Duxson P, Fernandez-Jimenez A, Provis JL, Lukey GC, Palomo A, Deventer JSJv. Geopolymer technology: the current state of the art. J Mater Sci 2007;42:2917–33.
[12] Zuhua Z, Xiao Y, Huajun Z, Yue C. Role of water in the synthesis of calcined kaolin-based geopolymer. Appl Clay Sci 2009;43:218–23.
[13] Nematollahi B, Ranade R, Sanjayan J, Ramakrishnan S. Thermal and mechanical properties of sustainable lightweight strain hardening geopolymer composites. Arch Civil Mech Eng 2017;17:55–64.
[14] Nematollahi B, Sanjayan J, Shaikh FUA. Synthesis of heat and ambient cured one-part geopolymer mixes with different grades of sodium silicate. Ceram Int 2015;41:5696–704.
[15] Szczotok AM, Carmona M, Kjøniksen A-L, Rodriguez JF. Equilibrium adsorption of polyvinylpyrrolidone and its role on thermoregulating microcapsules synthesis process. Colloid Polym Sci 2017;40:4061–71.
[16] http://www.micronal.de. datasheet of DS-5038X.
[17] http://www.microteklabs.com/data-sheets.html. Data sheet of MPCM24D.
[18] Cao VD, Pilehvar S, Salas-Bringas C, Szczotok AM, Valentini L, Carmona M, et al. Influence of microcapsule size and shell polarity on thermal and mechanical properties of thermoregulating geopolymer concrete for passive building applications. Energy Convers Manage-Data Brief 2018.
[19] Pilehvar S, Cao VD, Szczotok AM, Carmona M, Valentini L, Lanzon M, et al. Physical and mechanical properties of fly ash/slag geopolymer concrete containing different types of micro-encapsulated phase change materials; 2018 [Submitted for publication].
[20] Nematollahi B, Sanjayan J. Efficacy of available superplasticizers on geopolymers. Res J Appl Sci Eng Technol 2014;7:1278–82.
[21] Nematollahi B, Sanjayan J. Effect of different superplasticizers and activator combinations on workability and strength of fly ash based geopolymer. Mater Des 2014;57:667–72.
[22] Jang JG, Lee NK, Lee HK. Fresh and hardened properties of alkali-activated fly ash/slag pastes with superplasticizers. Constr Build Mater 2014;50:169–76.
[23] Feldkamp LA, Davis LC, Kress JW. Practical cone-beam algorithm. J Opt Soc Am A 1984;1:612–9.
[24] Standard BS EN 12390–7. Testing hardened concrete. Part 7: Density of hardened concrete; 2009.
[25] Liu MYJ, Alengaram UJ, Jumaat MZ, Mo KH. Evaluation of thermal conductivity, mechanical and transportproperties of lightweight aggregate foamed geopolymer concrete. Energy Build 2014;72:238–45.
[26] Safiuddin M, Hearn N. Comparison of ASTM saturation techniques for measuring the permeable porosity of concrete. Cem Concr Res 2005;35:1008–13.
[27] Cui H, Liao W, Mi X, Lo TY, Chen D. Study on functional and mechanical properties of cement mortar with graphite-modified microencapsulated phase-change materials. Energy Build 2015;105:273–84.
[28] Tittelein P, Gibout S, Franquet E, Johannes K, Zalewski L, Kuznik F, et al. Simulation of the thermal and energy behaviour of a composite material containing encapsulated-PCM: influence of the thermodynamical modelling. Appl Energy 2015;140:269–74.
[29] Joulin A, Zalewski L, Lassue S, Naji H. Experimental investigation of thermal characteristics of a mortar with or without a micro-encapsulated phase change material. Appl Therm Eng 2014;66:171–80.
[30] Cengel YA. Heat transfer: a practical approach. 2nd ed. Mcgraw-Hill; 2002.
[31] Mucteba U, Kemalettin Y. Effect of mineral admixtures on properties of self-compacting concrete. Cem Concr Compos 2011;33:771–6.
[32] Nikbin IM, Beygi MHA, Kazemi MT, Vaseghi Amiri J, Rabbanifar S, Rahmani E, et al. A comprehensive investigation into the effect of water to cement ratio and powder content on mechanical properties of self-compacting concrete. Constr Build Mater 2014;57:69–80.
[33] Chad Norvell DJS, Dusicka Peter. The effect of microencapsulated phase-change material on the compressive strength of structural concrete. J Green Build 2013;8:116–24.
[34] Dehdezi PK, Hall MR, Dawson AR, Casey SP. Thermal, mechanical and microstructural analysis of concrete containing microencapsulated phase change materials. Int J Pavement Eng 2012;14:449–62.
[35] Borreguero AM, Serrano A, Garrido I, Rodríguez JF, Carmona M. Polymeric-SiO_2-PCMs for improving the thermal properties of gypsum applied in energy efficient buildings. Energy Convers Manage 2014;87:138–44.
[36] Moosberg-Bustnes H, Lagerblad B, Forssberg E. The function of fillers in concrete. Mater Struct 2004;37:74–81.
[37] Fedroff D, Ahmad S, Savas B. Mechanical properties of concrete with ground waste tire rubber. Transpor Res Board 1996;1532:66–72.
[38] Khatib ZK, Bayomy FM. Rubberized Portland cement concrete. J Mater Civ Eng 1999;11:206–13.
[39] Ukrainczyk SKN, Šipušiæ J. Thermophysical comparison of five commercial paraffin waxes as latent heat storage materials. Chem Biochem Eng Q 2010;24:129–37.
[40] Vahedi F, Shahverdi HR, Shokrieh MM, Esmkhani M. Effects of carbon nanotube content on the mechanical and electrical properties of epoxy-based composites. New Carbon Mater 2014;29:419–25.
[41] Elkady H, Serag MI, Elfeky MS. Effect of nano silica de-agglomeration, and methods of adding super-plasticizer on the compressive strength, and workability of nano silica concrete. Civil Environ Res 2013;3:21–34.

Paper VI

Thermal performance and numerical simulation of geopolymer concrete containing different types of thermoregulating materials for passive building applications.

Vinh Duy Cao, Shima Pilehvar, Carlos Salas-Bringas, Anna M. Szczotok, Tri Quang Bui, Manuel Carmona, Juan F. Rodriguez, Anna-Lena Kjøniksen.

Energy and Buildings **2018**, 173, 678-688.

Energy & Buildings 173 (2018) 678–688

Contents lists available at ScienceDirect

Energy & Buildings

journal homepage: www.elsevier.com/locate/enbuild

Thermal performance and numerical simulation of geopolymer concrete containing different types of thermoregulating materials for passive building applications

Vinh Duy Cao[a,b], Shima Pilehvar[a,c], Carlos Salas-Bringas[b], Anna M. Szczotok[a,d], Tri Quang Bui[a], Manuel Carmona[d], Juan F. Rodriguez[d], Anna-Lena Kjøniksen[a,*]

[a] Faculty of Engineering, Østfold University College, Halden N-1757, Norway
[b] Faculty of Science and Technology, Norwegian University of Life Sciences, Ås N-1432, Norway
[c] Department of Material Engineering and Manufacturing, Technical University of Cartagena, Cartagena, Murcia, Spain
[d] Department of Chemical Engineering, University of Castilla – La Mancha, Ciudad Real 13004, Spain

ARTICLE INFO

Article history:
Received 6 December 2017
Revised 26 February 2018
Accepted 7 June 2018
Available online 20 June 2018

Keywords:
Microencapsulated phase change materials
Geopolymer concrete
Thermal performance
Implicit method
Finite differences

ABSTRACT

Geopolymer concrete (GPC) containing microencapsulated phase change materials (MPCM) were fabricated in order to achieve a high thermal energy storage capacity of an environmental friendly concrete. Different kinds of MPCM were utilized to investigate the influence of the hygroscopic nature, latent heat, and size of microcapsules on the microstructure and thermal properties of GPC. A combination of polar functional groups on the polymer shell and microcapsules with a small size was found to improve the interface bonds between microcapsules and the GPC matrix, how well the MPCM is dispersed in the GPC, and the thermal insulation properties of the GPC. The energy storage capacity of GPC increases at higher concentrations of MPCM and with a higher latent heat of the MPCM. To determine the thermal impact of buildings utilizing GPC containing MPCM, a numerical model was utilized. The model is based on the implicit finite differences method using an energy balance approach and the heat capacity method. In order to improve the model, a new equation was successfully utilized to fit the specific heat capacity of GPC containing MPCM as function of temperature. The numerical model was verified by experimental measurements of the thermal performance of the GPC. The simulated numerical values obtained for GPC containing MPCM were in good agreement with the experimental data. Higher amounts of MPCM and thicker concrete walls reduce the power consumption needed to maintain an indoor temperature of 23 °C. A power reduction of nearly 35% was achieved when utilizing a 75 mm concrete wall containing 5.2 wt.% MPCM. These building materials are therefore promising for improving human comfort and for reducing the energy consumption of buildings.

1. Introduction

A promising solution for reducing indoor temperature fluctuations, maintaining thermal comfort, and minimizing the peak of the cooling and heating loads is integration of microencapsulated phase change materials (MPCM) in building materials. This will enhance the heat storage capacity during the phase transition of the phase change materials and reduce the thermal conductivity of the building materials. Portland cement concrete is among the best known materials for integration of MPCM due to the high mechanical strength and the possibility of changing the properties by varying the concrete recipe [1–9]. However, the main drawback of producing Portland cement is the CO_2 emission, which contributes to about 5–8% of the total CO_2 emissions, and is the third man-made CO_2 source after transport and energy generation [10]. Accordingly, it is advantageous to use green materials to partly replace Portland cement concrete. Geopolymer synthesized by alkali activation of aluminosilicate materials in amorphous form (from industrial waste) is environmentally friendly [11,12]. Replacing Portland cement by geopolymer as the main concrete binder can significantly reduce the CO_2 emission from the cement industry. Although geopolymer concrete containing microencapsulated phase change materials is very interesting, research regarding

* Corresponding author.
E-mail address: anna.l.kjoniksen@hiof.no (A.-L. Kjøniksen).

https://doi.org/10.1016/j.enbuild.2018.06.011

Table 1
The fundamental data of the microencapsulated phase change materials.

MPCM name	Hygroscopic nature of shell	Size (μm)		T_{melt}(°C)	ΔH(J/g)	Core/Shell ratio	Ref
		Single	Aggregates (mean size)				
PS-DVB/RT27	nonpolar groups	10–100	130	24.9	100	11:9	[25]
MF/PCM24	polar groups	10–30	21	21.9	154	9:1	[26]

these materials is limited [3,5]. In addition, previous publications have mainly been investigating the effect of one type of microcapsules [1–7]. There are very few investigations comparing different types of microcapsules to examine the effect of the polarity of the polymer shell, as well as the size and the heat storage capacity of the microcapsules.

It is helpful to utilize numerical models to estimate the thermal impact of geopolymer concrete containing MPCM in buildings. Some numerical methods have been developed to simulate the effect of heat transfer during the solid–liquid phase change. These are the temperature transforming model, the heat source method, the enthalpy method and the heat capacity method [13–18]. One of the most commonly used numerical methods is the heat capacity method [16–18]. For this method a good agreement between experimental data and the numerical methods are found. Nevertheless, this method defines the apparent specific heat capacity as a stepwise function of temperature, which exhibits a discontinuity of the specific heat capacity at the start and end of the melting point range. This can produce a mismatch between the model and realistic conditions. Furthermore, most studies assume that the melting peak is symmetric, and define $C_p(T)$ as a piecewise function of temperature [16,17] or a Gaussian function of temperature [19]. However, for concrete containing microcapsules this assumption is not in agreement with the experimental curve of $C_p(T)$, which exhibit an asymmetric melting peak [3,20–22].

Previously, it was found that agglomeration of the microcapsules have an important effect on the properties of geopolymer concrete [3]. Accordingly, the current work utilizes microencapsulated phase change materials that do not form large agglomerates. Unlike the previous study [3], two types of microcapsules with different polymer shells, heat storage capacity and sizes were utilized to explore their influence on the microstructure and thermal properties of geopolymer concrete. In addition, a simple equation is developed to reproduce the heat capacity for GPC containing microencapsulated phase change materials. This equation was utilized in the numerical model to predict the thermal impact of GPC containing MPCM. Finally, a simple experimental system was designed to verify the performance of the numerical model. Previous studies have compared the thermal impact based on numerical calculations with experimental results for Portland cement plastering mortars containing MPCM [23,24]. There is however a lack of studies where this kind of comparison have been conducted on concretes or geopolymer materials containing MPCM.

2. Experimental

2.1. Materials

Two different kinds of microcapsules were utilized:

- PS-DVB/RT27 microcapsules consists of a paraffin Rubitherm®RT27 core coated with a PS-DVB (polystyrene cross-linked with divinylbenzene) shell. These microcapsules were made by a polymerization suspension process in our lab [25].
- Commercial Microtek MPCM24D (MF/PCM24) which contains a paraffin core and a melamine-formaldehyde polymer shell (MF).

The properties of the microcapsules are summarized in Table 1.

Table 2 summarizes the composition of geopolymer concrete containing MPCM (MPCM-GPC). The main components of the geopolymer concrete are sand (Gunnar Holth and Skolt Pukkverk AS, Norway), aggregates (Gunnar Holth and Skolt Pukkverk AS, Norway), fly ash (FA) (Norcem, Germany), ground granulated blast furnace slag (GGBFS) (Cemex, Germany), retarder (FLUBE OS 39, Bozzetto Group, Italy), an alkaline activator solution and microcapsules. The alkaline activator solution is a mixture of a sodium silicate solution Na_2SiO_3 (35 wt.% solid) and 14 M sodium hydroxide NaOH (560 g/L). Based on a previous study [27], the mixing ratio between Na_2SiO_3 and NaOH is 1.5 corresponding to $m_{Na2SiO3(aq)} = 120$ g, and $m_{NaOH(aq)} = 80$ g. MPCM was mixed into the GPC as the final mixing step to minimize the shear forces on the microcapsules during the mixing process. For more information about the recipe and the mixing process, see Pilehvar et al. [5,27].

In order to investigate the effect of MPCM concentration on the thermal properties of MPCM-GPC, The MPCM concentration was varied from 0 to 5.2 wt.% in steps of 2.6 wt.%. After mixing, MPCM-GPC were cast into molds at a size of 200 × 200 × 25 mm, and precured at room temperature for 24 h. The samples were then demolded and kept in water at room temperature for 28 days to reach a fully cured state. Finally, they were gently dried in an oven at 40 °C (to avoid shrinkage, thermal cracks, and broken microcapsules) until the sample weight remained unchanged [3].

2.2. Scanning electron microscopy

The fractured surfaces of MPCM-GPC samples containing 2.6 wt.% of MPCM were investigated using Zeiss EVO50 EP Scanning electron microscopy (Norway).

2.3. Density and porosity

The density and open porosity of the concrete samples were determined by EN 12390-7 (Eq. (1)) [28] and ASTM C1202-12 (Eq. (2)), respectively [29,30].

$$\rho = \frac{m_d}{V} \tag{1}$$

$$Open\ Porosity\ (\%) = \frac{m_s - m_d}{m_s - m_b} \times\ 100 \tag{2}$$

where ρ is the dry density of the sample, V is the volume of the sample, and m_d, m_b and m_s are oven-dried weight, the buoyant mass of the saturated sample in water and the mass of the saturated sample in air, respectively.

2.4. Thermal properties

A homemade guarded hot plates device [3,20,31] was designed to measure the thermal properties of concrete containing MPCM such as the thermal conductivity, the specific heat capacity and the heat storage capacity. The sample was placed in the middle of two aluminum plate heat exchangers. Each aluminum plate heat exchanger was connected to a programmable thermal regulated bath that defines the thermal conditions. A 40 mm thick polyethylene expanded foam (PEF) is used to cover the sample and minimize the heat losses from the sides of the samples. Accordingly,

Table 2
Composition of geopolymer concrete.

MPCM(wt.%)	Alkaline solution(g)	Water(g)	FA*(g)	GGBFS**(g)	Sand(g)	Aggregate(g)	Retarder(g)	MPCM(g)
0	200	50	300	200	871.8	851.7	5	0
2.6	200	50	300	200	696.9	851.7	5	63
5.2	200	50	300	200	522.7	851.7	5	117

(*) FA: Flyash (**) GGBFS: Ground granulated blast-furnace slag

the heat transfer through the sample can be assumed to behave according to one-dimensional thermal conditions. Calibrated heat flux sensors (Captecv, France) and calibrated T-type thermocouples (OMEGA, US) were utilized to record the temperature variations and heat fluxes through sample during testing.

Thermal conductivity

The thermal conductivity of the samples is defined according to the European standard EN-12667. The thermal conductivity of the samples in the liquid and solid states of PCM were determined by applying different temperature gradients between the top and bottom aluminum plate heat exchangers corresponding to a liquid state temperature range ($T > 30\,°C$) and a solid state temperature range ($T < 20\,°C$). After the samples reached a steady-state, the temperature and heat fluxes on both surfaces of the samples were collected. The thermal conductivity of the samples in the liquid and solid states of PCM was determined by [3]:

$$k = \frac{\varphi d}{\Delta T} \tag{3}$$

where $d = 25 \pm 1$ mm is the thickness of the sample, ΔT is the difference in temperature between the surfaces of the sample and φ is the average heat fluxes on both faces of the concrete sample.

Specific heat capacity/ heat storage capacity

The specific heat capacity of the concrete containing MPCM was determined by homogeneously raising the temperature of both aluminum plate heat exchangers from 5 °C and 45 °C at a heating rate of 10 °C/hour. It should be noted that a steady-state must be achieved at the initial and final temperatures of this process. The data including the heat flux (φ) and temperature (T) on both surfaces of the sample were collected during the process using calibrated heat flux sensors and calibrated thermocouples. The specific heat capacity as a function of temperature of the samples can be determined by [3,21]:

$$C_p(T) = \frac{A\varphi(T)}{m\frac{dT}{dt}} \tag{4}$$

The total heat storage capacity was calculated in the temperature range of 10–35 °C by Eq. (5) [21] using OriginPro 2016 Sr2.

$$Q = \frac{A}{m}\left(\int_{T1}^{T2} \varphi(T)dT\right) \tag{5}$$

where $T_1 = 10$ °C and $T_2 = 35$ °C. $A = 400$ cm^2 is the area of the sample.

In addition, the thermal conductivity and specific heat capacity of a homogeneous reference sample (granite rock-Nero Assoluto, Zimbabwe) were determined by using the homemade hot plate system and a TPS2500 hotdisk system (Lund) to evaluate the accuracy of the homemade system compared to the commercial one. The test was performed at room temperature (≈20 °C) for the TPS2500 hotdisk system and a temperature range of 15–25 °C for the homemade system. The results are summarized in Table 3. There is a good agreement between the results measured by the homemade device and the TPS2500 with approximately 7% and 10% relative differences for the specific heat capacity and the thermal conductivity, respectively. In addition, the values are close to the litterature values of the specific heat capacity and thermal conductivity of granite rock (approximately 790 J/kg °C and 2.68–3.07 W/m °C [32]). Accordingly, the homemade sytem can be utilized to determine the thermal properties of building materials.

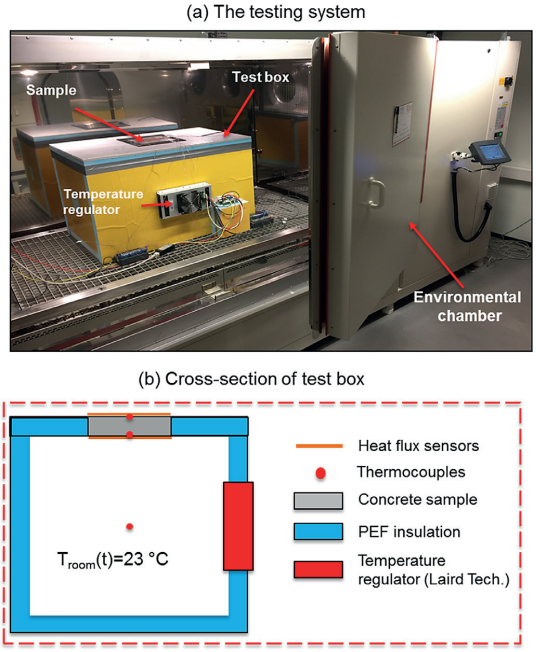

Fig. 1. The thermal performance testing system (a) test box placed in an environmental chamber, (b) sketch of the cross-section of the test box.

2.5. Energy saving aspects

Experimental test

Fig. 1 shows the thermal testing system which was utilized to investigate the thermal impact of geopolymer concrete containing microcapsules and to verify the numerical model. A small test box with inner dimensions of 600 × 800 × 600 mm was made of 50 mm panels of polyethylene expanded foam (PEF) (Fig. 1) and was placed inside an environmental chamber to model outdoor temperature fluctuations. The concrete sample was placed in a rectangular opening (200 × 200 mm) in the middle of the top insulation panel.

For the test, the small test box was exposed to a daily sinusoidal temperature oscillation T_{out} (t) (Eq. (6)) using an environmental chamber (VT^3 4250, Vötsch, Germany) while the temperature inside the test box (T_{room}) was kept constant at 23 °C by a temperature regulator (AA150-Laird Technologies). For more information regarding the environmental chamber and temperature regulator, see the supporting document [33]. The maximum outdoor temperature T_{max} were set at 14:00 during the temperature

Table 3
Summarization of the specific heat capacity and thermal conductivity of granite rock determined by a homemade device and the TPS2500.

	Methods			Relative differences (%) $\frac{TPS2500-Homemade}{TPS2500} * 100\%$
	Homemade device	TPS2500	Literature	
Specific heat capacity (J/Kg °C)	704 ± 9	755	790	6.7
Thermal conductivity	2.65 ± 0.03	2.93	2.68–3.07	9.6

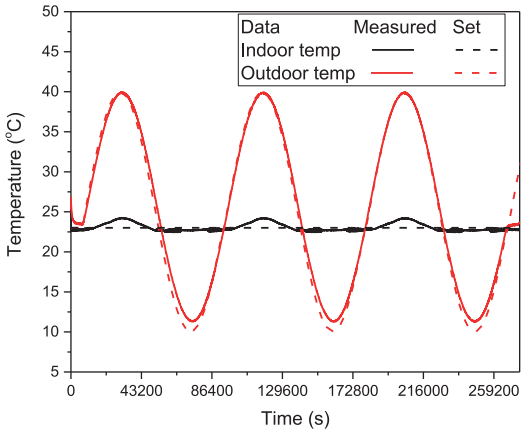

Fig. 2. The setting and measured temperatures of the indoor (inside text box) and outdoor (outside test box) environnments.

variation of the outdoor conditions:

$$T_{out}(t) = \frac{T_{max} + T_{min}}{2} + \frac{T_{max} - T_{min}}{2} \sin\left(\frac{\pi}{43200} t - \frac{2\pi}{3}\right) \quad (6)$$

where $T_{max} = 40$ °C and $T_{min} = 10$ °C are the maximum and minimum outdoor temperatures during one day, respectively. In order to simplify the thermal system, the effect of solar radiation is not considered. At the initial stage, both the indoor temperature (T_{room}) and outdoor temperature (T_{out}) were set at 23 °C for 2 h to reach a steady-state condition. Afterwards, the outdoor temperature cycles (Eq. (6)) were run continuously for 72 h.

Thermocouples were installed at different depths through the concrete wall in steps of 25 mm to measure the temperature across the samples. Heat flux sensors were installed on both surfaces of the concrete. Thermocouples were also placed at different positions both in the test box and in the environmental chamber to record the indoor temperature (T_{room}) and the outdoor temperature (T_{out}). All data were recorded every 60 s using a multichannel multimeter (LR8410-20 Hioki, Japan).

The outdoor and indoor temperatures during the experiments were recorded and is shown in Fig. 2. There is the slight mismatch between the setting temperature (Eq. (6)) and the mean collected temperature for both the outdoor and indoor temperature. This is more pronounced for the indoor temperature (T_{room}), which is probably due to the limits of the heating/cooling capacity of the temperature regulator. Therefore, the real experimental data collected using the calibrated thermal couples was utilized as input temperature data for the numerical calculation to improve the reality and accuracy of the method.

It is assumed that the insulation panels of the test box are perfectly thermally insulated. The heat will transfer to the test box via the concrete sample and be compensated for by the temperature regulator to maintain an inside temperature (T_{room}) of 23 °C. Accordingly, the total heat transfer to the test box can be calculated by Eq. (7) and corresponds to the energy (power consumption) of the temperature regulator (for heating when the temperature is below 23 °C and cooling when the temperature is higher than 23 °C):

$$P = \frac{\int_0^{24h} |\varphi_{indoor}| dt}{3600 \cdot 10^3} \quad (7)$$

where φ_{indoor} is the heat flux on the indoor side of the sample.

The power reduction Pr is defined as:

$$Pr = \frac{P_{GPC} - P_{MPCM-GPC}}{P_{GPC}} \cdot 100\% \quad (8)$$

where P_{GPC} and $P_{MPCM-GPC}$ are the power consumption of the heating/cooling system during 24 h for geopolymer concrete without and with MPCM, respectively.

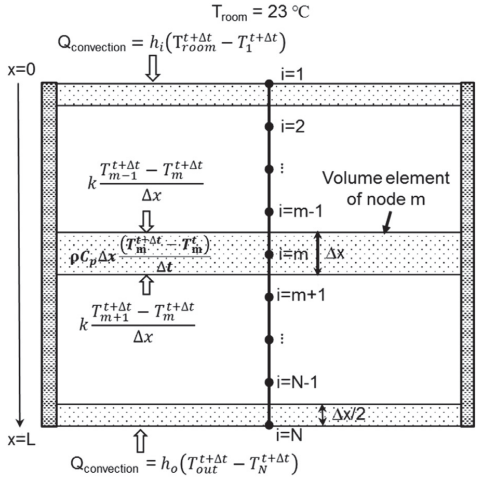

$$T_{out}(t) = \frac{T_{max} + T_{min}}{2} + \frac{T_{max} - T_{min}}{2} \sin(\frac{\pi}{43200} t - \frac{2\pi}{3})$$

Fig. 3. Schematic representation of the MPCM-concrete wall, and implicit finite differences method using the energy balance approach with boundary conditions. The energy balance states that heat transferred into the volume element from all of the surfaces is equal to the change in the energy content of the volume element during Δt [34].

2.6. Numerical method

A numerical model was developed to investigate the effect of MPCM addition on the thermal properties of a concrete wall. A simplified and uninsulated concrete wall was utilized. The thermal performance including the indoor surface temperature of the concrete wall, and the power consumption and power reduction for the heating and cooling system to maintain a constant indoor temperature were numerically calculated.

The model used to investigate the thermal behavior of the concrete wall is shown in Fig. 3. In order to simplify the model, it is assumed that:

- The heat transfer through the wall is a one-dimensional condition.
- The GPC containing microcapsules is homogeneous and isotropic.
- There is no heat generation in the samples.
- The convection effect in the melted PCM and super-cooling effects are neglectable.
- The indoor and outdoor heat transfer coefficients are assumed to be constant and are obtained from the literature.

The thermal conductivity, specific heat capacity, and density of the concrete walls which were used as input data for the numerical calculation were experimentally determined.

The mathematical model for one-dimensional heat transfer through the wall is [16,17,34]:

$$k\frac{\partial^2 T}{\partial x^2} = \rho C_p(T)\frac{\partial T}{\partial t} \quad (9)$$

where k, ρ, x are the thermal conductivity, density, and thickness of the wall, respectively. $C_p(T)$ is the specific heat capacity as a function of temperature of GPC containing microcapsules.

- **Numerical solution procedure**

The implicit finite difference method using the energy balance approach is used to solve the mathematic model and is illustrated in Fig. 3 [34]. The concrete wall is first discretized into a number of nodes (N) with a distance of Δx between two adjacent nodes. The volume elements over the nodes, where energy balance is applied, are formed to determine the temperatures at all nodes of the sample. The resulting implicit finite differences using the energy balance approach equations are:

◦ Interior node i = 1 (x = 0, indoor wall surface) (boundary condition [34]):

$$k\frac{T_2^{t+\Delta t} - T_1^{t+\Delta t}}{\Delta x} + h_i\left(T_{room}^{t+\Delta t} - T_1^{t+1\Delta t}\right) = \rho C_p\frac{\Delta x}{2}\frac{\left(T_1^{t+\Delta t} - T_1^{t}\right)}{\Delta t} \quad (10)$$

$$T_1^t = (1 + 2Bi_iFo)T_1^{t+\Delta t} - 2FoT_2^{t+\Delta t} - 2Bi_iFoT_{room}^{t+\Delta t} \quad (11)$$

◦ Inner node i = 2 to i = N-1

$$k\frac{T_{m-1}^{t+\Delta t} - T_m^{t+\Delta t}}{\Delta x} + k\frac{T_{m+1}^{t+\Delta t} - T_m^{t+\Delta t}}{\Delta x} = \rho C_p\Delta x\frac{T_m^{t+\Delta t} - T_m^t}{\Delta t} \quad (12)$$

$$T_m^t = -FoT_{m-1}^{t+\Delta t} + (1 + 2Fo)T_m^{t+\Delta t} - FoT_{m+1}^{t+\Delta t} \quad (13)$$

◦ Exterior node i = N (x = L, outdoor wall surface) (boundary condition [17,19,34,35]):

$$k\frac{T_{N-1}^{t+\Delta t} - T_N^{t+\Delta t}}{\Delta x} + h_o\left(T_{out}^{t+\Delta t} - T_N^{t+\Delta t}\right) = \rho C_p\frac{\Delta x}{2}\frac{\left(T_N^{t+\Delta t} - T_N^{t}\right)}{\Delta t} \quad (14)$$

$$T_N^t = -2FoT_{N-1}^{t+\Delta t} + (1 + 2\mathrm{Fo} + 2Bi_oFo)T_N^{t+1} - 2Bi_oFoT_{out}^{t+\Delta t} \quad (15)$$

where Bi_i and Bi_o are the Biot numbers in the room and in the outdoor environment, respectively:

$$Bi_i = \frac{h_i\Delta x}{k} \text{ and } Bi_o = \frac{h_o\Delta x}{k} \quad (16)$$

Fo is the Fourier number calculated as:

$$Fo = \frac{k\Delta t}{\rho C_p(\Delta x)^2} \quad (17)$$

T_m^t, $T_m^{t+\Delta t}$ are the temperatures of node m at time t and time (t + Δt), respectively. In addition, $\Delta t = 60$ s and $\Delta x = 0.005$ m were selected for all cases. The initial temperature of the system was set to 23 °C. T_{out} and T_N are the outdoor temperature and the outdoor wall surface temperature (x = L). h_i and h_o are the indoor heat transfer coefficient (test box) and the outdoor heat transfer coefficient (environmental chamber), respectively. The heat transfer coefficient depends on the surface orientation, the direction of the heat flow and the velocity of the heat flow [36], which are collected from the experimental setup. To simplify the complex determination, the heat transfer coefficient values were selected from the literature based on the experimental setup information. Both h_i and h_o were considered to have the same value of 8 W/m^2 K for the horizontal wall. This is similar to the recommended values of ASHEA [36] and has been utilized for similar calculations previously [17,37,38].

MATLAB (Mathworks Inc., Natick, MA, USA) was employed to solve Eq. (10)Eq. (15) for all nodes. Relevant output data including the temperature across the thickness of the concrete samples, and the heat flux on the indoor surface (φ_{indoor}) were collected:

$$\varphi_{indoor}(t) = h_i\left(T_{room}^t - T_1^t\right) \quad (18)$$

Accordingly, the power required for a heating/cooling system to keep the indoor temperature stable was determined from Eq. (7) while the power reduction Pr was calculated from Eq. (8).

- **Testing conditions**

In order to evaluate the effect of microcapsules on the thermal impact on buildings using MPCM-GPC walls, various conditions were employed. Those conditions were carefully selected and applied on both the numerical model and the experimental tests.

◦ **Outdoor and indoor temperature**

In order to verify the numerical model, the actual outdoor temperature (environmental chamber) and indoor temperature (test box) were collected through the experiments using calibrated thermal couples. These data are utilized as the input temperature data for the numerical calculation to improve the reality and accuracy of the method.

◦ **MPCM concentration**

MPCM concentrations were selected at 0, 2.6 and 5.2 wt.% of the total weight of the concrete, to evaluate effect of MPCM concentration on the thermal performance of the concrete. The concentration of MPCM was limited to 5.2 wt.% since higher concentrations of MPCM resulted in a too low workability of the concrete.

◦ **Concrete thickness**

Due to the importance of the wall thickness on the heat transfer process of buildings, the thickness of the concrete walls was varied to investigate the effect on the thermal performance. GPC without microcapsules and GPC containing 5.2 wt.% microcapsules at thicknesses of 25, 50 and 75 mm were utilized.

3. Results and discussion

3.1. MPCM-GPC density and porosity

The open porosity of GPC as a function of MPCM concentration is shown in Fig. 4(a). The porosity increases when the MPCM concentration is raised. The smaller size of the microcapsules compared to the sand particles (see Fig. 1 in the supporting document [33]) is a possible explanation for this trend and in good agreement with previous findings [3]. The porosity of GPC containing PS-DVB/RT27 is lower than for MF/PCM24, especially after adding 2.6 wt.% microcapsules. MF/PCM24 has a polymer shell containing polar amine groups, which give rise to two opposite effects. Due

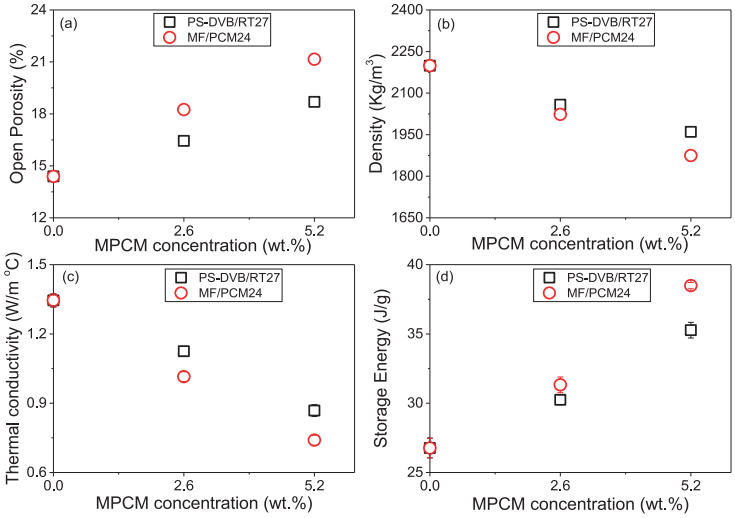

Fig. 4. (a) Open porosity, (b) density, (c) thermal conductivity and (d) storage energy as function of MPCM concentration of GPC containing PS-DVB/RT27 and GPC containing MF/PCM24.

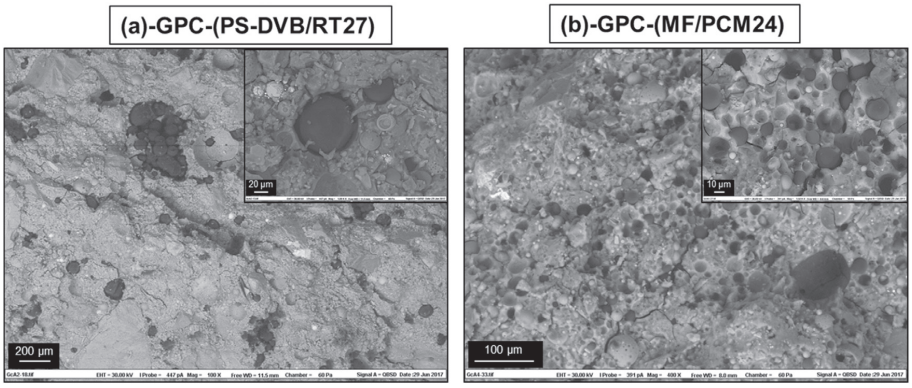

Fig. 5. SEM images of GPC containing 2.6 wt.% of (a) PS-DVB/RT27, (b) MF/PCM24.

to the polar groups, the polymer shell of MF/PCM24 is more compatible with the GPC. This causes better interface bonds between microcapsules and the geopolymer. This can reduce the air gaps between MPCM and GPC. PS-DVB/RT27 has a hydrophobic polymer shell which repel water. This causes more air gaps to be formed between the microcapsules and the GPC during the mixing process [3,39,40]. As is evident from the SEM images in Fig. 5, obvious gaps are observed between the concrete matrix and PS-DVB/RT27, while there is almost no air gaps between MF/PCM24 and the concrete matrix. This observation is supported by Zhang et al. [41] who concluded that the interface bonds between MPCM and Portland cement mortar can be improved by modifying the surface of the microcapsules using a silane coupling agent. On the other hand, the polar groups on the MF polymer shell and the smaller size of MF/PCM24 promotes adsorption of more water on the surface of the MF/PCM24 microcapsules [42]. This results in higher viscosities [3,5], which increases the probability of forming entrapped air voids during the mixing and pouring process. The higher porosity of GPC containing MF/PCM24 compared to GPC containing PS-DVB/RT27 is probably due to this effect.

The lower density of microcapsules compared to the sand it replaces and the increase of the porosity cause a decrease of the density of the MPCM-GPC samples when the MPCM concentration increases (Fig. 4(b)). Similar observations were also found previously [1,3]. The density decreases more for MF/PCM24, which has the highest porosity increase.

The average thermal conductivity of GPC containing different amounts of MPCM is summarized in Fig. 4(c). The thermal conductivity of MPCM-GPC decreases when the concentration of microcapsules is raised. This is due to the lower thermal conductivity of the microcapsules compared to that of replaced sand [3] and the enhanced porosity (Fig. 4(a)) after adding microcapsules. Furthermore, GPC containing MF/PCM24 has a lower thermal conductivity than GPC containing PS-DVB/RT27, which is in good agreement with the porosity data which rises faster for MF/PCM24 (Fig. 4(a)). Additionally, the better distribution of MF/PCM24 in the concrete matrix compared to PS-DVB/RT27 (Fig. 5) can provide an improved

thermal pathway through the concrete matrix and cause a lower thermal conductivity.

Fig. 4d summarizes the heat storage capacity of GPC as a function of microcapsule concentration within the temperature range of 10–35 °C. The heat storage capacity increases as more microcapsules are added to the concrete. This is in good agreement with Shadnia et al. [43] who demonstrated that the heat storage capacity of geopolymer mortar increases when the amount of MPCM increases. A similar observation has been observed for the integration of MPCM in Portland cement mortar [20,21], and Portland cement concrete [1,2]. In addition, the increase is more pronounced for MF/PCM24 due to the higher enthalpy of fusion (Table 1).

SEM images (Fig. 5) show that the microcapsules remain stable with a spherical shape in the concrete matrix. This demonstrates that both PS-DVB/RT27 and MF/PCM24 microcapsules have a good mechanical strength which can withstand the concrete mixing process. Hunger et al. [17] found that Micronal D5008X (polymethyl methacrylate/paraffin) MPCM was broken during the mixing process leading to a reduction of the Portland cement concrete compressive strength. Accordingly, both types of microcapsules utilized in the current study are probably stronger than the Micronal D5008X.

3.2. Specific heat capacity curve of MPCM-GPC

In order to accurately simulate the thermal performance of GPC containing MPCM, it is important to utilize an accurate equation to represent the experimental data of the specific heat capacity function ($C_p(T)$). This fitted $C_p(T)$ can be utilized for simulating the phase transition process.

Most previous studies define $C_p(T)$ assuming that the melting peak is symmetric, utilizing a piecewise function of temperature [16,17] or a Gaussian function of temperature [19] for modeling purposes. However, for concrete containing microcapsules this assumption is not in agreement with the experimental curve of $C_p(T)$, which presents an asymmetric shape of the melting peak [3,20–22]. We have therefore, utilized a new equation (Eq. (19)) based on the Pearson IV function to fit the specific heat capacity ($C_p(T)$) to the asymmetric shape:

$$Cp(T) = \begin{cases} Cp_o + h * \dfrac{{w_l}^{2m_l}}{\left({w_l}^2 + \left(2^{\frac{1}{m_l}} - 1\right) * (2T - 2T_m)^2\right)^{m_l}} & for\ T \le T_m \\ Cp_o + h * \dfrac{{w_r}^{2m_r}}{\left({w_r}^2 + \left(2^{\frac{1}{m_r}} - 1\right) * (2T - 2T_m)^2\right)^{m_r}} & for\ T > T_m \end{cases} \quad (19)$$

where Cp_o and h are the specific heat capacity outside the melting range and the height of the melting peak, respectively; T_m, w_l and w_r are the melting peak temperature, the phase change temperature range on the left side and right side of the melting peak, respectively; m_l and m_r are shape parameters for the left and right side of the peak, respectively.

The experimental data of the specific heat capacity versus temperature of GPC containing 5.2 wt.% microcapsules MF/PCM24 fitted to Eq. (19) is shown in Fig. 6(a). The high value of R^2 (0.99) and the non-systematic residuals (Fig. 6(b)) illustrate that this model is well suited for characterizing these systems.

Fig. 7 shows the fitted parameters obtained from Eq. (19). The specific heat capacity outside the melting range (Cp_o) of both GPC containing PS-DVB/RT27 and GPC containing MF/PCM24 increase when the concentration of microcapsules is raised (Fig. 7(a)). This is due to the higher specific heat capacity of the microcapsules compared to geopolymer concrete [3]. This is inconsistent with previous findings [3], where the specific heat capacity of MPCM-concrete remained almost unchanged after adding 2.7 wt.% of MPCM. The discrepancy is probably due to the higher microcapsule concentration applied in the current study (5.2 wt.%) which

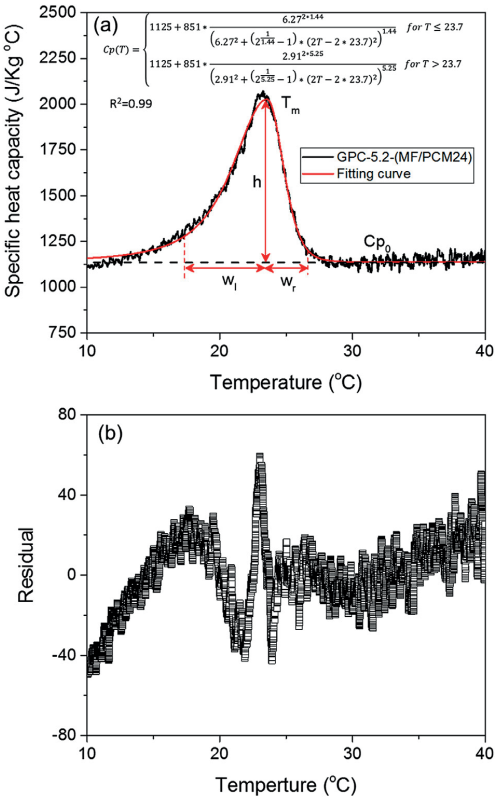

Fig. 6. (a) The specific heat capacity of GPC containing 5.2 wt.% of MF/PCM24 as function of temperature. The black solid line is experimental values. The red line shows the fitted values according to Eq. (19). (b) Residual plot between the measured and fitted values. (For interpretation of the references to color in this figure legend, the reader is referred to the web version of this article.)

is high enough to cause a significant increase of the specific heat capacity. This observation is in agreement with Joulin et al. [21], who studied effect of MPCM on the specific heat capacity of Portland cement mortar. Interestingly, the melting peak temperature of GPC containing microcapsules increases as the concentration of microcapsules is raised. The reason for this is unclear, but it might be caused by the reduced thermal conductivities of the samples (Fig. 4(c)) and the airgaps between the concrete matrix and the microcapsules (Fig. 5). When the thermal conductivity decreases it takes longer for the heat to reach the microcapsules to melt them, thereby shifting the melting peak to higher temperatures. In addition, the airgaps between PS-DVB/RT27 and the concrete matrix will act as an insulation layer, preventing the heat to efficiently reach the microcapsules. This will further delay the melting of the MPCM core.

3.3. Energy saving aspects

In order to evaluate the thermal impact of MPCM-concrete structures, numerical simulations and experimental measurements were carried out. The numerical model presented in this study is validated using the experimental results obtained by using the system show in Fig. 1. Results from the numerical model was compared with the experimental measurements.

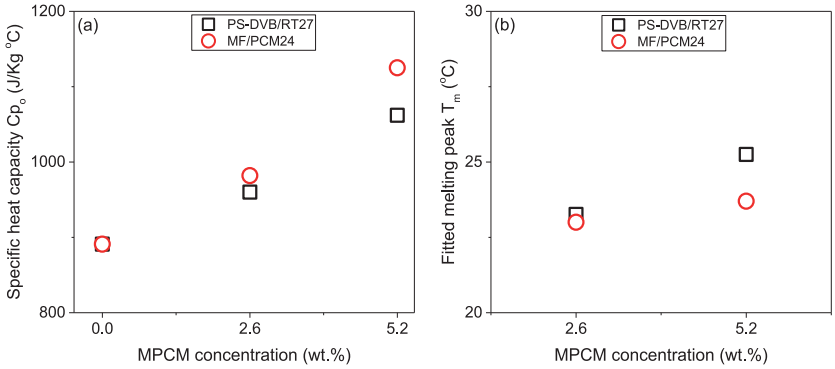

Fig. 7. (a) The specific heat capacity Cp_o and (b) the fitted melting peak T_m of GPC containing microcapsules as a function of microcapsule concentration obtained by fitting to Eq. (19).

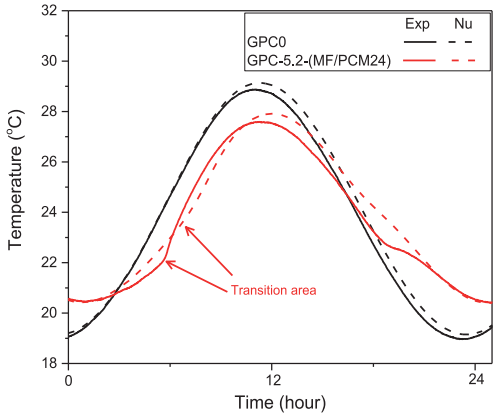

Fig. 8. Comparison of numerical model with experimental measurements for the indoor surface temperature of GPC0 and GPC-5.2-(MF/PCM24). The wall thickness of all samples is 75 mm.

Fig. 8 presents a comparison of the numerical model with experimental measurements for the indoor surface temperature of GPC0 and GPC-5.2-(MF/PCM24). There is a reasonable agreement between the experimental data and the numerical calculations. Both numerical and experimental data show that the variation of the indoor surface temperature of GPC containing 5.2 wt.% of MPCM is smaller than that of GPC without MPCM. This due to the higher heat storage capacity and lower thermal conductivity of GPC after the addition of MPCM. Accordingly, the integration of MPCM into the geopolymer concrete significantly reduce the influence of the outdoor temperature on the indoor surface temperature. This can be utilized to reduce the energy consumption for heating and cooling. However, the temperature peak occurs later in the numerical model than in the experimental work, and the melting transition is much clearer in the experimental data than in the numerical model (Fig. 8).

Fig. 9 shows a comparison of the numerical results with experimental measurements for the temperature variations across the concrete thickness at different times for GPC without MPCM and containing 5.2 wt.% of MPCM (PS-DVB/RT27 and MF/PCM24). For this test, the thermocouples were inserted through the 75 mm thick concrete sample with distance of 25 mm to determine the temperature across the concrete sample at different times (3 h, 6 h, 12 h and 22 h). Fig. 9 shows that the temperature across the thickness of the concrete obtained by experimental and numerical calculation exhibit the same trends for all samples. For GPC without MPCM (Fig. 9(a)) there is no significant deviation between the numerical model and the experimental data, illustrating that the numerical model provides a very good simulation at these conditions. In the presence of MPCM, there is a small deviation between the numerical model and the experimental data (<1 °C). This is probably due to the small deviations between the numerical calculations and the experimental data around the transition areas and the slightly different positions of the peaks (Fig. 8).

The heat flux on the indoor side of concrete samples were collected and compared to the numerical calculations. Fig. 10 shows the experimental curves and numerical curves of the heat flux on the indoor side of concrete wall without MPCM and containing 5.2 wt.% of MF/PCM24. For the GPC without MPCM there is a very good agreement between the simulation and the experimental data. In the presence of MPCM, the agreement is good except for a small deviation around the melting/solidifying transition points. The transition zones are more evident for the experimental data than in the simulations. There are several possible reasons for this discrepancy. The utilized model assumes a homogeneous sample, which is not strictly correct when microcapsules are distributed in the concrete matrix. In addition, the phase change process depends not only on temperature but also on the time it takes to completely convert the PCM to a liquid phase (melting process) or to a solid phase (solidifying process). Furthermore, the model does not take into account the effect of the interface between concrete and microcapsules, which can influence the heat transfer process especially when there are air gaps between the microcapsules and the concrete matrix. It is also possible that the heat capacity $C_p(T)$ utilized in the model is lower than the actual values and/or that the thermal conductivity is lower than expected.

The total heat transfer at the indoor surface can be used to determine the heat gain/loss toward the indoor environment. This must be compensated by a heating/cooling system in order to keep a constant indoor temperature. Accordingly, the total heat gain/loss toward the indoor environment can be considered as the energy consumption of the heating/cooling system to maintain a constant indoor temperature. In this study, the total energy consumption of the heating/cooling system is the sum of the heating power consumption when the indoor surface temperature $T_{x=0} < T_{room}$, and the cooling power consumption when the indoor surface temperature $T_{x=0} > T_{room}$. In order to verify the model, the simulated power consumption and power reduction were compared to exper-

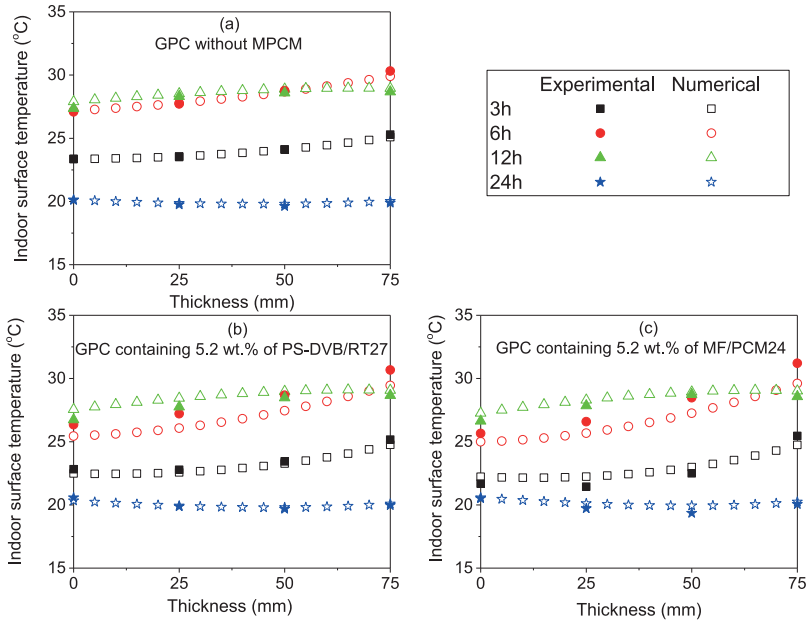

Fig. 9. Comparison of numerical model with experimental measurements for temperature variations across the concrete thickness at different times for (a) GPC0, (b) GPC-5.2-(PS-DVB/RT27) and (c) GPC-5.2-(MF/PCM24). The thickness of all samples is 75 mm.

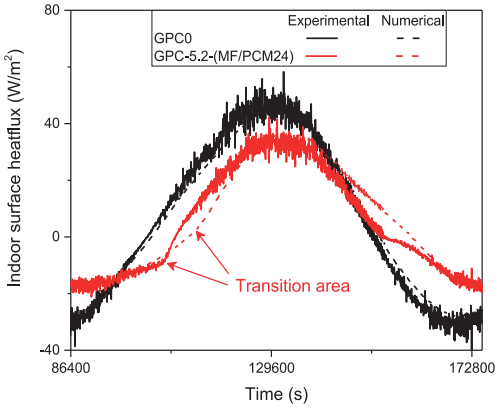

Fig. 10. Comparison of simulation model with experimental measurements for the indoor surface heat flux variations with time of GPC0 and GPC-5.2-(MF/PCM24). The thickness of all samples is 75 mm.

imental data. Furthermore, the effect of MPCM concentration, concrete wall thickness and different kinds of microcapsules on the thermal performance were investigated.

Fig. 11 presents the total calculated power consumption (Eq. (18)) and the power reduction (Eq. (19)) for the heating/cooling system to maintain an indoor temperature of 23 °C for both the experimental test and the numerical calculation. Two kinds of microcapsules PS-DVB/RT27 and MF/PCM24 were utilized. Fig. 11(a) reveals that the power consumption for the heating/cooling system to maintain an indoor temperature of 23 °C decreases substantially when the MPCM concentration is raised. The experimental data shows that the system can reduce the power consumption with up to 18.5% for PS-DVB/RT27 and 25.9% for MF/PCM24 after adding 5.2 wt.% of microcapsules (Fig. 11(b)). This demonstrates the promising thermal impact of GPC containing MPCM on the building envelope. The effect is due to a combination of a higher heat storage capacity and the better insulation properties of GPC after adding microcapsules. This is in agreement with previous experiments [1,3] and numerical calculations [17]. The simulations and experimental data exhibit the same trends. However, the simulations underestimate the amount of power that can be saved utilizing MPCM. This might be due to the deviations between the experimental and simulated data illustrated in Fig. 10. Furthermore, it is possible that the heat transfer coefficients for the indoor (h_i) and outdoor conditions (h_o) chosen from the literature might be higher than the actual values.

Fig. 12(a) shows the experimental curves of the indoor surface heat flux of GPC containing 5.2 wt.% of MF/PCM24 as a function of the concrete thickness. There is a reduction of the indoor surface heat flux when the wall becomes thicker. This is expected since the rate of heat conduction through the wall is inversely proportional to the wall thickness (Eq. (6)). This results in a lower power consumption to maintain the indoor temperature stable at 23 °C (Fig. 12(b)). Fig. 12(c) illustrates the power reduction of GPC containing 5.2 wt.% of microcapsules (GPC-5.2-(PS-DVB/RT27) and GPC-5.2-(MF/PCM24)) compared to corresponding samples without microcapsules as a function of concrete thickness (Eq. (19)). The experimental power reduction increase from 6.8% to 24.3% for GPC-5.2-(PS-DVB/RT27) and from 12.5% to 34.8% for GPC-5.2-(MF/PCM24) when the concrete thickness increases from 25 mm to 75 mm. This is probably due to a combination of the heat transfer reduction for the thicker samples and the effect of a high heat storage capacity after adding microcapsules.

GPC containing MF/PCM24 have a better thermal impact than GPC containing PS-DVB/RT27. This is expected since GPC with MF/PCM24 has lower thermal conductivity and higher heat storage

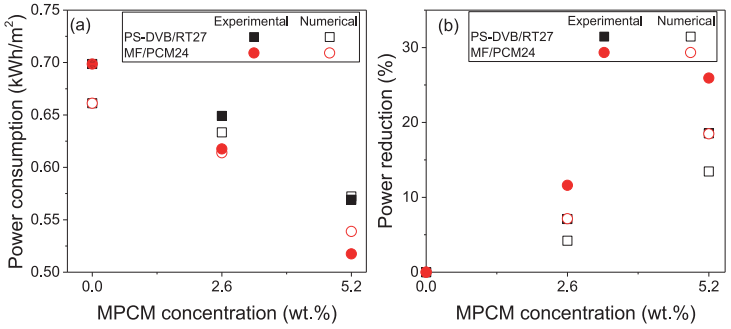

Fig. 11. Experimental data and simulation values of (a) the power consumption and (b) the power reduction of GPC as function of microcapsule concentration. Two kinds of microcapsules (PS-DVB/RT27 and MF/PCM24) were utilized. The thickness of the sample is 50 mm.

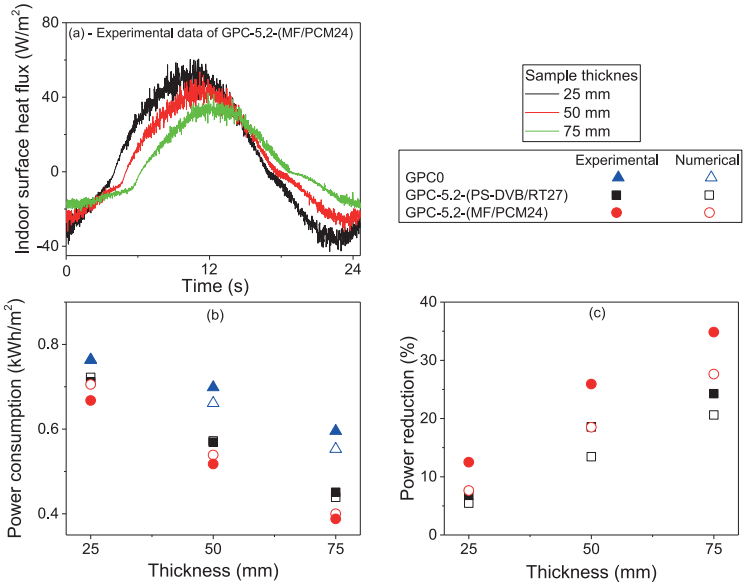

Fig. 12. The effect of wall thickness on (a) indoor surface heat flux GPC-5.2- (MF/PCM24), (b) the power consumption of GPC without microcapsules and GPC containing 5.2 wt.% microcapsules and (c) the power reduction of GPC containing 5.2 wt.% microcapsules compared to GPC without microcapsules.

capacity than that GPC containing PS-DVB/RT27 (Fig. 4). Although there are differences between the power consumption and power reduction between the experimental and numerical data, they exhibit the same trends.

The numerical model work well, with small deviations from the experimental data. Accordingly, this numerical model can be used as a quantitative tool to predict the thermal impact of concrete containing microcapsules at different climate conditions and for varying building designs.

4. Conclusion

Environmental friendly geopolymer concrete with a high thermal energy storage capacity containing microencapsulated phase change materials was achieved. By integrating microencapsulated phase change materials (MPCM) into geopolymer concrete (GPC), the thermal energy storage capacity of GPC is improved while the thermal conductivity and the density of geopolymer concrete (GPC) decrease. This results in an enhancement of the energy efficiency of the building envelope. A higher amount of MPCM in GPC or thicker MPCM-GPC walls can reduce the power consumption needed to stabilize the indoor temperature at 23 °C. The experimental data show that the power consumption can be reduced by up to 34.8% and 24.3% when utilizing a 75 mm concrete wall containing 5.2 wt.% of MF/PCM24 and PS-DVB/RT27, respectively.

The influence of the hygroscopic nature, the latent heat and the size distribution of microencapsulated phase change materials on the microstructure and thermal properties of geopolymer concrete (GPC) were explored. MF/PCM24 which has a polymer shell containing polar functional groups, a higher latent heat and small sizes (≈21 μm) exhibited a higher porosity, better interfacial bonds between microcapsules and the concrete matrix, a higher thermal energy storage capacity, and a lower thermal conductivity than PS-DVB/RT27, which has a hydrophobic polymer shell and larger sizes (≈130 μm).

Although there is a small deviation between numerical data and experimental results, the numerical values obtained for GPC containing MPCM was in good agreement with the experimental data. Accordingly, the numerical model, based on the implicit finite differences method using the energy balance approach and the heat capacity method, can be utilized to theoretically predict the thermal performance of building materials containing microencapsulated phase change materials. A new equation was successfully utilized to describe the specific heat capacity of GPC containing MPCM as function of temperature, which improved the accuracy of the numerical model.

Acknowledgments

We gratefully acknowledge funding from the Research Council of Norway, project number 238198. The authors gratefully acknowledge Rino Nilsen, Trond Atle Drøbak at Østfold University College, Prof. Lars Wadsö at Lund University and Van Thi Ai Nguyen for their assistance with laboratory work.

Supplementary materials

Supplementary material associated with this article can be found, in the online version, at doi:10.1016/j.enbuild.2018.06.011.

References

[1] A.G.E.M. Hunger, I. Mandilaras, H.J.H. Brouwers, M. Founti, The behavior of self-compacting concrete containing micro-encapsulated phase change materials, Cem. Concr. Compos. 31 (2009) 731–743.
[2] J.L.M. María Fenollera, ItziarI. Goicoechea, JaimeJ. Lorenzo, MiguelM. Ángel Álvarez, The influence of phase change materials on the properties of self-compacting concrete, Materials 6 (2013) 3530–3546.
[3] V.D. Cao, S. Pilehvar, C. Salas-Bringas, A.M. Szczotok, J.F. Rodriguez, M. Carmona, N. Al-Manasir, A.-L. Kjøniksen, Microencapsulated phase change materials for enhancing the thermal performance of Portland cement concrete and geopolymer concrete for passive building applications, Energy Convers. Manag. 133 (2017) 56–66.
[4] A. Eddhahak-Ouni, S. Drissi, J. Colin, J. Neji, S. Care, Experimental and multi-scale analysis of the thermal properties of Portland cement concretes embedded with microencapsulated phase change materials (PCMs), Appl. Therm. Eng. 64 (1–2) (2014) 32–39.
[5] S. Pilehvar, V.D. Cao, A.M. Szczotok, L. Valentini, D. Salvioni, M. Magistri, R. Pamies, A.-L. Kjøniksen, Mechanical properties and microscale changes of geopolymer concrete and Portland cement concrete containing micro-encapsulated phase change materials, Cem. Concr. Res. 100 (2017).
[6] A.L. Pisello, A. D'Alessandro, C. Fabiani, A.P. Fiorelli, F. Ubertini, L. F.Cabeza, A.L. Materazzi, Franco Cotana, Multifunctional analysis of innovative PCM-filled concretes, Energy Procedia 111 (2017) 81–90.
[7] Z. Wei, G. Falzone, B. Wang, A. Thiele, G. Puerta-Falla, L. Pilon, N. Neithalath, G. Sant, The durability of cementitious composites containing microencapsulated phase change materials, Cem. Concr. Compos. 81 (2017) 66–76.
[8] V.V. Rao, R. Parameshwaran, V.V. Ram, PCM-mortar based construction materials for energy efficient buildings: a review on research trends, Energy Build. 158 (2018) 95–122.
[9] S. Mengjie, N. Fuxin, M. Ning, H. Yanxin, D. Shiming, Review on building energy performance improvement using phase change materials, Energy Build. 158 (2018) 776–793.
[10] E. Benhelal, G. Zahedi, E. Shamsaei, A. Bahadori, Global strategies and potentials to curb CO2 emissions in cement industry, J. Cleaner Prod. 51 (2013) 142–161.
[11] P. Duxson, A. Fernandez-Jimenez, J.L. Provis, G.C. Lukey, A. Palomo, J.S.J.v. Deventer, Geopolymer technology: the current state of the art, J. Mater. Sci. 42 (2007) 2917–2933.
[12] Z. Zuhua, Y. Xiao, Z. Huajun, C. Yue, Role of water in the synthesis of calcined kaolin-based geopolymer, Appl. Clay Sci. 43 (2009) 218–223.
[13] S.N. AL-Saadi, Z.J. Zhai, Modeling phase change materials embedded in building enclosure: a review, Renew. Sustain. Energy Rev. 21 (2013) 659–673.
[14] J. Darkwa, O. Su, Thermal simulation of composite high conductivity laminated microencapsulated phase change material (MEPCM) board, Appl. Energy 95 (2012) 246–252.
[15] B.L. Gowreesunker, S.A. Tassou, M. Kolokotroni, Improved simulation of phase change processes in applications where conduction is the dominant heat transfer mode, Energy Build. 47 (2012) 353–359.
[16] P. Lamberg, R. Lehtiniemi, A.-M. Henell, Numerical and experimental investigation of melting and freezing processes in phase change material storage, Int. J. Therm. Sci. 43 (2004) 277–287.
[17] A.M. Thiele, G. Sant, L. Pilon, Diurnal thermal analysis of microencapsulated PCM-concrete composite walls, Energy Convers. Manag. 93 (2015) 215–227.
[18] A.M. Borreguero, M.L. Sánchez, J.L. Valverde, M. Carmona, J.F. Rodríguez, Thermal testing and numerical simulation of gypsum wallboards incorporated with different PCMs content, Appl. Energy 88 (2011) 930–937.
[19] B.M. Diaconu, M. Cruceru, Novel concept of composite phase change material wall system for year-round thermal energy savings, Energy Build. 42 (2010) 1759–1772.
[20] H. Cui, W. Liao, X. Mi, T.Y. Lo, D. Chen, Study on functional and mechanical properties of cement mortar withgraphite-modified microencapsulated phase-change materials, Energy Build. 105 (2015) 273–284.
[21] A. Joulin, L. Zalewski, S. Lassue, H. Naji, Experimental investigation of thermal characteristics of a mortar with or without a micro-encapsulated phase change material, Appl. Therm. Eng. 66 (2014) 171–180.
[22] M. Lachheba, M. Karkri, S.B. Nasrallah, Development and thermal characterization of an innovativegypsum-based composite incorporating phase change material asbuilding energy storage system, Energy Build. 107 (2015) 93–102.
[23] A.V. Sá, M. Azenha, H. de Sousa, A. Samagaio, Thermal enhancement of plastering mortars with phase change materials: experimental and numerical approach, Energy Build. 49 (2012) 16–27.
[24] M. Kheradmand, M. Azenha, J.L.B. de Aguiar, J. Castro-Gomes, Experimental and numerical studies of hybrid PCM embedded in plastering mortar for enhanced thermal behaviour of buildings, Energy 94 (2016) 250–261.
[25] A.M. Szczotok, M. Carmona, A.-L. Kjøniksen, J.F. Rodriguez, Equilibrium adsorption of polyvinylpyrrolidone and its role on thermoregulating microcapsules synthesis process, Colloid Polym. Sci. 40 (2017) 4061–4071.
[26] http://www.microteklabs.com/data-sheets.html, Data sheet of MPCM24D, in.
[27] S. Pilehvar, V.D. Cao, A.M. Szczotok, M. Carmona, R. Pamies, A.-L. Kjøniksen,
[28] Standard BS EN 12390-7. Testing hardened concrete, in: Part 7: Density of hardened concrete, 2009.
[29] M.Y.J. Liu, U.J. Alengaram, M.Z. Jumaat, K.H. Mo, Evaluation of thermal conductivity, mechanical and transportproperties of lightweight aggregate foamed geopolymer concrete, Energy Build. 72 (2014) 238–245.
[30] M. Safiuddin, N. Hearn, Comparison of ASTM saturation techniques for measuring the permeable porosity of concrete, Cem. Concr. Res. 35 (2005) 1008–1013.
[31] P. Tittelein, S. Gibout, E. Franquet, K. Johannes, L. Zalewski, F. Kuznik, J.-P. Dumas, S. Lassue, J.-P. Bédécarrats, D. David, Simulation of the thermal and energy behaviour of a composite material containing encapsulated-PCM: influence of the thermodynamical modelling, Appl. Energy 140 (2015) 269–274.
[32] E. Lev, I. Kutasov, A. Pilchin, Applied Geothermics, Springer-Verlag Berlin Heidelberg, 2014.
[33] V.D. Cao, S. Pilehvar, C. Salas-Bringas, A.M. Szczotok, T.Q. Bui, M. Carmona, J.F. Rodriguez, A.-L. Kjøniksen, Thermal performance and numerical simulation of geopolymer concrete containing different types of thermoregulating materials for passive building applications, Energy and Buildings.
[34] Y.A. Cengel, Heat Transfer: A Practical Approach, 2nd ed., Mcgraw-Hill, 2002.
[35] L.A.A. Pasupathy, R. Velraj, R.V. Seeniraj, Experimental investigation and numerical simulation analysis on the thermal performance of a building roof incorporating phase change material (PCM) for thermal management, Appl. Therm. Eng. 28 (2008) 556–565.
[36] ASHRAE, Handbook of Fundamentals, American Society of Heating, Refrigerating and Air-Conditioning Engineers, Inc., Atlanta, 2013.
[37] E.M. Alawadhi, Thermal analysis of a building brick containing phase change material, Energy Build. 40 (3) (2008) 351–357.
[38] S.A. Al-Sanea, Thermal performance of building roof elements, Build. Environ. 37 (2002) 665–675.
[39] D. Fedroff, S. Ahmad, B. Savas, Mechanical properties of concrete with ground waste tire rubber, Transp. Res. Board 1532 (1996) 66–72.
[40] Z.K. Khatib, F.M. Bayomy, Rubberized portland cement concrete, J. Mater. Civil Eng. 11 (1999) 206–213.
[41] J. Zhang, H. Yan, S.L. Chen, X.M. Wang, Z.D. Gu, The preparation and properties of the low melting point microencapsulated paraffin insulation mortar, Appl. Mech. Mater. 71-78 (2011) 4835–4838.
[42] V.D. Cao, S. Pilehvar, C. Salas-Bringas, A.M. Szczotok, L. Valentini, M. Carmona, J.F. Rodriguez, A.-L. Kjøniksen, Influence of microcapsule size and shell polarity on thermal and mechanical properties of thermoregulating geopolymer concrete for passive building applications, Energy Convers. Manag. 164 (2018) 198–209.
[43] R. Shadnia, L. Zhang, P. Li, Experimental study of geopolymer mortar with incorporated PCM, Constr. Build. Mater. 84 (2015) 95–102.

Paper VII

Thermal analysis of Geopolymer concrete containing microencapsulated phase change materials for passive building applications.

Vinh Duy Cao, Shima Pilehvar, Carlos Salas-Bringas, Anna M. Szczotok, Tri Quang Bui, Manuel Carmona, Juan F. Rodriguez, Anna-Lena Kjøniksen.

Submitted to *Solar Energy* (Under review)

Thermal analysis of geopolymer concrete walls containing microencapsulated phase change materials for building applications

Vinh Duy Cao[1, 2], Shima Pilehvar[1,3], Carlos Salas-Bringas[2], Anna M. Szczotok[1, 4], Tri Quang Bui[1], Manuel Carmona[4], Juan F. Rodriguez[4], and Anna-Lena Kjøniksen[1*]

[1]Faculty of Engineering, Østfold University College, N-1757 Halden, Norway

[2]Faculty of Science and Technology, Norwegian University of Life Sciences, N-1432 Ås, Norway

[3]Department of Material Engineering and Manufacturing, Technical University of Cartagena, Cartagena, Murcia, Spain

[4]Department of Chemical Engineering, University of Castilla – La Mancha, 13004 Ciudad Real, Spain

[*]**Corresponding author:** anna.l.kjoniksen@hiof.no

Abstract

The potential of utilizing geopolymer concrete (GPC) walls containing microencapsulated phase change material (MPCM) in buildings at different environmental conditions has been investigated. The effect of climate conditions (temperature, solar radiation) and MPCM design (shell thickness, concentration) on the energy efficiency of buildings was systematically analyzed based on numerical calculations utilizing the finite differences method with an energy balance approach. The energy efficiency of buildings was found to increase at higher levels of MPCM addition and for thicker concrete walls. When the outdoor temperature is higher than the indoor temperature, increasing the maximum solar radiation causes a higher power consumption, a lower power reduction, and accordingly a reduced energy efficiency of the buildings. Utilizing a PCM with a melting temperature close to the average outdoor and indoor temperatures has a positive effect on enhancing the energy efficiency of buildings. Numerical calculations were used to evaluate the efficiency of using GPC containing two different types of MPCM (PS-DVB/RT27 with a paraffin Rubitherm®RT27 core and a shell of polystyrene cross-linked with divinylbenzene and MF/PCM24 with a paraffin mixture core and a melamine–formaldehyde polymer shell) at the environmental conditions of Oslo and Madrid throughout one year. It was found that a significant reduction of the annual power consumption

for heating/cooling can be achieved in both Oslo and Madrid. It was also found that the wall orientation and the season have significant effects on the power consumption and power reductions. The GPC containing MPCM was found to exhibit better performance in Madrid than in Oslo. The developed model can be used as a quantitative tool to design MPCM-concrete walls in different climates.

Keywords: Microencapsulated phase change materials, Geopolymer concrete, Energy efficiency, Solar radiation.

1. Introduction

Approximately 40 % of the total energy consumption is related to buildings, and a significant amount of this energy is due to heating and cooling (EU Directive 2002/91/EC; EU Directive 2010/31/UE). Accordingly, reducing the energy consumption of buildings is important for achieving the energy and climate targets of the world. Improved construction techniques and advanced material technology can significantly reduce the energy consumption needed to keep a comfortable indoor temperature.

Integration of microencapsulated phase change materials (MPCM) into building materials has been investigated to create materials with a high thermal energy storage capacity (Borreguero et al., 2014; Cao et al., 2017; Cui et al., 2018; Eddhahak-Ouni et al., 2014; M. Hunger, 2009; Pilehvar et al., 2017; Pisello et al., 2017; Shadnia et al., 2015; Wei et al., 2017). Phase change materials are materials that can store and release high amounts of thermal energy, utilizing the phase transition of the materials. The main parameters that influence the storage and release of thermal energy are the heat storage capacity, the thermal conductivity, the melting temperature of the PCM, and the outdoor environment. Incorporating MPCM into a building material is expected to improve the thermal energy storage capacity, resulting in higher energy efficiency and reduced power consumption for heating and cooling. Another advantage of utilizing PCM in building materials is the possibility of moving the maximum thermal load of the buildings to periods where the electricity demand is low (e.g., at night), thereby reducing the peak electricity demand.

Concrete-based materials are among the most used materials for buildings. This is due to their high mechanical strength and the possibility of changing the properties by varying the concrete recipe. Concrete has a moderate thermal energy storage capacity, which can be improved by integration of MPCM (Cao et al., 2017; Cui et al., 2018; M. Hunger, 2009; Pilehvar et al., 2017; Wei et al., 2017). The enhancement of the thermal energy storage capacity of concrete will improve the energy efficiency of buildings.

Experimental studies of the thermal response of concrete walls containing MPCM show very promising results regarding saving building energy consumption (Cao et al., 2017; Cao et al., 2018b; M. Hunger, 2009). However, experimental studies are usually costly and time consuming, especially when it is desirable to compare a range of potential designs to evaluate their respective performance. Alternatively, simulation studies are able to determine the efficiency of a design without physically building the systems. This significantly reduces the investigation time and the overall cost of building the system. Due to the benefit of numerical models, some numerical methods have been developed to simulate the thermal impact of building materials containing PCM/MPCM (AL-Saadi and Zhai, 2013; Biswas and Abhari, 2014; Borreguero et al., 2011; Darkwa and Su, 2012; Diaconu and Cruceru, 2010; Gowreesunker et al., 2012; Lamberg et al., 2004; Marin et al., 2016; Thiele et al., 2015; Xie et al., 2018; Zwanzig et al., 2013). The heat capacity method is one of the most commonly used numerical methods, and show good agreement with experimental data (Borreguero et al., 2011; Lamberg et al., 2004). Nevertheless, while the building materials containing PCM/MPCM exhibit an asymmetric melting area (Cao et al., 2017; Cui et al., 2015; Joulin et al., 2014; Lachheba et al., 2015), most studies define $C_p(T)$ as a piecewise function of temperature (Lamberg et al., 2004; Thiele et al., 2015) or a Gaussian function of temperature (Diaconu and Cruceru, 2010), which assume that the melting area is symmetric. A mismatch between the model and realistic conditions induces inaccuracies in the models.

Few studies have numerically calculated the energy consumption of building over an entire year in different cities to explore the role of various seasons on the thermal impact of building materials containing PCM/MPCM (Biswas and Abhari, 2014; Diaconu and Cruceru, 2010; Xie et al., 2018; Zwanzig et al., 2013).There are the conflictive observations regarding seasonal variations of the energy efficiency of buildings utilizing PCM/MPCM. Some studies found that the energy reduction in the summer was higher than in the winter (Biswas and Abhari, 2014; Zwanzig et al., 2013) while other studies came to the opposite conclusion (Diaconu and Cruceru, 2010). The discrepancies could be due to different climate conditions with dissimilarities in solar radiation and outdoor temperatures. However, further investigations are required to present clear evidence on how the seasons and climates can affect the thermal impact of concrete containing MPCM.

The objective of the present work is to numerically investigate how the variation of different climate conditions influence the thermal impact of buildings utilizing concrete walls containing microencapsulated phase change materials. A geopolymer concrete (GPC) was selected for this work. GPC is environmentally friendly with low CO_2 emission and

competitive mechanical and thermal properties compared to the traditional Portland cement concrete. A mathematical model was developed to simulate the effect of MPCM addition on the thermal performance of buildings. In addition, the heat capacity as function of temperature for concrete containing microencapsulated phase change materials was utilized in the numerical model. The effect on the energy efficiency of buildings of MPCM type and concentration, the thickness of the concrete walls, solar radiation, and outdoor temperature was investigated. The possibility of utilizing concrete containing MPCM walls at the climate conditions of Oslo and Madrid over a span of one year was evaluated with special attention on the effect of wall orientation and seasons. The main purpose is to explore the combined effect of different climates conditions such as solar radiation and outdoor temperature on the energy efficiency of MPCM addition.

2. Experimental

2.1. Materials

Geopolymer concrete containing microencapsulated phase change materials (MPCM-GPC) was fabricated by mixing class F fly ash (FA), ground granulated blast furnace slag (GGBFS), sand, aggregates, retarder, an alkaline activator solution and MPCM. Table 2 summarizes the composition of geopolymer concrete containing MPCM (MPCM-GPC) (Pilehvar et al., 2018; Pilehvar et al., 2017). MPCM was incorporated into GPC at 0, 2.6 and 5.2 wt.%. The concentration of MPCM was limited to 5.2 wt.% since higher concentrations of MPCM resulted in too low workability of the geopolymer concrete.

Two different kinds of microcapsules were utilized. PS-DVB/RT27 microcapsules consists of a paraffin Rubitherm®RT27 core coated with a PS-DVB (polystyrene cross-linked with divinylbenzene) shell. The commercial Microtek microcapsules, MPCM24D (MF/PCM24) have a paraffin core and a melamine-formaldehyde polymer shell (MF). The MPCM properties are summarized in Table 1.

The concrete samples containing 0 wt.%, 2.6 wt.% and 5.2 wt.% of MPCM were named GPC0, GPC-2.6-X and GPC-5.2-X, respectively. X is the name of integrated MPCM (PS-DVB/RT27 or MF/PCM24).

Sand (density of 2.7 g/cm^3) and aggregates (density of 2.6 g/cm^3) were supplied by Gunnar Holth and Skolt Pukkverk AS, Norway. In addition, the class F fly ash (density = 2.26±0.02

g/cm^3) and ground granulated blast furnace slag (GGBFS) (density = 2.85±0.02 g/cm^3) was purchased from Norcem, Germany and Cemex, Germany, respectively.

The alkaline activator solution consists of a mixture of a sodium silicate solution (density = 1.93 g/cm^3, 35 wt.% solid) and a 14M NaOH (560 g/L) solution. The ratio between the sodium silicate solution and NaOH(aq) is 1.5 (Pilehvar et al., 2018). For the current recipe, $m_{Na2SiO3(aq)}$ = 120 g, and $m_{NaOH(aq)}$ = 80 g. In order to improve the workability as well as the mixing ability of MPCM into GPC, a naphthalene based retarder (density of 1.2 g/cm^3; FLUBE OS 39, Bozzetto Group, Italy) was selected (Jang et al., 2014; Nematollahi and Sanjayan, 2014a, b; Pilehvar et al., 2018).

Table 1: The properties of the microencapsulated phase change materials

MPCM name	Size (μm)		T_{melt}	ΔH	Ref
	Single	Aggregates (mean size)	(ºC)	(J/g)	
PS-DVB/RT27	10-100	130	24.9	100	(Szczotok et al., 2017)
MF/PCM24	10-30	21	21.9	154	(Cao et al., 2018b)

Table 2: Composition of Geopolymer concrete

MPCM (wt.%)	Alkaline solution (g)	Water (g)	FA* (g)	GGBFS** (g)	Sand (g)	Aggregate (g)	Retarder (g)	MPCM (g)
0	200	50	300	200	871.2	851.7	5	0
2.6					696.9			63
5.2					522.7			117

(*) FA: Flyash (**) GGBFS: Ground granulated blast-furnace slag

The properties of GPC containing various concentrations of MPCM were determined previously (Cao et al., 2018a) and are summarized in Table 3 and Table 4.

The specific heat capacity as a function of temperature of GPC containing microcapsules can be described by (Cao et al., 2018a):

$$Cp(T) = \begin{cases} Cp_o + h * \dfrac{{w_l}^{2m_l}}{\left({w_l}^2 + \left(2^{\frac{1}{m_l}} - 1 \right) * (2T - 2T_m)^2 \right)^{m_l}} & for\ T \le T_m \\ Cp_o + h * \dfrac{{w_r}^{2m_r}}{\left({w_r}^2 + \left(2^{\frac{1}{m_r}} - 1 \right) * (2T - 2T_m)^2 \right)^{m_r}} & for\ T > T_m \end{cases} \quad \text{Eq. 1}$$

Where T_m is the melting temperature of phase change materials. w_l and w_r are the phase change temperature range on the left side and right side of the melting peak, respectively. m_l and m_r are shape parameters for the left and right side of the peak, respectively. Cp_o and h are respectively the specific heat capacity outside the melting range and the height of the melting peak. For more information about Cp(T) fitting process, see (Cao et al., 2018a).

Table 3. Summarization of the thermal properties of GPC containing PS-DVB/RT27 (Cao et al., 2018a)

MPCM (%)	k (W/m ºC)	C_p (J/Kg ºC)							ρ (Kg/m^3)
		Cp_o	h	w_l	w_r	m_l	m_r	T_m	
0	1.35	891	-	-	-	-	-	-	2199
2.6	1.13	960	199	9.0	3.3	159	275	23.3	2057
5.2	0.87	1062	568	7.8	2.3	1.7	3.4	25.3	1960

Table 4. Summarization of the thermal properties of GPC containing MF/PCM24 (Cao et al., 2018a)

MPCM (%)	k (W/m ºC)	C_p (J/Kg ºC)							ρ (Kg/m^3)
		Cp_o	h	w_l	w_r	m_l	m_r	T_m	
0	1.35	891	-	-	-	-	-	-	2199
2.6	1.02	982	404	5.6	1.6	1.3	2.8	23	2023
5.2	0.74	1125	851	6.3	2.9	1.4	5.3	23.7	1875

2.2. Numerical method

The effect of MPCM addition on the thermal performance of concrete walls was numerically evaluated. The indoor surface temperature reduction, the time delay of the maximum thermal load, the power consumption, and the power reduction for the heating and cooling system were calculated based on a simplified, uninsulated concrete wall and a constant indoor temperature.

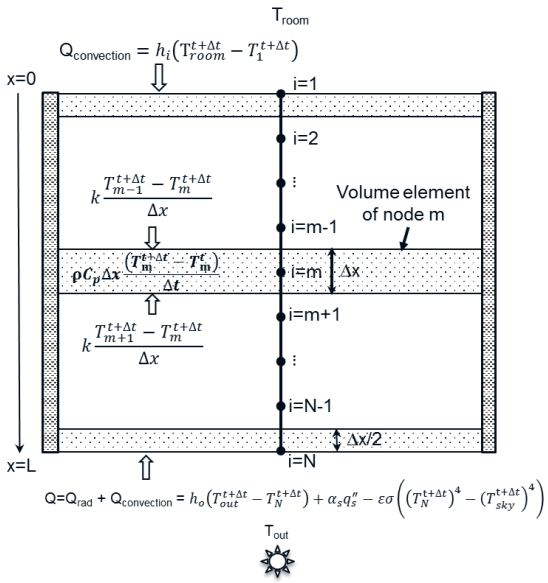

Figure 1. Schematic representation of the MPCM-concrete wall, and finite differences method using the energy balance approach with boundary conditions. The energy balance states that heat transferred into the volume element (Q) from all of its surfaces is equal to the change in the energy content of the volume element ($\Delta E_{element}$) during Δt (Cengel, 2002).

Figure 1 shows the model used to investigate the thermal behavior of the concrete walls. The following assumptions of the material properties and environmental conditions were made to simplify the calculation process:

- The thickness of the concrete wall is significantly smaller than the other dimensions. Therefore, the heat transfer process across the concrete walls is assumed as a one-dimensional problem.
- The MPCM concrete sample is homogeneous and isotropic.
- There is no heat generation in the concrete samples.
- The convection effect in the melted PCM is omitted.

- The convection coefficients for the indoor and outdoor environment are assumed to be constant.
- The heat from people and devices are neglected.

Based on these assumptions, the equation for one-dimensional heat transfer across the MPCM-concrete wall is (Cengel, 2002; Lamberg et al., 2004; Thiele et al., 2015):

$$k\frac{\partial^2 T}{\partial x^2} = \rho C_p(T)\frac{\partial T}{\partial t} \quad \text{Eq. 2}$$

where k, ρ, x are the thermal conductivity, density, and thickness of the wall, respectively. $C_p(T)$ is the specific heat capacity as a function of temperature of GPC containing microcapsules and can be described by Eq.1.

The model is solved by the implicit finite difference method using the energy balance approach (Cengel, 2002). This method is based on discretizing the medium into a number of nodes where the distance (thickness) between two adjacent nodes is Δx. The volume elements over the nodes, where energy balance is applied, are formed to determine the temperatures at all nodes of the sample (Figure 1).

In addition, boundary conditions were applied to solve Eq. 2:

- Interior node i=1 (x=0, indoor wall surface) (boundary condition (Cengel, 2002)): For the room, a constant indoor temperature T_{room} is maintained at 23 ºC by a HVAC (heating, ventilation and air conditioning) system. Only the convective heat transfer is imposed at the interior wall surface while the radiative heat transfer due to the different temperature between the indoor wall surface and the room temperature is neglected.

$$k\frac{\partial T}{\partial x}(x,t) + h_i\big(T(room,t) - \mathrm{T(x,t)}\big) = \rho C_p(T)\frac{\Delta x}{2}\frac{\partial T}{\partial t}(x,t) \quad \text{Eq. 3}$$

- Exterior node i=N (x=L, outdoor wall surface) (boundary condition (A. Pasupathy, 2008; Cengel, 2002; Diaconu and Cruceru, 2010; Thiele et al., 2015)): the exterior wall surface is subjected to a time dependent outdoor temperature (T_{out}) and a time dependent solar radiation heat flux (q''_s). The combined convective and radiative heat transfer is imposed at the exterior wall surface.

$$k\frac{\partial T}{\partial x}(x,t) + h_o\big(T(out,t) - \mathrm{T(x,t)}\big) + \alpha_s q''_s - \varepsilon\sigma\big((T^{\mathrm{t}}_N)^4 - (T^{\mathrm{t}}_{sky})^4\big) = \rho C_p(T)\frac{\Delta x}{2}\frac{\partial T}{\partial t}(x,t) \quad \text{Eq. 4}$$

Different values of Δt and Δx were tested to determine values for the simulation where the simulated data is stable and there is no difference when the values of Δt and Δx are changed. Based on this test, Δt=60 s and Δx=0.005 m were used.

The initial temperature of the system was set as 23 ºC.

T_{out}, T_{sky} and T_N represent the outdoor temperature, the average sky temperature and the outdoor wall surface temperature (x=L), σ is the Stefan–Boltzmann constant, α_s and ε are the total absorptivity and emissivity of the outdoor wall surface, respectively (Kreith et al., 2012; Thiele et al., 2015). The indoor heat transfer coefficient h_i was set to 8 W/m^2 K while the outdoor heat transfer coefficient h_o was set to 20 W/m^2 K. These values are similar to the values recommended by ASHAE (ASHRAE, 2013), and has been utilized for similar calculations previously (Al-Sanea, 2002; Alawadhi, 2008; Thiele et al., 2015). The total hemispherical solar absorptivity and surface emissivity of the outdoor wall surface were 0.65 and 0.87, respectively (Kreith et al., 2012). An average sky temperature $T_{sky} = (T_{out}-12)$ ºC was used (Al-Sanea, 2002; Garg, 1982).

The above equations for all nodes was programmed and solved in MATLAB (Mathworks Inc., Natick, MA, USA). The indoor surface temperature ($T_{x=0}$), and the heat flux on the indoor surface (φ_{indoor}) was calculated:

$$\varphi_{indoor}(\mathrm{t}) = h_i(\mathrm{T(room,t)} - \mathrm{T(x=0,t)}) \quad \text{Eq. 5}$$

- **Energy efficiency of MPCM addition under various simulated environmental conditions**

In the simulations, the outer wall surface of the concrete wall was exposed to a sinusoidal outdoor temperature variation (Eq.9) and solar radiation (Eq.8) while the indoor room temperature was kept constant at 23 ºC. The effect of MPCM concentration, wall thickness, the maximum solar radiation and the average outdoor temperature on the power consumption, power reduction and delay time of the maximum thermal load were numerically investigated. In order to achieve a steady state, simulations were run for 4 cycles (days) of varying outdoor temperatures and solar radiation, the temperature and heat flux for the third day were determined.

The power needed for a heating/cooling system to keep the indoor temperature stable was determined as:

$$P = \frac{\int_0^{24h} |\varphi_{indoor}| dt}{3600 \cdot 10^3} \quad \text{Eq. 6}$$

The power reduction Pr is:

$$Pr = \frac{P_{Con} - P_{MPCM-Con}}{P_{Con}} \cdot 100\% \quad \text{Eq. 7}$$

where P_{Con} and $P_{MPCM-Con}$ are the power consumption of a heating and cooling system working within one day, for concrete without MPCM and with MPCM, respectively.

- **MPCM concentration**

The MPCM concentration was varied to evaluate effect on the thermal performance of concrete. Accordingly, three MPCM concentrations of 0, 2.6 and 5.2 wt.% MPCM per solid of content of concrete were selected. The concentration of MPCM was limited to 5.2 wt.% since higher concentrations of MPCM resulted in too low workability of the concrete.

- **Concrete thickness**

The thickness of the concrete wall affects the heat transfer process, and is therefore important for the thermal performance of buildings. The thickness of the concrete walls was varied from 5 to 15 cm to investigate the effect on the thermal performance.

- **Solar radiation**

The time dependent solar radiation heat flux q''_s which mimics maximum solar radiation conditions during summer time (July) of the city of Madrid, Spain (Pérez-Burgos et al., 2014) was utilized:

$$q''_s = \begin{cases} 0 & for\ 21{:}00 \le t \le 5{:}00 \\ q''_{s,max} \sin\left(\frac{\pi}{57600} t - \frac{5\pi}{16}\right) & for\ 5{:}00 < t < 21{:}00 \end{cases} \quad \text{Eq. 8}$$

where $q''_{s,max}$ is the maximum daily solar radiation heat flux. In this article, the maximum daily solar radiation heat flux was varied from 0-1000 W/m^2 in steps of 250 W/m^2 to cover European conditions during summer time. The maximum daily solar heat flux was assumed to occur at 13:00 (Pérez-Burgos et al., 2014).

- **Outdoor temperature**

To mimic outdoor conditions, the ambient outdoor temperature T_{out} was imposed as a sinusoidal function of time as:

$$T_{out}(t) = \frac{T_{max}+T_{min}}{2} + \frac{T_{max}-T_{min}}{2} \sin\left(\frac{\pi}{43200} t - \frac{2\pi}{3}\right) \quad \text{Eq. 9}$$

where T_{max} and T_{min} are the maximum and minimum outdoor temperatures during a day, respectively. The maximum outdoor temperature T_{max} were set at 14:00. The efficiency of MPCM addition on the thermal performance of concrete buildings is strongly dependent on the interplay between the phase change temperature and the outdoor temperature. Therefore, the outdoor temperature conditions were varied to evaluate the optimal temperature conditions for the MPCM utilized in this study. An outdoor temperature variation of (T_{max}-T_{min})/2 = 5, 7.5 and 10 ºC were utilized, and the average outdoor temperatures (T_{max}+T_{min})/2 was varied from 0 ºC to 40 ºC.

- **Evaluation of building envelopes using single wall geopolymer concrete containing MPCM at the conditions of two European cities (Oslo and Madrid).**

The possibility of utilizing the geopolymer concrete containing MPCM as a simple single wall for a single family home in the climate zones of Oslo and Madrid were evaluated. The outdoor temperature and solar radiation as function of time for a typical year in Oslo and Madrid for Eq.1 were obtained from weather data (Climate Consultant software (energy-design-tools.aud.ucla.edu.)). The effect of wall orientation (south, east, north and west facing walls) and the season during a typical year on power consumption and power reduction were evaluated. GPC without MPCM and GPC containing 5.2 wt.% of PS-DVB/RT27 and MF/PCM24 were selected for the evaluation.

The power consumption of a heating and cooling system during each season for each wall orientation is:

$$P_{n,j} = \frac{\int_{t1}^{t2} |\varphi_{indoor}| dt}{3600 \cdot 10^3} \qquad \text{Eq. 10}$$

where $P_{n,j}$ is the power consumption of a wall facing the *n* direction (south, east, north and west) during season j (spring, summer, autumn and winter). t1 and t2 are the initial and final time of each season. For this work, the spring, summer, autumn and winter were set as 21st March-20th June, 21st June-23rd September, 24th September-21st December and 22nd December to 20th March, respectively.

Furthermore, the average power consumption through all four wall orientations of a single house was also determined:

$$P_{ave,j} = \sum \frac{P_{n,j}}{4} \qquad \text{Eq. 11}$$

3. Results and discussions

Effect of MPCM concentration

In order to explore how MPCM-concrete structures work when they are exposed to different operating conditions, numerical simulations were carried out. In the simulations, the outer wall surface of the concrete wall was exposed to a sinusoidal outdoor temperature variation (Eq.9) with T_{min} = 15 ºC and T_{max} = 35 ºC while the indoor room temperature was kept constant at 23 ºC. The thickness of the concrete wall was set to 10 cm. The simulations also include solar radiation (Eq.8), with a maximum of 750 W/m^2, which mimics the maximum solar radiation during summer time (July) of the city of Madrid, Spain (Pérez-Burgos et al., 2014).

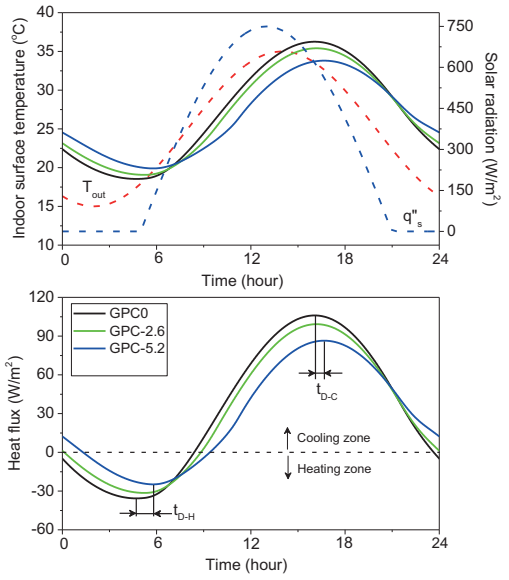

Figure 2. (a) The simulated indoor surface temperature and (b) the simulated indoor surface heat flux through a 10 cm thick GPC containing PS-DVB/RT27 wall after exposing it to a sinusoidal outdoor temperature fluctuation (T_{out}) and maximum solar radiation (q''_s) of 750 W/m^2.

The effect of MPCM concentration on the simulated indoor surface temperature (Figure 2a) and inner wall heat flux (Figure 2b) as function of time within a 24 h period are shown in Figure 2. The addition of MPCM causes a slight transition point around the melting point of PCM for both the indoor surface temperature and the heat flux. This is especially evident at the highest MPCM concentration. This transition is the effect of the PCM latent heat, and is in good agreement with previous findings (Borreguero et al., 2014; Cui et al., 2015; M. Hunger, 2009). The inclusion of MPCM in the concrete structure reduces the effect of outdoor temperature variations on the indoor surface temperature. This is due to the higher heat storage capacity and lower thermal conductivity of MPCM-concrete. The variation of the indoor surface temperature of the MPCM-concrete samples is smaller than that of concrete without MPCM, and decreases as the concentration of MPCM is increased (Figure 2a). The maximum and minimum indoor surface temperature as a function of MPCM concentration are summarized in Figure 3a.

In order to keep a constant indoor temperature, the total heat transfer at the indoor surface (heat gain/loss) should be compensated by a heating/cooling system. The heat gain and loss can be determined by integrating the heat flux on the indoor surface of the concrete wall (Figure 2b). The total energy consumption for the heating/cooling system is the sum of the heating power

consumption when the indoor surface temperature $T_{x=0} < T_{room}$ (heating zone), and the cooling power consumption when the indoor surface temperature $T_{x=0} > T_{room}$ (cooling zone). The total calculated power consumption (Eq.6) for the heating/cooling system to maintain an indoor temperature of 23 ºC and the power reduction (Eq.7) as a function of MPCM concentration are shown in Figure 3b.

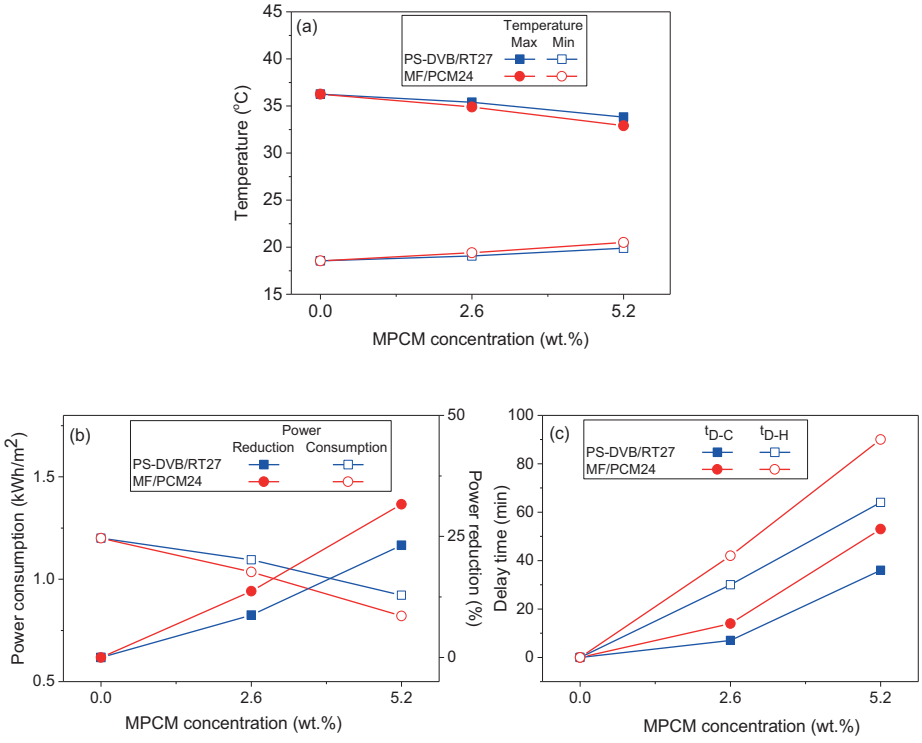

Figure 3. (a) The maximum and minimum indoor surface temperature; (b) the power consumption and the power reduction; (c) the delay time of the maximum (t_{D-H}) and minimum (t_{D-C}) power consumption of the MPCM-concrete wall compared to GPC without MPCM as a function of MPCM concentration.

The effect of MPCM addition on the regulation of the indoor environment can be observed by examining the indoor surface temperature. According to Figure 3a, the maximum indoor surface temperature of MPCM-concrete decreases with approximately 3 ºC while the minimum indoor surface increases with almost 1.5 ºC after adding 5.2 wt.% PS-DVB/RT27. This indicates that an increase of MPCM concentration results in a smaller indoor temperature variation, thereby maintaining the temperature closer to the human comfort zone. Accordingly, a lower power

consumption is needed for the heating and cooling system to maintain the indoor environment at the desired temperature (Figure 3b).

Figure 3b shows that the power consumption to maintain the indoor temperature at 23 ºC decreases substantially with increasing MPCM concentration. The addition of 5.2 wt.% PS-DVB/RT27 can reduce the power consumption with approximately 25 %. This demonstrates that the utilization of MPCM will have a significant effect on the energy efficiency of buildings. The effect is not only due to the higher heat storage capacity but also due to the better insulation properties of MPCM-concrete, which is in agreement with previous experiments (Cao et al., 2017; M. Hunger, 2009) and numerical calculations (Thiele et al., 2015).

The addition of MPCM to concrete also delays the peak of the cooling (t_{D-C}) and heating loads (t_{D-H}) as shown in Figure 2b. This effect comes from the ability of PCM to store and release a high amount of energy during the phase change in combination with the lower thermal conductivity after the addition of MPCM into concrete. As can be seen from Figure 2b, there are two main peaks for the indoor surface heat flux: the heating peak from 03:00 to 06:00 and the cooling peak from 14:00 to18:00, depending on the amount of MPCM in the samples. They are correlated to the outdoor temperature peaks where the lowest temperature occurs at 02:00 and the highest temperature at 14:00. The effect of adding MPCM on the delay time of the power consumption peaks is shown in Figure 3c. The delay time increases with higher MPCM concentrations, reaching approximately 65 min for the heating peak (minimum indoor surface temperature) and 40 min for the cooling peak (maximum indoor surface temperature) after adding 5.2 wt.% of PS-DVB/RT27.

As can be seen in Figure 3, geopolymer concrete containing MF/PCM24 has lower power consumption, higher power reduction and longer delay time of the heating/cooling peak than GPC containing PS-DVB/RT27. This indicates that MF/PCM24 has a greater thermal impact on GPC compared to PS-DVB/RT27. This is probably caused by the higher heat storage capacity of MF/PCM24 compared to PS-DVB/RT27 (Table 1), and the lower thermal conductivity of GPC containing MF/PCM24 (Table 3 and Table 4)

Effect of solar radiation

In order to evaluate the effect of solar radiation on the energy efficiency of MPCM-concrete walls, corresponding simulations were also carried out at different solar radiation maximums (0 to 1000 W/m^2). The MPCM concentration and the thickness of concrete samples were kept at 5.2 wt.% and 10 cm, respectively. The outdoor temperature, which is based on summer time (July) in Madrid, is described by Eq.9 with T_{max}=35 ºC, and T_{min}=15 ºC. The indoor surface

temperature, the power consumption, power reduction and delay times are summarized in Figure 4.

As expected, increasing the maximum solar radiation leads to a higher power consumption to maintain an indoor temperature of 23 ºC (Figure 4b). As is evident from Figure 4b, the power reduction decreases from 29 to 22 % when the maximum solar radiation is raised from 0 to 1000 W/m^2. The heat transfer through the wall will increase with more solar radiation, while the MPCM can only absorb a certain amount of heat. During a hot summer, the capacity of the PCM will not be sufficient to compensate for the additional solar radiation. The delay time for the cooling peak decreases from 75 min for 0 W/m^2 to 33 min for 1000 W/m^2 while the heating peak remains approximately stable. This is in good agreement with the indoor surface temperature (Figure 4a) where the maximum indoor surface temperature increases while the minimum indoor surface temperature remains stable as the maximum solar radiation is raised. This is because the solar radiation is only affecting the samples during the daytime (cooling zone), as illustrated in Figure 2a.

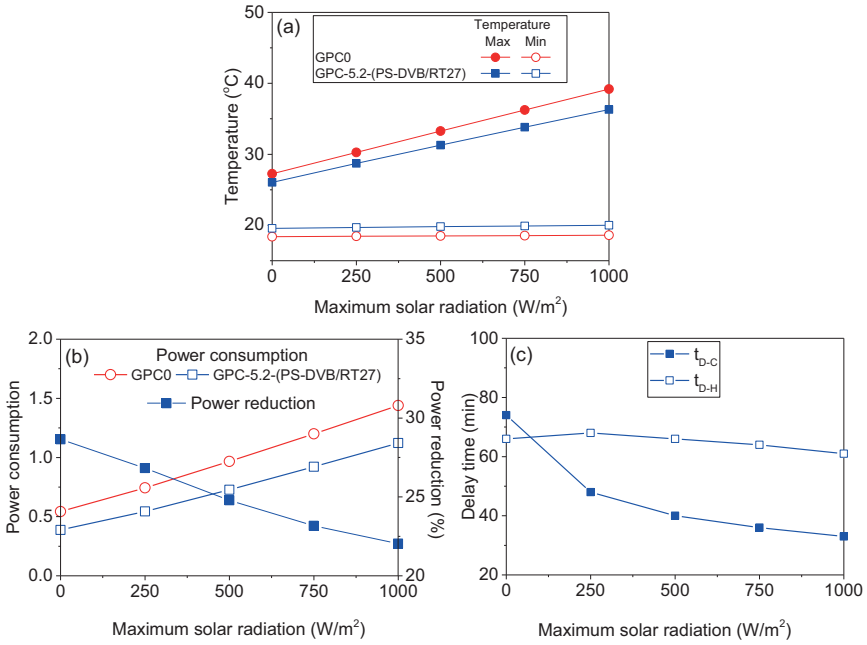

Figure 4. (a) The maximum and minimum indoor surface temperature; (b) The power consumption of GPC0 and GPC-5.2-(PS-DVB/RT27), and the power reduction of GPC-5.2-(PS-DVB/RT27) compared to GPC0; (c) the delay time of the maximum (t_{D-H}) and minimum

(t_{D-C}) power consumption of GPC-5.2-(PS-DVB/RT27) compared to GPC0 as a function of maximum solar radiation.

Effect of concrete wall thickness

For this work, the thickness of wall was varied from 5 to 15 cm in step of 2.5 cm. The outdoor temperature and the solar radiation were described by Eq. 9 and Eq. 8 with T_{max}=35 ºC, T_{min}=15 ºC and a maximal solar radiation of 750 W/m^2.

The temperature regulating capacity of the walls strongly depends on the combination of wall thickness and the content of MPCM. Figure 5a and Figure 5b shows the simulated indoor surface heat flux and indoor surface temperature during a 24 hour period for different thicknesses of the MPCM-concrete samples containing 5.2 wt.% PS-DVB/RT27. Figure 5a shows that the indoor surface heat flux decreases as the sample becomes thicker. The decline in indoor surface heat flux is caused by the rate of heat conduction through a sample, which is inversely proportional to the thickness of the sample (Eq.6). The reduced heat transfer through the concrete for the thicker samples combined with the effect of MPCM cause a smaller variation of the indoor surface heat temperature (Figure 5b) and lower power consumption to maintain the indoor temperature stable at 23 ºC (Figure 5c).

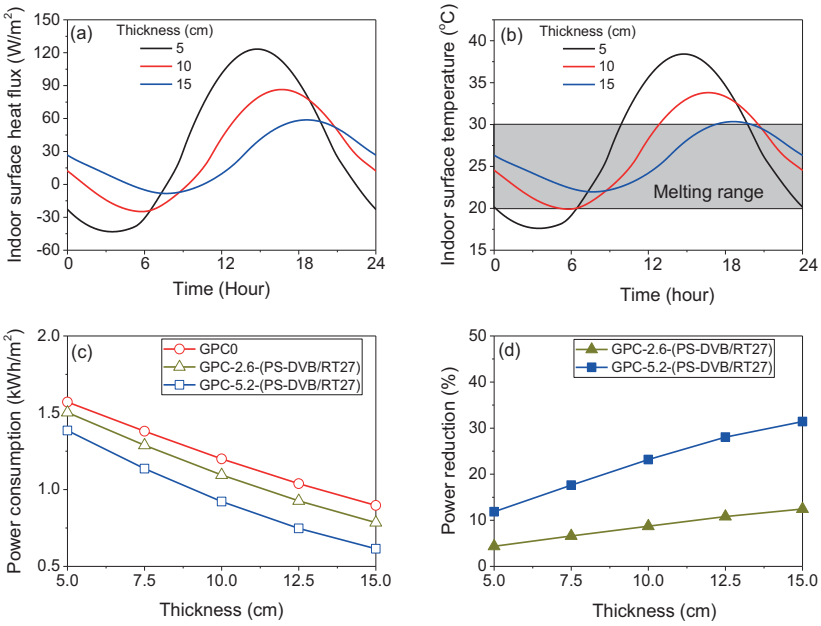

Figure 5. The effect of thickness on (a) indoor surface heat flux, (b) indoor surface temperature of GPC-5.2-(PS-DVB/RT27), (c) The power consumption and (d) the power reduction of GPC after adding various concentrations of MPCM as a function of concrete thickness.

The reduction of power consumption of concrete samples containing different amounts of MPCM compared to corresponding samples without MPCM (GPC0) was calculated as a function of concrete thickness and is illustrated in Figure 5c.The power reduction increases when the thickness of the sample increases and when the MPCM concentration increases. The cause of the increased efficiency of MPCM addition for the thicker walls can be divulged from Figure 5b, where it can be seen that the temperature variations of the 15 cm sample covers most of the PCM melting range. This provides good conditions for utilizing the MPCM effect. It is important to point out that although the energy efficiency increases with thicker concrete walls, the thicker walls have higher cost and occupy more housing space.

Effect of outdoor temperature

In order to find the optimum outdoor environment for utilizing the MPCM concrete as building materials, the relation between different outdoor temperature range variations and the energy efficiency was investigated. In these simulations, the MPCM concentration, concrete thickness and maximum solar radiation were set as 5.2 wt.%, 10 cm and 750 W/m^2, respectively. The

average outdoor temperature (T_{max}+T_{min})/2 was varied from 0 ºC to 40 ºC while the outdoor temperature amplitude (T_{max}-T_{min})/2 was set to 5, 7.5 and 10 ºC. The power consumption, power reduction and delay time as a function of the average outdoor temperature are presented in Figure 6.

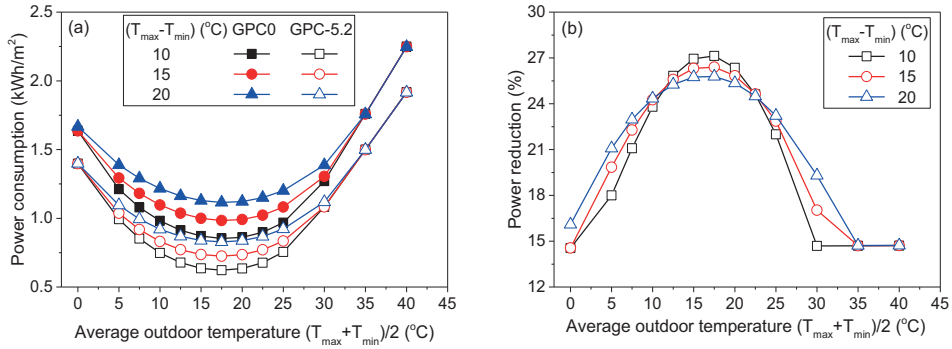

Figure 6. The effect of average outdoor temperature and the outdoor temperature amplitude on (a) power consumption, (b) power reduction. The thickness of PS-DVB/RT27-concrete wall was 10 cm, and the maximum solar radiation was set at 750 W/m^2.

The power consumption for both GPC0 and GPC-5.2-(PS-DVB/RT27) decreases when the average outdoor temperature is increased, reaching a minimum power consumption when the average outdoor temperature is 15-20 ºC, before it increases again at higher temperatures (Figure 6a). The minimum power consumption is naturally occurring when the average outdoor temperature is close to the desired indoor temperature. The power consumption is much lower when MPCM is added to the concrete, and when the outdoor temperature fluctuations throughout the day is low.

As can be seen from Figure 6b, the power reduction with the addition of MPCM was about 25-27 % at the optimum outdoor temperature average (15-20 ºC) for all outdoor temperature amplitudes. At higher or lower outdoor temperature averages, the effect of MPCM is diminished. This demonstrates that MPCM has less effect on the power reduction in extreme cold and hot weather, since the power consumption is strongly dependent on the melting range of MPCM. The efficiency of utilizing MPCM will be higher when the melting range of PCM is fully covered by the temperature variations of walls. Figure 7 shows the correlation between the indoor and outdoor surface temperature of the concrete and the melting range of the PCM. As can be seen from Figure 6b, too hot (40 ºC) or cold (0 ºC) outdoor temperature averages greatly reduce the efficiency of MPCM addition. At these conditions the temperature

fluctuations are mostly outside the melting range of the PCM (Figure 7). It is important to point out that although the effect of phase change is hindered, the reduction of the thermal conductivity of concrete after adding MPCM becomes the dominating effect at these conditions. Interestingly, the power reduction after adding 5.2 wt.% PS-DVB/RT27 can reach up to 15 % even in extreme hot or cold climate compared to GPC without MPCM.

Furthermore, the power consumption increases while the power reduction decreases as the amplitude of the outdoor temperature oscillations is raised (Figure 6b). As expected, a broader temperature range require more energy to keep the room temperature stable.

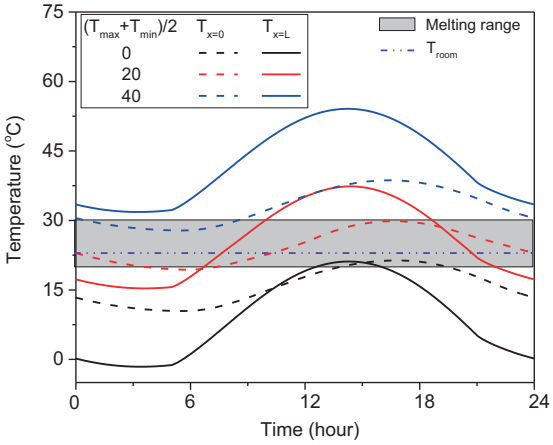

Figure 7. The correlation between melting temperature range and indoor ($T_{x=0}$) and outdoor surface temperature ($T_{x=L}$) of GPC-5.2-(PS-DVB/RT27) after exposure to average outdoor temperatures of 0, 20, and 40 ºC. The amplitude of the outdoor temperature was set to 10 ºC, the maximum solar radiation was 750 W/m^2 and the thickness of the concrete wall was 10 cm.

Evaluation of building envelopes using single wall geopolymer concrete containing MPCM at the climate conditions of Oslo and Madrid

Figure 8 shows the indoor surface heat flux as a function of time for a south-facing wall over one year at the climate conditions of Oslo and Madrid for GPC without MPCM and GPC containing 5.2 wt.% PS-DVB/RT27. The indoor surface heat flux throughout the year is decreased after adding MPCM, leading to a reduced power consumption for the heating and cooling system to maintain the indoor temperature. This is in good agreement with Figure 3.

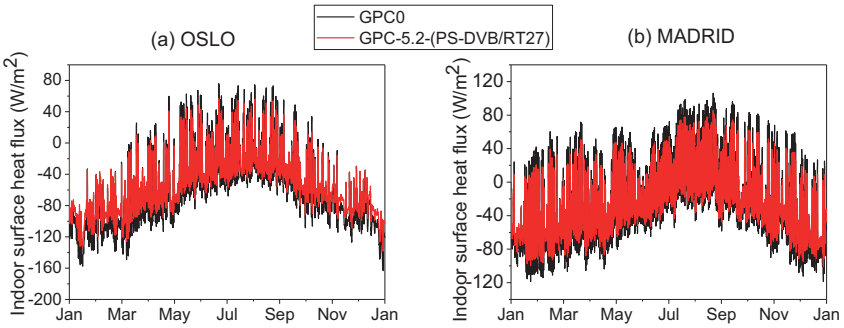

Figure 8. Indoor surface heat flux as a function of time for a south-facing wall over one year at the climate conditions of (a) Oslo and (b) Madrid for GPC without MPCM and GPC containing 5.2 wt.% PS-DVB/RT27.

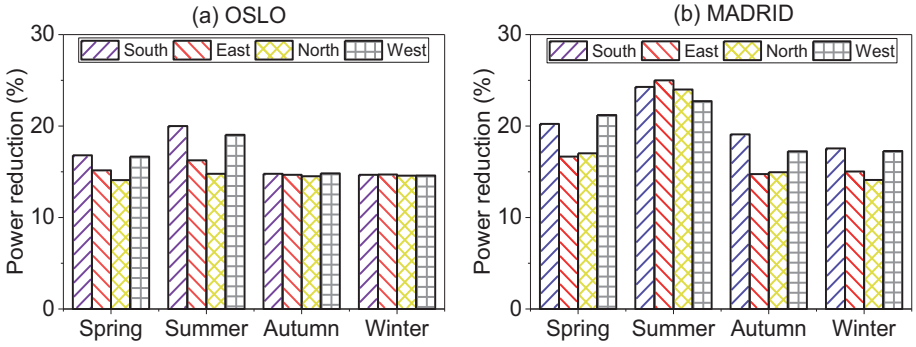

Figure 9. The power reduction of for South, East, North and West facing walls in Oslo and Madrid utilizing GPC-5.2-(PS-DVB/RT27) compared to GPC0 at different seasons during a year in (a) Oslo and (b) Madrid.

The power reduction of concrete samples containing 5.2 wt.% MPCM compared to corresponding samples without MPCM (GPC0) for walls facing different directions (south, east, north and west) in Oslo and Madrid during different seasons are presented in Figure 9. During spring and summer in Oslo, the power reduction for the south and west facing walls are higher than for the walls facing east and north, while all directions are almost the same during autumn and winter. The different solar radiation combined with the outdoor temperature contribute to this effect. Since the outdoor temperature in Oslo is lower than the maintained indoor temperature during most of the year (Figure 10), the heat provided by solar radiation reduces the heat transfer from the indoor environment toward the outdoor environment. This

shifts the indoor wall surface temperature on the south and west walls (which receives most direct sunlight) closer to the indoor temperature (Figure 10). This effect is most pronounced during spring and summer when the average outdoor temperature is closer to the indoor temperature, and the solar radiation on the south and west facing walls are relatively strong. During autumn and winter (24th September to 20th March), the days are much shorter and the solar radiation is too low to cause significant changes (Figure 11).

The power reduction in Madrid is highest for the south and west facing walls except during the summer. Unlike Oslo, the solar radiation in Madrid is significant through the whole year (Figure 11). Interestingly, during summer the power reduction in Madrid is lower for the south and west walls than for the east and north walls. Madrid experiences several summer days with temperatures higher than the indoor temperature. Accordingly, during these periods the added heat from the solar radiation results in a higher power consumption for cooling down the indoor environment.

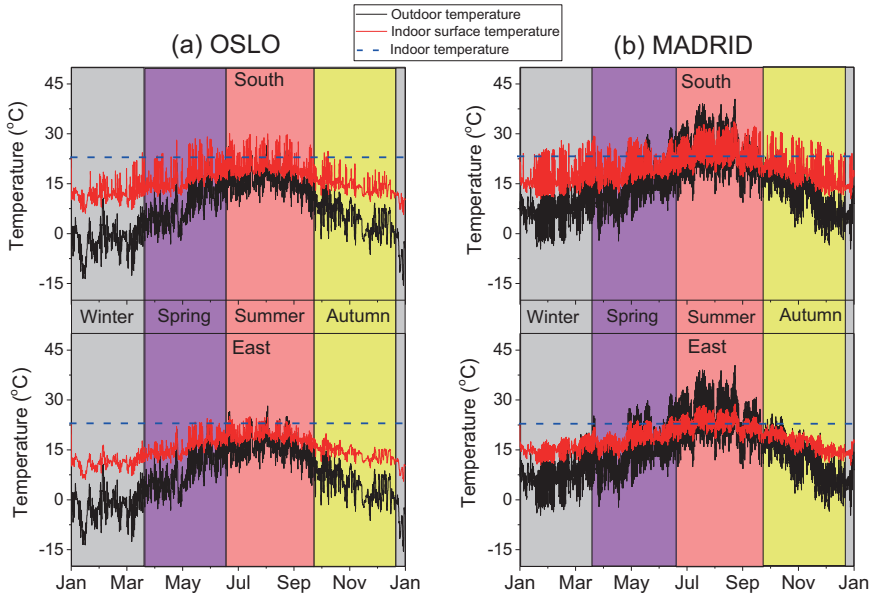

Figure 10. The outdoor temperature (obtained from weather data-Climate Consultant software (energy-design-tools.aud.ucla.edu.) and the effect of solar radiation on the indoor surface temperature of the south and east facing walls in (a) Oslo and (b) Madrid.

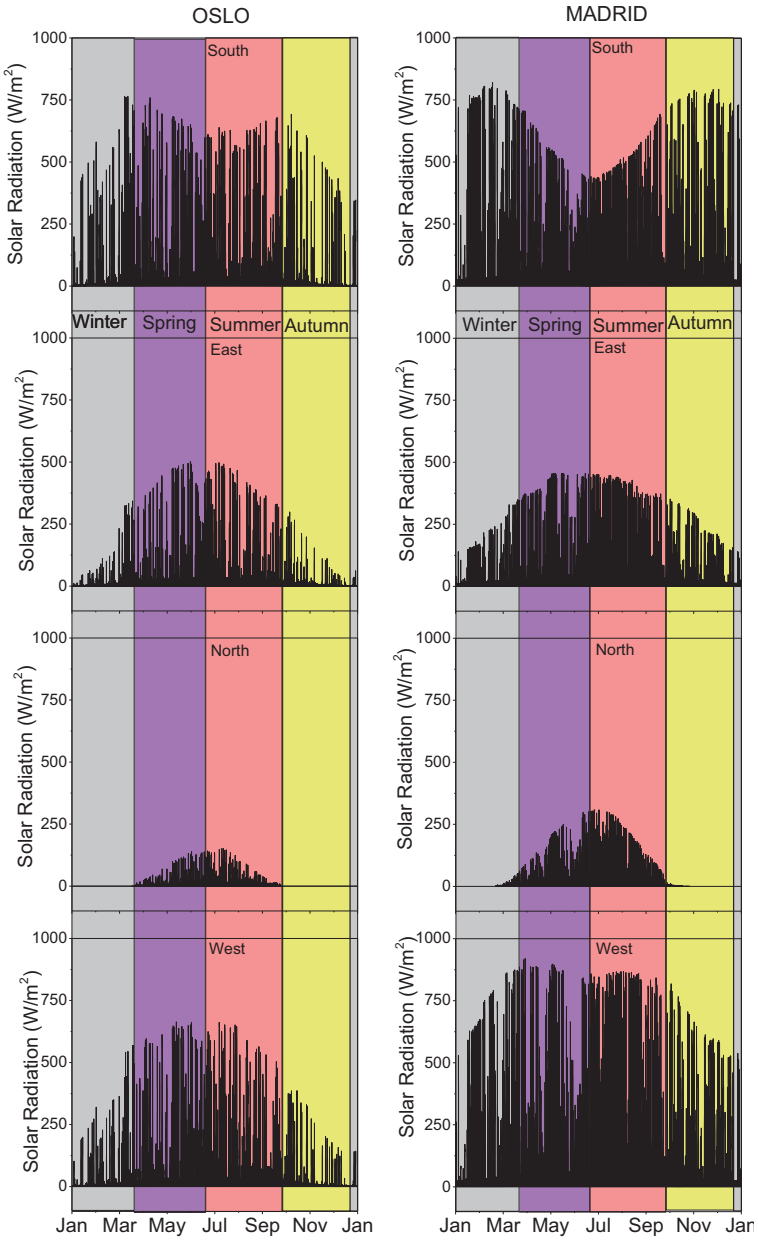

Figure 11. The solar radiation incident upon a south, east, north and west facing walls as functions of time Oslo and Madrid (obtained from weather data-Climate Consultant software (energy-design-tools.aud.ucla.edu.).

In order to evaluate the effect of MPM addition on the power consumption of the single house at different seasons during one year in Oslo and Madrid, the average power consumption and power reduction from different wall orientations were calculated (Figure 12). The power consumption is lowest during the summer and highest during winter in both cities and for all samples. Furthermore, the power reduction is highest in the summer and lowest during winter. The average outdoor temperature during the summer months (15±2 ºC in Oslo and 22±2 ºC in Madrid) (Figure 10) is close to the indoor temperature (23 ºC) and within the melting range of MPCM, which will improve the efficiency of utilizing the high latent heat of MPCM. The effect of high latent heat during phase change is hindered during winter due to too low temperatures. This is in good agreement with Figure 6. In addition, the lower power consumption and higher power reduction in Madrid compared to Oslo demonstrates that the utilized MPCM has a higher impact on the warmer climate in Madrid. This is due to an average yearly temperature in Madrid which is closer to the melting range of MPCM (Figure 10). Accordingly, by adding 5.2 wt.% of MPCM to GPC, a single family house in Madrid can reduce the power consumption with up to 24 % when utilizing PS-DVB/RT27 and 33 % for MF/PCM24 during summer and 16 % (PS-DVB/RT27) and 22 % (MF/PCM24) during winter (Figure 12). In Oslo, the power reduction can reache 18 % and 24 % during summer and 15 % and 20 % during winter after adding 5.2 wt.% of PS-DVB/RT27 and MF/PCM24, respectively. The higher power reduction of concrete containing MF/PCM24 is expected since the heat storage capacity of MF/PCM24 is higher than that of PS-DVB/RT27 (Table 1).

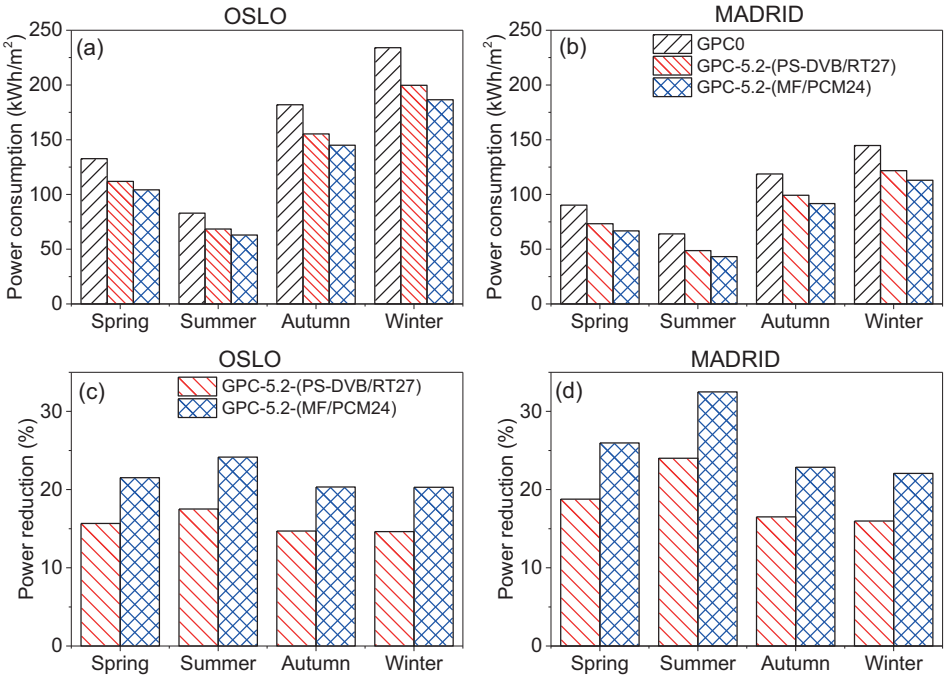

Figure 12. (a-b) The average power consumption (Eq.11) and (c-d) average power reduction (four wall orientations) of utilizing GPC-5.2-(PS-DVB/RT27) and GPC-5.2-(MF/PCM24) compared to GPC0 at different seasons during a year in Oslo and Madrid.

4. Conclusion

A numerical model based on the finite differences method using the energy balance approach was developed to predict the energy saving aspects of buildings utilizing GPC containing 2 types of MPCM at different environmental conditions. Increasing the MPCM concentration and the wall thickness significantly reduce the power consumption and increase the power reduction of buildings. The energy efficiency of the buildings was reduced at higher levels of solar radiation when the outdoor temperature is higher than the indoor temperature (cooling zone). This illustrates the importance of utilizing a PCM with a melting temperature close to the average outdoor and indoor temperatures, where the effect of the high heat storage capacity during the phase change can be fully utilized. The power reduction with the addition of 5.2 wt.% PS-DVB/RT27 was about 25-27 % when the average outdoor temperature was15-20 ºC for all outdoor temperature amplitudes. Interestingly, the addition of MPCM reduced the power

consumption up to 15 % even at conditions where the outdoor temperature is extremely warm or cold due to the increased concrete porosity and the resulting lower thermal conductivities. The numerical model was applied at the conditions of Oslo and Madrid. The annual power reduction was dependent on the orientation of the wall, and was found to be highest for the south and west walls in both Oslo and Madrid. The combined effect of solar radiation and outdoor temperature contribute to this effect. The influence of MPCM addition was highest during summer and lowest in winter. This is probably due to that the average outdoor temperature in the summer months (15±2 ºC in Oslo and 22±2 ºC in Madrid) is close to the indoor temperature (23 ºC) and within the melting range of the MPCM. The lower power consumption and higher power reduction of Madrid compared to Oslo is caused by temperatures closer to the melting range of the MPCM. GPC containing MF/PCM24 exhibits a better thermal performance than GPC containing PS-DVB/RT27 due to the higher heat storage capacity and lower thermal conductivity of GPC containing MF/PCM24.

Acknowledgement

We gratefully acknowledge funding from the Research Council of Norway, project number 238198. The authors gratefully acknowledge Rino Nilsen, Trond Atle Drøbak at Østfold University College and Van Thi Ai Nguyen for their assistance with laboratory work.

References

A. Pasupathy, L.A., R. Velraj, R.V. Seeniraj, 2008. Experimental investigation and numerical simulation analysis on the thermal performance of a building roof incorporating phase change material (PCM) for thermal management. Applied Thermal Engineering 28, 556–565.

AL-Saadi, S.N., Zhai, Z.J., 2013. Modeling phase change materials embedded in building enclosure: Areview. Renewable and Sustainable Energy Reviews 21, 659-673.

Al-Sanea, S.A., 2002. Thermal performance of building roof elements. Building and Environment 37, 665-675.

Alawadhi, E.M., 2008. Thermal analysis of a building brick containing phase change material. Energy and Buildings 40(3), 351-357.

ASHRAE, 2013. Handbook of Fundamentals. Atlanta: American Society of Heating, Refrigerating and Air-Conditioning Engineers. Inc.

Biswas, K., Abhari, R., 2014. Low-cost phase change material as an energy storage medium in building envelopes: Experimental and numerical analyses Energy Conversion and Management 88, 1020-1031.

Borreguero, A.M., Sánchez, M.L., Valverde, J.L., Carmona, M., Rodríguez, J.F., 2011. Thermal testing and numerical simulation of gypsum wallboards incorporated with different PCMs content. Applied Energy 88, 930-937.

Borreguero, A.M., Serrano, A., Garrido, I., Rodríguez, J.F., Carmona, M., 2014. Polymeric-SiO2-PCMs for improving the thermal properties of gypsum applied in energy efficient buildings. Energy Conversion and Management 87, 138-144.

Cao, V.D., Pilehvar, S., Salas-Bringas, C., Szczotok, A.M., Bui, T.Q., Carmona, M., Rodriguez, J.F., Kjøniksen, A.-L., 2018a. Thermal performance and numerical simulation of geopolymer concrete

containing different types of thermoregulating materials for passive building applications. Submitted for publication.
Cao, V.D., Pilehvar, S., Salas-Bringas, C., Szczotok, A.M., Rodriguez, J.F., Carmona, M., Al-Manasir, N., Kjøniksen, A.-L., 2017. Microencapsulated phase change materials for enhancing the thermal performance of Portland cement concrete and geopolymer concrete for passive building applications. Energy Conversion and Management 133, 56-66.
Cao, V.D., Pilehvar, S., Salas-Bringas, C., Szczotok, A.M., Valentini, L., Carmona, M., Rodriguez, J.F., Kjøniksen, A.-L., 2018b. Influence of microcapsule size and shell polarity on thermal and mechanical properties of thermoregulating geopolymer concrete for passive building applications. Energy Conversion and Management-Data in Brief, Submitted.
Cengel, Y.A., 2002. Heat Transfer: A Practical Approach, 2nd ed. Mcgraw-Hill.
Cui, H., Feng, T., Yang, H., Bao, X., Tang, W., Fu, J., 2018. Experimental study of carbon fiber reinforced alkali-activated slagcomposites with micro-encapsulated PCM for energy storage. Construction and Building Materials 161, 442-451.
Cui, H., Liao, W., Mi, X., Lo, T.Y., Chen, D., 2015. Study on functional and mechanical properties of cement mortar withgraphite-modified microencapsulated phase-change materials. Energy and Buildings 105, 273-284.
Darkwa, J., Su, O., 2012. Thermal simulation of composite high conductivity laminated microencapsulated phase change material (MEPCM) board. Applied Energy 95, 246-252.
Diaconu, B.M., Cruceru, M., 2010. Novel concept of composite phase change material wall system for year-round thermal energy savings. Energy and Buildings 42, 1759-1772.
Eddhahak-Ouni, A., Drissi, S., Colin, J., Neji, J., Care, S., 2014. Experimental and multi-scale analysis of the thermal properties of Portland cement concretes embedded with microencapsulated Phase Change Materials (PCMs). Applied Thermal Engineering 64(1–2), 32-39.
energy-design-tools.aud.ucla.edu., U.E.D.T.G.C.C.h.w.
EU Directive 2002/91/EC, E.P., Brussels, 2003.
EU Directive 2010/31/UE, E.P., Strasburg, 2010.
Garg, H.P., 1982. Treatise on solar energy: Fundamentals of Solar Energy, Chichester: Wiley.
Gowreesunker, B.L., Tassou, S.A., Kolokotroni, M., 2012. Improved simulation of phase change processes in applications where conduction is the dominant heat transfer mode. Energy and Buildings 47, 353-359.
Jang, J.G., Lee, N.K., Lee, H.K., 2014. Fresh and hardened properties of alkali-activated fly ash/slag pastes with superplasticizers. Construction and Building Materials 50, 169-176.
Joulin, A., Zalewski, L., Lassue, S., Naji, H., 2014. Experimental investigation of thermal characteristics of a mortar with or without a micro-encapsulated phase change material. Applied thermal engineering 66, 171-180.
Kreith, F., Manglik, R.M., Bohn, M.S., 2012. Principles of Heat Transfer, SI Edition. Cengage Learning.
Lachheba, M., Karkri, M., Nasrallah, S.B., 2015. Development and thermal characterization of an innovativegypsum-based composite incorporating phase change material asbuilding energy storage system. Energy and Buildings 107, 93-102.
Lamberg, P., Lehtiniemi, R., Henell, A.-M., 2004. Numerical and experimental investigation of melting and freezing processes in phase change material storage. International Journal of Thermal Sciences 43, 277-287.
M. Hunger, A.G.E., I. Mandilaras, H.J.H. Brouwers, M. Founti, 2009. The behavior of self-compacting concrete containing micro-encapsulated Phase Change Materials. Cement & Concrete Composites 31, 731-743.
Marin, P., Saffari, M., Gracia, A.d., Zhu, X., Farid, M.M., Cabeza, L.F., Ushak, S., 2016. Energy savings due to the use of PCM for relocatable lightweight buildings passive heating and cooling in different weather conditions. Energy and Buildings 129, 274-283.
Nematollahi, B., Sanjayan, J., 2014a. Effect of different superplasticizers and activator combinations on workability and strength of fly ash based geopolymer. Materials and Design 57, 667-672.
Nematollahi, B., Sanjayan, J., 2014b. Efficacy of Available Superplasticizers on Geopolymers. Research Journal of Applied Sciences, Engineering and Technology 7, 1278-1282.
Pérez-Burgos, A., Bilbao, J., Miguel, A.d., Román, R., 2014. Analysis of solar direct irradiance in spain. Energy Procedia 57, 1070-1076.

Pilehvar, S., Cao, V.D., Szczotok, A.M., Carmona, M., Valentini, L., Lanzón, M., Pamies, R., Kjøniksen, A.-L., 2018. Physical and mechanical properties of fly ash and slag geopolymer concrete containing different types of micro-encapsulated phase change materials. Construction and Building Materials 173, 28-39.
Pilehvar, S., Cao, V.D., Szczotok, A.M., Valentini, L., Salvioni, D., Magistri, M., Pamies, R., Kjøniksen, A.-L., 2017. Mechanical properties and microscale changes of geopolymer concrete and Portland cement concrete containing micro-encapsulated phase change materials. Cement and Concrete Research 100.
Pisello, A.L., D'Alessandro, A., Fabiani, C., Fiorelli, A.P., Ubertini, F., F.Cabeza, L., Materazzi, A.L., FrancoCotana, 2017. Multifunctional Analysis of Innovative PCM-filled Concretes. Energy Procedia 111, 81-90.
Shadnia, R., Zhang, L., Li, P., 2015. Experimental study of geopolymer mortar with incorporated PCM. Construction and Building Materials 84, 95-102.
Szczotok, A.M., Carmona, M., Kjøniksen, A.-L., Rodriguez, J.F., 2017. Equilibrium adsorption of polyvinylpyrrolidone and its role on thermoregulating microcapsules synthesis process. Colloid and Polymer Science 40, 4061-4071.
Thiele, A.M., Sant, G., Pilon, L., 2015. Diurnal thermal analysis of microencapsulated PCM-concrete composite walls. Energy Conversion and Management 93, 215-227.
Wei, Z., Falzone, G., Wang, B., Thiele, A., Puerta-Falla, G., Pilon, L., Neithalath, N., Sant, G., 2017. The durability of cementitious composites containing microencapsulated phase change materials. Cement and Concrete Composites 81, 66-76.
Xie, J., Wang, W., Liu, J., Pan, S., 2018. Thermal performance analysis of PCM wallboards for building applicationbased on numerical simulation. Solar Energy 162, 533-540.
Zwanzig, S.D., Lian, Y., Brehob, E.G., 2013. Numerical simulation of phase change material composite wallboard in a multi-layered building envelope. Energy Conversion and Management 69, 27-40.

Norwegian University of Life Sciences
Faculty of Science and Technology

Philosophiae Doctor (PhD)
Thesis 2018:72

Geopolymer Concrete Incorporated with Microencapsulated Phase change materials for Energy Efficient Buildings

Geopolymer Betong med Mikrokapslede Faseendringsmaterialer for Energieffektive Bygninger

Vinh Duy Cao